Instituto Andaluz de Ciencias de la Tierra
Consejo Superior de Investigaciones Científicas

A multiproxy approach for reconstructing environmental responses to climate variability in western Mediterranean over the last deglaciation

Jose Manuel Mesa Fernández
PhD Thesis

Supervisors:
Francisca Martínez Ruiz
Marta Rodrigo Gámiz

Granada, 2022

Editor: Universidad de Granada. Tesis Doctorales
Autor: José Manuel Mesa Fernández
ISBN: 978-84-1117-410-7
URI: http://hdl.handle.net/10481/75949

Esta Tesis Doctoral ha sido realizada en la unidad de Geociencias Marinas del Instituto Andaluz de Ciencias de la Tierra (CSIC-UGR) en el marco de los proyectos CGL2015-66830-R y PID2019-104624RB-I00 del Plan Estatal de Investigación Científica y Técnica y de Innovación (MCIN/AEI/ 10.13039/501100011033)

Para la realización de la tesis doctoral, el doctorando disfrutó de un contrato de Personal Investigador en Formación (FPI) BES-2016-077024 adscrito al proyecto CGL2015-66830-R. Además, realizó una estancia en el departamento de Microbiología y Biogeoquímica Marina en el Royal Netherlands Institute for Sea Research (NIOZ) en Países Bajos.

Esta tesis ha sido financiada, además, por los proyectos CGL2017-92600-EXP (AEI), P18-RT-3804 y Grupo de Investigación RNM-179 (Junta de Andalucía), cofinanciados con fondos de desarrollo regional (FEDER).

Table of contents

Abstract

This Thesis provides a high-resolution paleoclimate and paleoceanographic reconstruction for the past 20 ka in the western Mediterranean, obtained from a multiproxy approach in a suite of marine and continental sediment records. Previous work in this region has demonstrated the rapid response and high sensitivity of the Mediterranean region to the North Atlantic oceanic and atmospheric processes. Nevertheless, most of the previous studies have focused on one or very few records and the comparison between different basins and between marine and continental realms has not been fully addressed. Thus, this thesis aims to compare the climatic and sedimentary signals from different sub-basin in the western Mediterranean, and from marine and continental sedimentary records in order to provide new insights into the evolution of the western Mediterranean climate since the end of the Last Glacial Maximum to the present. To do so, diverse geochemical proxies have been obtained at high-resolution from seven marine records located in the Algero-Balearic and Alboran basins, and from one alpine continental record in Sierra Nevada. Major and trace element composition as well as elemental ratios in hemipelagic marine sediments support that the relative variation between terrigenous and carbonate fraction at suborbital scale is controlled by the deep current intensity while the surface productivity, the sea level variations and the riverine and eolian inputs have a minor influence. A palynological study was also performed in the alpine wetland record, which has provided a detailed environmental reconstruction of vegetation variations during the Holocene. The stable carbon and hydrogen isotopic composition measured in long-chained *n*-alkanes has been obtained in two of the studied marine records located in the eastern and western Alboran basins, which are influenced by different river catchments demonstrating the importance of sedimentary processes in the organic matter deposition.

This collective multiproxy approach performed in the different studied sedimentary records has allowed us to characterize the main climate intervals over the last 20 ka: The Heinrich Stadial 1 (HS1; 18-15 cal ka BP) is depicted by pervasive cold and arid conditions with a lesser influence of Atlantic sourced precipitation due to less humid westerlies. The advance of the sea ice sheets to lower latitudes could have promoted the influence of cold and dry winds over the Gulf of Lions and the WMDW formation and thus, increase the terrigenous input into the western Mediterranean basins. During the Heinrich Event 1 (HE1; 16.3-15.6 cal ka BP), the influx of meltwater derived from the

Laurentide and Fennoscandian ice sheets into the Mediterranean weakened the formation of deep water. During this period, the marine records located in the Alboran Sea basins show a decrease in the terrigenous fraction in comparison with the carbonate fraction that is not recognized in the Algero-Balearic basin.

The Bölling-Alleröd (B-A; 15-13 cal ka BP) is characterized by overall warm and humid conditions due to a greater influence of Atlantic sourced precipitation. The alpine glacial melting supplied fresh water into the Gulf of Lions, which considerably reduced the surface salinity and prevented the deep water formation thus promoting the formation of the Organic Rich Layer 1 in the Alboran Sea (ORL1; 15-9 cal ka BP). This ORL1 is characterized by high sedimentation rates, which enhanced organic matter preservation. The sea level rise during the meltwater pulse-1a flooded the shelf, remobilizing the loose sediments and destabilizing the shelf edge. The stable isotopes on specific organic compounds analyzed in the two Alboran records also suggest that terrestrial organic matter supplied into the basin was highly degraded at this time. Furthermore, redox-sensitive geochemical proxies have allowed to distinguishing two phases within the ORL1: ORL1a (15-11.7 cal ka BP) characterized by highly reduced oxygen seafloor conditions and the ORL1b (11.7-9 cal ka BP) depicted by more oxic seafloor conditions. The transition between the two sub-phases was marked by a reactivation of the bottom currents during the Younger Dryas (YD; 13-11.7 cal ka BP) due to the pervasive cold and arid conditions. The ORL1 demise at around 9 cal ka BP does not seem to be related to a reactivation of the deep currents since the redox-sensitive proxies show relatively stable values after the YD period. Instead, the demise was coeval with a sudden decrease of the sedimentation rates, which would promote the organic matter oxidation.

The Early Holocene (11.7-8.2 cal ka BP) was characterized by the warmest and most humid conditions over the last 20 ka as a result of maximum boreal summer insolation. Stable hydrogen isotopic records point to an Atlantic source of the precipitation, suggesting a higher influence of the westerlies over the western Mediterranean area. The retreat of the glacial in the southern Mediterranean mountains promoted the formation of alpine wetlands and lakes, such as Laguna Hondera (LH), the studied record in Sierra Nevada. This record evidences a high surface runoff and scarce preservation of the pollen grains during the Early Holocene. The Middle Holocene (8.2-4.2 cal ka BP) is depicted by an aridification trend with a vegetation assemblage composed of an increasing development of herbs species and by a trend towards more enriched δ^2H values in the

sedimentary *n*-alkanes, which suggest a reduction of the precipitation of Atlantic moisture source. During this period, there was a clear increasing influence of Saharan dust input in the Sierra Nevada lakes and wetlands that was less evident in the marine records. Only the marine records with low sedimentation rates showed such an increase, likely because high sedimentation rates diluted the eolian input.

Regarding the sedimentary condition in the marine basins, another interval of no correlation between terrigenous and carbonate fractions is evidenced in the Alboran and the Algero-Balearic basins. This fact could be related to the onset of the Alboran gyres that enhanced aspiration of deep waters in the Alboran Sea while the deep water currents were relatively stable in the Algero-Balearic basin.

The Middle-Late Holocene is characterized by an increase in arid-adapted vegetation and by a transition from pervasive Atlantic moisture source to more Mediterranean conditions, punctuated by a rapid see-saw fluctuation of Mediterranean-Atlantic-Mediterranean moisture source, between 4.8 and 3.8 cal ka BP which could be tentatively related to the 4.2 ka event.

The Late Holocene (4.2 cal ka BP-present) is characterized by high climatic variability and the first clear signal of human activities. An increase in the Pb content in the studied sediment records is recognized at around 3.8 cal ka BP and 3.5-2.5 cal ka BP in the Sierra Nevada and the Alboran records, respectively. At 2.5-2 cal ka BP, during the Iberian Roman Humid Period, there was a sharp increase in the terrigenous content recorded in all the marine records. Such an increase could be related to a higher effective erosion as a result of enhanced soil use for agrarian or mining activities. The last 150 years are characterized by an enhanced anthropic signal. An increase in *Olea* pollen marked the onset of extensive olive cultivation in southern Spain. In addition, a sharp increase in the Pb/Al ratio is recognized in both marine and continental records coinciding with the Industrial Period and the use of leaded fuels.

Resumen

Esta tesis presenta una reconstrucción paleoclimática y paleoceanográfica de alta resolución para los últimos 20 ka en el oeste del Mediterráneo, obtenida mediante un estudio multidisciplinar llevado a cabo en diversos registros sedimentarios marinos y continentales. Distintos trabajos previos en esta región han demostrado la alta sensibilidad del Mediterráneo a los cambios oceanográficos y atmosféricos del Atlántico Norte, así como la rapidez de su respuesta a dichos cambios. Sin embargo, la mayoría de los estudios realizados se han basado en un número limitado de registros y, además, la comparación entre las diferentes cuencas del oeste del Mediterráneo y la correlación entre registros marinos y terrestres no se han abordado suficientemente. Por tanto, esta tesis pretende comparar la señal climática y sedimentaria en las diferentes cuencas del oeste del Mediterráneo, así como la de registros marinos y continentales, para avanzar en el conocimiento sobre la evolución del clima en el oeste del Mediterráneo desde el último máximo glaciar hasta la actualidad. Con este fin, se han analizado diferentes indicadores geoquímicos a muy alta resolución en siete registros marinos de las cuencas Argelino-Balear y del mar de Alborán, y en un registro alpino en Sierra Nevada. La composición de los sedimentos hemipelágicos analizados, así como los diferentes indicadores geoquímicos utilizados, sugieren que la variación relativa entre las fracciones terrígena y carbonatada a escala suborbital está controlada principalmente por la intensidad de las corrientes de fondo, mientras que la productividad superficial, las variaciones del nivel del mar y los aportes fluviales y eólicos tienen una menor influencia. Además, se ha llevado a cabo un estudio palinológico en un registro alpino de Sierra Nevada, que ha proporcionado información paleoambiental detallada sobre la evolución de la vegetación durante el Holoceno. Así mismo, se ha analizado la composición de los isótopos estables de carbono e hidrógeno en cadenas largas de *n*-alcanos en dos registros marinos situados en las cuencas este y oeste del mar de Alborán, los cuales están influenciados por diferentes cuencas de drenaje, demostrando así la importancia de los procesos sedimentarios en el depósito de la materia orgánica terrestre en las cuencas marinas.

El estudio integrado y multidisciplinar llevado a cabo en los diferentes registros sedimentarios ha permitido diferenciar y caracterizar los principales periodos climáticos durante los últimos 20 ka. El estadío Heinrich 1 (HS1; 18-15 cal ka BP) se caracteriza por condiciones climáticas predominantemente frías y áridas con una menor influencia de precipitación de origen atlántico, debido a unos vientos del oeste menos húmedos, como

resultado de una temperatura superficial del mar más baja. El avance de la capa de hielo marina hacia latitudes bajas pudo incrementar la influencia de vientos fríos y áridos de latitudes más altas en el golfo de León, aumentado así la formación de agua profunda y, por lo tanto, el contenido de material terrígeno en las cuencas del oeste del Mediterráneo. Durante el evento Heinrich 1 (HE; 16.3-15.6 cal ka BP), el aporte de agua del deshielo de los casquetes Laurentino y Fenoescandinavo en el Mediterráneo debilitó la formación de agua profunda. Durante este periodo, los registros marinos en las cuencas del mar de Alborán muestran una disminución de la fracción terrígena con respecto a la carbonatada, mientras que este descenso no se reconoce en la cuenca Argelino-Balear.

El periodo Bölling-Alleröd (B-A; 15-13 cal ka BP) se caracteriza por condiciones climáticas predominantemente cálidas y húmedas, debido a una mayor influencia de la precipitación de origen atlántico. El deshielo de los glaciares alpinos también aportó agua dulce al golfo de León, lo que redujo considerablemente la salinidad superficial, impidiendo la formación de agua profunda y promoviendo la formación de la capa rica en materia orgánica 1 (en inglés, *Organic Rich Layer 1*, ORL1; 15-9 cal ka BP). La ORL1 en el mar de Alborán se caracteriza por una alta tasa de sedimentación, lo que contribuyó a una mayor preservación de la materia orgánica. El aumento del nivel del mar durante el pulso de agua de deshielo 1a (14.5-12.8 cal ka BP) inundó la plataforma, removilizando el sedimento no consolidado y desestabilizando el borde de la plataforma. Los análisis de isótopos estables de carbono e hidrógeno en compuestos orgánicos específicos, en concreto cadenas de *n*-alcanos, analizados en dos registros marinos del mar de Alborán, demostraron que la materia orgánica terrígena depositada durante este periodo estaba bastante degradada. Además, el estudio de indicadores elementales sensibles a cambios en condiciones redox ha permitido distinguir dos fases en el depósito de la ORL1: la ORL1a (15-11.7 cal ka BP), caracterizada por unas condiciones muy reductoras en el sedimento del fondo de la cuenca, y la ORL1b (11.7-9 cal ka BP) caracterizada por un aumento de la ventilación y oxigenación del fondo. La transición entre estas dos fases queda bien marcada por la reactivación de las corrientes profundas durante el Dryas Joven (YD; 13-11.7 cal ka BP) debido a las condiciones predominantemente frías y áridas. El final de la ORL1, en torno a 9 cal ka BP, no parece coincidir con una reactivación de las corrientes profundas, ya que los indicadores redox se mantuvieron relativamente estables después del Dryas Joven.

Durante el Holoceno temprano (11.7-8.2 cal ka BP) se registraron las condiciones climáticas más cálidas y húmedas de los últimos 20 ka. El registro de isótopos estables en *n*-alcanos apunta a que la precipitación procedía del Atlántico, sugiriendo una mayor influencia y humedad de los vientos del oeste en el Mediterráneo occidental.

La retirada de los glaciares en las montañas del sur de Europa dio lugar a la formación de lagos y humedales en Sierra Nevada, como es el caso del registro estudiado de Laguna Hondera (LH). Dicho registro muestra un gran aporte de escorrentía superficial y una mala preservación de los granos de polen durante el Holoceno temprano. El Holoceno medio (8.2-4.2 cal ka BP) se caracteriza por una tendencia a la aridificación, con una vegetación compuesta principalmente por especies herbáceas y una tendencia hacia valores más altos del δ^2H en los registros sedimentarios de *n*-alcanos, sugiriendo una reducción de la precipitación de origen atlántico. Durante este periodo, tuvo lugar un incremento en el aporte del polvo sahariano en los lagos y humedales de Sierra Nevada, que es menos evidente en los registros marinos. Solo aquellos registros marinos que presentan una baja tasa de sedimentación registran este incremento, probablemente porque la señal eólica queda diluida por las altas tasas de sedimentación.

Con respecto a las condiciones sedimentarias de las cuencas Argelino-Balear y del mar de Alborán durante este periodo, se registra un nuevo intervalo de no correlación en la variación relativa de terrígenos y carbonatos. Este hecho se puede deber a que el inicio de los giros superficiales en el mar de Alborán dio incrementó la aspiración de Bernoulli del agua profunda de la cuenca, mientras que las corrientes profundas se mantuvieron relativamente estables en la cuenca Argelino-Balear.

El tránsito del Holoceno medio al Holoceno tardío se caracteriza por un incremento de la vegetación adaptada a la aridez y por la transición de una precipitación con una fuente de humedad principalmente atlántica a una fundamentalmente mediterránea, que finalizó con una fluctuación rápida, mediterránea-atlántica-mediterránea, entre los 4.8 y 3.8 cal ka BP, lo que puede relacionarse tentativamente con el evento 4.2 ka.

El Holoceno tardío (4.2 ka cal BP-presente) se caracteriza por una alta variabilidad climática, evidenciando la primera señal clara de actividades humanas. Se ha reconocido un aumento del contenido de Pb en los registros de sedimentos continentales de Sierra Nevada en torno a 3.8 cal ka BP y en los registros marinos de Alborán entre 3.5 y 2.5 cal ka BP. Entre 2.5 y 2 cal ka BP, durante el Período Húmedo Romano Ibérico, se produjo un fuerte aumento del contenido de material terrígeno en todos los registros marinos.

Dicho aumento podría estar relacionado con una mayor erosión efectiva como resultado de un incremento del uso del suelo para actividades agrícolas o mineras. Los últimos 150 años registran una señal antrópica muy clara. El aumento del polen de *Olea europaea* está relacionado con el inicio del cultivo extensivo del olivo en el sur de España. Además, se reconoce un fuerte aumento de la relación Pb/Al tanto en registros marinos como continentales, coincidiendo con el Período Industrial y el uso de combustibles fósiles con plomo.

I GENERAL BACKGROUND

I. GENERAL BACKGROUND

1. Introduction

It is well known that climate change is a major challenge for the scientific community (e.g., IPCC, 2021). At the present-day, as society becomes more aware of the effects of climate change, governments are investing vast resources for investigating and mitigating its negative impact on the population and the economy. The Earth's temperature has risen 0.8ºC since the pre-industrial era as a result of the anthropIic greenhouse gas emissions, and future temperature projections point to a continuous increase in the next decades (e.g., IPCC, 2012, 2021). In the Paris agreement signed in 2015, 195 states vowed to limit global warming below 2ºC (with respect to pre-industrial levels), and try not to exceed 1.5ºC. Within this context, the Mediterranean region is a particularly vulnerable area, since in both scenarios of 1.5ºC and 2ºC of mean temperature increase, it will experiment severe droughts and extremely high temperatures implying numerous socio-economic challenges (IPCC, 2018, 2021). A reduction of winter and summer precipitation in the Mediterranean basin of 7 mm/K is expected (Lionello and Scarascia, 2018). The irregular and scarce precipitation will affect crop productivity, such as olive or grapevine, as well as the populations of southern Mediterranean countries, which already have water availability problems (Lionello et al., 2012; IPCC, 2018, 2021). Given the emergency marked by model projections (Fig. 1) (Collins et al., 2013; IPCC, 2018; Jacob et al., 2018), it is essential to provide a reliable scenario for future climate variability, for which purpose we need more precise knowledge of past climate changes that occurred under natural conditions, without human interference (e.g., Ruddiman et al., 2001; Masson-Delmotte et al., 2013; Fischer et al., 2018).

Paleoclimatology is a discipline that aims to investigate the response of the climate system to different natural forcings. In past decades, paleoclimatologists have studied climatic responses through natural paleo-archives, such as ice and sediment cores, tree rings, etc. (e.g., Shackleton et al., 2000; Lowe et al., 2008). Among these climate archives, marine sediment cores recovered in continental margins are highly sensitive to elucidate changes in the atmospheric, oceanic and sedimentary conditions. In addition, lacustrine sedimentary records are excellent paleo-archives since they present high sedimentation

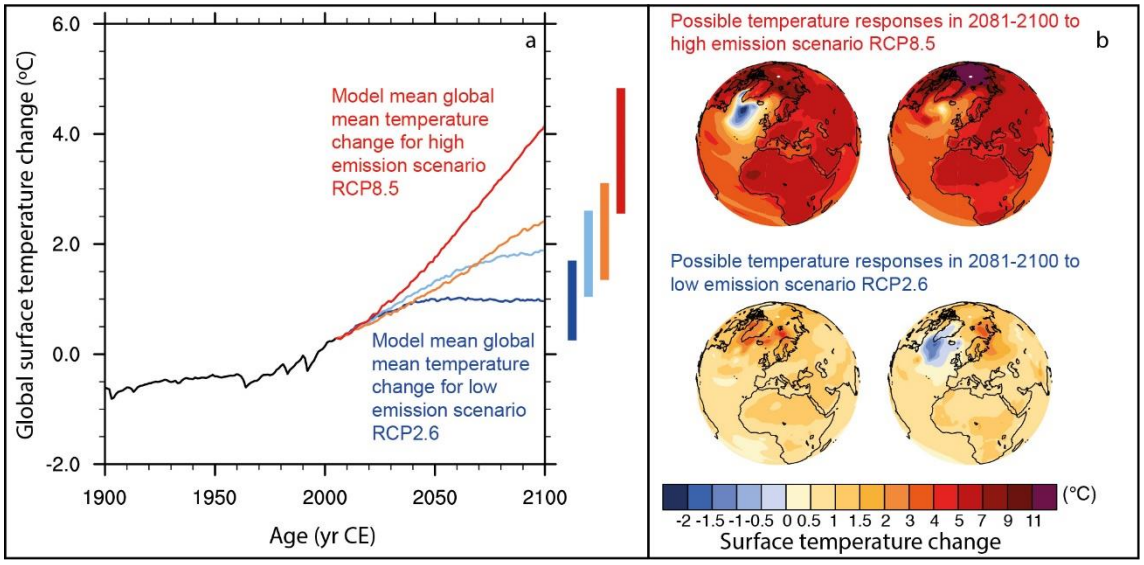

Figure 1. a) Global mean temperature change averaged across all Coupled Model Intercomparison Project Phase 5 (CMIP5) models (relative to 1986–2005) for the four Representative Concentration Pathway (RCP) scenarios: RCP2.6 (dark blue), RCP4.5 (light blue), RCP6.0 (orange) and RCP8.5 (red); b) Surface Temperature Change between 2081-2100 and 1986-2005 of RCP scenarios RCP8.5 and RCP2.6. Modified from Collins et al. (2013).

rates, allowing for high resolution studies, and they are also very sensitive to changes in precipitation and vegetation. Therefore, the recovery and study of both kinds of sedimentary records from strategic locations will certainly provide relevant paleoclimate information. The western Mediterranean region is a key location for reconstructing past climate changes, having shown a rapid response to the North Atlantic climate variability; thus, it sheds light on the interplay between oceanic and atmospheric processes and between high- and low-latitude dynamics (e.g., Thomson et al., 1999; Cacho et al., 1999, 2002; Martrat et al., 2004, 2007; Sierro et al., 2005; Hodell et al., 2013, 2017). The teleconnection between the North Atlantic dynamics and the western Mediterranean climate is highly influenced by the westerly system, which brings humidity and warm conditions to Europe (e.g., Trigo et al., 2002; Lionello et al., 2006; Fletcher et al., 2013, Sánchez Goñi et al., 2018; Li et al., 2019). At orbital timescales, variations in the position and intensity of the westerlies have been modulated by insolation and precession cycles, while at millennial timescales the Atlantic Meridional Overturning Circulation intensity and Arctic ice sheet have played a key role (Brauer et al., 2008; Jackson et al., 2015; Li et al., 2019).

1.1 Climate variability at orbital and suborbital timescales in the western Mediterranean

1.1.1 Present-day teleconnections and oceanographic conditions

Present-day climate variability in the western Mediterranean region is mainly driven by the North Atlantic Oscillation (NAO), which controls the region´s winter precipitation (Trigo et al., 2004). The NAO is governed by the difference between the surface sea-level pressure of the subpolar Icelandic cyclone and the subtropical Azores anticyclone (Wanner et al., 2001; Trigo et al., 2004; Lionello et al., 2006). An intensified Azores anticyclone and a deeper Icelandic cyclone, hence a positive NAO phase, generate northward migration of the westerlies, resulting in a more arid climate in the southern Mediterranean area (Fig. 2). Conversely, during a negative NAO phase, the Azores anticyclone is weaker and the Icelandic cyclone shallower, so that the westerlies deviate southward, resulting in humid conditions and increased precipitation in the southern Mediterranean (Fig. 2) (Wanner et al., 2001; Trigo et al., 2004).

Along the eastern and southeastern coast of the Iberian Peninsula, annual precipitation is controlled by the Western Mediterranean Oscillation (WeMO), and convective precipitation represents most of the annual precipitation (Martín-Vide and López-Bustins et al., 2006; Gonzalez-Hidalgo et al., 2009; Serrano-Notivoli et al., 2018). The WeMO is defined as a dipole of high pressure in the Azores and low pressure in the Gulf of Geneva, and the Western Mediterranean Oscillation Index (WeMOi) results from the differences in the atmospheric surface pressure between Cádiz and Padua (Martín-Vide and López-Bustins et al., 2006; López-Bustins et al., 2008). During its positive phase, the high pressure over the Gulf of Cadiz and the low pressure over the Gulf of Geneva promote the cyclonic rains of Mediterranean origin over the northern coast (Martín-Vide and López-Bustins, 2006). Conversely, the negative phase is characterized by an anticyclone over northern Italy and low pressure over the southwestern Iberia, promoting precipitation over the eastern coast of the Iberian Peninsula (Martin-Vide and López-Bustins, 2006). The orographic barriers also play an important role, preventing the arrival of the Atlantic front to the east (Martín-Vide and López-Bustins et al., 2006). On the other hand, during spring and summer, the convective or cyclonic precipitation of Mediterranean origin can

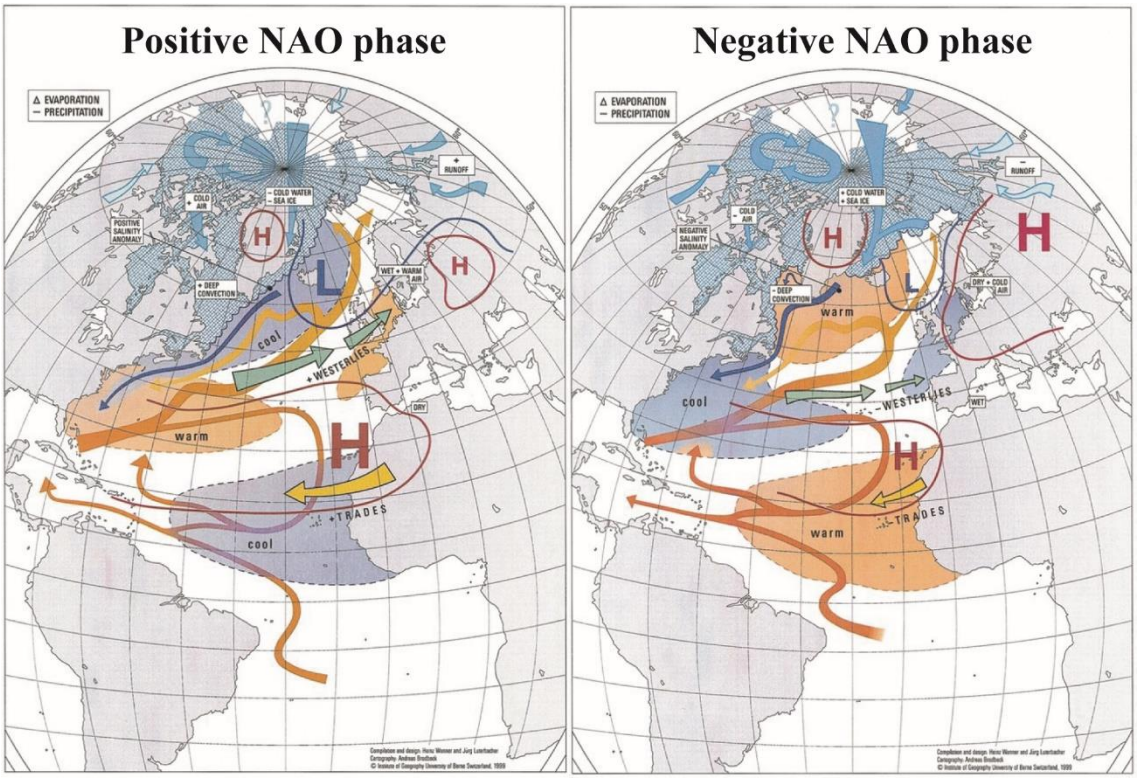

Figure 2. Schematic representation of the positive and negative states of the NAO, ice sheet extension, sea surface temperature and sea level pressure. Modified from Wanner et al. (2001). (a) Positive NAO phase: high pressure gradient between the Iceland low and the Azores high and northward migration of the westerlies; (b) Negative NAO phase: low pressure gradient between the Iceland low and the Azores high and southward migration of the westerlies, entering the Mediterranean region.

bear a major influence even on regions far from the coast (Romero et al., 1999; Celle-Jeanton et al., 2001).

The atmospheric teleconnections between the western Mediterranean and the North Atlantic influence not only the hydrological conditions of southwestern Mediterranean, but also the formation of Western Mediterranean Deep Water (WMDW) through heat loss of the surface waters (MEDOC group, 1970; Smith et al., 2008; Canals et al., 2013). In recent years, several studies point to the East Atlantic Pattern (EAP) as the main mechanism leading to heat loss in the Gulf of Lions, triggering the WMDW formation (Josey et al., 2011; Papadopoulus et al., 2012; Canals et al., 2013; Martínez-Asensio et al., 2014). The EAP is characterized by a low pressure cell located west of Ireland, between the two poles of the NAO (Josey et al., 2011); at a decadal timescale it can influence the position of the NAO dipole (Hernández et al., 2020). During a negative

phase, the EAP turns into a high pressure pole that promotes north-northwestern winds (Tramontane/Mistral) blowing into the Gulf of Lions (Josey et al., 2011; Papadopoulos et al., 2012). A positive phase of the WeMO, with a low pressure cell in the Gulf of Geneva, can also intensify these northerly winds (Lionello and Sanna, 2005; Martín-Vide and López-Bustins, 2006, López-Bustins et al., 2008; Martín et al., 2012).

From an oceanic point of view, the Mediterranean Sea is a semi-enclosed marine basin with a mean depth of 1500 meters below sea level (mbsl) (Schroeder, 2018), located between 30ºN and 45ºN latitude and between 5ºW and 35ºE longitude, surrounded by continental areas (Europe to the North, Africa to the South, Asia to the East) and connected with the Atlantic Ocean through the Gibraltar Strait to the West, and the Black Sea to the East. The present-day circulation in the Mediterranean is forced by the negative water balance in the basin, with more evaporation than precipitation in the basin, resulting in one of the saltiest sea water masses in the world. Due to the negative water balance and its connection with the less saline waters from the Atlantic Ocean, the Mediterranean Sea is characterized by a general anti-estuarine circulation: the fresher Atlantic waters enter the Mediterranean and flow as a shallower layer eastward, while the denser Mediterranean water flows westward, residing in the deeper part of the basin (Millot et al., 1999, 2009.

The Mediterranean Sea is subdivided in two main basins, with different temperature and salinity conditions, separated by the Sicilia Strait (500 mbsl) (Fig. 3). The western Mediterranean basin is subdivided from East to West in several sub-basins: The Tyrrhenian Sea, the Liguro-Provençal basin, the Algero-Balearic basin and the Alboran Sea basin. The formation of the western Mediterranean basin and its sub-basins is closely related to the evolution of the Alpine mountain ranges and the convergence between the African and Eurasian plates (Rehault et al., 1984; Comas et al., 1999 for a review).

The oceanographic circulation in the western Mediterranean can be simplified as three main water masses separated by differences in temperature, salinity and density (Fig. 3) (Millot, 1999, 2009, 2013). The Surface Atlantic Water (SAW) and the North Atlantic Central Water (NACW) enter the Mediterranean through the Gibraltar Strait and mix with the Mediterranean Outflow Water (MOW), forming the light Modified Atlantic Water (MAW), which flows eastward occupying the top 200 m of the seawater column (Fig. 3)

(Millot, 1999, 2009, 2013). In the Alboran Sea basin, the MAW forms two anticyclonic gyres —the quasi-permanent Western Alboran Gyre (WAG) and the seasonal Eastern Alboran Gyre (EAG) (Heburn and La Violtte, 1990; Tintoré et al., 1991; Millot, 1999; Bárcena et al., 2001; Fabres et al., 2002; Ercilla et al., 2016). Two high productivity fronts are associated with these gyres: the Málaga Front and the Almería-Orán Front (Sanchez-Vidal et al., 2004).

Below the MAW, three intermediate water masses flow westward (Fig. 3): between 200 and 600 mbsl along the southern Iberian margin and the central Alboran basin, between 200 and 400 mbsl along the Moroccan margin and between 300 and 1500 mbsl in the Algero-Balearic basin. The shallowest of these three water masses is the Winter Intermediate Water (WIW), which forms when the MAW is cooled in the Liguro-Provençal sub-basin during wintertime. The middle is the Levantine Intermediate Water (LIW) results from cooling and evaporation of the MAW in the Levantine sub-basin and it is characterized by a relatively warm temperature and high salinity. The deeper of these intermediate water is the Tyrrhenian Dense Water (TDW), formed by the mixing of Eastern Mediterranean Deep Water (EMDW) with water masses from the Tyrrhenian, WMDW, old TDW and old LIW (Fig. 3) (Millot, 2009). The TDW shows two different behaviours: the upper part of TDW behaves like the LIW and flows through the northern margin, while the lower part behaves like the WMDW and flows through the Moroccan margin.

The WMDW is restricted to 600 mbsl in the northern and central Alboran basin, below 400 m in the Moroccan margin and below 1500 m in the Algero-Balearic basin (Fig. 3) (Millot, 1987, 2013). It is formed in the Gulf of Lion as a result of Dense Shelf Water Cascading or Offshore Convection triggered by the buoyancy loss of the surface waters (see Canals et al., 2013 for a review). The WMDW formation is associated with the presence of the Mistral and Tramuntana winds blowing cold and dry air into the NW Mediterranean. Apart from the surface water heat loss, other factors that influence the WMDW formation include the LIW input into the Provençal subbasin. The warm and saltier LIW can induce OC events that result in a warmer but saltier WMDW (Toucanne et al., 2007, 2012; Smith et al., 2008; Martin et al., 2010).

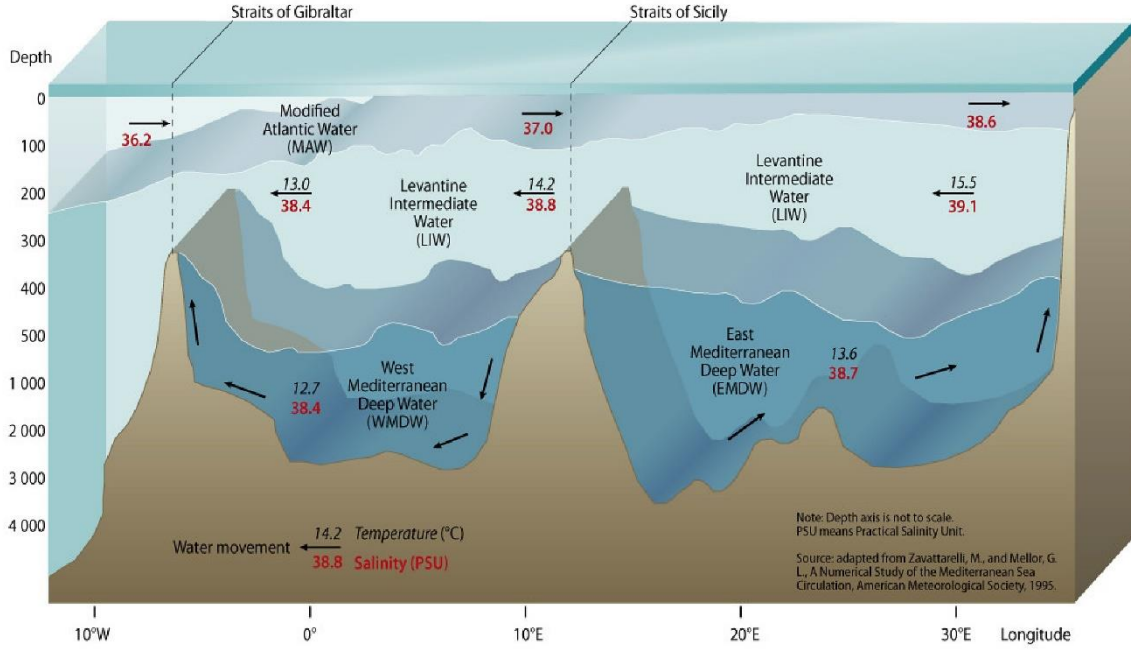

Figure 3. Schematic representation of the main water masses in the Mediterranean Sea. Numbers in black (red) indicate temperature (salinity) and black arrows indicate the water movement. From GRIDArendal. 2013.

In turn, the Atlantic Meridional Overturning Circulation (AMOC) is an overturning cell located in the North Atlantic, responsible for the northward transport of surface warm water, and balanced by the southward transport of deep cold water (Buckley and Marshall, 2015; Lynch- Stieglitz, 2017; Weijer et al., 2019). The AMOC plays a central role in transporting heat from low to high latitudes (Buckley and Marshall, 2015), and controlling the position of the Inter Tropical Convergence Zone (ITCZ), thus influencing the climate of the Northern Hemisphere (Brayshaw et al., 2009; Buckley and Marshall, 2015; Li et al., 2019).

1.1.2 Past climate variability and oceanographic evolution

The global climate over the last 900 ka has been characterized by glacial-interglacial intercalations related to insolation changes linked to orbital oscillations (Berger, 1980). Within the orbital oscillations, known as Milankovitch cycles, eccentricity (100 ka periodicity) has been suggested as the main insolation driver, modulated by obliquity and

precession cycles (with 41 ka and 23 ka periodicities, respectively) over the past 900 ka (Milankovic, 1941; Hays et al., 1976; Berger and Jansen, 1994; Tzedakis et al., 2017). The last 20 ka are characterized by minima in summer insolation around 20 cal ka BP, followed by a gradual increase until 11 cal ka BP, when a maximum was reached (Wanner et al., 2008). In general, the last 12 cal ka BP are characterized by a decreasing trend until present-day (Laskar et al., 2004).

The orbital cycles are superimposed upon high-frequency climatic variability at a suborbital timescale (Imbrie et al., 1984). They include the Dansgaard-Oeschger (D-O) cycles, characterized by rapid warming and progressive cooling, with a frequency of 1.5 ka (Daansgard et al., 1984; Alley et al., 2001). The D-O cycles show a progressive trend toward colder cycles, known as Bond cycles, which sometimes culminate in Heinrich events (HEs) (Bond et al., 1992, 1993). The HEs are described as the deposition of ice-rafted debris (IRD) layers in the North Atlantic (Heinrich et al., 1988) as a consequence of iceberg melting, and have been recognized in almost all of the last glacial periods (Hodell et al., 2008). The IRD deposition is accompanied by large meltwater inputs in the North Atlantic, which have had a great influence in the AMOC intensity and the climate variability of the North Hemisphere (Fig. 4) (Heinrich et al., 1988; Hodell et al., 2015; Repschläger et al., 2015; 2021; Lynch-Stieglitz, 2017; Weijer et al., 2019). Changes in the intensity of the AMOC during the D-O cycles bear a direct impact on the European and Mediterranean climates by controlling the humidity and/or position of the westerlies (Brayshaw et al., 2009; Jackson et al., 2015; Lynch-Stieglitz, 2017; Naugthon et al., 2019; Li et al., 2019; Toucanne et al., 2021). The freshwater input in the North Atlantic prevented the overturning and thus the transport of heat from the Equator to the Poles, resulting in a cooling over the Northern Hemisphere, the advance of continental and sea ice sheets, intensification of the westerlies, and reorganization in the ITCZ position, with the concomitant consequences for humidity transport over Europe (Baldini et al., 2015).

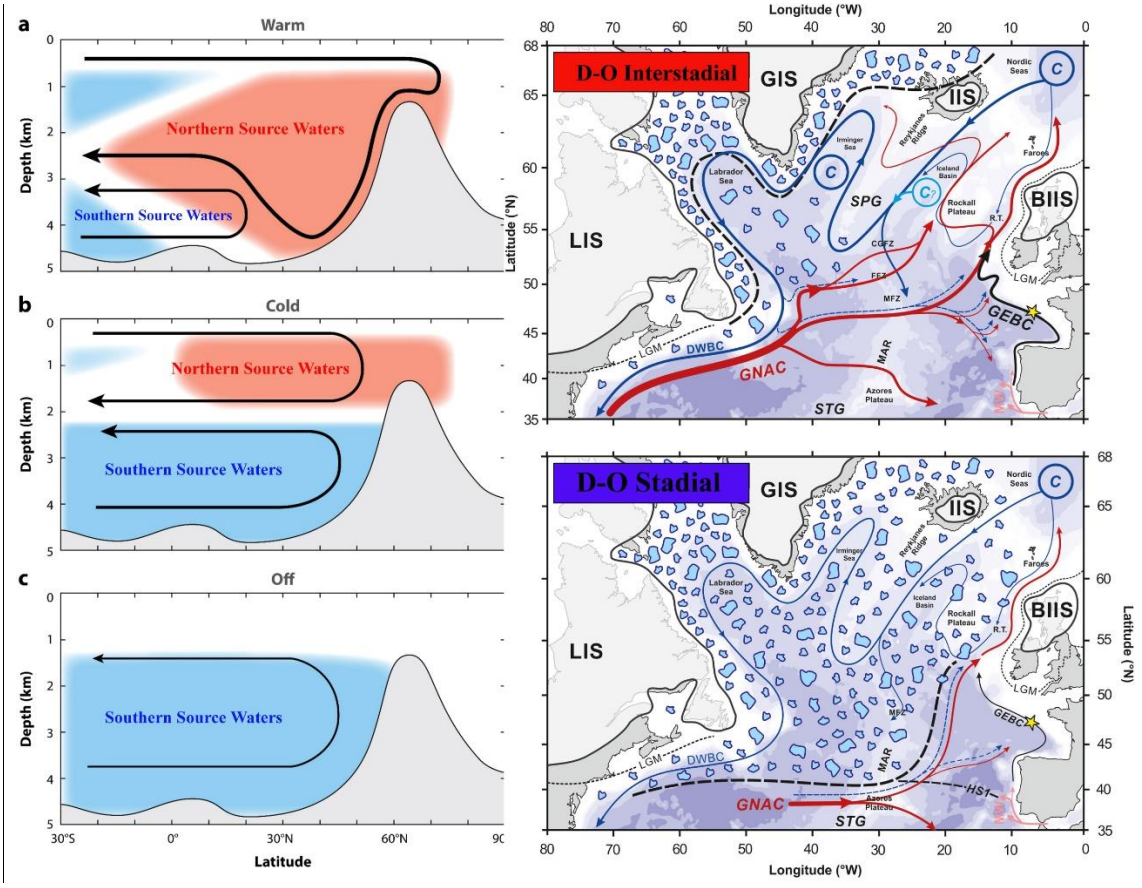

Figure 4. Different phases of the AMOC. LIS: Laurentide Ice Sheet; GIS: Greenland Ice Sheet; IIS: Iceland Ice Sheet; BIIS: British-Irish Ice Sheet; SPG: Sub-Polar Gyre; STG: Sub-Tropical gyre; GNAC: Glacial North Atlantic Current; C: Convection zones. Modified from Lynch-Stieglitz (2017) and Toucanne et al. (2021).

1.2 Sediment records from the western Mediterranean region

1.2.1 Marine sediment records

The sedimentary column of the western Mediterranean basin is around 7 km thick, and it comprises three main formations or units: the oldest one consists of marly sediments of Lower and Middle Miocene age; the middle unit consists of evaporites formed during the Messinian salinity crisis; and the upper formation consists of marly sediments with the occurrence of turbidites and contourites of Pliocene and Quaternary age (Rehault et al., 1984).

Nowadays, sedimentation in the western Mediterranean basin and its sub-basins represents an interaction between vertical settling, downslope and along-slope processes

(Rehault et al., 1984; Comas et al., 1999; Lobo et al., 2006; Frigola et al., 2007; Jiménez-Espejo et al., 2007; Lombo Tombo et al., 2015; Ercilla et al., 2016). In the Algero-Balearic basin several turbidite systems occurred along the continental slopes, the most prominent ones being the Rhone, Ebro/Valencia and Var fans (Rothwell et al., 1998; Dennielou et al., 2019). Similarly, contouritic deposits are located around the Balearic Promontory (Sierro et al., 2005; Frigola et al., 2007; Cisneros et al., 2019). In the Alboran Sea basin, the different sedimentary environments have been accurately characterized (Ercilla et al., 2016, 2019; Juan et al., 2016). Turbidite systems are mainly located along the northern coast of the Alboran Sea, likely due to the current intensity by the northern and southern coasts (Ercilla et al., 2019); the largest are the Almeria and Fuengirola turbidite systems. The interaction of deep water currents with the complex seafloor morphology of the basin promote the formation of contouritic deposits along the Alboran Sea basin (Ercilla et al., 2016). Hemipelagic sedimentation dominated throughout the different sub-basins, mainly in zones without the influence of turbidites and conturites. In particular, the Alboran Sea basin presents a higher lithogenic content and sedimentation rates than the Algero-Balearic basin due to its narrow and semi-enclosed morphology (Fabres et al., 2002; Sierro et al., 2005; Jiménez-Espejo et al., 2007; Zuñiga et al., 2007a; Rodrigo-Gámiz et al., 2011).

Therefore, the sedimentary sequences recovered in the western Mediterranean sub-basins are excellent paleo-archives, highly sensitive to different climate sub-systems such as the atmosphere (wind patterns), the hydrosphere (water circulation and sea floor oxygenation), and the biosphere (productivity). The westernmost Mediterranean basin in particular is an outstanding location for paleoclimate reconstructions because the erosion of the relatively young massifs around the basin promote high and continuous sedimentation rates, allowing for high resolution paleoclimate studies (e.g., Cacho et al., 2001; Sierro et al., 2005; Jiménez-Espejo et al., 2007; Nieto-Moreno et al., 2011; Rodrigo-Gámiz et al., 2011; Martínez-Ruiz et al., 2015).

1.2.2 Alpine continental records in southern Iberia

Continental sedimentary records recovered in lakes, peat bogs and wetlands have also been useful for reconstructing the paleoclimate evolution, contributing to high resolution studies since they usually present higher sedimentation rates than marine records. They are also sensitive to atmospheric processes, but they usually present greater local influences. Continental records tend to be shorter than marine records and can be especially influenced by anthropic actions in the most recent times. Furthermore, alpine lakes, peat bogs and wetlands are highly valuable paleo-archives in that the anthropic signal is expected to be almost negligible (e.g., Tinner et al., 2003, 2005; Anderson et al., 2011; Jiménez-Moreno and Anderson 2012; Sánchez-López et al., 2016; Cartier et al., 2018).

Within this framework, the Sierra Nevada mountain range, located in the southern Iberian Peninsula, is one of the highest mountain range in the southern Europe. The bedrock of the high elevations of Sierra Nevada is mostly composed by metamorphic rocks, principally mica schists (Castillo Martín, 2009). During the Late Pleistocene, the Sierra Nevada was one of the southernmost mountains supporting alpine glaciers, and its last advance was recorded during the Little Ice Age (LIA) (Palma et al., 2017; Oliva et al., 2018; Palacios et al., 2020). The erosion and subsequent melting of glaciers at the end of the Last Glacial Maximum (LGM; 21-18 cal ka BP) formed wetlands and small lakes between 2451 and 3227 m above sea level (masl) (Schulte, 2002; Castillo Martín, 2009; Palma et al., 2017), which are excellent paleo-archives, as previously explained. In the last decade, numerous paleoclimate studies have been carried out on lakes and peatbog in Sierra Nevada (Anderson et al., 2011; Jiménez-Moreno and Anderson, 2012; García-Alix et al., 2012, 2013, 2017; Oliva and Gómez-Ortiz, 2012; Oliva et al., 2018; Jiménez-Moreno et al., 2013, 2020; Jiménez-Espejo et al., 2014; Ramos-Román et al., 2016), which allow for comparisons with previously published studies.

As usually occurs in mountainous regions, vegetation in Sierra Nevada is distributed with respect to elevation, depending on the temperature and rainfall gradients (e.g., El Aallali et al., 1998; Valle, 2003). In Sierra Nevada, the crioromediterranean flora occurs as tundra-like open grassland above 2800 masl. The oromediterranean belt (1900-2800

masl) mostly includes dwarf *Juniperus* (juniper), xerophytic shrublands and pasturelands, with *Pinus sylvestris* and *P. nigra*. The supramediterranean belt (~1400-1900 masl) is characterized by mixed deciduous and evergreen forest species (i.e., evergreen and deciduous *Quercus*, with *Pinus spp.* and others). Mesomediterranean vegetation (600-1400 masl) includes sclerophyllous shrublands and evergreen *Quercus* woodlands. The natural vegetation has been strongly altered by human activities and cultivation in the last centuries, significantly increasing the abundance of *Olea europaea* (olive), due to cultivation at lower altitudes (Anderson et al., 2011, and references therein), and *Pinus* due to reforestation, primarily at higher elevations (Valbuena-Carabaña, 2010).

The southern Iberian Peninsula has a long history of settlement since the Chalcolithic or Copper Age (5.3-4.2 cal ka BP). Los Millares (Almería), dated as 5.15 cal ka BP, is one of the first settlements, whose population worked with metallurgy and fortified the settlement (Molina-González et al., 2004; Blanco-González et al., 2018). Early human modification of landscapes by grazing and agricultural activities are found since the Middle Holocene (Carrión et al., 2010), and the first signal of mining around Sierra Nevada is dated at around 3.8 cal ka BP (García-Alix et al., 2012). During the Roman occupation of the Iberian Peninsula the mining of galena was intensified, and the signal of lead pollution is recorded in several locations around southern Iberia and in the Alboran Sea (Martín-Puertas et al., 2010; García-Alix et al., 2013). During the Middles Ages, grazing activities have also been evidenced at various alpine peat bogs from Sierra Nevada (Anderson et al., 2011; Ramos-Román et al., 2016). The anthropogenic signal in paleoclimatic records from the southern Iberia become clearer from the LIA until the present-day, with the onset of intensive olive cultivation and an increase in the Pb content coinciding with the industrial revolution (González Portilla, 1998).

1.3 Paleoenvironmental responses over the Last Glacial Maximum, the deglaciation and the Holocene

The last glacial cycle is culminated with the Last Glacial Maximum (LGM; 21-18 cal ka BP), defined as the maximum extension of mountain glaciers and sea ice sheets (Hudges et al., 2013) and the lowest sea level of the entire cycle (Lambeck et al., 2014).

Afterwards, a progressive trend to warmer conditions occurred, with the subsequent melting of both mountain glaciers and sea ice sheets, leading to a sea level rise (Ivy-Ochs et al., 2008; Clark et al., 2009; Lambeck et al., 2014). This period is known as the last deglaciation, and it spans from the end of LGM to the end of the Younger Dryas (YD; 12.8-11.7 cal ka BP). The last deglaciation is characterized by a progressive warming trend punctuated by several cold spells, such as the Heinrich Stadial 1 (HS1; 18-15 cal ka BP; Hodell et al., 2017) and the YD. At most high altitude settings from the western Mediterranean region, e.g. the Alps and Sierra Nevada, the glaciers reached their maximum expansion (Ivy-Ochs et al., 2008; Palacios et al., 2020). The onset of the deglaciation, around 19 cal ka BP, is characterized by a retreat of Alpine glaciers and an increase in the sea level (Ivy-Ochs et al., 2008; Lombo Tombo et al., 2015; Palacios et al., 2020). Between 18 and 15 cal ka BP, the melting of the Fennoscadian and Laurentide ice sheet triggered freshwater input into the North Atlantic, resulting in an AMOC slowdown or collapse (Hodell et al., 2015, 2017; Repschläger et al., 2015, 2021), with the concomitant effect on the western Mediterranean climate (Torres et al., 2020; Camuera et al., 2021). In the southern Iberia, the HS1 is characterized by cooler and more arid conditions than during the LGM (Cacho et al., 2002; Fletcher et al., 2010; Rodrigo-Gámiz et al., 2014; Camuera et al., 2021), the arid conditions over tropical Africa increasing the Saharan dust input over the whole Mediterranean area (Rodrigo-Gámiz et al., 2011; Scheuvens et al., 2013). After the HS1, reactivation of the AMOC during the B-A period triggered warmer and more humid climate conditions over the western Mediterranean (Combourieu-Nebout et al., 2009; Fletcher et al., 2010; Ng et al., 2018; Skinner et al., 2021). In addition, the melting of the alpine glaciers discharging in the Gulf of Lions triggered the melt-water pulse 1a and the collapse of the WMDW formation, which resulted in the Organic Rich Layer 1 (ORL1) deposition in the Alboran Sea (Cacho et al., 2002; Rogerson et al., 2008). During this period, the onset of the African Humid Period (AHP) occurred (ca. 14 cal ka BP) due to a northward migration of the ITCZ and the African monsoon, and a southward migration of the Atlantic Storm track (Cheddadi et al., 2021). The YD is depicted by cold and arid conditions related to a new release of freshwater in the North Atlantic, owing to drainage of the Lake Agassiz, resulting in a

new AMOC slowdown (Fanning and Weaver, 1997; Repschläger et al., 2015; Naughton et al., 2016, 2019).

The Holocene spans the last 11.7 cal ka BP until present-day (Wanner et al., 2008, Walker et al., 2019), and is characterized as a relatively stable and warm period, with short cold spells (Mayewski et al., 2004). Cooling pulses in the North Atlantic similar to those taking place during the deglaciation have been recognized during the Holocene period; known as Bond events (Bond et al., 1997, 2001), they also affected the thermohaline circulation and Northern Hemisphere climate variability (Alley and Ágústsdóttir, 2005; Wiersma and Jongma, 2010). The Early Holocene (11.7-8.2 cal ka BP) is characterized by the boreal summer insolation maximum, which triggered the AMOC reactivation and humid conditions over the Mediterranean area (Oppo et al., 2003; Repschläger et al., 2015). The northward migration of the ITCZ resulted in a precipitation increase in the Nile watershed, and thus an increase of freshwater input into the Eastern Mediterranean (de Lange et al., 2008; Revel et al., 2015). The extreme reduction in the surface salinity prevented the formation of deep water, resulting in anoxic conditions in the bottom basin, allowing for the formation of the Sapropel 1 (S1; 10-6.4 cal ka BP). At around 9 cal ka BP there was a demise of the ORL1 deposition (Cacho et al., 2006; Jiménez-Espejo et al., 2007; Pérez-Asensio et al., 2020), which has been related to a reactivation of the WMDW (Frigola et al., 2008). In the southern Iberian high altitude mountains, the glaciers underwent a great retreat, giving rise to the formation of several alpine lakes and wetlands. In the Sierra Nevada mountain range, all the lakes located above 2400 m altitude were formed during this interval (Anderson et al., 2011).

The transition between the Early and the Middle Holocene (8.2-4.2 cal ka BP) is characterized by the cold event 8.2 ka, which was triggered by meltwater release in the North Atlantic (Alley et al., 2001). Although this event has not been recognized in most of the northern Mediterranean records (Magny et al., 2013), it triggered a northward migration of the ITCZ, resulting in a reactivation of the thermohaline circulation in the eastern basin and an interruption of the S1 deposition (Rohling and de Rijk, 1999; de Lange et al., 2008; Filippidi et al., 2016). Another cold event in the North Atlantic was recorded around 7.6-7.0 cal ka BP, which in the Mediterranean resulted in arid conditions over the basin and a new interruption of the S1 deposition (Rohling and de Rijk, 1999;

Ariztegui et al., 2000; Filippidi et al., 2016). In the southwestern Mediterranean, xerophytic vegetation started to replace the more humid-adapted vegetation predominant during the Early Holocene. This aridity trend culminated at 5 cal ka BP with the demise of the AHP, which meant the transition of a vegetated Sahara-Sahel region to the present-day desertic conditions (de Menocal et al., 2000; Schefuß et al., 2005; Castañeda et al., 2009; Chedaddi et al., 2021). This change enhanced dust export from the Sahara Desert to other Mediterranean locations.

The Late Holocene (4.2 cal ka BP to present-day) is characterized by high variability: pervasive warm and humid conditions during the Iberian Roman Humid Period (IRHP; 2.60-1.45 cal ka BP; Martín-Puertas et al., 2009, 2010), cold and arid conditions during the Dark Ages (DA; 1.45-1.05 cal ka BP; Helama et al., 2017); warm and arid conditions during the Medieval Climate Anomaly (MCA; 1.05-0.65 cal ka BP; Moreno et al., 2012); and cold and humid conditions during the Little Ice Age (LIA; 0.65-0.15 cal ka BP, Oliva et al., 2018). Nevertheless, there was a dissimilar response across the Mediterranean basin (Sánchez-López et al., 2016). In addition, during this period there was a change in the teleconnection between the North Atlantic and the Mediterranean —during the Early and the Middle Holocene and the deglaciation, the Atlantic cooling events corresponded with arid conditions over the Mediterranean, but during the Late Holocene these coolings were coeval with humid conditions over the Mediterranean (Zielhofer et al., 2017). This change in the N-S teleconnections is not well understood, yet changes in insolation and the AMOC strength have been postulated as possible forcing mechanisms (Fletcher and Zielhofer 2013; Zielhofer et al., 2017).

1.4 Multi-proxy approach for paleoclimate reconstruction

1.4.1 Inorganic geochemical proxies

Early works and oceanic expeditions aiming to reconstruct past climate variability from deep marine sediment records realized that the lithology and the mineral composition mainly responded to glacial-interglacial cycles (Bramlette and Bradley, 1940; Arrhenius, 1952). Later on, it was discovered that the geochemical composition of deep marine sediment records offers valuable information about the ocean dynamics, allowing for the

study of geochemical cycles (Goldberg, 1954; Goldberg and Arrhenius, 1958; Berner, 1971). The elemental composition of marine sediments is usually the result of processes involved in its deposition: (1) source area; (2) transport mechanisms; (3) climate conditions on the surrounding continents; (4) oceanic dynamics and seafloor oxygen conditions; (5) productivity; and (6) physical and chemical post-depositional processes; although sometimes, the same element can be enriched in the sediment by more than one of the processes described above (Calvert and Pedersen, 2007).

Furthermore, sediments are conformed by different fractions, including lithogenic, biogenic, hydrogenous, cosmogenous and diagenetic fractions. Potentially, all sediments are made up of an admixture of these fractions, and elements in the sediments reflect the relative proportion of each fraction (Calvert and Pedersen, 2007). Thus, if one element resides only in one fraction, its abundance would be subjected to the dilution between fractions. In order to elucidate the real abundance of one element within a fraction, it should be normalized. Aluminum (Al) normalization is most commonly used for elucidating the variation of an element within the terrigenous fraction, since Al is supposed to be conservative (Van der Weijden, 2002; Calvert and Pedersen, 2007; Martínez-Ruiz et al., 2015). Nevertheless, some studies warn about pitfalls in the use of normalizations (Van der Weijden, 2002). Another element cited in the literature for disentangling the variation of a terrigenous element within the lithogenic fraction is Ti (Murray and Leinen, 1993). The use of Ti for normalizations may be preferred when the elemental data are obtained by X-ray fluorescence core-scanning, since the Al and other light elements are not always accurately measured by this method (Tjallingii et al., 2007).

Geochemical ratios can also serve to discern the source area or transport mechanisms of terrigenous sediment (Calvert and Pedersen, 2007). Elemental ratios such as Si/Al, Ti/Al and Zr/Al have been used to reconstruct eolian input in the Pacific and Atlantic Ocean and in the Mediterranean area (Calvert and Pedersen, 2007; Martínez-Ruiz et al., 2015). Si is enriched in quartz grains, while Ti and Zr are enriched in heavy minerals such as zircons and rutiles, which are mostly sourced from Saharan eolian dust (Wehausen and Brumsack, 1999). These elements have been used for elucidating paleocurrent intensity in different deposits, as the high density of these minerals impedes their winnowing by currents (Dypvik and Harris, 2001; Bahr et al., 2014; de Castro et al., 2020). This aspect

is necessary for understanding the sedimentary environment in which the core was recovered prior to using a geochemical ratio, since the same ratio can have different meanings depending on the sedimentary conditions.

Other studies may normalize one terrigenous-derived element by one carbonate-derived element (i.e., Fe/Ca, Ti/Ca), in which case the increase of one of the two elements would imply the decrease of the other one, because they are subjected to the closed-sum effect (Govin et al., 2012). Likewise, the variation of a two element enriched in the carbonate fraction (i.e., Sr/Ca ratio) also gives relevant information about the carbonate characteristic. The Sr is enriched in aragonite, a mineral that is scarce in the basin, since the bottom waters are undersaturated in Sr. When sediments from deep marine basins are enriched in the Sr/Ca ratio, they can be traced to input into the basin of shallow carbonates from the shelf, high productivity of aragonite rich planktonic organisms such as pteropods, or to authigenic precipitation under suboxic conditions (Thomson et al., 2004; Reitz et al., 2006).

Meanwhile, geochemical ratios based on redox elements can provide information about the seafloor oxygen conditions (Algeo and Trivobillard, 2009). Uranium (U) and molybdenum (Mo) are two elements used for this purpose (Liu and Algeo, 2020). Both are predominantly of authigenic origin in sediments, being scarce in the upper continental crust. They are indicative of sub-oxic or euxinic conditions, since they need at least a small amount of H_2S for precipitating in the sediment (Canfield and Thamdrup, 2008; Algeo and Liu, 2020). The precipitation of U and Mo occurs after the ferruginous threshold, in which the Fe^{3+} is reduced to Fe^{2+} (Algeo and Liu, 2020). In turn, manganese (Mn) is dissolved in the column water under euxinic conditions and precipitates under oxic bottom conditions (Canfield and Thamdroup, 2008; de Lange et al., 2008).

1.4.2 Leaf wax lipids and stable isotopes

Biomarkers are organic compounds ideally derived from a restricted biological source (Bossard et al., 2013). In the very beginning, Eglinton and Calvin (1967) designated these organic compounds as chemical fossils, and later on, as biological markers, although nowadays they are better known as biomarkers (Simoneit, 2002). Biomarkers provide

valuable information about the organisms that produce the lipids and environmental factors that influence their production (Peters et al., 2005). In particular, the lipids from the leaf wax of vascular plants are useful proxies in paleoclimatology due to their chemical inertness, water insolubility and resistance to biodegradation (Eglinton and Eglinton, 2008). These lipids are formed by long-chained n-alkyl compounds including straight chains of *n*-alkanes, *n*-alkanols and *n*-alkanoic acid with a variable number of carbon and hydrogen atoms (Eglinton and Hamilton, 1963). These characteristics allow them to be transported to marine and lacustrine environments as aerosols, or on mineral phases by rivers or the wind, and to be preserved in the sedimentary record (Eglinton and Eglinton, 2008). In addition, the strong covalent bounds C-C and C-H enable preservation of the isotopic signature of both C and H incorporated by the plants during biosynthesis (Eglinton and Eglinton, 2008).

The carbon incorporated by plants is comes primarily from atmospheric CO_2, while the H proceeds from precipitation during the growing season (Diefendorf and Freimuth, 2017). The $\delta^{13}C$ measured in *n*-alkanes depends on several factors, such as the photosynthetic pathway of the plant and hydric stress. During photosynthesis plants discriminate the ^{13}C versus the ^{12}C, the former being heavier and forming stronger bounds than the latter, for which reason plants show depleted $\delta^{13}C$ values with respect to the atmosphere (O'Leary, 1988). The enzyme Rubisco converts CO_2 into sugars, and together with the photosynthetic pathway, are the two main factors behind the fractioning of ^{13}C. Plants that use the C_3 pathway (Calvin-Benson) would have a stronger fractionation than those using the C_4 pathway (Hatch-Slack) (O'Leary, 1988), whereas those using the crassulacean acid metabolism (CAM) show values ranging between C_3 and C_4 (O'Leary, 1982). There may also be fractionation depending on hydric stress —during arid/humid conditions the plants close/open their stomata to control de/hydration, hence reducing or increasing the intracellular CO_2 and the fractionation, resulting in more positive (or negative) $\delta^{13}C$ values (Farquhar et al., 1982; O'Leary, 1995; Zech et al., 2007).

$$R = {}^{13}C/{}^{12}C$$

$$\delta^{13}C = ((R_{sample}/R_{standard}) - 1) \times 1000$$

where the $R_{standard}$ is the VPDB (Vienna Pee Dee Belemnite), which corresponds to 0.01123720.

Because water is the main source of H used during photosynthesis, the study of stable ^{2}H isotopes on the *n*-alkanes provides information about the water source used by these organisms during their growth (e.g., Englebrecht and Sachs 2005; Sasche et al., 2012), after a significant biological fractionation effect (Saschse et al., 2012).

The $\delta^{2}H$ from water precipitation, and thus recorded in the *n*-alkanes, depends on several factors, such as the humidity source, the altitude effect, the temperature of the rainfall, the precipitation amount, the continental effect, and the evapotranspiration in soils (Dansgaard, 1964; Vogts et al., 2016). The net fractionation of the ^{2}H by plants therefore involves soil-water and biochemical processes (Sachse et al., 2012).

$R = {}^{2}H/H$

$\delta^{2}H = (R_{sample} - R_{standard})/R_{standard}$

where the $R_{standard}$ is the Vienna Standard Mean Ocean Water (VSMOW) = 155.76 ± 0.1 ppm.

1.4.3 Pollen

The study of pollen grains has been widely used for paleoclimate reconstructions. It traces a reliable picture of the past vegetation assemblages, in turn depending on the temperature and humidity conditions. Pollen grains are the masculine gametophyte of angiosperm and gymnosperm plants, and contain the male nucleus that will fertilize the female nucleus in an ovule (Smol et al., 2002). This process is called pollination, namely, the transport of pollen grains from the anther, where they are produced, to the stigma, usually of a different plant. This transport can be by wind (anemophilous), by insects (entomophilous), or by water (hygrophilous), the two former means being the most usual. Depending on the pollination strategy, the pollen can be dispersed farther from or closer to the parent plant, and produced in greater or lesser quantity. For example, plants with anemophilous pollination tend to produce more pollen grains and disperse them farther than plants with entomophilous pollination. Nevertheless, most of the produced pollen

never reach the ovule and fall onto the ground (Smol et al., 2002). When the pollen falls in an anoxic environment, such as peat bogs or lakes, it can be preserved for a long time, since its walls are made of sporopollenine, which is an organic material very resistant to alkaline environments, thus allowing for its preservation in sediments. Paleopalynology works because of: (1) the ubiquity of palynomorphs; (2) the abundance and resistance of palynomorphs; (3) its fast evolution over geological time (Traverse, 2007). In paleontology, palynology has three main purposes: geochronology, biostratigraphy and paleoecology (Traverse, 2007), the latter proving the most important for this thesis. By reconstructing the assemblages of pollen grains in sediment records we can infer the vegetation changes throughout the period represented in the sediments.

In the case of high altitude lakes and wetlands in Sierra Nevada (southern Iberian Peninsula), the presence of arboreal taxa (deciduous and evergreen *Quercus*, *Olea*, *Pistacia*, *Pinus*) are related to more humid and/or warm conditions and the migration of the vegetation belt to higher altitudes. Conversely, the occurrence of pollen grains of Asteraceae, including Chenopodiaceae, Asteroideae, *Artemisia*, and Poaceae, among others, point to arid and/or colder conditions. The occurrence of aquatic and wetland species, such as Cyperaceae, Ranunculaceae and *Typha*, are controlled by local factors, i.e., the aquatic taxa can increase because there are more humid conditions; or because more arid conditions dry the lake and these taxa proliferate in the wetland, so that aquatic and wetland species does not usually provide much information.

2. Motivation, Objectives and Thesis framework

Future climate projections point to hazardous scenarios for the Mediterranean region, with increasing droughts and the concomitant effects for the economy and human migrations (IPCC, 2021). Moreover, there is a consensus within the scientific community that the current climate change is the result of human activities. Given the severe future consequences of the climatic crisis (IPCC, 2013, 2021), it is essential to improve the accuracy of prediction models by extending our knowledge of the climatic system beyond historical data, which only cover until 1850 of the current era. In order to anticipate socio-environmental impacts and vulnerability for planning adaptations, it is also critical to understand the links between the occurrence of extreme events and natural climate variability at both orbital and suborbital timescales.

To achieve this, it is important to understand the processes and climate triggers that caused past rapid climate variability under natural conditions and the response of the different components of the climate system (atmosphere, hydrosphere, cryosphere, lithosphere and biosphere), at both orbital and suborbital timescales. Within this context, deciphering how and why extreme climate events occurred in the past calls for understanding present-day oceanic and atmospheric configurations, as well as climate models for the studied area, to elucidate the climate proxies sensitive to recognizing these events. In this regard, the studied time period takes in the end of the LGM, the last deglaciation and the Holocene, two time intervals in which the climate system has undergone an important reconfiguration. Superimposed upon the general warming trend, several cold periods have occurred in response to changes in the AMOC and in the atmospheric patterns. These disruptive events can be extrapolated to a future climate scenario if ice sheet melting in the poles continues. The Late Holocene is a particularly interesting interval, since the anthropic influence began to be evident, registered in diverse sedimentary records. Although these time intervals have been widely studied during the last decades, there is still a lack of correlation between marine and continental paleoclimate records, and the response to climatic events in different sedimentary basins is not well established.

Within this context, the present PhD thesis aims to advance knowledge of climate variability in the western Mediterranean over the deglaciation and the Holocene, as well as its causes and effects in both marine and continental settings. Previous work in the region has demonstrated the rapid response and high sensibility of the Mediterranean region to the North Atlantic oceanic and atmospheric processes. Still, most studies to date have presented just a few records, and comparisons between basins or between marine and continental realms have not been fully addressed. In this thesis, a new continental record from an alpine lake located in Sierra Nevada, plus several marine sediment records from the Alboran Sea and Algero-Balearic basins, were collectively studied in order to compare the climatic imprints recorded in each kind of setting. The alpine record was integrated with previously studied lake and wetland records from Sierra Nevada. The thesis also aims to discern between natural or anthropic climate variability, and evaluate the anthropogenic impact. To accomplish these goals, a multiproxy approach was adopted, encompassing geochemical analysis including major and trace elemental ratios, stable isotopes on specific organic compounds, and pollen assemblages in sediments. Within this framework, the following specific objectives have also been defined:

- To compare the paleoenvironmental information obtained from different proxies and to evaluate the similarities and differences recognized in marine records in order to discern between climatic and sedimentary-biased signals.

- To elucidate what factors control the terrigenous *vs.* carbonate input in the studied records from the western Mediterranean since the end of the LGM.

- To reconstruct changes in the vegetation and in precipitation sources in the western Mediterranean during the deglaciation and the Holocene periods.

- To reconstruct the vegetation and the hydrological evolution in Sierra Nevada as responses to the Holocene climatic variability, and to compare the results with previously studied records for the area.

- To compare the multiproxy data from Sierra Nevada and the western Mediterranean basin with other regional and local records in order to understand the factors influencing western Mediterranean climate variability.

- To identify anthropic influence in the sedimentary records from alpine wetlands and marine basins.

The results obtained to fulfill the main and specific objectives are presented in four chapters:

Chapter II comprises the published paper titled: *Paleocirculation and paleoclimate conditions in the western Mediterranean basins over the last deglaciation: New insights from sediment composition variations*. Global and Planetary Change, 2022, 209, 103732. This chapter discusses the main factors controlling the terrigenous *vs.* carbonate dilution in the deep western Mediterranean basins during the last 20 ka. Geochemical proxies from seven marine sediment cores in a transect from the Algero-Balearic to the Alboran Sea basin were studied. Furthermore, in this chapter, a new hypothesis about the onset and demise of the ORL1 based on some redox geochemical proxies is provided.

Chapter III comprises the published paper: *Vegetation and geochemical responses to Holocene rapid climate change in the Sierra Nevada (southeastern Iberia): the Laguna Hondera record*. Climate of the Past, 2018, 14, 1687-1706. This chapter reports the climatic evolution of an alpine wetland in Sierra Nevada deduced from geochemical proxies and pollen analysis over the Holocene. In addition, the onset of the Saharan eolian input in the oligotrophic lakes of Sierra Nevada was approached due to its important influence in the lake ecology.

Chapter IV includes the paper titled: *Stable hydrogen and carbon isotope records of plant wax n-alkanes from the Alboran Sea basin (westernmost Mediterranean) indicate precipitation and sediment dynamics during the last deglaciation*. Submitted to Palaeogeography, Palaeoclimatology, Palaeoecology, under review. This chapter is focused on reconstructing the hydrological and climatic evolution in the Alboran Sea based on the study of stable isotopes of leaf wax derived *n*-alkanes. This chapter studies the terrestrial organic-derived proxies in two marine sediment records recovered from the two Alboran basins, remarking on the possible bias that the terrigenous organic matter could suffer during its transport.

Chapter V includes an integrated discussion of the results obtained in the previous chapters in order to merge and synthetize the contribution of this thesis to advance knowledge on paleoclimate conditions in the western Mediterreanena region.

Finally, other works derived from different collaborations are listed in the Appendix.

3. Materials and Methods

3.1 Sediment records locations

3.1.1 Marine sediment records

The studied marine sediment records have been recovered during different oceanographic cruises in the western Mediterranean, in the Alboran Sea and the Algero-Balearic basins (Table 1). These cruises were aimed at reconstructing the paleoceanographic and paleoclimate evolution in the western Mediterranean basin (Fig 5).

Core 975B was recovered in the Algero-Balearic basin, in the south of the Balearic Promontory, during the Ocean Drilling Program (ODP) Leg 161 in 1996 using a piston corer (Table 1; Comas et al., 1996). This cruise aimed to monitor the history of both, the inflowing Atlantic waters as they flow to the east, and the outflowing Mediterranean waters on their way west to the Alboran Sea (Zahn et al., 1999). The lithology consisted in a nannofossil clay with calcareous olive-gray silty-clay without the presence of turbidites (Comas et al., 1996).

Cores located in the Alboran Sea were recovered during several UNESCO/IOC Training Through Research (TTR) cruises on board RV Professor Logachev (St. Petersburg, Russia) (Table 1). During the TTR cruise 12 Leg 3 in 2002 were recovered cores 292G and 293G in the western and eastern Alboran basins, respectively, using a gravity corer (Kenyon et al., 2003). Core 292G was recovered in the eastern east and west basins. This site was selected on base of the present-day circulation pattern in the Alboran Sea with the aim of reconstruct changes in the past oceanic circulation and paleoproductivity conditions. The lithology consisted of 371 cm of hemipelagic sediment with a variable degree of bioturbation. The top 5 cm showed brownish oxidized marls rich in foraminifera (Kenyon et al., 2003). Core 293G was recovered in the eastern Alboran basin, in the opposite side of the Alboran Though and relatively close to the Almeria turbidite system, this marine sequence provided a very good record of 402 cm of hemiplegic sediments. The top 10 cm consisted in a soupy marl with rich in foraminifera and the rest of the core consist in a homogeneous mud-clay with some intervals with foraminifera and high bioturbation (Kenyon et al., 2003). During the TTR cruise 14 Leg 2, cores 300G, 302G

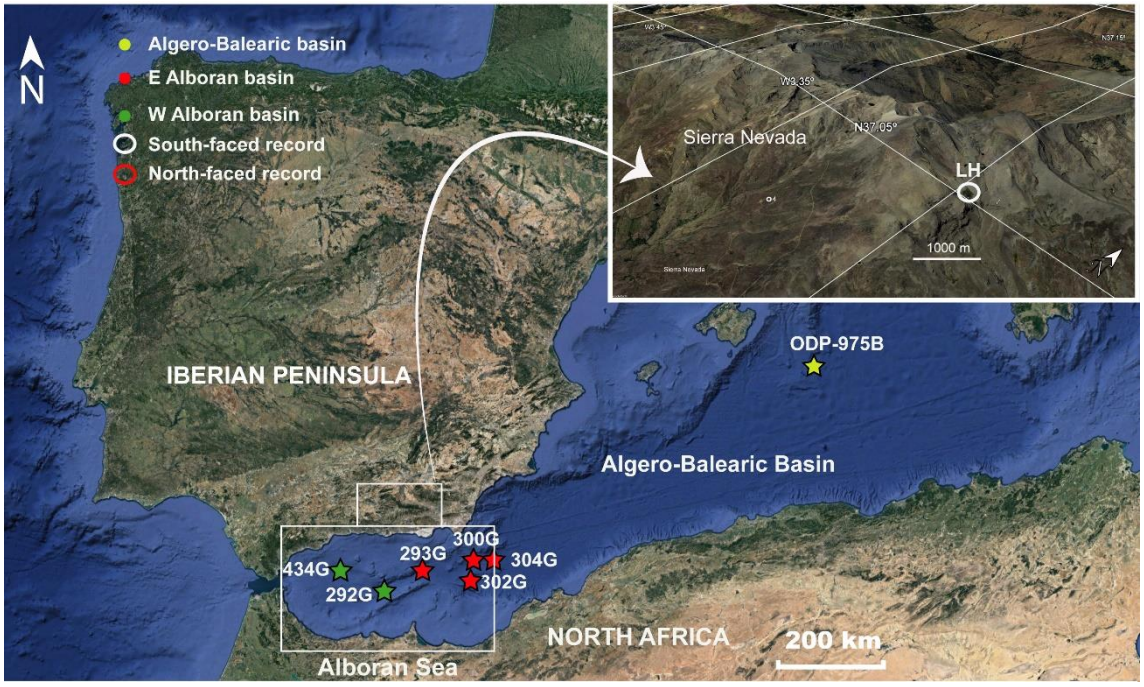

Figure 5. Location of the sediment cores used during this thesis in the eastern and western Alboran basins, the Algero-Balearic basin and Sierra Nevada mountains range.

and 304G were recovered in the eastern Alboran basin (Kenyon et al., 2006). Core 300G was recovered at the south-east of the Cabo de Gata (Almería) and consisted of 458 cm of hemiplegic sediments. The lithological composition is grey clays, brownish in the upper 7 cm, with foraminifera and some silty intervals (Kenyon et al., 2006). Core 302G was recovered at the same site than the ODP core 977A Leg 161, located in a graben that is limited by the Yusuf Ridge to the south and the Maimonides Ridge to the north. The sediments consisted of brownish marl with foraminifera in the upper 14 cm and grey clay bottomward (Kenyon et al., 2006). Core 304G was recovered in the transition between the eastern Alboran basin and the Algero-Balearic basin. It consisted of 454 cm of greyish clay hemipelagic sediment, brownish in the upperpart, with some silty admixture (Kenyon et al., 2006). During the TTR cruise 17, Leg 3 core 434G was recovered in the western Alboran Sea, at the same site as the ODP Site 976, located in a structural high close to the Fuengirola turbidite system. The sediments consist of green-brownish hemipelagic mud with some intervals rich in foraminifera (Comas et al., 2009).

Table 1. Core description, coordinates, altitude and location of each sedimentary record studied.

Site	Coordinates	Depth / Altitude	Location
ODP161–975B	38° 53.7950 N 4° 30.5960 E	2416 mbsl	Algero-Balearic basin
TTR14-304G	36° 19.873 N 1° 31.631 W	2383 mbsl	East Alboran basin
TTR14-302G	36° 01.906 N 1°57.317 W	1989 mbsl	
TTR14-300G	36° 21.532 N 1° 47.507 W	1860 mbsl	
TTR12-293G	36º 10.414 N 2º 45.280 W	1840 mbsl	
TTR12-292G	35º 53.85' N 3º 36.33' W	1536 mbsl	West Alboran basin
TTR17-434G	36º 12.313 N 4º 18.735 W	1108 mbsl	
LH12-03	37º02.88 N 3º17.66 W	2899 masl	Sierra Nevada

3.1.2 Continental sediment records

In the last decade, several field campaigns have been carried out in Sierra Nevada mountains for recovering sedimentary sequences deposited during the last deglaciation in different peat bogs, wetlands and lakes in order to reconstruct the climatic and vegetation evolution as well as the anthropic impact on alpine ecosystems (Anderson et al., 2011García-Alix et al., 2012, 2017, 2018; Jiménez-Moreno and Anderson, 2012; Jiménez-Moreno et al., 2013, 2020; Manzano et al., 2019; López-Avilés et al., 2021, 2022; Ramos-Román et al., 2016, 2018; 2019).

Laguna Hondera (LH) is an alpine wetland located in the South face of Sierra Nevada, at 2899 masl, at the lowest elevation of a set of lakes known as Cañada de Siete Lagunas. LH12-03 was one of the six sediment cores recovered from LH in 2012 using a Livingstone piston corer. The catchment basin is in the lower part of the Caldera

Formation and its lithology mainly consists in mica-schist (Díaz de Federico et al., 1980). LH12-03 was selected since with 83cm was the longest core in the depocenter of the lake (Table 1). The lithology of core LH12-03 is composed by sand in the bottom part, followed by an interval of intercalation of clays and peat. The upper part of the core is mainly dominated by peat with some clayey intervals (Mesa-Fernández et al., 2018).

3.2 Mineralogical and sedimentological analyses

3.2.1 Scanning electron microscopy

Mineralogical composition and morphological analyses were performed using scanning electron microscopy (SEM), an AU-RIGA model microscope (Carl Zeiss SMT) coupled with energy-dispersive X-ray microanalysis (EDX) and electron backscatter diffraction (EBSD) mode at the Center for Scientific Instrumentation of the University of Granada (CIC-UGR, Spain). Mineral grains were analyzed to determine provenance and transport mechanisms for detrital particles, in particular, those from eolian dust origin .

3.2.2 Grain size analysis

The grain size distribution of selected cores was determined on the raw sample and carbonate-free samples using a Mastersizer 2000 at CIC-UGR. The output data was treated by using the GRADISTAT package (Blott and Pye, 2001) in order to obtain the mean size and the percentages of sand (>63μm), silt (4-63μm) and clay (<4μm). In addition, the percentage of the sortable silt (SS, 10-63μm) and mean size of the non-carbonated fractions were calculated following McCave et al. (1995).

3.3 Major and trace elements analyses

3.3.1 X-ray fluorescence core-scanner

All studied cores (Table 1) have been measured by X-ray fluorescence (XRF) core-scanner, though only the results from those that have not been measured by using discrete samples by wavelength dispersion XRF were used. XRF core-scanner was performed at

the MARUM—University of Bremen (Germany), except core LH12-03 that was measured at the University of Barcelona (Spain), using an Avaatech XRF core-scanner. The XRF core-scanner is a non-destructive methodology that offers qualitative information of the chemical element distributions. An X-ray current of 650 µA, a 10 s count time and 10kV X-ray voltage were used for measuring light elements, whereas 1700µA X-ray current, 35 s count time and 30 kV X-ray voltage were used for heavy elements. The analysis resolution for these analyses was every 0.5 cm. For our studies only three elements (K, Ca and Ti) have been considered.

3.3.2 Wavelength Dispersive X-Ray Fluorescence

Major elements were measured with a Wavelength Dispersion X-Ray Fluorescence (WDXRF) S4 Pioneer BRUKER with a maximum power of 4 kW after fusion with lithium tetraborate at the Andalusian Institute of Earth Science (IACT). The instrument is equipped with a Rh anode X-ray tube (60 kV, 150 mA), three analyzer crystals (OVO-55; LiF 200 and PET) and a collimator of 0.26º and 0.46º, with an analytical detection limit of 0.1% and an instrumental error <1%. Typical precision was better than 61.5% for an analyte concentration of 10 wt.%. Zirconium was determined by XRF on pressed pellets, with a precision better than 64% for 100 ppm Zr. The samples were prepared by melting 0.3/1g of bulk sediment.

3.3.3 Inductively Coupled Plasma-Mass Spectrometry and Optical Spectrometry

Prior to the measurements, 0.1 g of ground sample was digested with $HClO_4$, H_2O_2, HNO_3 and HF in a Teflon-lined vessel at 180°C evaporated to dryness, and subsequently diluted in 100 mL bi-distiller water with 4 vol.% HNO_3.

Minor and trace elements from all studied cores were measured by inductively coupled plasma-mass spectrometry (ICP-MS) using a Perkin Elmer NexION 300d. The samples were measured in triplicate through spectrometry using Re and Rh as internal standards. The instrumental error is 2% for elemental concentrations of 50 ppm (Bea, 1996).

Major elements in the sediment samples with low material availability, such as core LH12-03, were measured by inductively coupled plasma optical spectrometry (ICP-OES) using a Perkin Elmer Optima 8300. Prior to the measurements, 0.1000 g of ground sample was digested with HNO_3 and HF in a Teflon-lined vessel at 180°C and 200 psi during 30 min, evaporated to dryness, and subsequent diluted in 100 mL bi-distiller water with 4 vol.% HNO_3. Blanks and international standards were used for quality control; the analytical accuracy was higher than ±2.79% and 1.89% for 50 ppm elemental concentrations of Al and Ca, respectively, and better than ±0.44% for 5 ppm elemental concentrations.

3.4 Organic geochemical analyses

3.4.1 Gas chromatography

A total of 66 samples from the marine core 293G (East Alboran Sea) and 56 samples from the marine core 434G (West Alboran Sea), previously extracted by Rodrigo-Gámiz et al. (2014), were selected to study the *n*-alkanes distribution included in the apolar fraction from the total lipid extracts. The apolar fractions were re-dissolved in 100 μL of *n*-hexane. Analysis of *n*-alkanes was performed on a Hewlett Packard 6890 Gas Chromatograph (GC) equipped with flame ionization detector (FID) using a fused silica column CP Sil-5 (25 m × 0.32 mm internal diameter, 0.12 μm film thickness), an on-column injector and He as mobile phase, at the NIOZ, The Netherlands.

3.4.2 Gas chromatography/isotope ratio mass spectrometry

The stable carbon ($\delta^{13}C$) isotope analyses on *n*-alkanes were performed in duplicate using a Thermo Trace GC (1310) coupled with a Thermo Delta-V advantage isotope ratio mass spectrometer (IRMS) at the NIOZ, The Netherlands. A total of 42 samples were measured for the marine core 293G and 46 samples for the marine core 434G. Results were expressed with respect to the Vienna Pee Dee Belemnite (V-PDB) standard.

The stable hydrogen ($\delta^{13}C$) isotopic composition on *n*-alkanes was determined using a Thermo Trace GC (1310) coupled with a Thermo Electron Delta V irMS via a GC-isolink

II and conflo 4, at the NIOZ, The Netherlands. Compounds were pyrolyzed at 1450ºC in an empty ceramic tube, which was pre-activated with hexane. H_2 gas with a predetermined stable isotopic composition was used as monitoring gas. Mix B (Schimmelmann, Indiana University) was used to check machine functioning at the beginning of every day. Samples were only analyzed if the average deviation of Mix B from the off-line determined values was 5‰ or less for hydrogen isotopic analyses. Analyses were done in duplicate and squalene standard was co-injected with every sample. 22 samples were analyzed for core 293G and 27 samples for core 434G. Results were expressed with respect to and Vienna Standard Mean Ocean Water (V-SMOW) standard. The δ^2H values were corrected for the potential influence of sea ice volume on the marine water isotopic composition following Niedermeyer et al. (2010).

3.5 Pollen analysis

The extraction of the pollen grains from the sediments was carried out following Faegri and Iversen, (1989). Prior to the acid digestion, a pill of a kwon number of the spore *Lycopodium* was added to each sample in order to quantify the pollen concentration. The carbonates were removed from the sample by HCl digestion, the silicates by HF and humic acid was removed by adding NaOH. Afterward, the sample was sieved with a naylon sieve of 10µm, and the resulting residue was suspended in glycerine and mounted on microscope slides. The slides were analyzed using a Zeiss transmitted light microscope at 400x magnification and counting a minimum of 300 pollen grains in each sample. The pollen grains identification was based on the pollen atlas from Beug (2004). The pollen grains counting was transformed to percentages based on the total pollen sum, excluding aquatics and wetland pollen (Cyperaceae, Ranunculaceae and *Thypa*), since they record a local signal.

3.6 Chronological analysis

Absolute age determinations have been previously performed in samples from some of the marine and continental records used in this thesis, and a later update of the radiocarbon calibration and age models has been performed. Table 2 shows the radiocarbon dates

using Accelerator Mass Spectrometry (AMS), the radiocarbon laboratories and previous publication when applicable.

3.6.1 Radiocarbon dating

Radiocarbon AMS dates ^{14}C measured in at least 10 mg of monospecific planktonic foraminifera tests of the *Globigerina bulloides* hand-picked from the size fraction >125 μm. As explained above, ages from some marine cores have been previously published (Table 2). In core ODP 975B from the Algero-Balearic basin, four samples were measured (Jiménez-Espejo et al., 2007). In cores 300G and 302G from the eastern Alboran basin, three and two samples, respectively were previously dated (Jiménez-Espejo et al., 2008). In core 293G, also from the eastern Alboran basin, ten samples were initially dated (Rodrigo-Gámiz et al., 2011), and later on the age model was updated with two more samples (Rodrigo-Gámiz et al., 2014). Lastly, in core 434G, six samples were AMS previously dated (Rodrigo-Gámiz et al., 2014).

To complete radiocarbon dating, a total of seven samples have been selected in core 292G.

On the other hand, in the alpine continental records, radiocarbon AMS dates were performed in plants remains and bulk sediment when plants remains were absents. In LH record, a total of seven samples were measured.

Table 2. Accelerator Mass Spectrometry (AMS) dates (in years, yr) from selected samples from the different sedimentary records studied, associated errors, depth of the sample (cm), radiocarbon laboratory and previous references.

Lab ID	**AMS date (yr)**	**Error (yr)**	**Depth (cm)**	**Laboratory**	**Reference**
975B 1 8-10	2455	30	9	Leibniz-Labor for Radiometric Dating (Germany)	Jiménez-Espejo et al., 2007
975B 1 50-52	7070	35	51		
975B 1 130-132	15870	80	131		
975B 2 45-47	19460	110	190		

292G 1 43.5-45	2105	30	44.25	Poznan radiocarbon laboratory (Poland)	This thesis
292G 2 4.5-6	2810	35	63.25		
292G 2 40.5-42	4390	35	99.25		
292G 3 9-10.5	5860	80	127.75		
292G 3 45-46.5	6900	50	163.75		
292G 6 58.5-59.5	11800	70	354.25		
293G 1 16.5-18	1520	60	17.25	National Centre for Accelerators, CNA (Spain) and Poznan radiocarbon laboratory (Poland)	Rodrigo-Gámiz et al., 2011, 2014
293G 2 24-25.5	4780	80	82.75		
293G 3 40.5-42	8705	45	157.75		
293G 4 19.5-21	9760	60	194.75		
293G 5 6-7.5	10440	90	238.75		
293G 5 22.5-24	11120	70	255.25		
293G 6 3-4.5	12230	110	293.75		
293G 6 33-34.5	12680	100	323.75		
293G 6 42-43.5	13280	90	332.75		
293G 7 40.5-42	16540	160	390.25		
293G 5 9-10.5 (Poznan)	10760	80	241.75		
293G 6 30-31.5 (Poznan)	12940	70	320.75		
434G 0 27-28.5	1350	35	27.75	Poznan radiocarbon laboratory (Poland)	Rodrigo-Gámiz et al., 2014
434G 1 30-31.5	3350	40	66.75		
434G18-19.5	4680	40	108.75		
434G 27-28.5	7960	50	173.75		
434G 30-31.5	11140	60	232.25		
434G 49.5-51	12200	70	251.75		
300G 2 17-19	6470	40	75		

300G 3 54-56.5	11690	60	168	Poznan radiocarbon laboratory (Poland)	Jiménez-Espejo et al., 2008
300G 4 6-7.5	11890	60	179		
302G 5 8-10	11950	50	225	Poznan radiocarbon laboratory (Poland)	
302G 7 53-55	20480	100	374		
LH 01 7.0	40	40	7	Poznan radiocarbon laboratory (Poland)	This thesis
LH 02 6.0	1112	32	22	DirectAMS	
LH 03 3.0	2675	30	39		
LH 03 9.0	3350	30	44	BETA Analytics	
LH 04 6.25	5480	30	55.5		
LH 04 7.5-8.0	5510	50	57.5	Poznan radiocarbon laboratory (Poland)	
LH 04 11.5-12.0	6450	50	62		
LH 05 3.0-3.5	8620	70	74		

3.6.2 Age model

The radiocarbon AMS dates were calibrated with different curves according with the nature of the sedimentary records. The continental Laguna Hondera record, LH03-12, was calibrated with the IntCal13 curve (Reimer et al., 2013), and the depth-age model was built using the R-code package "Clam software v2.2" (Blaauw, 2010), using the smooth spline curve. The marine record, 292G, was calibrated with the Marine20 curve (Heaton et al., 2020). Previous age models for marine cores 293G (Rodrigo-Gámiz et al., 2011) and 434G (Rodrigo-Gámiz et al., 2014) both calibrated to the Marine09 curve, and cores 975B (Jiménez-Espejo et al., 2007), 300G and 302G (Jiménez-Espejo et al., 2008) calibrated to the Marine04 curve, were updated to the Marine20 curve (Heaton et al., 2020). In order to constrain better age models for cores 975B, 300G, 302G and 304G, which has no dated samples, their Ba/Al profiles were compared with that of the well-dated record 293G (Rodrigo-Gámiz et al., 2011, 2014). Ba peaks have been correlated with cold events clearly recognized in the Alboran and Algero-Balearic basins for the last 20 ka (Jiménez-Espejo et al., 2007, 2008; Martínez-Ruiz et al., 2015), being useful tie-

points to establish a more robust age models in those marine sediment cores. Then, the depth-age model of the marine cores 292G, 293G, 434G, 300G, 302G, 304G and 975B were built using the R-code package "rbacon 2.4.2 software" (Blaauw and Christen, 2011), giving similar age models to those previously published for cores 293G and 434G (Rodrigo-Gámiz et al., 2011, 2014).

3.7 Statistical analyses

3.7.1 Cluster

R-mode cluster analysis constrained by age was performed on the pollen percentages of the taxa with > 1% in order to obtain pollen zonation. The cluster analysis was conducted by the Tilia software CONISS (Grimm, 1987).

3.7.2 Principal Component analysis (PCA)

R-mode principal component analysis (PCA) was performed on the geochemical datasets run with the PAST software v.4.03 (Hammer et al., 2001). PCA identifies hypothetical variables accounting for as much as possible variance in a multivariate data (Davis, 1986; Harper, 1999). The principal components (PC) (hypothetical variables) obtained were ordered by significance, whereas the PC1 would explain more variance of the dataset than the PC2, and so on. As data pretreatment, every sample was normalized to z-scores by subtracting the mean and dividing the result by the standard deviation (Davis, 1986). When the sample resolution of the variables was not the same, a linear interpolation was conducted to obtain equivalent time series.

3.7.3 Stacked curves

Stacked curves were performed to synthesize proxies in every basin and to reduce the age model dependence. The selected ratios were converted to z-scores and binned in every sub-basin. In order to equalize the time series, all cores were interpolated to those which

has a lower resolution. The value and the error of every sample were expressed as the mean and the standard deviation of the samples with the same age, respectively.

II

PALEOCIRCULATION AND PALEOCLIMATE CONDITIONS IN THE WESTERN MEDITERRANEAN BASINS OVER THE LAST DEGLACIATION: NEW INSIGHTS FROM SEDIMENT COMPOSITION VARIATIONS

II. Paleocirculation and paleoclimate conditions in the western Mediterranean basins over the last deglaciation: New insights from sediment composition variations

Jose Manuel Mesa-Fernández[1*], Francisca Martínez-Ruiz[1], Marta Rodrigo-Gámiz[2], Francisco J. Jiménez-Espejo[1], Marga García[3], Francisco J. Sierro[4]

[1] Instituto Andaluz de Ciencias de la Tierra (IACT), CSIC-UGR, Avenida de las Palmeras 4, 18100, Armilla, Granada, Spain

[2] Departamento de Estratigrafía y Paleontología, Universidad de Granada (UGR), Avda. Fuente Nueva s/n, 18071, Granada, Spain

[3] Spanish Institute of Oceanography, Centre of Cadiz, Muelle Pesquero s/n, Cadiz, Spain

[4] Departamento de Geología, Universidad de Salamanca, Salamanca, Spain

* *Corresponding author:* Jose Manuel Mesa-Fernández (jmesa@iact.ugr-csic.es)

Published in *Global and Planetary Change*, *103732*.

DOI: 10.1016/j.gloplacha.2021.103732

Impact factor: 5.11

Abstract

We present a high-resolution analysis of seven marine sediment records from the western Mediterranean in a transect from the Algero-Balearic basin to the Alboran Sea, spanning the last 20 ka, to decipher the paleoenvironmental and paleoceanographic evolution of the Western Mediterranean Sea. To do so, diverse elemental ratios have been used for reconstructing sediment input variations and paleo-oxygen conditions. In particular, the Ti/Ca ratio has been used to reconstruct variations in the terrigenous and carbonate fractions. However, the specific sedimentary processes controlling this ratio are still poorly understood thus, we also provide new insights for appropriate interpretations, in the studied zone. Our results suggest that the Ti/Ca ratio at the suborbital scale is mostly controlled by bottom current intensity, and less influenced by marine productivity, sea level variations, and the fluvial and eolian inputs. Comparison of diverse records within the western Mediterranean reveals that the Ti/Ca ratio depicted a similar trend in both regions, except during the Heinrich Stadial 1 (HS1) and the Middle Holocene. The HS1 is recorded as a single-phase event in the Algero-Balearic basin, whereas three phases are recognized in the Alboran Sea basin, with a relative minimum in the Ti/Ca ratio. Conversely, during the Middle Holocene, an increase in the Ti/Ca ratio is recorded in the Alboran Sea and the Atlantic Iberian margin, but not in the Algero-Balearic basin, which could be related to the establishment of the Alboran gyres. Redox sensitive proxies, in particular the Mo/Al, U/Al and Mn/Al ratios, point to different phases within the Organic Rich Layer 1 (ORL1): the ORL1a (15-11.7 ka cal BP), characterized by more reducing conditions in the Alboran Sea sediments, and the ORL1b (11.7- ~9 ka cal BP) characterized by suboxic-ferruginous conditions. The sea level transgression, the enhanced fluvial input and the shelf flooding played a key role during the ORL1 onset and demise, increasing the sedimentation rate in the basin and preventing the organic matter oxidation. During the last 2 ka cal BP, an unprecedented common response is recognized in all the studied regions, showing an overall increase in the Ti/Ca ratio, which may be related to intensified human activity in the Mediterranean area, promoting a greater terrigenous input.

1. Introduction

During the last decades a large number of studies have highlighted the climatic and oceanographic complexity over the Last Glacial Maximum (LGM), the deglaciation and the Holocene (Cacho et al., 2002, 2006; Eynaud et al., 2009; Fletcher and Sánchez Goñi, 2008; Moreno et al., 2010; Rohling et al., 2015; Tierney and DeMenocal, 2013; van Dijk et al., 2018). The overall warming which has characterized the climate since the end of the LGM has been interrupted by relatively rapid cold spells, such as the Heinrich Stadial 1 (HS1, 18-15 ka cal BP) and the Younger Dryas (YD, 12.8-11.7 ka cal BP) during the deglaciation, and the 8.2 ka and 4.2 ka events during the Holocene, with the concomitant oceanographic reorganizations and their imprint in the marine sediments (Alley et al., 1997; Bahr et al., 2015; Kaboth et al., 2015; Mayewski et al., 2004; Repschlager et al., 2015; Rohling et al., 2015; Schirrmacher et al., 2020; Sierro et al., 2005; Sierro et al., 2020).

These changes are particularly well recorded in the western Mediterranean basins, and especially in the Alboran Sea basin, which is highly sensitive to high and middle latitudes processes and influences from the western and eastern Mediterranean (e.g., Cacho et al., 1999; Rohling et al., 2015; Sanchez-Goñi et al., 2020). As examples, the ice rafted debris deposition during the Heinrich Event 1 (HE1) in the North Atlantic, also promoted the meltwater influx into the Mediterranean preventing Western Mediterranean Deep Water (WMDW) formation (Cacho et al., 2006; Frigola et al., 2008; Rogerson et al., 2008; Sierro et al., 2005); or the freshwater input from the alpine glacial melting in the northwestern Mediterranean during the deglaciation, induced the slowdown of the Mediterranean thermohaline circulation and promoted the deposition of Organic Rich Layers (ORLs) in the Alboran Sea basin (Rogerson et al., 2008; Martrat et al., 2014; Rohling et al., 2015). On the other hand, the Mediterranean Outflow Water (MOW) has a particular impact on the North Atlantic circulation, especially on the Atlantic meridional overturning circulation (AMOC) due to its high salinity (Ausín et al., 2020; Rogerson et al., 2012; van Dijk et al., 2018)

Recent works have also highlighted the complex interplay between hemipelagic, downslope and along-slope processes in the marine basins from the western

Mediterranean, in particular in the Alboran Sea basin (e.g., Alonso and Ercilla, 2003; Alonso et al., 2021; Ercilla et al., 2016; Ercilla et al., 2019). Nonetheless, although the western Mediterranean marine sediment records have been widely studied, some questions remain unresolved, including the main factors controlling marine sediment composition, especially during rapid climate changes since the LGM.

In order to solve this, geochemical ratios have been used as valuable tools for climatic and paleoceanographic reconstructions. In terms of sediment composition, the Ti/Ca ratio has been used as a proxy for the two end-members of marine sediments, being Ti indicative of terrigenous input, whereas Ca indicates the contribution of marine biogenic carbonate (e.g., Govin et al., 2012; Steinke et al., 2014; Stuut et al., 2014). The terrigenous fraction in marine sediments is mainly controlled by sea level changes, riverine and eolian input, and its distribution by bottom currents, while carbonates mainly derived from marine organisms' productivity (Calvert and Pedersen, 2007; Govin et al., 2012) or from detrital carbonates in settings where this lithology dominates the surrounding areas (Pasquier et al., 2019). Thus, the Ti/Ca is subjected to the "closed-sum effect" or the dilution effect, which means that any variation in the concentration of the terrigenous fraction directly affects the carbonate content (Calvert and Pedersen, 2007; Govin et al., 2012). Nevertheless, in zones with high productivity of biogenic silica or with high input of detrital carbonates, this relationship could lead to an overestimation of the terrigenous input and the carbonate marine productivity, respectively (Govin et al., 2012; Pasquier et al., 2019).

Hence, Ti/Ca and Fe/Ca ratios have been broadly used as proxies for reconstructing sea level variations (Thomson et al., 1999), marine productivity (Hodell et al., 2013), eolian input (Bouimetarhan et al., 2013; Lopez-González et al., 2019); riverine input (Dickson et al., 2010) or fine sediment winnowing by strong bottom currents (de Castro et al., 2020). However, assessment of the precise role of each factor requires detailed interpretations of the geologic and oceanographic interplay with climate controls (e.g., Calvert and Pedersen, 2007; Govin et al., 2012).

With this aim, this work investigates the main factors influencing sediments composition in a transect from the Algero-Balearic basin to the Alboran Sea, with a special focus on

the Alboran basin because of its unique location. To this end, diverse geochemical ratios obtained using continuous core-scanning and discrete sample analysis were examined in seven marine sediment records spanning the last 20 ka with special emphasis on the Ti/Ca ratio profiles. This study is particularly focused on time periods covering the HS1 (18-15 ka cal BP) and the ORL1 deposition (15-9 ka cal BP), to assess the complexity of its onset and demise in the westernmost Mediterranean as a result of climatic and oceanographic variability. Thus, the main objectives are to: (1) evaluate the major factor/s controlling the relative variation between terrigenous and carbonate in the western Mediterranean deep basins; (2) elucidate the different response of the western Mediterranean basins to the major paleoclimatic and paleoceanographic events occurred during the deglaciation, such as the HE1 or the ORL1.

2. Study area

The Alboran Sea is the westernmost basin of the Mediterranean Sea and is located between South Iberia and North Africa (Fig. 1). This basin presents high sedimentation rates being a mixture of terrigenous particles with a lesser proportion of biogenic and detrital carbonates. The lithogenic fraction represents around 70% of contents, mainly derived from riverine discharge or eolian dust pulses from the African margin (Fabres et al., 2002; Martínez-Ruiz et al., 2015; Palanques et al., 2005; Rodrigo-Gámiz et al., 2015). The main rivers surrounding the Alboran Sea have a torrential nature, meaning most of the sediment load from the continent derives from flood events during late autumn, winter and spring (Fernández-Salas et al., 2003; Liquete et al., 2005; Palanques et al., 2005; Puig et al., 2017). The sediment deposited by riverine discharge onto the shelf is channelized by diverse canyons along the southern Iberian margin, and transported into the deep basin as hyperpycnal fluxes or turbidites (Ercilla et al., 2016; Palanques et al., 2005; Puig et al., 2017).

Moreover, the high African dust export can seasonally increase terrigenous input and fertilize the surface waters (Scheuvens et al., 2013; Zúñiga et al., 2008). Interaction between seafloor morphology and bottom currents led to the formation of contourite deposits in the basin (Ercilla et al., 2016; Juan et al., 2016). Thus, the sedimentation

resulted from a mixture of hemipelagic vertical processes, derived from marine productivity as well as fluvial and Saharan eolian dust contributions, downslope gravity processes along the turbiditic systems, and contouritic deposition resulting from the interaction of along-slope currents with complex bathymetry (Ercilla et al., 1994, 2016; Fabres et al., 2002; Jiménez-Espejo et al., 2008; Masqué et al., 2003; Rodrigo-Gámiz et al., 2011; Zúñiga et al., 2007). In turn, the sediment composition in the Algero-Balearic basin is richer in carbonates than the Alboran Sea basin, as the contribution of terrigenous input is lower and the surrounding lithology is rich in carbonates (Zúñiga et al., 2007).

Regarding to its oceanographic setting, the Alboran Sea is characterized by three main water masses with different temperature, salinity and density (Millot, 1999, 2009). The Modified Atlantic Water flows eastward, occupying the first 200 m of the water column and forming two anticyclonic gyres: the quasi-permanent Western Alboran Gyre, and the seasonal Eastern Alboran Gyre (Fabres et al., 2002; Millot, 1999). Two high productivity zones are associated with these Alboran gyres: the Malaga Front and the Almería-Orán Front (Sánchez-Vidal et al., 2005; Tintoré et al., 1988). The intermediate waters include the Winter Intermediate Water, the Levantine Intermediate Water (LIW) and the Tyrrhenian Dense Water (see Millot, 2009 for a review). The deeper part of the Alboran basin is filled by WMDW, formed in the Gulf of Lions, which is restricted to water depths below 600 m in the northern and central Alboran Sea and below 400 m along the Moroccan margin (Millot, 2013). Finally, the Mediterranean water flowing out through the Gibraltar Strait forms the MOW, which is mainly composed of LIW, with a minor amount of WMDW (Millot, 1999). Bottom water renewal and seafloor oxygenation in the western Mediterranean basins depend mainly on: (1) The formation rate of dense WMDW replacing older bottom water (Millot, 1999; Rogerson et al., 2008; Rohling et al., 2015; Schroeder et al., 2008, 2010); (2) The Bernoulli aspiration through the Gibraltar Strait in the case of the Alboran Sea basin, that depends on the outflow velocities, the tidal strength and the intensity of the Western Alboran Gyre (García-Lafuente et al., 2017; Naranjo et al., 2012; Stommel et al., 1973), although at millennial scale the density gradient between the Atlantic and the Mediterranean Sea waters and/or the density gradient below the sill, also have a great influence (Rogerson et al., 2008, 2012; Rohling et al., 2015).

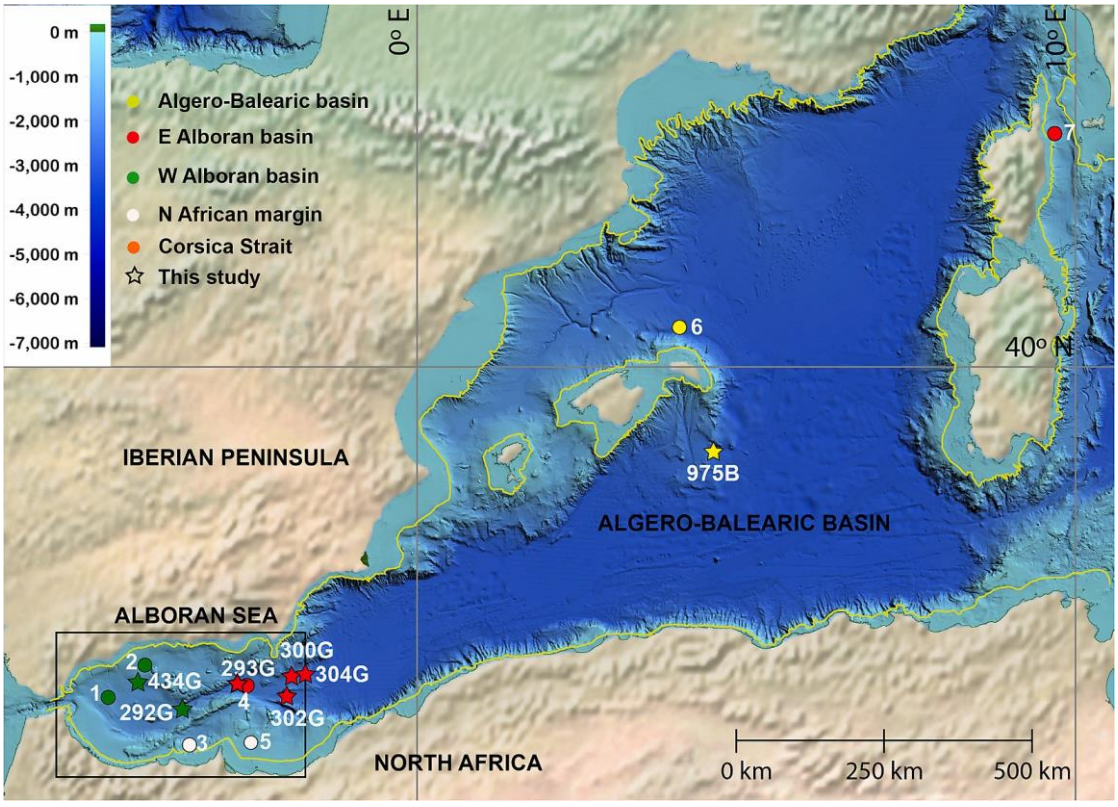

Fig. 1. Map showing the location of the studied marine sediment cores (stars; Table 1) and the main basins from the western Mediterranean Sea. Other marine sediment records (circles) used along the text for comparison are: 1) CEUTA10PC08 (914 mbsl; Ausín et al., 2015a); 2) HER-GC-T1 (659 mbsl; Ausín et al., 2015a); 3) GeoB18131-1 (457 mbsl; Wang et al., 2019); 4) MD95-2043 (1841 mbsl; Fletcher et al., 2010; Cacho et al., 1999, 2006); 5) GeoB 13731-1 (362 mbsl; Fink et al., 2013); 6) MD99-2343 (2391 mbsl; Sierro et al., 2005; Frigola et al., 2007); 7) MD01-2472 (501 mbsl; Toucanne et al., 2012). Yellow line indicates the shelf break.

Table 1

Core description, analyses and selected proxies.

Site	Location	Water depth	Methodology	Elements	Proxies	Basin	Reference
ODP161–975B	38° 53.7950 N 4° 30.5960 E	2416 m	Atomic Absorption	Al, Ca	Al/Ca, Mn/Al, Mo/Al	Algero-Balearic	Jiménez-Espejo et al., 2007
			ICP-MS	Mo, Mn			
			XRF Core Scanner	Ti, Ca	Ti/Ca		This study
TTR14-304G	36° 19.873 N 1° 31.631 W	2383 m	X-Ray Fluorescence	Ti, Ca, Al	Ti/Ca, Sr/Ca, Mo/Al	E Alboran	Jiménez-Espejo et al., 2008
			ICP-MS	Sr, Mo			
TTR14-302G	36° 01.906 N 1°57.317 W	1989 m	X-Ray Fluorescence	Ti, Ca, Al	Ti/Ca, Sr/Ca, Mo/Al, U/Al, Mn/Al		Jiménez-Espejo et al., 2008
			ICP-MS	Sr, Mo, U, Mn			
TTR14-300G	36° 21.532 N 1° 47.507 W	1860 m	X-Ray Fluorescence	Ti, Ca, Al, K, Zr	Ti/Ca, Sr/Ca, Ti/Al, K/Ca, K/Al, Zr/Ca, Zr/Al, Mo/Al, U/Al, Mn/Al		Jiménez-Espejo et al., 2008
			ICP-MS	Sr, Mo, U, Mn			
TTR12-293G	36º 10.414 N 2º 45.280 W	1840 m	X-Ray Fluorescence	Ti, Ca, Al, K, Zr	Ti/Ca, Sr/Ca, Ti/Al, K/Ca, K/Al, Zr/Ca, Zr/Al, Mo/Al, U/Al, Mn/Al		Rodrigo-Gámiz et al., 2011
			ICP-MS	Sr, Mo, U, Mn			
TTR12-292G	35º 53.85' N 3º 36.33' W	1536 m	X-Ray Fluorescence	Ti, Ca, Al	Ti/Ca, Sr/Ca, Mo/Al, U/Al, Mn/Al	W Alboran	This study
			ICP-MS	Sr, Mo, U, Mn			
TTR17-434G	36º 12.313 N 4º 18.735 W	1108 m	X-Ray Fluorescence	Ti, Ca, Al	Ti/Ca, Sr/Ca, Mo/Al, U/Al, Mn/Al		
			ICP-MS	Sr, Mo, U, Mn			

3. Material and methods

3.1. Core description

This study entails seven marine sediment records from a transect between the Algero-Balearic and the Alboran Sea basins (Fig. 1). They were recovered during diverse oceanographic cruises: Training Through Research (TTR) 12, 14, and 17, and ODP Leg 161 (Comas et al., 1999; Comas and Ivanov, 2006, Table 1). In the Alboran Sea basin, these marine records consist mostly of detrital minerals, including clays, with minor quantities of quartz, feldspars and accessory minerals, and less proportion of carbonates (Jiménez-Espejo et al., 2007, 2008; Martínez- Ruiz et al., 2015; Rodrigo-Gámiz et al., 2011). The marine record recovered in the Algero-Balearic basin (ODP Site 975B) shows similar sediment composition, though a higher content in carbonates (Jiménez-Espejo et al., 2007).

3.2. Age model

The age model for marine core 292G was derived for this study; those from marine cores 434G, 293G, 300G, 302G, 304G and ODP Site 975B were previously published (Jiménez-Espejo et al., 2007, 2008; Rodrigo-Gámiz et al., 2011, 2014a). The age model for core 292G was based on seven Accelerator Mass Spectrometry (AMS) ^{14}C dates by picking ca. 10 mg of planktonic foraminifera *Globigerina bulloides* (>125 μm), analyzed at the Poznan Radiocarbon Laboratory (Poland) (Fig. 2; Table 2). The radiocarbon dates were calibrated to calendar kilo-ages before present (ka cal BP) using the Marine20 curve (Heaton et al., 2020), and the age model was built by linear interpolation using the R-code package rbacon 2.4.2 software (Blaauw and Christeny, 2011). The mean sedimentation rate in core 292G is ~31 cm/ka. Previous age models for marine cores 293G (Rodrigo-Gámiz et al., 2011), 434G (Rodrigo-Gámiz et al., 2014a), 975B (Jiménez-Espejo et al., 2007) and 300G, 302G, 304G (Jiménez-Espejo et al., 2008) were updated to the Marine20 curve and contrasted with those obtained using the rbacon 2.4.2 software, giving similar results for cores 293G and 434G (Rodrigo-Gámiz et al., 2011, 2014b). Furthermore, the age models of cores 975B, 300G, 302G and 304G were constrained comparing their Ba/Al profiles with that of the well-dated record 293G (Rodrigo-Gámiz

et al., 2011) and then using the three maximum peaks as tie-points (Fig. S1). Ba peaks have been correlated with cold events clearly recognized in the Alboran basin and in the Algero-Balearic basin for the last 20 ka (Jiménez-Espejo et al., 2007, 2008; Martínez-Ruiz et al., 2015), making them useful tie-points to establish more robust age models in sediment cores. The mean sedimentation rates from previously published cores are 8.4 cm/ka in core ODP 975B from the Algero-Balearic basin; in the eastern Alboran cores are 20.5 cm/ka in core 293G, 13.8 cm/ka in core 300G, 16.1 cm/ka in core 302G and 14.4 cm/ka in core 304G; and in the western Alboran basin is 18.2 cm/ka in core 434G. Note that cores 292G, 293G, 434G, 300G, 302G and 304G are gravity cores, being three time more compressed than those recovered by a piston core like the ODP 975B (Crusius and Anderson, 1991).

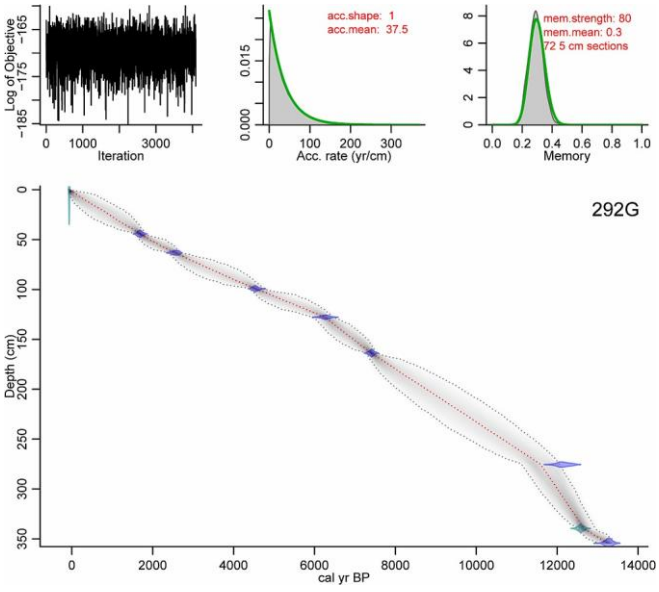

Fig. 2. Age-depth model of marine record 292G constructed using seven ^{14}C AMS. The blue points represent the calibrated age ranges corresponding to each radiocarbon date. The dotted red line corresponds to the bayesian age model developed using the R-code package rbacon 2.4.2 software (Blaauw and Christeny, 2011) and the Marine20 calibration curve (Heaton et al., 2020). The gray shaded area represents the error range in age estimations.

Table 2

AMS ^{14}C carbon dating of single planktonic foraminifera *Globigerina bulloides* (>125 μm) taken from marine record 292G.

Lab Number	*Depth (cm)*	*Dating Method*	*Age (14C yr BP±1σ)*	*Calibrated age (cal yr BP)2σ ranges*
Surface	0	Present	-63	-63
Poz-44814	44.25	14C	2105 ± 30	1340-1732
Poz-46170	63.25	14C	2810 ± 35	2140-2640
Poz-46171	99.25	14C	4390 ± 35	4107-4620
Poz-62841	127.75	14C	5860 ± 80	5682-6270
Poz-62840	163.75	14C	6900 ± 50	6953-7407
Poz-46587	275.5	14C	10720 ± 60	9742-11574
Poz-43213	354.25	14C	11800 ± 70	12849-13422

3.3. Geochemical analyses

Major elements were measured in records 292G and 434G by means of X-Ray Fluorescence (XRF) using a Wavelength Dispersive Spectrometry (WDXRF) Bruker AXS Pioneer S4 at the Andalusian Earth Science Institute (CSIC-University of Granada, Spain). Sampled were measured as pressed pellets prepared by pressing about 5 g of ground bulk sediment into a briquet with boric acid backing. The quality of the analysis was monitored with reference materials showing high precision with 1 sigma 1.0-3.4% on 16 data-sets at the 95% confidence level. Major elements from records 300G, 302G, 304G and 293G have been previously published by Jiménez-Espejo et al. (2007) and Rodrigo-Gámiz et al. (2011) (Table 1).

Trace elements in the 292G and 434G records were measured by inductively coupled plasma mass spectrometry (ICP-MS; Perkin Elmer Sciex Elan 5000) at the Centre of Scientific Instrumentation of the University of Granada (CIC-UGR, Spain). Samples were digested with HNO_3 and HF. Internal standard of Rh and Re were used. The instrumental error was ±2% for elemental concentration of 50 ppm (Bea et al., 1996). The trace elements in records 300G, 302G, 304G and 293G have been previously reported by

Jiménez-Espejo et al. (2007) and Rodrigo-Gámiz et al. (2011) (Table 1). Because the Ti from ODP Site 975B was not measured using WDXRF, we included XRF from the core scanner II (AVAATECH Serial No. 2) data obtained at the MARUM—University of Bremen (Germany).

Among all the elements measured, we selected Ti, Al, Ca, Sr, Mo, Mn and U, in view of their significance for paleoclimatic and paleoceanographic reconstructions (see section below). In addition, K and Zr from core 293G and 300G records were also selected (Table 1). The Ti/Ca ratios from three of the seven selected records (cores 434G, 292G and 975B) have not been previously studied. For the rest of records, although Ca and Ti data have been previously published, the Ti/Ca ratio in this form have not been previously interpreted (see Table 1 for a detailed summary of selected geochemical data used and references to the original papers) (i.e., Jiménez-Espejo et al., 2007, 2008; Rodrigo-Gámiz et al., 2011). We also used geochemical, grain size data and productivity data, available from the PANGAEA database, for comparison (i.e., Ausín et al., 2020; Frigola et al., 2008; Fink et al., 2013; Wang et al., 2019).

3.4. Selected elemental proxies

Apart from the Ti/Ca ratio, which will be discussed in detail in Section 5.1, diverse elemental proxies have been selected for reconstructing paleoclimate and paleoceanographic conditions in the Mediterranean region over the last deglaciation. For instance, the K/Al ratio has been used as a runoff proxy, since K is a major component in some clay minerals, such as illite, or in K-feldspar, and they are transported into marine basins mainly through riverine runoff (Calvert and Pedersen, 2007; Martínez-Ruiz et al., 2015). Ti/Al and Zr/Al ratios have been used as eolian input proxies since Ti and Zr are enriched in minerals such as rutile or zircon respectively, which are concentrated in the Saharan dust (Bouimetarhan et al., 2013; Calvert and Pedersen, 2007; Govin et al., 2012; Jiménez-Espejo et al., 2014; Moreno et al., 2006). Moreover, the Zr/Rb and Zr/Al ratios have also been used as sorting or winnowing proxies (Bahr et al., 2014; Dypvik and Harris, 2001; Lebreiro et al., 2018), since strong deep-water currents concentrate heavy minerals by winnowing the finest fraction (Bahr et al., 2014; de Castro et al., 2020).

The Mo/Al, U/Al and Mn/Al ratios have served as redox proxies in different Mediterranean records (e.g. de Lange et al., 2008; Filippidi et al., 2016; Gallego-Torres et al., 2007). Both, Mo and U are associated to authigenic precipitation in sediments since they are scarce in the upper continental crust, and thus, are indicative of bottom oxygen conditions (Liu and Algeo, 2020; Tribovillard et al., 2012). The precipitation of Mo as thiomolybdate requires the presence of aqueous H_2S, thus euxinic conditions of the bottom waters or in the pore water of the sediment (Algeo and Liu, 2020; Calvert and Pedersen, 2007). On the other hand, the U enrichment in sediments occurs earlier than that of the Mo, during the transition of FeIII-FeII (ferruginous phase) under suboxic conditions (Algeo and Li, 2020; Canfield and Thamdrup, 2009). In the same way, the precipitation of Mn in the sediment occurs under more oxygenated conditions, marking the transition from suboxic to oxic environment (Canfield and Thamdrup, 2009; de Lange et al., 2008).

The Sr/Ca ratio, confronts two elements from the carbonate fraction. Higher values in the Sr/Ca ratio in sediments from the Mediterranean usually indicate a higher percentage of aragonite in the sediment, as it is enriched in Sr (Reitz and De Lange, 2006; Thomson et al., 2004). Aragonite is typically abundant in shallow marine environments, because deep waters are undersaturated in Sr and it is commonly dissolved in the water column or in the sediment after its deposition (Fabry & Deuse, 1991; Reitz and De Lange, 2006). Nonetheless, several processes can trigger Sr enrichment in deep sediments, such as (1) authigenic formation as consequence of sulphate reduction during diagenesis, (2) *in situ* productivity of Sr rich organisms (i.e., pteropods), or (3) shallow-dwelling organisms transported basinward by density fluxes during enhanced precipitation events (Reitz and De Lange, 2006; Thomson et al., 2004). Therefore, a correct interpretation of this proxy has to be done in comparison with other geochemical data. The Sr enrichment in the sediment as consequence of sulphate diagenetic reduction should be well related with other elements enriched under euxinic conditions, such as Mo. On the other hand, high Sr/Ca ratio triggered by *in situ* productivity of Sr rich organisms should increase from the shelf to the deep and open marine settings. Conversely, high Sr/ Ca ratio triggered by sediment input from shallow depths should decrease toward deep marine settings (see Reitz and De Lange, 2006; Thomson et al., 2004, for a review).

3.5. Grain size analysis

The grain size distribution in core 293G was carried out on the carbonate and carbonate free fractions using a Mastersizer 2000 at Centro de Instrumentacion Científica. The output data was treated by using the GRADISTAT package (Blott and Pye, 2001) in order to obtain the mean size and the percentages of sand (>63μm), silt (4-63μm) and clay (<4μm). In addition, the sortable silt (SS, 10-63μm) percentage and mean size of the non-carbonated fraction were calculated following McCave et al. (1995), since these proxies have been successfully for reconstructing the current intensity.

3.6. Statistical analysis

Principal Component Analysis (PCA) on the geochemical data was performed using the PAST software© version 4.05 (Hammer et al., 2001), considering every element as a variable. As data pre-treatment, each value was converted to z-scores to eliminate the bias caused by the differences in the elements concentrations following the next formula $Z(Xi) = (Xi - \breve{u}(X1, X2, \ldots Xz))/\sigma(X1, X2, \ldots Xz)$, where X represent the selected ratio, ŭ and σ are the mean and the standard deviation of the dataset. In order to reduce the age model dependence of the different cores, we constructed a stacked plot for every sub-basin.

The z-score of the selected ratios obtained from the different cores were binned for every sub-basin: western Alboran (434G and 292G), eastern Alboran (293G, 300G and 302G) and the Algero-Balearic Basin (ODP Site 975B and MD99-2343). In order to equalize the time series, all cores were interpolated to those which has a lower resolution. The stacked plot is expressed as the mean of the samples with the same age and the error as its standard deviation.

4. Results

4.1. Elemental ratios profiles

Hereafter the new marine sediment record 292G together with the other marine sediment records obtained for this study will be referred to by location: western Alboran (434G and 292G); eastern Alboran (293G, 300G, 302G, 304G); or Algero-Balearic basin (ODP Site

975B) (Table 2). The Ti/Ca ratio in core ODP Site 975 was provided as Ln(Ti/Ca), in order to reduce the possible artifacts resulting of the water content and grain- size during the XRF core-scanner measurement (Tjallingii et al., 2007) (Weltje and Tjallingii, 2008).

The Ti/Ca ratios of the seven sediments records from the western and eastern basins of the Alboran Sea and from the Algero-Balearic basin show a remarkably similar pattern since the LGM (Fig. S2). The Ti/Ca ratio has maximum values between 18 and 15 ka cal BP in all the records, and a relative minimum between ~17 and ~16 ka cal BP, except in the Algero-Balearic basin (Fig. S2g). The missing of the relative minimum in the latter is not caused by the different methodology used for ODP Site 975, since the Al/Ca measured by XRF on discrete sample showed the same trend. We consider that it is not missed either by a lower resolution because the relative minimum is recorded in core 304G (Fig. S2f) which has a lower sample resolution than the 975B (273 yr/ sample *vs* 114 yr/sample). A general decrease in the Ti/Ca ratio occurs until ~13 ka cal BP in all the sites. A relative maximum at ~12.5-12 ka cal BP is seen in all the records (Fig. S2). A progressive increase in the Ti/ Ca ratio occurs in all the Alboran records at ~8 ka cal BP, peaking at ~6.5-6 ka cal BP, and showing higher values in western than in eastern records. In the Algero-Balearic basin a minor increase occurred but no such a peak as seen in the Alboran Sea cores. Another increase is evidenced in all records during the last ~2 ka cal BP. Since the Ti/Ca ratio from the ODP Site 975B is missing for the last 2 ka, we referred to the Al/ Ca ratio obtained by discrete sample analysis so as to have a record of the past 2 ka. The Ti/Ca from XRF core-scanning and the Al/Ca from discrete sampling show good correlation, both ratios indicating dilution between terrigenous and carbonate fractions (see discussion).

The Sr/Ca ratio in the Alboran basin decreases from shallow to deep marine setting, denoting higher values in the western than in the eastern cores (Fig. S3). The eastern Alboran records show minimum values between 18 and 15 ka cal BP, with a slight increase between 17 and 16 ka cal BP. Later on, an increase between 15 and 9 ka cal BP is recorded in all records but in core 434G, decreasing until 8 ka cal BP. The last 8 ka cal BP are characterized by high variability in all the studied records (Fig. S3a-e).

The Mo/Al ratio in the eastern Alboran basin traces an essentially flat pattern, interrupted by a prominent increase between 15 and 11.7 ka cal BP leading to a peak at ~13 ka cal BP (Fig. S3f-k). In the western Alboran basin, the Mo/Al ratio increases slightly along the same lines. The Mo/Al ratio in the Algero-Balearic basin depicts a flat pattern over the last 20 ka (Fig. S3k).

The U/Al ratio is characterized by low values from the LGM until 17 ka cal BP, when the records then show an increase peaking at 15.5 ka cal BP. Overall high values are recognized between 15 and 12.4 ka cal BP (Fig. S4a-e). Between 12.1 and 9 ka cal BP, relative high U/Al values are registered. During the Holocene, the U/Al ratio show a decreasing trend until the present, showing a sharped decrease during the last 2 ka (Fig. S4a-e).

The Mn/Al ratio show high values between 20 and 14.1 ka cal BP with some interval of relative minima; i.e. 17.4 to 16.6 ka cal BP and 16 to 14.7 ka cal BP. The lowest values of the entire record occurred between 14 and 12 ka cal BP. Minor variability is then recognized between 10.5 and 7.5 ka cal BP, with a subsequent minor decrease and increasing variability during the last 5 ka (Fig. S4f-j).

4.2. Grain size

The mean grain size distribution, the percentage of sortable silt (SS) and the mean SS of the carbon free fraction follow a similar evolution (Fig. S5). A first increase occurred between 18.6 and 17.4 cal ka BP, with a subsequent decrease between 16.5 and 17.4 cal ka BP. The highest values during the whole record occurred between 16.2 and 10.2 cal ka BP (Fig. S5). Minimum values occurred between 10.2 cal ka BP until the present. The sand content, which variates between 0.5% and 5.5 %, show a different pattern. Maximum values (>3%) occurred between 16.2 and 15.1 cal ka BP.

On the other hand, in the carbonated samples the mean grain size and the percentage of sand show a similar pattern (Fig. S5). A relative minimum occurred between 17.9 and 16.6 cal ka BP with a subsequent increase between 16.2 and 15 cal ka BP. A relative minimum is recorded between14.8 and 14.4 cal ka BP and a maximum between 12.8 and 12.4 cal ka BP. A relative minimum between 9.2 and 7.2 cal ka BP is followed by an

increase until 5.6 cal ka BP. A sample at 4.9 cal ka BP break a decreasing trend until the present (S5).

4.3. Statistical analysis

Regarding to the PCA performed on the geochemical data, the PC1 confronts aluminosilicates *vs* carbonate elements, suggesting terrigenous input *vs* marine-carbonate production (Fig. S6). Thus, geochemical ratios such as Ti/Ca, Fe/Ca, Al/Ca, K/Ca or Zr/Ca, are interpreted in the same way than the PC1, that is the dilution effect between terrigenous and carbonate fraction. The PC2 shows higher variability between cores, which likely are associated with site-specific bias, although influences during the sample preparation cannot be ruled out. It is characterized by typical elements hosted in heavy minerals (i.e. Zr) in one load, and the elements associated with fine-grained particles (i.e. Rb) in the opposite (Fig. S6). When significant, this relationship between heavy *vs* light elements is usually used as a sorting or winnowing proxy, or as terrigenous source proxy, i.e. fluvial-derived *vs* eolian-derived elements. Whether these ratios conforming the PC2 indicate winnowing or terrigenous provenance in our records is discussed in the next section.

Furthermore, selected correlations between the sedimentation rate (SR) and the K/Al and the Ti/Ca ratios in records 292G, 293G, 434G from the Alboran basin and ODP Site 975B of the Algero-Balearic basin are shown in Table 3. These comparisons evidence an anti-correlation between the K/Al and Ti/Ca ratios for all records, except for ODP Site 975, where the Al was measured by the core scanner technique, which present a low accuracy for measuring light elements (Table 3). In turn, SR is positively correlated with the K/Al ratio in core 293G from 20 to 9 ka cal BP ($r = 0.54$, $p < 0.01$) but is not correlated from 9 ka cal BP to the present ($r = -0.16$, $p > 0.05$). In the Algero-Balearic basin, a positive correlation between the SR and the Ti/Ca ratio is seen. Conversely, in the 434G sediment record from the western Alboran basin —which does not cover the interval between the LGM and the ORL1— the SR indicates a negative correlation with the K/Al ratio ($r = -0.35$, $p < 0.01$) and a positive correlation with the Ti/Ca ratio ($r = 0.72$, $p < 0.01$). Additionally, we have correlated the Ti/Ca ratio and the PC1 of the studied records with

those from other published records from the Minorca contourite drift in the Algero-Balearic basin and (Table S1, S2; Frigola et al., 2007). The Ti/Ca ratio and PC1 of all records show a positive correlation with the fraction upper than 10μm (UP10) and the silt/clay ratio from the Minorca contourite drift during the interval from the LGM to the ORL1 (Table S1). Conversely, such correlations become negative from the ORL1 to the present, except at ODP Site 975B record, likely because the last 2 ka are not recorded (Table S2).

5. Discussion

5.1. Main forcing controlling the terrigenous vs carbonate fraction variation at suborbital scale in the western Mediterranean

In order to elucidate the main forcing mechanism affecting the Ti/Ca ratio in the western Mediterranean over the last 20 ka, this section looks into the factors influencing the carbonate and terrigenous contributions: (1) marine productivity, (2) eolian dust input, (3) riverine input, (4) sea level variations, and (5) bottom water currents (e.g., Arz et al., 1999; Bahr et al., 2014; Dickson et al., 2010; Hodell et al., 2013; Hodell et al., 2015; Thomson et al., 1999).

(1) Hodell et al. (2013) suggested that the variation in the Ti/Ca ratio at a sub-millennial scale depends on productivity changes, being reduced during stadials and enhanced during interstadials. To test this hypothesis, we compared the Ti/Ca ratio from record 293G with the Nannofossil Accumulation Rate (NAR; expressed as coccoliths counts/ cm^2 ka) from cores CEUTA10PC08 and HER-GC-T1, located in the western Alboran basin (Fig. 3f, g; Ausín et al., 2015a) and with the Benthic Foraminifera Accumulation Rate (BFAC; benthic foraminifer counts × $10^3/cm^2$ ka) from core GeoB18131-1c, collected off-mound in the West Melilla cold-water coral mound province (Wang et al., 2019) (Fig. 3h).

A noteworthy decrease in the Ti/Ca ratio occurred during the B-A period, coinciding with a productivity increase in the Alboran Sea basin (Ausín et al., 2015a; Bazzicalupo et al., 2018; Wang et al., 2019). This biogenic Ca production could explain the Ti/Ca ratio decrease, but not the sharpest rise in SR in the Alboran Sea during the last 20 ka, which

could hardly be triggered by a mere increase in productivity (Fig. 3b). The increases in the NAR (from core CEUTA10PC08; Fig. 3g) and the BFAR (from core GeoB18131-1c; Fig. 3h) during the Early Holocene are synchronous with a decrease in the Ti/Ca ratio, yet their sudden drops are not reflected in the Ti/Ca ratio, meaning that the ratio is not only sensitive to productivity changes (Fig. 3; Ausín et al., 2015a; Wang et al., 2019). Furthermore, the increase in the NAR from core HER-GC-T1 at 7.7 ka cal BP —which resulted from a productivity increase related to the onset of Alboran gyres (Ausín et al., 2015b)— coincides with an increase in the Ti/Ca ratio in all the Alboran records (Fig. S2a-f). This suggests that the Ti/Ca ratio is controlled by terrigenous input variation rather than by productivity changes; when both the terrigenous and carbonate fractions increase, the Ti/Ca ratio records only a terrigenous rise, due to the "closed-sum" or dilution effect (Govin et al., 2012).

Such an interpretation is supported by the present-day sedimentation in the Alboran Sea basin, controlled by detrital input changes rather than by productivity changes (Fabres et al., 2002; Masqué et al., 2003). Most studies carried out in continental margins relate the Ti/Ca ratio (or Fe/Ca ratio) to terrigenous variations (Arz et al., 1999; Liu et al., 2016; Steinke et al., 2014; Thomson et al., 1999). Only in regions characterized by a high productivity regime —such as the Western Pacific Warm Pool— the carbonate production controls the detrital/carbonate variations (Tachikawa et al., 2011). In addition, if the Ti/Ca ratio was mainly controlled by the surface productivity, its variability should be also recorded in other shallow marine cores. Nevertheless, core GeoB13731- 1, which is located at 360 m below sea level (mbsl) in the northern Africa margin (Fink et al., 2013; number 5 in Figs. 1, 4f), does not record a Ca decrease during the HS1 and the YD and show a flat pattern during the whole deglaciation. Thus, the Ti/Ca ratio in the studied western Mediterranean records appears to be influenced, but not controlled, by productivity changes at the sub-orbital scale.

(2) The impact of eolian input in the terrigenous *vs* carbonate fraction can be also significant, given the proximity of the Saharan desert and the impact of eolian input in northern regions (Révillon et al., 2011) (Fig. 1). High Ti content in the Saharan eolian dust would affect the Ti/ Ca ratio, and thus indicate eolian input *vs* productivity (Bouimetarhan et al., 2013; Lopez-González et al., 2019). Still, as mentioned in Section

4, the elements Zr and Ti included in the PC2 have served as winnowing and eolian proxies in different sedimentary environments, i.e. countourites *vs.* hemipelagites (Bahr et al., 2014; Calvert and Pedersen, 2007; Govin et al., 2012; Martínez-Ruiz et al., 2015).

In order to confirm previous interpretations of Zr/Al ratios and the PC2 in the Alboran Sea (Fig. S6), we compared our data with other reliable proxies of deep water current intensity, i.e. the silt/clay and of deep water renewal, i.e. $\delta^{13}C$ from the benthic foraminifera *Cibicidoides pachydermus*, from cores MD99-2343 and MD95-2043, recovered in the Minorca contouritic drift and the eastern Alboran Sea, respectively (number 6 and 4, respectively, in Figs. 1 and 5) (Cacho et al., 2006; Frigola et al., 2008; Sierro et al., 2005). We have selected the Zr data from core 293G since it was obtained by XRF in discrete samples measured as pressed pellets, while in the other sediment records Zr was obtained by ICP-MS (434G, 292G, 300G, 302G and 304G), and therefore full digestion of heavy minerals may be difficult, or by XRF core-scanner (975B), which provides qualitative element contents. The $\delta^{13}C$ *C. pachydermus* depends on the isotopic composition of the WMDW, which in turn depend on the deep water formation in the Gulf of Lions, the exchange between Atlantic and Mediterranean waters and the organic matter export to the seafloor (Sierro et al., 2005). Furthermore, the $\delta^{18}O$ *Globigerina bulloides* from selected cores have been also plotted in Fig. 5 for a direct chronological comparison.

The Zr/Al ratio and the PC2 show the maximum values between 16.4 and 15.6 ka cal BP (Fig. 5, blue bar), coeval to the decrease in the $\delta^{18}O$ *G. bulloides*, from the selected records and in the $\delta^{13}C$ *C. pachydermus* from the MD95-2043 and the MD99-2343 (cores 4 and 6 in Figs. 1 and 5a-d) (Sierro et al., 2005; Cacho et al., 2006; Frigola et al., 2007; Rodrigo-Gámiz et al., 2011). This decrease in the isotopic signature of the different foraminifera species has been related to an influx of fresh meltwater from the Atlantic, which promote the WMDW slowdown, as shown by the silt/clay decrease, resulting in suboxic condition in the sediment and in increasing U concentration in the Alboran Sea (Fig. 5, blue bar). In addition, the sortable silt (SS) shows a more similar trend to the U/Al ratio than to the Zr/Al ratio (Fig. 5e, k, l), further suggesting that the Zr/Al ratio and the grain size in the 293G record are not controlled by the bottom current intensity.

Accordingly, since the PC2 coincided with the meltwater input and suboxic condition in the sediment it would be indicative of eolian *vs* fluvial input (positive *vs* negative loads) (Fig. 5e, f); as previously proposed by Rodrigo-Gámiz et al. (2011). The increase in the Zr/Al and Ti/ Al ratios likely respond to the increase aridity in the Saharan area during the HS1 and thus, enhanced eolian input. Then, we state that these ratios should be interpreted in these Alboran Sea records as an eolian dust input proxy rather than a deep water current winnowing proxy during the deglaciation.

In order to elucidate the contribution of eolian input to the sediment composition regarding the Ti/Ca ratio, we compared the variations in the K, Ti and Zr profiles with respect to the detrital and carbonate fractions in records 293G and 300G (Fig. S7). There are minimum variations between K/Ca, Ti/Ca and Zr/Ca ratios at both sites, and they depict the same trend as PC1 (Fig. S7). However, these elements present high variability with respect to the detrital fraction (K/Al, Ti/Al and Zr/ Al ratios), because they indicate fluvial and eolian input, respectively. High values in the Ti/Al ratio point to enhanced eolian input and coincided with relative minima in the Ti/Ca ratio, which indicate a terrigenous decrease with respect to the carbonate fraction (Fig. S7, gray bar). This finding highlights that the Ti/Ca and Zr/Ca ratios are not reliable eolian proxies for the Alboran Sea, and that eolian input does not control the relative variations between terrigenous and carbonate inputs in the western Mediterranean basin.

Table 3

Correlation between K/Al and Ti/Ca ratios and Sedimentation Rate (SR) from the cores 292G, 293G, 434G and 975B (Jiménez-Espejo et al., 2007; Rodrigo-Gámiz et al., 2011).

Core	SR vs K/Al			SR vs Ti/Ca			K/Al vs Ti/Ca			Remarks
	All	Post ORL	ORL-LGM	All	Post ORL	ORL-LGM	All	Post ORL	ORL-LGM	In black p-value >0.05
292G	0.22	0.09		-0.07	-0.01		-0.77	-0.88		
293G	0.33	-0.16	0.54	-0.28	-0.32	-0.53	-0.38	-0.30	-0.48	
434G	-0.35	-0.44		0.72	0.65		-0.66	-0.76		
975B				0.68	-0.37	0.64				Ti measured by core canner and K and Al by atomic absorption

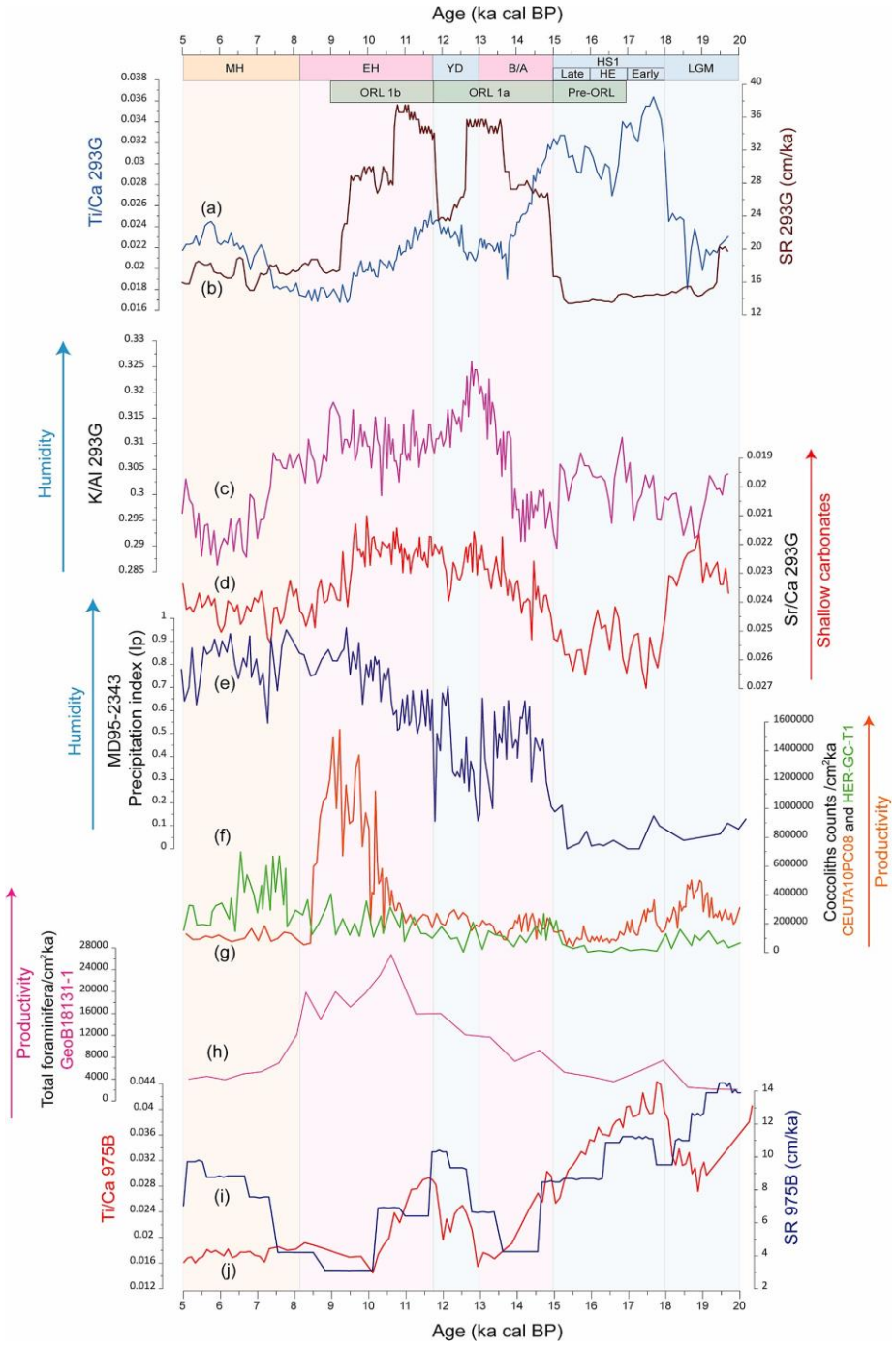

Fig. 3. Age profiles of the (a) Ti/Ca ratio from core 293G, (b) Sedimentation Rate (SR), (c) K/Al ratio, (d) Sr/Ca ratio (x 10^{-4}) from core 293G (Rodrigo-Gámiz et al., 2011); (e) Pollen-based precipitation index (PI) (deciduous *Quercus*/(semi-desertic taxa + deciduous *Quercus*)) from core MD95-2043 (Fletcher et al., 2010); Nannofossil Accumulation Rates (NAR) expressed as coccoliths counts/cm^2 ka from (f) core HER-GC-T1 (Ausín et al., 2015a) and (g) core CEUTA10PC08 (Ausín et al., 2015a); (h) Benthic Foraminifera Accumulation Rate (BFAR) from core GeoB18131-1 (Wang et al., 2019) expressed as foraminifera counts/cm^2 ka; (i) SR and (j) Ti/ Ca ratio from ODP Site 975B (Jiménez-Espejo et al., 2007). LGM: Last Glacial Maximum; HS1: Heinrich Stadial 1; HE1: Heinrich Event 1; B/A: Bolling-Alleröd; YD: ¨ Younger Dryas; EH: Early Holocene; MH: Middle Holocene, ORL: Organic Rich Layer.

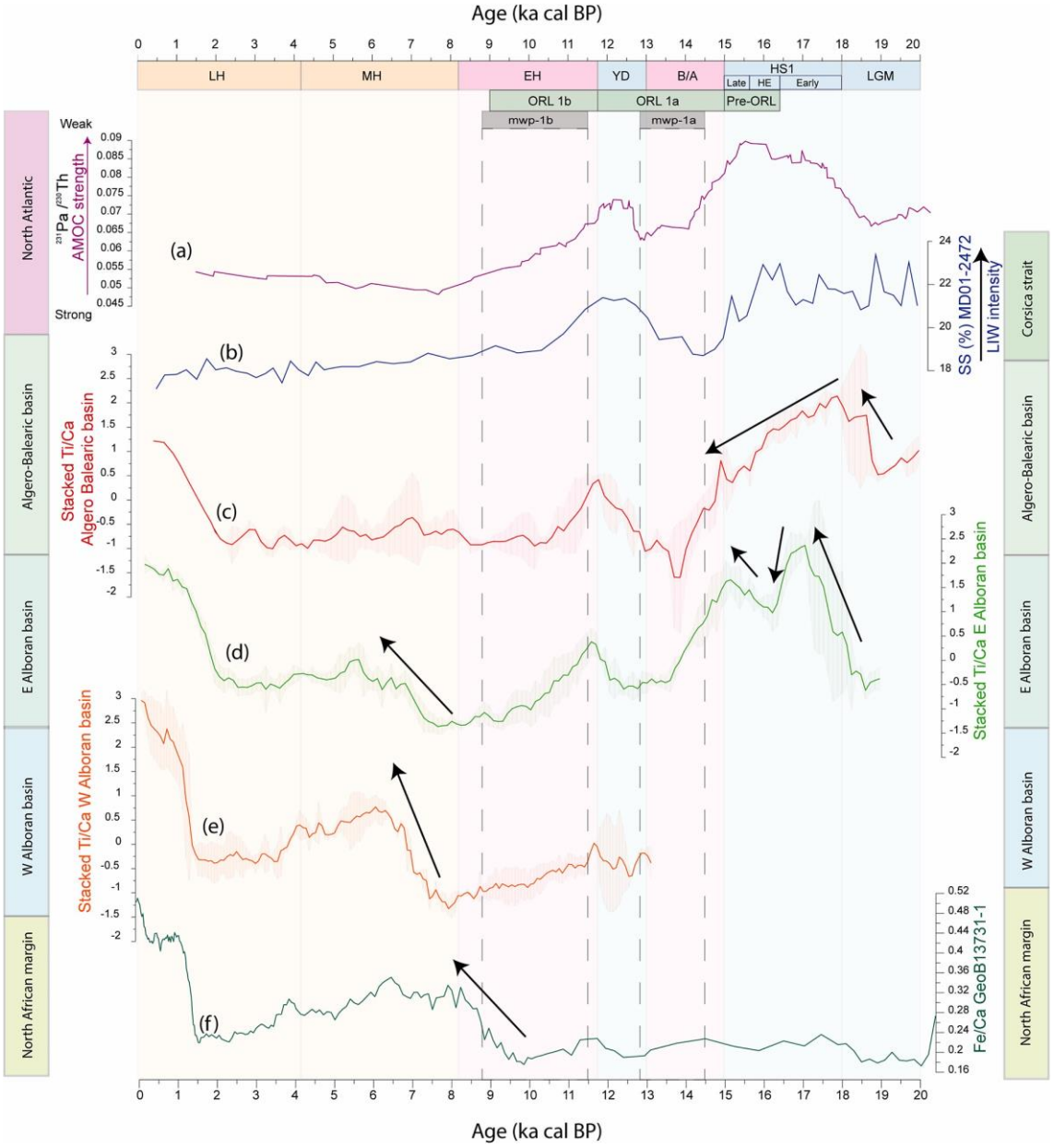

Fig. 4. Age profile of the (a) AMOC intensity reconstruction (Ng et al., 2018); (b) % Sortable Silt (SS) from the Corsica Strait (core MD01-2472; Toucanne et al., 2012); (c) Stacked Ti/Ca ratio from Algero-Balearic basin [ODP Site 975B (this study) + MD99-2343 (Frigola et al., 2007), using XRF core-scanner data]; (d) Stacked Ti/Ca ratio from eastern Alboran basin [cores 293G + 300G + 302G + 304G]; (e) Stacked Ti/Ca ratio from western Alboran basin [cores 292G + 434G] (f) Fe/Ca of core GeoB 13731-1 (Fink et al., 2013). LGM: Last Glacial Maximum; HS1: Heinrich Stadial 1; HE1: Heinrich Event 1; B/A: Bølling-Allerød; YD: Younger Dryas; EH: Early Holocene; MH: Middle Holocene; LH: Late Holocene; ORL: Organic Rich Layer; mwp: melt water pulse (Stanford et al., 2011).

(3) Regarding the role of the riverine input, if it controls the proportion of terrigenous *vs* carbonates in the western Mediterranean, different studies indicate that there should be a positive correlation between the Ti/Ca and the SR (Arz et al., 1999; Liu et al., 2017; Steinke et al., 2014; Stuut et al., 2014; Tachikawa et al., 2011; Xu et al., 2014; Zaragosi et al., 2006). Then, there should likewise be a positive correlation between the Ti/Ca ratio and other typical proxies of fluvial input such as the K/Al ratio (Dickson et al., 2010).

In the Alboran Sea records, a comparison of the K/Al and Ti/Ca ratios over the last 20 ka reveals that the Ti/Ca is negatively correlated overall with the K/Al ratio during the entire time interval (Table 3). This suggests that both proxies are sensitive to the fluvial input but in an opposite way. Furthermore, the comparison of these two ratios in core 293G with the pollen-based precipitation index (PI) from core MD95- 2043 (number 4 in Fig. 1)—as a continental humidity proxy, from Fletcher et al. (2010) (Fig. 3)—suggests that the K/Al ratio is positively related to humidity changes while the Ti/Ca ratio is strongly anti- correlated. If the Ti/Ca would be controlled by fluvial input, its anticorrelation with the PI and the SR could be explained by high amounts of detrital carbonate, but detrital carbonate is not representative in the Alboran Sea sediments. On the other hand, the decrease in the PI and the development of more xerophytic vegetation could increase the effective erosion and thus the Ti/Ca ratio during stadials (Cutmore et al., 2021). Nevertheless, the highest SR coincided with periods of more humid vegetation and the Fe/Ca ratio in core GeoB13731-1 —located on the northern African margin at 362 mbsl (number 5 in Fig. 1)—did not record any variation during the deglaciation (Fig. 4e; Fink et al., 2013).

In addition, there is a slight positive correlation between the SR and the K/Al ratio from the LGM to the ORL1 in the Alboran Sea, suggesting that riverine input influenced the SR, as occurs at present day (Fabres et al., 2002; Masqué et al., 2003) (Fig. 3). In contrast, the Algero-Balearic cores 975B and MD99-2343 (number 6 in Fig 1), evidence a high correlation between SR and the Ti/Ca ratio, although the Ti/Ca ratio decreases when continental humidity increases (Fig. 3), suggesting terrigenous decreases with enhanced fluvial input. In view of these observations, riverine input is unlikely to be the main trigger of Ti/Ca ratio variations at the studied locations.

(4) Sea level is also known to highly influence the terrigenous input of continental margins and thus, the Ti/Ca ratio (e.g., Hodell et al., 2013; Thomson et al., 1999). In sediments from continental margins at mid- and high-latitudes it is well known that during glacial lowstands, river mouths were connected to the marine slope, implying greater sediment input into the deep basins and increasing the SR and the Ti/Ca ratio. Yet during interglacial highstands, the river mouths step back towards the continent, leaving sediment trapped in the shelf and diminishing terrigenous input into the deep basin, thus reducing the SR and the Ti/Ca ratio (e.g., Hodell et al., 2013; Thomson et al., 1999). Although the sea level has risen over the last 20 ka, intervals of rapid rise occurred during the B-A and the Early Holocene, and intervals of relatively stable or even drop sea level took place during the HS1 and the YD (Lambeck et al., 2014); consequently, similar sedimentation conditions can be expected for the glacial period and stadials, as well as during interglacial periods and interstadials but probably with lower amplitudes.

Our data show a relative minimum in the Ti/Ca ratio in the Algero- Balearic basin and absolute minimum values in the Alboran Sea cores during the LGM, when, according to Thomson et al. (1999), supposedly the highest values occurred, as the sea level reached its lower point in the entire record (Fig. 4). The minimum in the Ti/Ca ratio between 20 and 18 ka, coincided with an increase in the SR and the occurrence of turbidites in the Gulf of Lions, favored by the connection of the Rhone river with the canyon head (Lombo Tombo et al., 2015; Dennielou et al., 2019). This would support the interpretation by Thomson et al. (1999), but it could not explain the minimum in the Ti/Ca ratio.

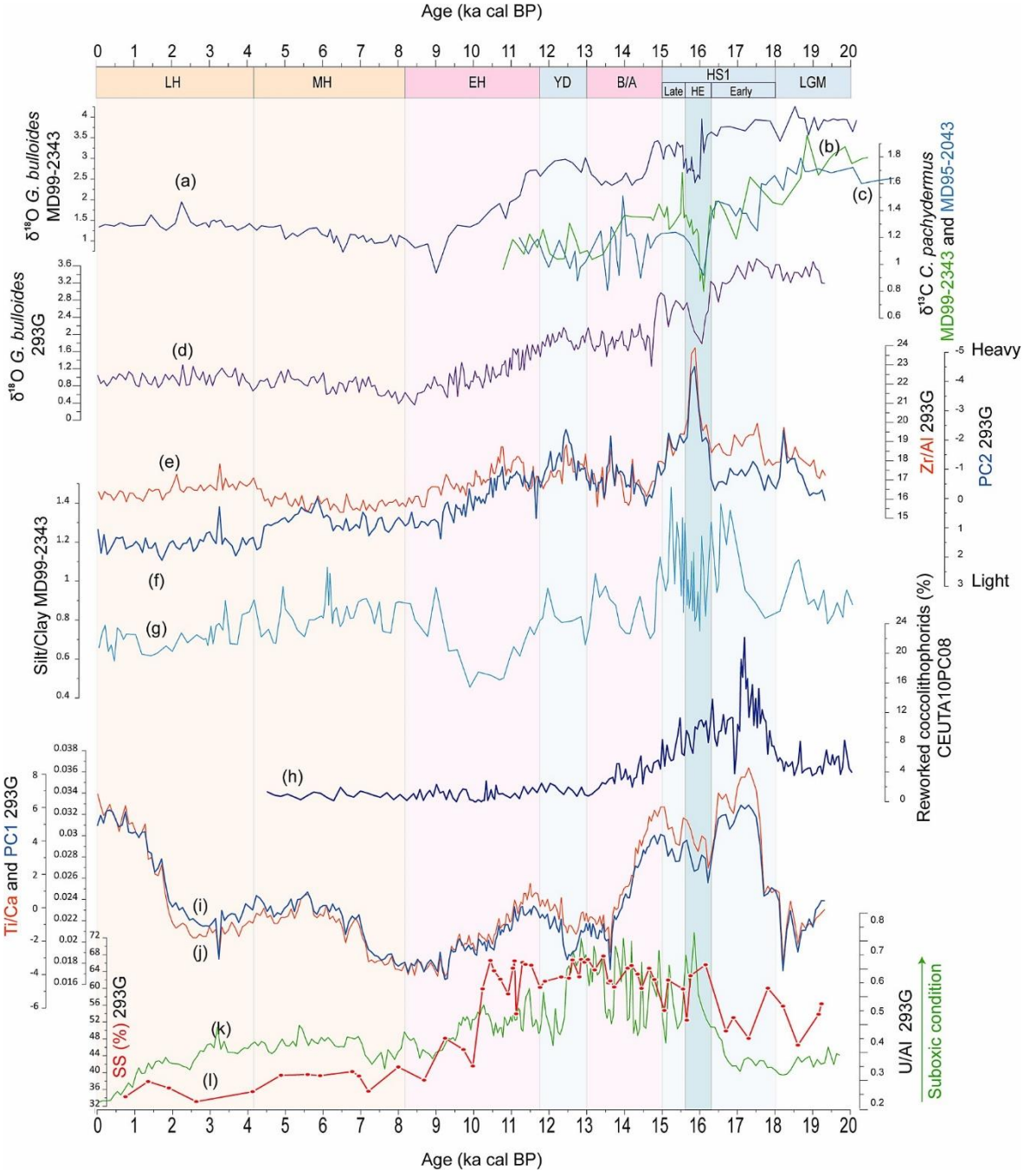

Fig. 5. (a) $\delta^{18}O$ *Globigerina bulloides* from core MD99-2343 (Frigola et al., 2007); $\delta^{13}C$ *Cibicidoides pachydermus* from core (b) MD99-2343 (Sierro et al., 2005) and (c) MD95-2043 (Cacho et al., 2006); (d) $\delta^{18}O$ *Globigerina bulloides* from core 293G (Rodrigo-Gámiz et al., 2011); (e) Zr/Al ratio (x 10^{-4}) and (f) PC2 from core 293G (Rodrigo-Gámiz et al., 2011); (g) silt/clay ratio from core MD99-2343 (Frigola et al., 2008); (h) reworked coccolitophorids from core CEUTA10PC08 (Ausín et al., 2015a); (i) PC1 and (j) Ti/Ca from 293G core; (k) U/Al ratio (x 10^{-4}) from core 293G (Rodrigo-Gámiz et al., 2011); (l) Sortable Silt (SS) from 293G core. LGM: Last Glacial Maximum; HS1: Heinrich Stadial 1; HE1: Heinrich Event 1; B/A: Bolling-Aller¨ od; YD: Younger Dryas; EH: Early Holocene; MH: Middle Holocene; ORL: Organic Rich Layer. Blue bar indicates the HE1 deposition time

The increase in the Ti/Ca ratio during HS1 in the Algero-Balearic and Alboran basins coincides with the disconnection between the Rhone river and the canyon head at 18 ka, hence the reduction of terrigenous input to the basin (Lombo Tombo et al., 2015). This further suggests that the Ti/Ca ratio variation cannot be explained merely by higher terrigenous input during lowstand conditions. Meanwhile, in the Alboran records, the maximum in SR occurred during the B-A and the Early Holocene, coinciding with a rapid sea level increase related to melt- water pulses 1a and 1b (Rogerson et al., 2006; Stanford et al., 2011), when a minimum would be expected, since the sediment load of the retrograding rivers mouths would become trapped on the shelf (Fig. 6b, c; Thomson et al., 1999). In addition, the Fe/Ca ratio in core GeoB13731-1 records a flat pattern during the LGM and deglaciation, when it should in fact record higher terrigenous inputs during the lowstand, thus suggesting other factors than the sea level are controlling the terrigenous *vs* carbonates variability (Fink et al., 2013; Fig. 4f). A possible explanation could be that the sedimentation depends more on changes in fluvial input than on the advance or retreat of the shoreline, due to the narrow size of the Alboran shelves and to the lack of big rivers. To sum up, the maximum turbiditic activity described in the Gulf of Lions (Lombo Tombo et al., 2015) coincided with the relative minimum of the Ti/Ca ratio, and the shallow core GeoB13731-1 shows a minimum of terrigenous input during the deglaciation (Fink et al., 2013), thus suggesting that the Ti/Ca ratio is not controlled by typical lowstand and highstand sedimentation in the western Mediterranean Sea.

On the other hand, sea level can affect the terrigenous flux into the deep basin by shelf erosion during transgressions by wave ravinement, when the shelf is flooded, and the loose sediment becomes trapped by the canyons and is transported basinward (Hemming et al., 1998; Henrich et al., 2010; Liu et al., 2016; Marret et al., 2008). This mechanism can be significant meanwhile the storm wave base level is affecting the shelf edge (Catuneanu, 2006). Due to the terrigenous nature of the Alboran margin, an increase in the Ti/Ca ratio in the studied records might be caused during the shelf flooding. In the Alboran Sea, the shelf break is located at around 100-110 mbsl and the storm wave base between 30-35 mbsl (Bárcenas et al., 2015), indicating that wave ravinement could influence the deep basin sedimentation from the melt-water pulse 1a (15-13 ka cal BP), when the shelf was flooding, until the onset of the melt-water pulse 1b (11.5-8.8) when

the storm wave base level was above the shelf break (Catuneanu, 2006; Lambeck et al., 2014; (Stanford et al., 2011)).

This rapid sea level rise during the melt-water pulse 1a coincided with an increase in the SR and the Sr/Ca ratio in the Alboran Sea (Figs. 3b, d, 6b, d). Since the Sr/Ca ratio decreases from shallow to the deep cores and it is not constrained by the bottom oxygen condition, it can be used as a proxy for shallow carbonates input (Thomson et al., 2004; Reitz and De Lange, 2006). Increases in the Sr/Ca ratio indicates enhanced input of shallow carbonates into the deep basin, likely derived from wave ravinement on the flooded shelf (Catuneanu, 2006). Nevertheless, the values of the Sr/Ca ratio remained high until 9-8.5 ka cl BP indicating that other mechanisms are transporting the shallow carbonates to the deep basin, i.e. dense fluxes triggered by river flooding (Reitz and De Lange, 2006). The anti-correlation of the SR and the Sr/Ca ratio with the Ti/Ca ratio would suggest that the input of shallow carbonates could influence the Ti/Ca, but as stated above, the shelves in the Alboran Sea are richer in terrigenous than in carbonates and then, an increase in the Ti/Ca would be expected when the Sr/Ca increase (Fabres et al., 2002; Masqué et al., 2003). Moreover, this supports that the rise in the SR between 15 and 9 ka was triggered by a combination of both, an increase in the shelf erosion during the early phase of the transgression and enhanced fluvial input during the B-A and the Early Holocene (Fig. 3).

(5) Lastly, another important factor that controls the Ti/Ca ratio is the bottom water currents intensity. In order to test the importance of this factor, we have compared the Ti/Ca ratio with other proxies for bottom water current intensity (Fig. 5).

During the deglaciation, and especially during the HE1, patterns similar to the Ti/Ca ratio are recorded in the silt/clay ratio from the Minorca drift (core MD99-2343; Frigola et al., 2007), the $\delta^{18}O$ *G. bulloides* in the eastern Alboran basin (core 293G; Rodrigo-Gámiz et al., 2011) and the $\delta^{18}O$ *G. bulloides* and the $\delta^{13}C$ *C. pachydermus* in the Minorca drift and eastern Alboran Sea basin (cores MD95-2043 and the MD99-2343; Sierro et al., 2005; Cacho et al., 2006; Frigola et al., 2007) (Fig. 5a-d). The HE1 meltwater influx in the Mediterranean triggered a decrease in the WMDW formation, coinciding with a decrease in the Ti/ Ca ratio and an increase in the U/Al ratio, suggesting more stagnated bottom

waters (Sierro et al., 2005; Cacho et al., 2006; Frigola et al., 2007; Rodrigo-Gámiz et al., 2011; Fig. 5k, blue bar). In addition, the Ti/ Ca ratio show a good correlation with the percentage of reworked coccolitophorids in the Ceuta contourite drift (core CEUTA10PC08), which could be due to an increase in the WMDW (Ausín et al., 2015a). These facts suggest that the Ti/Ca ratio could be sensitive to bottom currents intensity.

The bottom currents could increase the terrigenous content in the marine sediments in two ways: (a) pirating the fine carbonates, such as the coccoliths, resulting in a SR decrease; or (b) concentrating the fine terrigenous fraction, such as sortable silt or aggregates of clays and cohesive silt, resulting in a SR increase (McCave and Hall, 2006). Regarding to the relationship between the Ti/Ca and the SR, a good correspondence between both is recorded in the Algero-Balearic basin, particularly at the ODP Site 975 located in an hemipelagic setting at 2416 mbsl with reduced continental influence (Fig. 3). This suggests that the bottom currents are concentrating fine terrigenous fraction at this site and controlling the SR in the basin. Present-day studies have demonstrated that the total mass flux and the terrigenous input at the bottom of the Algero-Balearic basin increased during months of enhanced WMDW (Zúñiga et al., 2008), supporting that high terrigenous concentration and high SR occurred during periods of more intense bottom currents.

In contrast, the Alboran Sea basin depicted the opposite pattern, being the SR anti-correlated with the Ti/Ca ratio (Fig. 3). Differences between these basins explain this apparent contradiction: although the bottom currents concentrate the terrigenous fraction and the SR also rises in the Alboran basin (Fig. 3), this increase is negligible when compared with the amount of sediment delivered to the basin during the shelf flooding or the enhanced fluvial input, which is amplified by its semi-enclosed and narrow morphology. Conversely, the Algero-Balearic basin is wider and deeper, so the wave ravinement and the increase fluvial input likely had a lesser impact in the SR than in the Alboran basin.

We discard that the anti-correlation between the SR and the Ti/Ca ratio in the Alboran Sea was due to the pirating of fine carbonates by bottom currents, because present-day studies showed that ~50-70% of the particulate matter deposited in the deep Alboran basin

was advected by bottom currents (Fabres et al., 2002; Masqué et al., 2003), and because the SR increase during B-A can be explained by the shelf flooding and enhanced fluvial input (see above).

In summary, bottom current activity concentrates the fine and cohesive terrigenous fraction and increases the SR in the whole western Mediterranean, but this SR increase is only significant in those records having a low SR background, such as the hemipelagic ODP Site 975 in the Algero-Balearic basin. This is supported by the differences in the SR between the Alboran cores and ODP Site 975B with maxima of 39 cm/ka and 14 cm/ka, respectively (Fig. 5). We, therefore, propose that the Ti/ Ca ratio is controlled by the bottom current intensity over the deglaciation, which concentrates the fine terrigenous fraction when increases.

5.2. Evolution of the Ti/Ca ratio over the last 20 ka

Considering that the Ti/Ca ratio is highly influenced by bottom current intensity in the western Mediterranean, this section is focused on three time windows, related to the main changes in WMDW intensity over the last 20 ka (Rogerson et al., 2008): (1) from the LGM to the end of the HS1 (20-15 ka cal BP), (2) the ORL1 deposition time period (15-9 ka cal BP) and (3) from the demise of the ORL1 to the present (9 ka cal BP-Present).

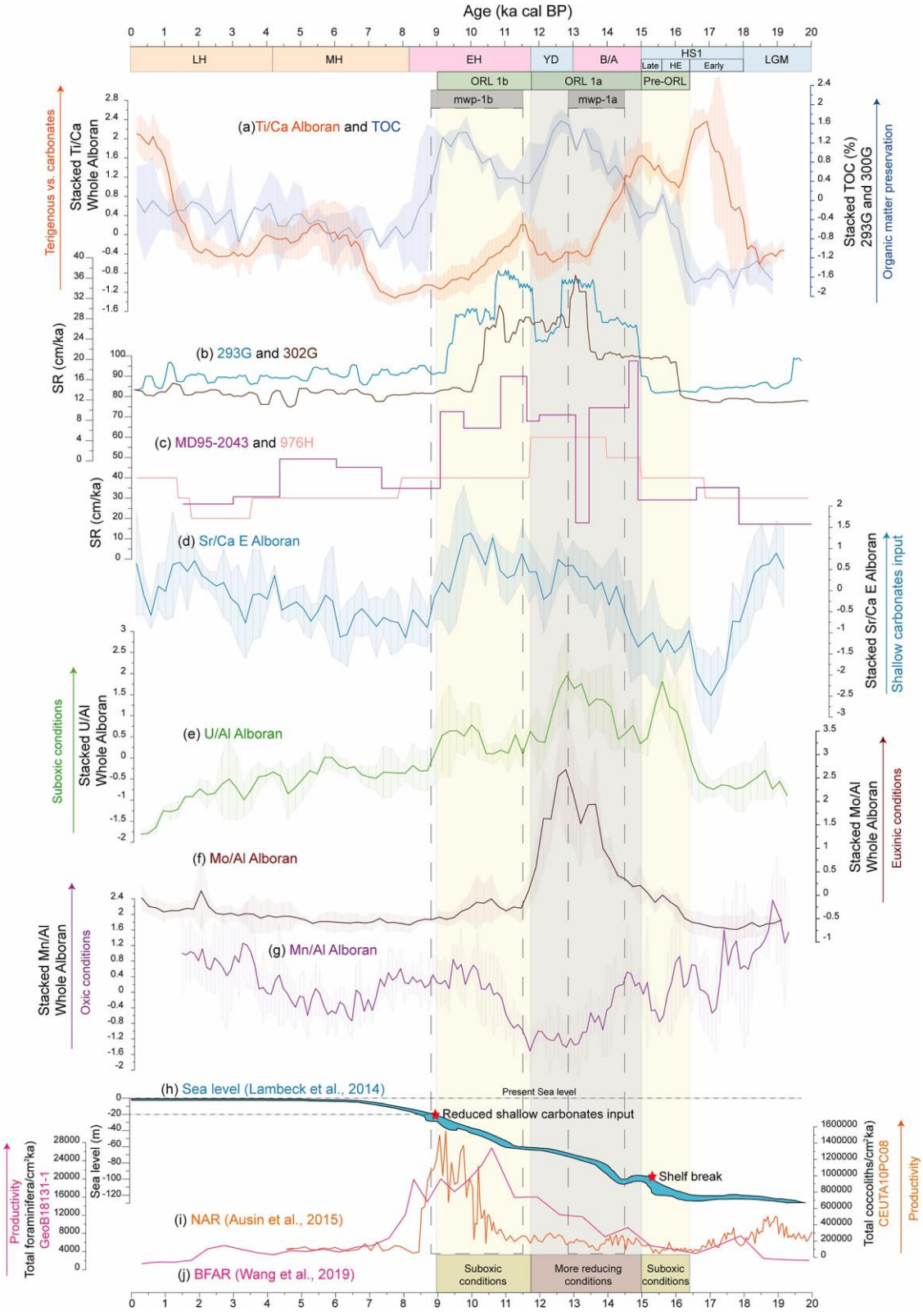

Fig. 6. Age profile of the (a) Ti/Ca ratio and Total Organic Carbon (TOC) content (in %) from core 293G (Rodrigo-Gámiz et al., 2011); (b) Sedimentation Rate (SR) from cores 293G and 302G (Rodrigo-Gámiz et al., 2011; Jiménez-Espejo et al., 2008); (c) SR from cores MD95-2043 (Cacho et al., 1999) located in the eastern Alboran basin and ODP Site 976H located in the western Alboran basin (Martrat et al., 2014); (d) Stacked Sr/Ca ratio from eastern Alboran basin [cores 293G + 300G + 302G]; (e) Stacked U/Al ratio from Alboran basins [cores 292G + 293G + 300G + 302G + 434G]; (f) Stacked Mo/Al ratio from Alboran basins; (g) Stacked Mn/Al ratio from Alboran basins; (h) sea level

5.2.1. Changes in bottom water intensity from the Last Glacial Maximum to the end of Heinrich Stadial 1

During the LGM, the Alboran records show minimum values of the Ti/Ca ratio, whereas the Algero-Balearic core gives higher values, suggesting differences in the bottom current intensity in the two basins between 20 and 18 ka cal BP (Fig. 4). The minimum values in the Ti/Ca ratio of the Alboran cores could be linked to reduced Bernoulli aspiration of the bottom waters as a consequence of low sea level and reduced water exchange between the Atlantic and the Mediterranean, although overall oxic bottom conditions prevailed (Fig. 6; Bárcena et al., 2001; Rogerson et al., 2010; Rohling et al., 2015). In a context of cold and arid climate and lower water exchange, the surface Mediterranean water became saltier and promoted the WMDW´s formation and spreading through the Algero-Balear basin (Rohling et al., 2015), resulting in higher fine terrigenous concentrations and Ti/Ca values than in the Alboran Sea basin.

Later on, overall high values in the Ti/Ca ratio during the HS1 are recorded in the Alboran and the Algero-Balearic records, which suggested high WMDW formation rates increasing fine terrigenous concentration (Fig. 4). Interestingly, although the Ti/Ca ratio increased in all records, those located in the Alboran Sea basin showed a three-step pattern, whereas those from the Algero-Balearic basin recorded the HS1 as a single event (Frigola et al., 2008; Fig. 4).

The HS1 is characterized by colder and more arid conditions over the western Mediterranean region than during the LGM, related to southward displacement of the Polar Front and a weakening of the AMOC (Camuera et al., 2021; Eynaud et al., 2009; Fletcher and Sánchez-Goñi, 2008; Moreno et al., 2010; Sierro et al., 2020) (Fig. 4). Within the HS1, two events of ice rafted detritus deposition occurred in the North Atlantic (Bond et al., 2001; Heinrich, 1988; Hodell et al., 2017), although only one was recorded in the NE Atlantic near the Gibraltar Strait (Naughton et al., 2016; Sierro et al., 2020; Voelker et al., 2006; Voelker and de Abreu, 2011), triggering the meltwater influx into the

reconstruction (Lambeck et al., 2014); (i) Nannofossil Accumulation Rate (NAR expressed as coccoliths counts/cm^2 ka from core CEUTA10PC08 (Ausín et al., 2015a); (j) Benthic Foraminifera Accumulation Rate (BFAR) expressed as foraminifera counts/cm^2 ka from core GeoB18131-1 (Wang et al., 2019). LGM: Last Glacial Maximum; HS1: Heinrich Stadial 1; HE1: Heinrich Event 1; B/A: Bølling-Allerød; YD: Younger Dryas; EH: Early Holocene; MH: Middle Holocene; LH: Late Holocene; ORL: Organic Rich Layer; mwp: melt water pulse (Stanford et al., 2011).

Mediterranean Sea (Hodell et al., 2017; Sierro et al., 2020). Hereafter we will refer to the HE1 deposition time to the H1.1 layer differentiated by Hodell et al. (2017), at ~16.2 ka cal BP. Accordingly, the early HS1 spans from 18 to 16.3 ka cal BP; the HE1 from 16.3 to 15.6 ka cal BP; and the late HS1 from 15.6 to 15 ka cal BP, after Hodell et al. (2017).

The early and late HS1 are characterized by an enhanced WMDW formation, reflected by high values in the Ti/Ca ratio (Figs. 4, 6), and suggesting fine terrigenous concentration in the entire basin. This interval coincided with a rise in the silt/clay ratio within the Algero- Balearic basin, suggesting a strong WMDW (Figs. 5, 6) (Frigola et al., 2008; Sierro et al., 2005). This enhanced WMDW formation is coeval with high LIW input in the Liguro-Provençal sub-basin (Fig. 4b), which could have preconditioned the WMDW formation (Duhamel et al., 2020; Rohling et al., 2015; Toucanne et al., 2012; van Dijk et al., 2018). This enhancement in the Mediterranean thermohaline circulation resulted in an intensification of the MOW in the Gulf of Cadiz and along the Atlantic Iberian margin (Rogerson et al., 2005, 2006) (Fig. 7a).

The HE1 (16.3-15.6 ka cal BP) is characterized by an incursion of depleted $\delta^{18}O$ and low salinity Atlantic waters derived from the Laurentide ice-sheet melting into the Mediterranean (Fig. 5) (Colmenero- Hidalgo et al., 2004; Jiménez-Amat and Zahn, 2015; Jiménez-Espejo et al., 2007; Lombo Tombo et al., 2015; Melki et al., 2009; Pérez-Asensio et al., 2020; Rodrigo-Gámiz et al., 2011; Sierro et al., 2005, 2020). The reduction of surface water salinity led to reduced WMDW formation and a less intense and deeper MOW as result of reduced density of the Atlantic waters (Rogerson et al., 2008; Sierro et al., 2005, 2020) (Fig. 7b).

It is also noteworthy that cores from the Alboran Sea basin depicted a different signal to those from the Algero-Balearic basin during the HE1, showing a Ti/Ca decrease in the former that was not recognized in the latter (Fig. 4). The possible mechanism controlling this difference could be the Bernoulli aspiration. On the Gulf of Cadiz, the deeper MOW recorded during this interval as result of less dense Atlantic water column could promote enhanced Bernoulli aspiration in the westernmost Alboran sea (Rogerson et al., 2012; Sierro et al., 2020). Nevertheless, a relative stagnation of the WMDW in the Alboran Sea basin is supported by high TOC content and an increase in the U/Al ratio during the pre-ORL1, indicating lesser renewal of the deep waters, suboxic conditions in the sediments and major organic matter preservation in the basin (Cacho et al., 1999, 2001; Casanova-Arenillas et al., 2021; Jiménez- Espejo et al., 2008; Pérez-Asensio et al., 2020; Rodrigo-

Gámiz et al., 2011) (Fig. 6a, e). Thus, our results suggest that fresh water input from the Atlantic into the Mediterranean during the HE1 reduced the density gradient in the Gibraltar Strait, resulting in a shoaling of the Bernoulli aspiration depth (Rohling et al., 2015). The shoaling of the aspiration depth could explain the decrease in the Ti/Ca ratio in the Alboran Sea basin, as the bottom waters were relatively stagnated and thus accumulated less fine sediment. Furthermore, a stagnated water column could reduce the piracy of fine-grained biogenic carbonate, such as coccoliths, by water currents, improving their vertical settlement from the surface waters to the deep basin.

The decreased Ti/Ca ratio in the Alboran cores during the HE1 could be also influenced by the input of detrital carbonate transported by icebergs, as occurred in the North Atlantic (Hodell et al., 2017). Yet the Sr/Ca ratio in the Alboran cores increased during this time, and Heinrich layers are characterized by low values in the Sr/Ca ratio (Hodell et al., 2017; Ausín et al., 2020) (Fig. 5). This would support that the drop in the Ti/Ca ratio during the HE1 was triggered by a reduction in the terrigenous concentration by bottom currents, as a result of shoaling in the Bernoulli aspiration depth, rather than by a carbonate input transported by icebergs (Fig. S3).

The Ti/Ca ratio from the Algero-Balearic core did not record this decrease, suggesting that although the WMDW had lesser intensity, it continued to concentrate fine terrigenous fraction during the HE1 (Frigola et al., 2008; Sierro et al., 2005) (Figs. 4, 6, 7b). These differences in the Ti/Ca ratio between the Alboran and Algero-Balearic basins during HE1 support the model proposed by Rogerson et al. (2008), in which the shoaling depth of Bernoulli aspiration along with the formation of less dense WMDW prevented the total renewal of the bottom waters in the Alboran basin, favoring organic matter preservation (Figs. S2, 6, 7a-b).

In short, our results suggest that the HE1 was characterized by weak Bernoulli-aspiration while the WMDW formation was reduced but still active, resulting in lower Ti/Ca values in the Alboran basin than in the Algero-Balearic basin.

5.2.2. The Organic Rich Layer 1 deposition

The ORL1 deposition time interval encompasses the B-A period, the YD and part of the Early Holocene, and is characterized by high variability in the Ti/Ca ratio, indicating reduced WMDW during the B-A and the Early Holocene, and enhanced during the YD

(Cacho et al., 2002; Murat, 1999) (Fig. 6). This interval features high organic matter preservation in the Alboran Sea basin (e.g. Cacho et al., 2002; Jiménez- Espejo et al., 2008; Martrat et al., 2004, 2014; Pérez-Asensio et al., 2020; Rodrigo-Gámiz et al., 2011) (Fig. 6) related to low oxygen bottom basin conditions because of a substantial slowdown in the western Mediterranean thermohaline circulation (Rogerson et al., 2008). An increase of fresh-water influx into the Gulf of Lions triggered by the alpine glaciers retreat during the interstadials (Ivy-Ochs et al., 2007, 2008) and the rapid sea level rise during the melt-water pulse 1a prevented WMDW formation and caused stagnation of the water column (Rogerson et al., 2006, 2008; Rohling et al., 2015(Stanford et al., 2011)) (Fig. 7c). The demise of the ORL1 has been related to a reactivation of the WMDW that could have re-oxygenated the western Mediterranean basins, this reactivation appears to be diachronic along the western Mediterranean basins, dated at 9.2-7.6 cal ka BP (Pérez-Asensio et al., 2020), 8.2 cal ka BP (Rogerson et al., 2008) or ~7.7 cal ka BP (Jiménez-Espejo et al., 2008). The abrupt reactivation is not reflected by redox proxies in the Alboran Sea records (Rodrigo-Gámiz et al., 2011), indicating that other factors may have also affected the demise of the ORL1 in the basin.

In this work we refer to the ORL1a from 15 to 11.7 ka cal BP (B-A and YD), and the ORL1b from 11.7 to 9 ka cal BP (Early Holocene) based on the Mo/Al ratio, which indicates that more reducing conditions prevailed until 11.7 ka (Fig. 6). Our data support that the ORL1a onset was related to a marked reduction in the WMDW depicted by a Ti/Ca ratio decrease, and also shown by the drop in the Mn/Al ratio and the rise in the Mo/Al ratio (Figs. 6, 7c), which are reliable redox proxies (Algeo and Tribovillard, 2009; Algeo and Liu, 2020). Interestingly, this is coeval to a sharp rise in the Sr/Ca ratio and the SR in the Alboran Sea cores, tied to an increase of shallow carbonate input, resulting from the shelf flooding during the rapid sea level transgression and/or the humid condition over the continent and thus, the enhanced fluvial input (Figs. 5, 6) (Combourieu Nebout et al., 2009; Fletcher et al., 2010; García-Alix et al., 2014; Rodrigo-Gámiz et al., 2011). The general SR increase in the deep basin could have also prevented organic matter oxidation (Jung et al., 1997).

The demise of the ORL1a coincides with a relative minimum in the TOC content from the Alboran records that is coeval with the WMDW reactivation during the YD and the termination of extremely reducing conditions in the deep Alboran Sea basin, further indicated by an increase in the Ti/Ca ratio and in the Mn/Al ratio and a decrease in the

Mo/Al ratio, going back to the background levels at ~11.7 ka cal BP (Figs. 6, 7c-d). The demise of strong reducing conditions in the Alboran Sea basin is also supported by a stronger LIW recorded in the Corsica Strait, which could promote the WMDW formation (Toucanne et al., 2012) (Fig. 4b) and an enhanced MOW as registered in several records from the Gulf of Cadiz between 12 and 11.7 cal ka BP (Bahr et al., 2014, 2015; Kaboth et al., 2015; Sierro et al., 2020).

The ORL 1b spans from 11.7 to 9 ka, and is characterized by an early recovery of the TOC values in the Alboran Sea records as well as reduced WMDW formation, coeval with a reduction of LIW input as result of the last sapropel formation (S1) in the eastern Mediterranean basin (de Lange et al., 2008; Rohling et al., 2015; Toucanne et al., 2012) (Figs. 6, 7e). This phase is characterized by more eutrophic conditions in the surface water and still high SRs in the Alboran basin (Ausín et al., 2015a; Cacho et al., 2002; Jiménez-Espejo et al., 2008; Martrat et al., 2004, 2014; Pérez-Asensio et al., 2020; Rodrigo-Gámiz et al., 2011; Wang et al., 2019) (Fig. 6).

Conversely to the ORL1a, the ORL1b interval is characterized by more oxygenated bottom conditions. Redox-sensitive proxies suggest suboxic-ferruginous conditions, since the Mo/Al ratio shows background levels and the U/Al ratio shows relatively high values (Fig. 6) (Algeo and Liu, 2020). The Mn/Al recovers from 11.7 ka, after the WMDW reactivation during the YD and supports the demise of strong reducing conditions that stabilized at 10.5 ka, as indicated by relatively stable Mn/Al values until the end of the ORL 1b (Figs. 6f, 7c-d). This suggests that the re-oxygenation of the deep Alboran basin by the bottom currents occurred at the end of ORL1a and not at the demise of ORL1b. An analogy can be found in the eastern Mediterranean during the last phase of the sapropel S1, between 7.4 and 6.4 ka cal BP, which occurred under sub-oxic or even oxic conditions (Filippidi et al., 2016).

The ORL1 demise coincides with a decrease in both the SR and the Sr/Ca ratio in the Alboran Sea records, but with constant values for the Ti/Ca and Mn/Al ratio (Fig. 6). All this suggests that a reduction in sediment from the shelf and less fluvial input reduced the SR in the deep basin and increased the exposure of organic matter to the oxygenated deep waters. This could also explain why the ORL1 demise shows a slightly diachronic pattern that could reflect differences in the SRs and depths, among other factors. A similar pattern has been described for sapropel S1 demise over the Holocene in the eastern Mediterranean Sea (Filippidi and De Lange, 2019).

Previous studies related the ORL1 demise with a resumption of the WMDW formation recorded in the Algero-Balearic basin (Frigola et al., 2008; Jiménez-Espejo et al., 2007; Rogerson et al., 2008; Rohling et al., 2015), but the Ti/Ca and the Mn/Al ratio in the Alboran basins points to relatively stable seafloor conditions (Fig. 6). Consequently, we propose (1) that strong reducing conditions were only restricted to the ORL1a, and that ORL1b was caused by high organic matter flux due to more eutrophic conditions in the Alboran Sea and high SR at the bottom basin, which prevented the oxidation of organic matter (Jung et al., 1997) (Figs. 7c-d); (2) that sea level and the humid condition over the mainland played a key role in the ORL1 deposition. The shelf flooding during the melt-water pulses 1a and 1b along with the enhanced fluvial input increased the SR in the basin, and the rapid burial prevented the organic matter from being oxidized (Fig. 6) (Cacho et al., 2002; Jiménez-Espejo et al., 2008; Martrat et al., 2004, 2014; Pérez-Asensio et al., 2020; Rodrigo-Gámiz et al., 2011).

5.2.3. Ti/Ca variability during the Holocene

During the Middle and Late Holocene, the Ti/Ca ratio is not correlated with the silt/clay ratio from core MD99-2343, located in the Minorca contourite drift (Frigola et al., 2008) (Table S2), and it shows different patterns in the Algero-Balearic basin and in the Alboran Sea records, indicating that the bottom currents are not controlling the variation between terrigenous and carbonate fractions (Figs. 4, 5). Whereas the Algero-Balearic basin — especially ODP Site 975B— recorded an almost flat pattern for the Ti/Ca ratio, the Alboran records showed increases trends around 8 and 7.5 ka cal BP (Figs. S2, 4c-f). Interestingly, a similar increase is also recorded by the Fe/Ca from core GeoB13731-1 located in the north African margin, beyond the influence of the WMDW (Fink et al., 2013) at around 9.6 cal ka BP. The decoupling between the Algero-Balearic and the Alboran basins, would suggest that the WMDW formation does not control the Ti/Ca ratio, but that the Bernoulli aspiration through the Gibraltar Strait seems to play a major role (Figs. 4, 7f). The early Ti/Ca ratio increase recorded in core GeoB13731-1 with respect to the deeper Alboran Sea cores could be due to natural reasons but we cannot rule out age model discrepancies (Fig. 4c-f).

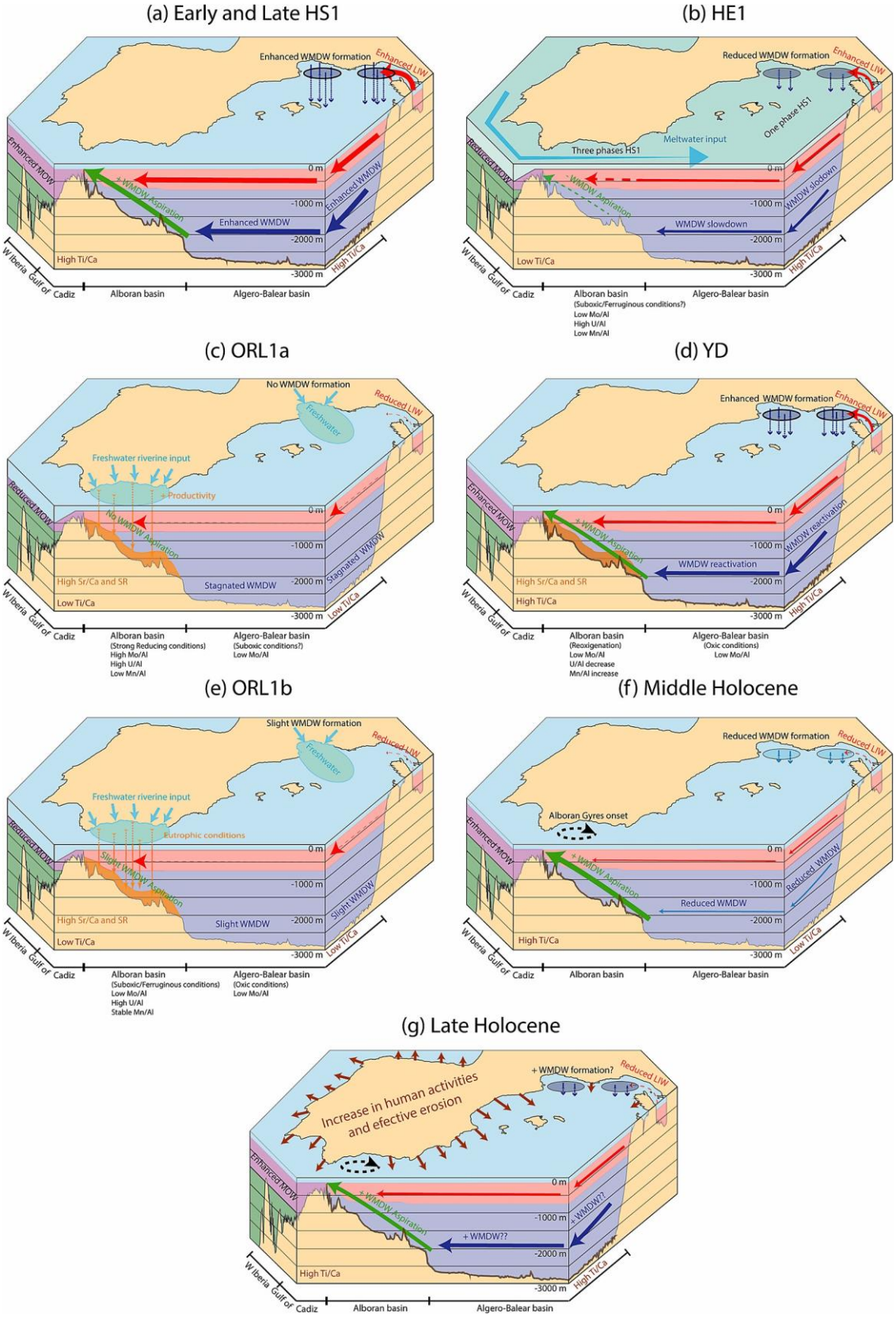

Fig. 7. Theoretical paleoclimate and paleoceanographic model in the western Mediterranean and southern Iberian margin for the last 20 ka. (a) Early and Late Heinrich Stadial 1 (HS1); (b) Heinrich Event 1 (HE1); (c) Organic Rich Layer 1a (ORL1a); (d) Younger Dryas (YD); (e) ORL1b; (f) Middle Holocene; (g) Late Holocene. Main water masses are indicated as Modified Outflow Water (MOW), Western Mediterranean Deep Water (WMDW) and Levantine Intermediate Water (LIW).

The increases in the Ti/Ca and Fe/Ca ratios in the Alboran basins roughly coincided with the establishment of the anticyclonic Alboran gyres at around 8 to 7.7 ka cal BP (Ausín et al., 2015b; Pérez-Folgado et al., 2003; Rohling et al., 1995). Nowadays, the Alboran gyres highly influence the increase of particulate fluxes to the deep Alboran Sea basin, increasing when the gyres are well-developed (Fabres et al., 2002). Furthermore, the intensity of the western Alboran gyre influences the aspiration of the WMDW by the Gibraltar Strait (García-Lafuente et al., 2017; Naranjo et al., 2012; Stommel et al., 1973). The onset of the Alboran gyres could erode or remobilize loose sediments from the shelf and slope and transport them as gravitational fluxes downslope, and/or funnel them to the deep basin (Fabres et al., 2002; Masqué et al., 2003; Miramontes et al., 2019). This could explain why the shallow core GeoB13731-1 in the north African margin, not bathed by the WMDW, and western Alboran cores recorded a sharper increase in the detrital fraction than the deeper cores from the eastern basin during this time interval with respect to the YD (Fig. 4c-f).

Furthermore, an enhanced Bernoulli aspiration though the Gibraltar Strait promoted by the onset of the gyres would increase the WMDW velocity in the Alboran Sea, which in turn would have increased the transport of terrigenous material into the basin, generating a W-E gradient, as shown in the Ti/Ca ratio plots (Fig. 4c-f; García-Lafuente et al., 2017; Naranjo et al., 2012; Stommel et al., 1973). The maximum values of the Ti/Ca ratio related to the onset of the Alboran gyres occurred at ~6-6.5 ka cal BP (Figs. S2, 4c-f), coinciding with the demise of sapropel S1 in the eastern Mediterranean and increased contourite deposition in the Gulf of Cadiz resulting from enhanced MOW (de Lange et al., 2008; Lebreiro et al., 2018; Sierro et al., 2020).

A final sharp increase in the Ti/Ca ratio during the last 2 ka cal BP was recorded in all the studied cores, suggesting a common response in the Alboran and Algero-Balearic basins (Figs. S2a-f, h, 4c-f). Increasing WMDW formation could explain the rise in the Ti/Ca values in the Algero-Balearic basin and the deep records in the Alboran basin, but not in core GeoB13731-1, located at 362 mbsl and nowadays bathed by the LIW (Fink et al., 2013). We discard an intensification of the Alboran gyres behind the increased Ti/Ca ratio (Fe/Ca ratio), because the increase is also observed in the Algero-Balearic basin (Fig. 4c). Higher LIW export into the western Mediterranean is also unlikely, because greater LIW input was not recorded at the Corsica Strait (Toucanne et al., 2012),

suggesting that the terrigenous increase might be related to anthropic impact rather than paleoceanographic changes (Fig. 7g) (Cutmore et al., 2021).

Furthermore, the increasing anthropogenic activity in the Mediterranean area during the last 2 ka is well established (Anderson et al., 2011; Carrión et al., 2010; Jalut et al., 2009; Miebach et al., 2016; Ramos-Román et al., 2019; Oldfield et al., 2003). Although human activity is recognized in the Iberian Peninsula since the Chalcolithic (5.3- 4.2 ka cal BP), with settlements and more frequent fire events during the last 4.5 ka cal BP, activity increased substantially during the Iberian- Roman Period (Aranbarri et al., 2014; Carrión et al., 2010; Martín- Puertas et al., 2010; Molina González et al., 2004; Schirrmacher et al., 2020). During this interval, the deforestation of woodlands as a result of mining, agricultural and grazing activities is recorded in the Iberian Peninsula, even at high altitude sites (Anderson et al., 2011; Aranbarri et al., 2014; García-Alix et al., 2013; Jiménez-Moreno et al., 2013; López-Avil es et al., 2021; Mesa-Fernández et al., 2018; Morellón et al., 2009; Ramos-Román et al., 2016, 2018). Greater land use and deforestation would have enhanced effective erosion, resulting in major terrigenous input into the marine basins and higher values in the Ti/Ca ratio for the western Mediterranean basin.

6. Conclusions

Diverse geochemical ratios analyzed in seven marine sediment records from the western Mediterranean, in a transect from the Algero-Balearic basin to the Alboran Sea basin, have served to elucidate the main factors controlling marine sediment composition over the last 20 ka. The Ti/Ca ratio has been used as a proxy for the relative variations between the terrigenous and the carbonate fractions. Although this ratio is influenced by marine productivity, eolian and riverine inputs, shelf erosion and sea level variations, our data support that the Ti/Ca ratio in the western Mediterranean mostly records bottom current intensity. In other nearby records from the Algero-Balearic basin, this ratio shows a similar pattern, except for the HE1 and the Middle Holocene. During the HE1, the melt-water influx into the Mediterranean reduced the density gradient in the Gibraltar Strait, further reducing the Bernoulli aspiration depth in the Alboran Sea and resulting in a local decrease of bottom current intensity. Despite a reduction in the WMDW formation and intensity in the Algero-Balearic basin, this reduction was not recorded by the Ti/Ca ratio, suggesting that it only affected the coarse fraction. During the Middle Holocene, the onset

of the Alboran gyres promoted the Bernoulli aspiration through the Gibraltar Strait, leading to higher WMDW velocities in the Alboran Sea which in turn increased the terrigenous input in the basin.

Regarding paleoceanographic variability and bottom water ventilation, the Mo/Al and the U/Al ratios support two phases within the ORL1: the ORL1a (15-11.7 ka cal BP) featured strong reducing conditions, while the ORL1b (11.7-9 ka cal BP) deposited under suboxic ferruginous conditions. We propose that the high SR, deriving from shelf erosion during rapid sea level rise along with pervasive humid condition in the continent, played a key role in organic matter preservation —especially during the ORL1b— when the deep basin was more oxygenized. We also relate the ORL1 demise to a sudden decrease in the SR, rather than to a resumption of the WMDW, since re-oxygenation of the basin occurred during the YD, as depicted by the Mn/Al and Mo/Al ratios. Low SR and slower organic matter burial after around 9 ka cal BP meant increased exposition to the oxygenated bottom water, reducing its preservation.

Over the last 2 ka cal BP, the Ti/Ca ratio increases in all the studied records, thereby suggesting an unprecedented common response in the studied basins. Heightened human land use and deforestation in the western Mediterranean region could have led to an increase in effective erosion, in turn increasing the terrigenous input into the basin.

Supplement to:

Paleocirculation and paleoclimate conditions in the western Mediterranean basins over the last deglaciation: New insights from sediment composition variations

Jose Manuel Mesa-Fernández[1*], Francisca Martínez-Ruiz[1], Marta Rodrigo-Gámiz[2], Francisco J. Jiménez-Espejo[1], Marga García[3], Francisco J. Sierro[4]

[1] Instituto Andaluz de Ciencias de la Tierra (IACT), CSIC-UGR, Avenida de las Palmeras 4, 18100, Armilla, Granada, Spain

[2] Departamento de Estratigrafía y Paleontología, Universidad de Granada (UGR), Avda. Fuente Nueva s/n, 18071, Granada, Spain

[3] Spanish Institute of Oceanography, Centre of Cadiz, Muelle Pesquero s/n, Cadiz, Spain

[4] Departamento de Geología, Universidad de Salamanca, Salamanca, Spain

* *Corresponding author:* Jose Manuel Mesa-Fernández (jmesa@iact.ugr-csic.es)

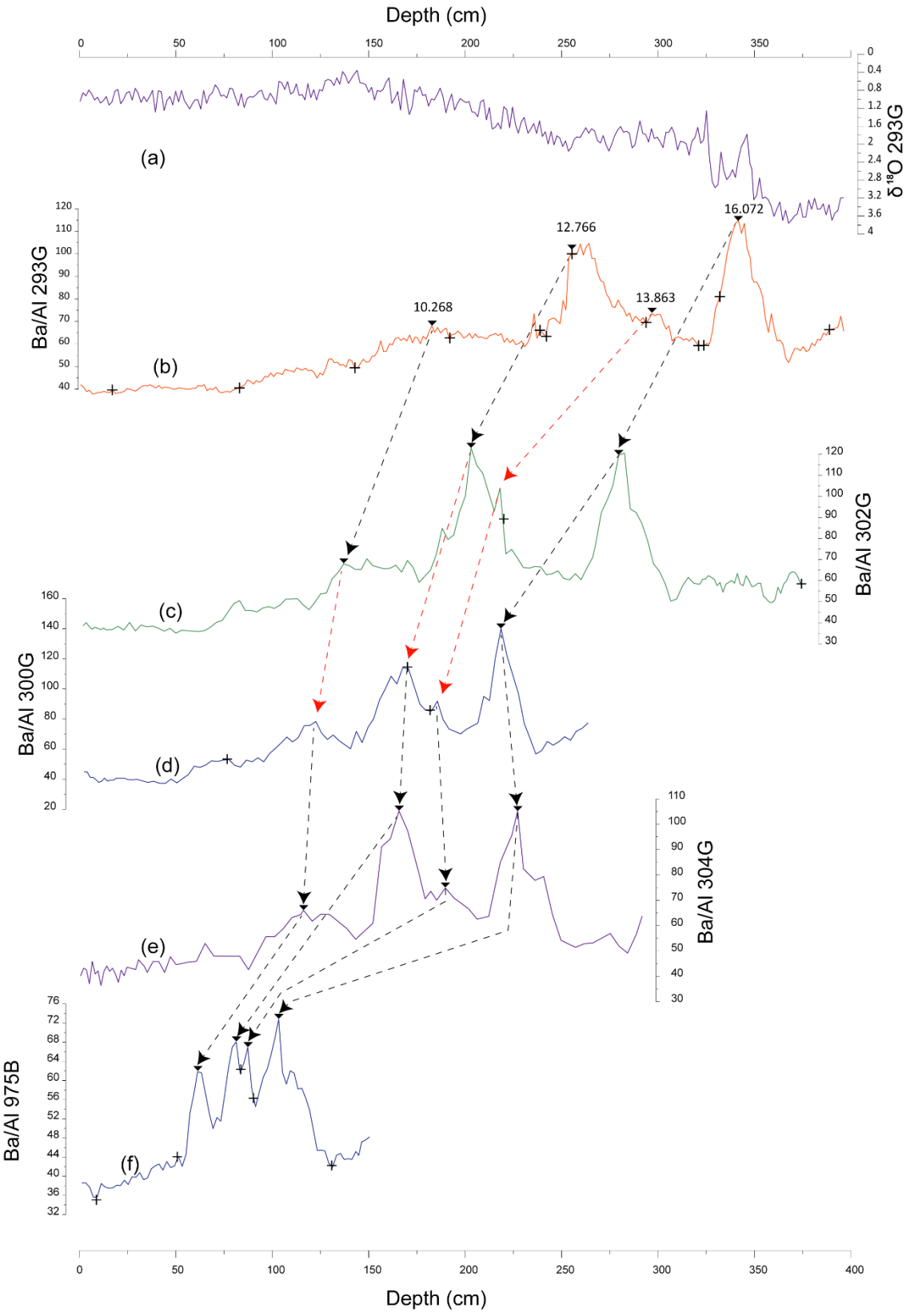

Figure Supplementary 1. (a) $\delta^{18}O$ *Globigerina bulloides* and (b) Ba/Al profile from core 293G; Ba/Al profile and tie-points used in cores (c) 302G, (d) 300G, (e) 304G and (f) 975B. Crosses indicate dated points. The black dashed arrows indicate the tie-points included in the age model update. The red dashed arrows indicate the tie-points not used because there is a nearby dated sample. In core 975B all the tie-points were used because the resolution between the sample is lower due to a lower Sedimentation Rate (SR).

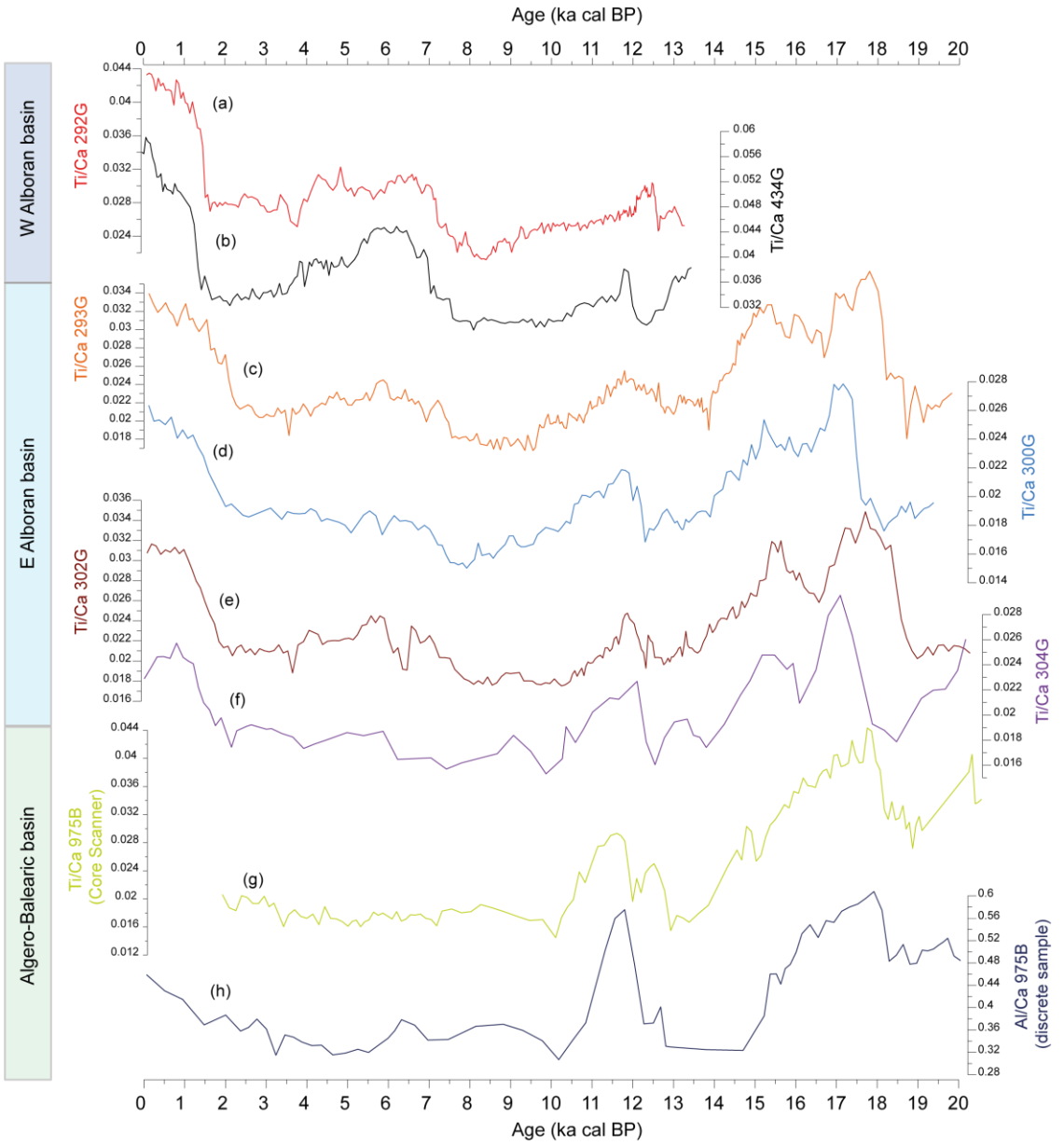

Figure Supplementary 2. Age profiles of the Ti/Ca ratio from the studied marine records: (a) 434G, (b) 292G, (c) 293G, (d) 300G, (e) 302G, (f) 304G; (g) Ti/Ca ratio from ODP Site 975B analyzed by core-scanner method and (h) Al/Ca ratio from ODP Site 975B analyzed by XRF on discrete sample.

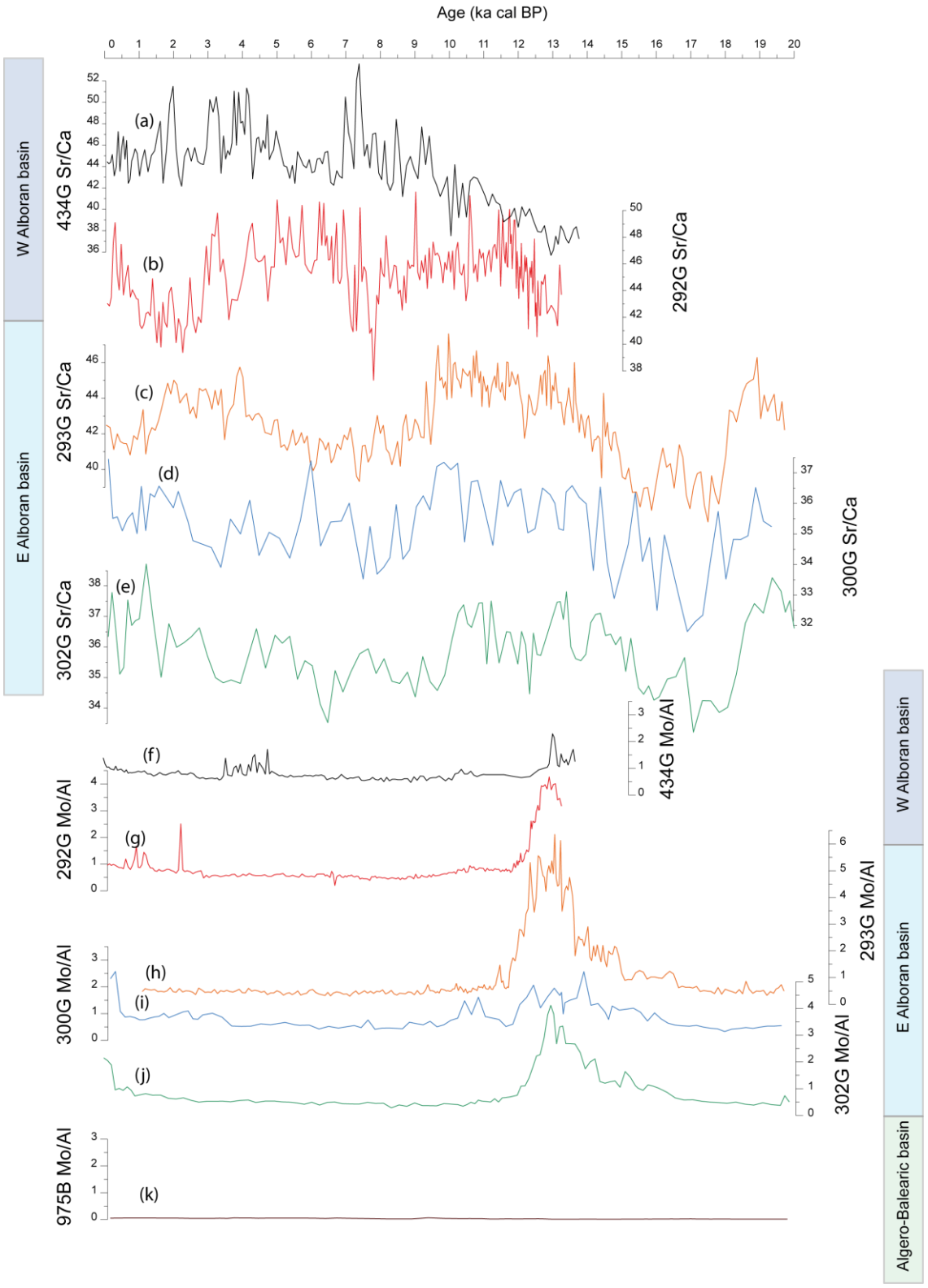

Figure Supplementary 3. Age profiles of the Sr/Ca ratio (x 10^{-4}) from cores (a) 293G, (b) 300G, (c) 302G, (d) 292G, (e) 434G; and the Mo/Al (x 10^{-4}) ratio from cores (f) 293G, (g) 300G, (h) 302G, (i) 292G, (j) 434G, and (k) ODP Site 975B.

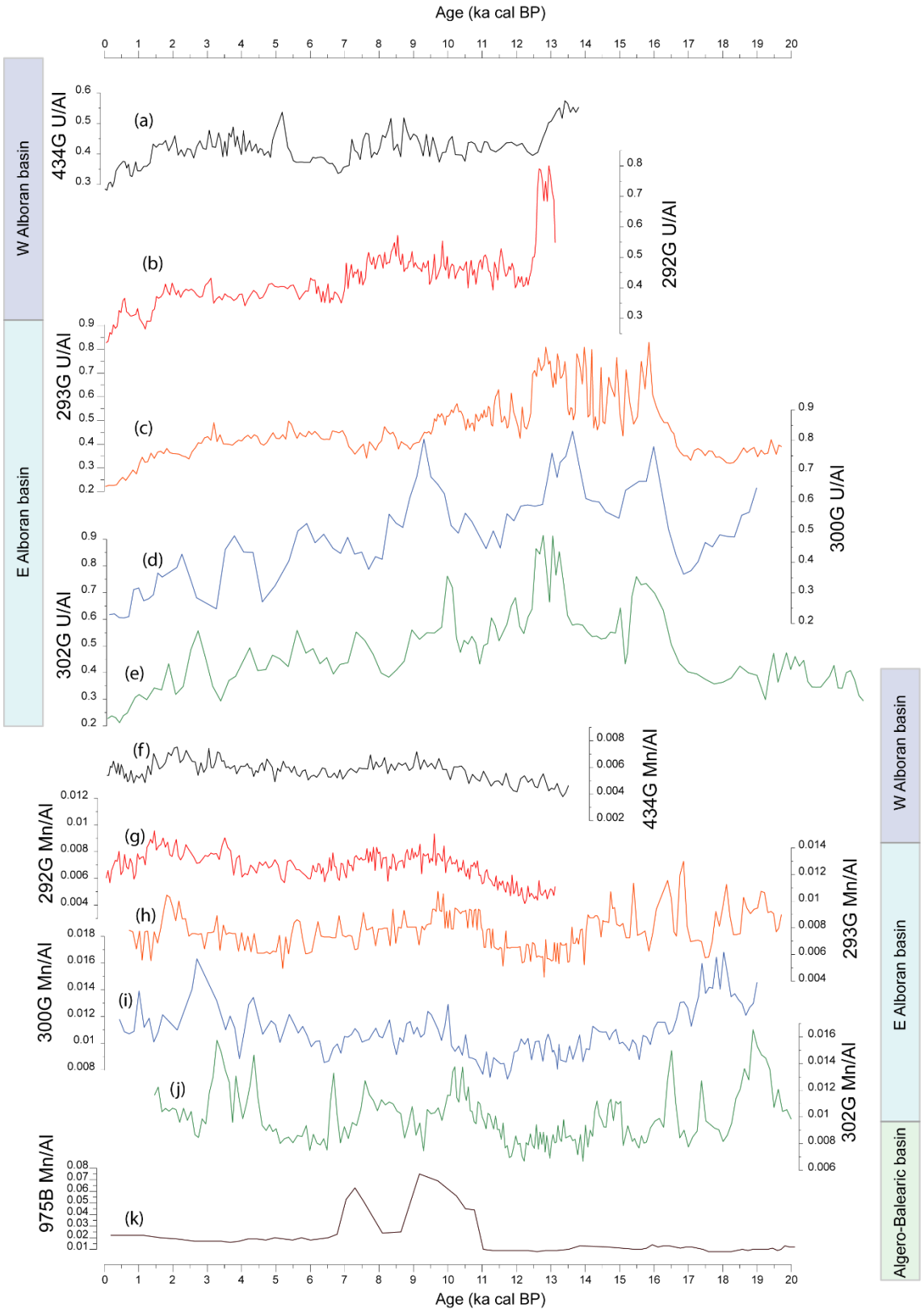

Figure Supplementary 4. Age profiles of the Sr/Ca ratio (x 10^{-4}) from cores (a) 293G, (b) 300G, (c) 302G, (d) 292G, (e) 434G; and the Mo/Al (x 10^{-4}) ratio from cores (f) 293G, (g) 300G, (h) 302G, (i) 292G, (j) 434G, and (k) ODP Site 975B.

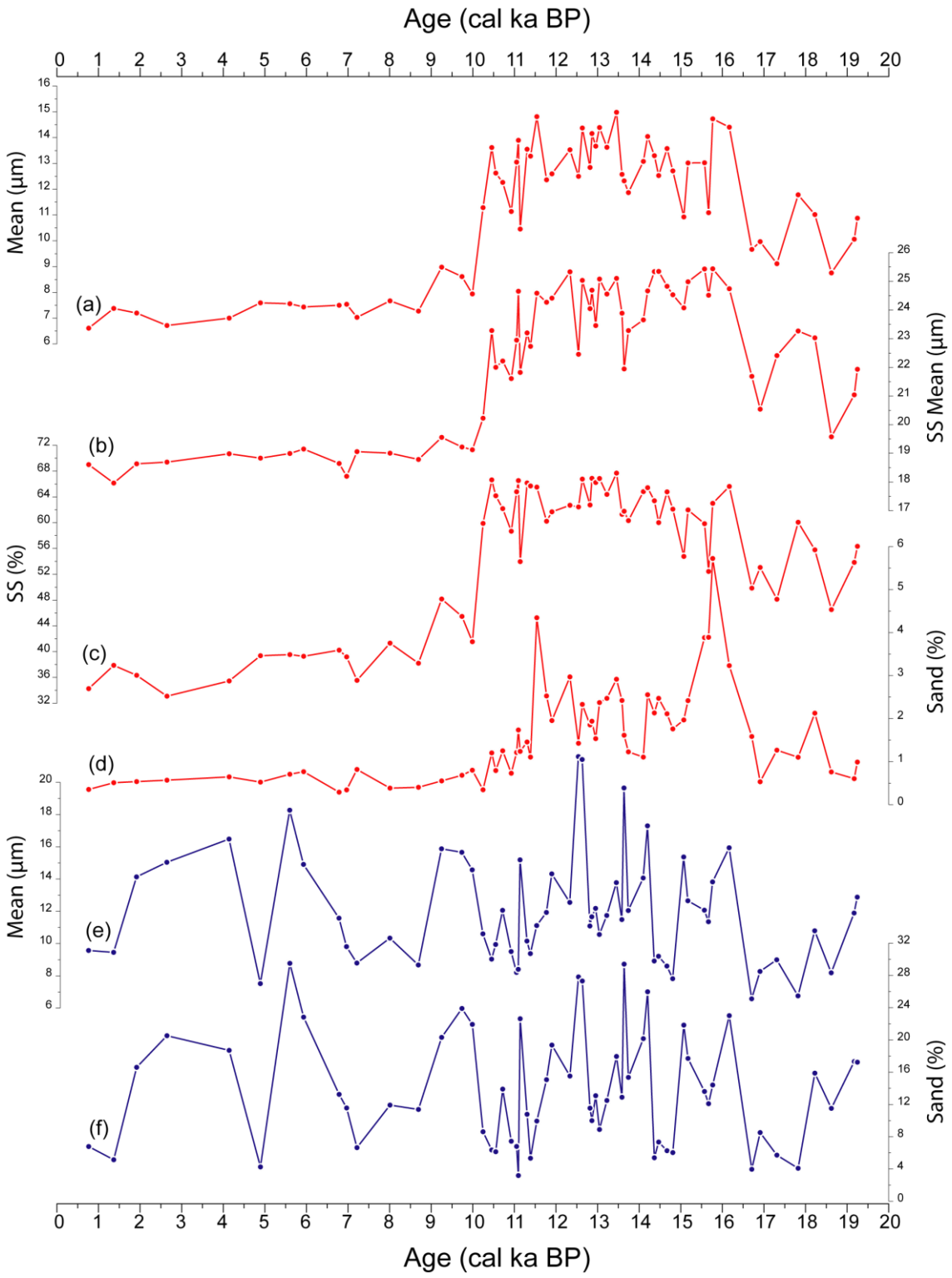

Figure Supplementary 5. Grain size of core 293G measured on the carbonate-free (red) fraction: (a) mean grain size; (b) Sortable Silt (SS) mean; (c) SS percentage; (d) sand percentage; and carbonated (blue) fraction: (e) mean grain size and (f) sand percentage.

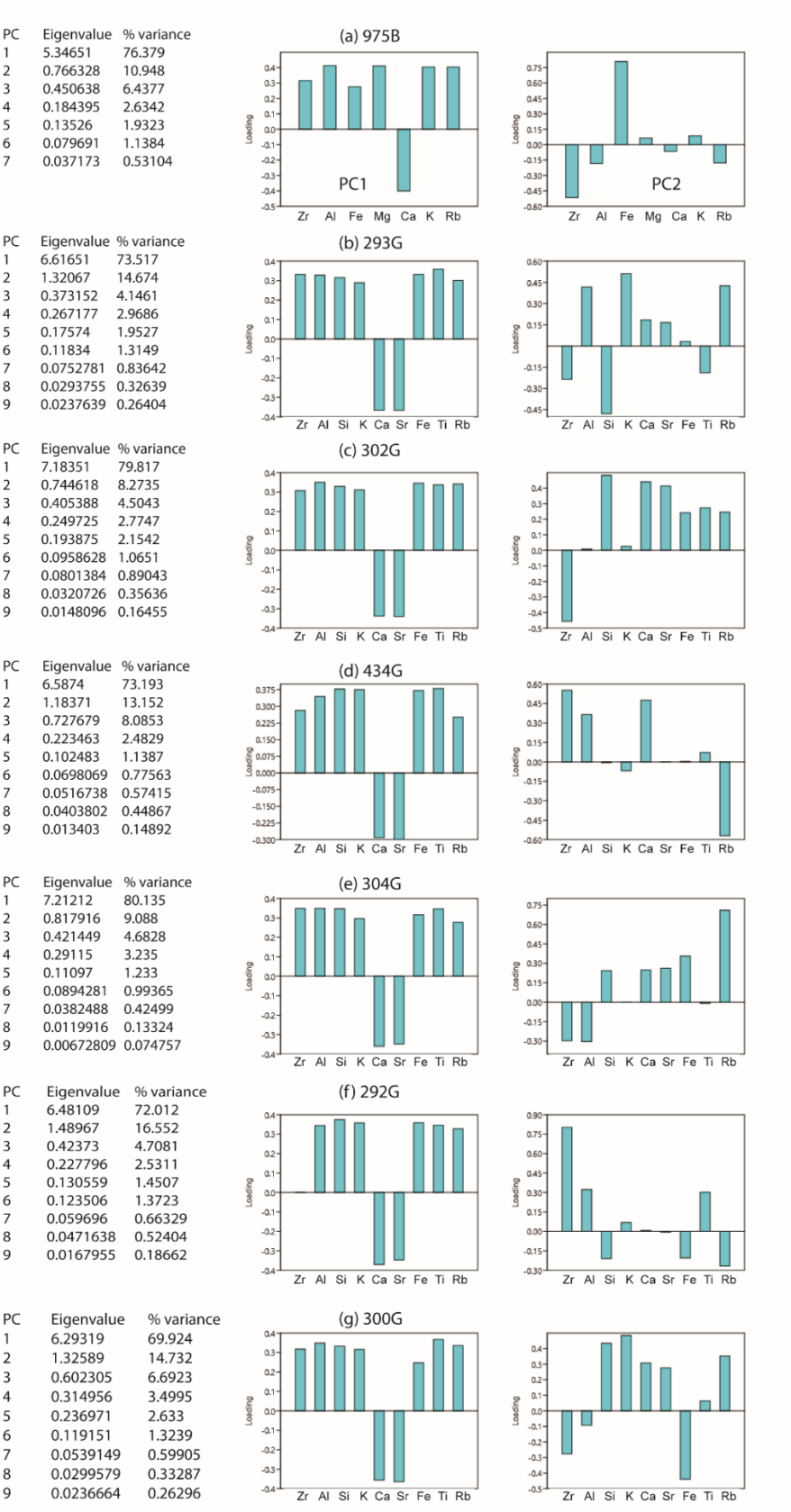

Figure Supplementary 6. Principal Component Analysis (PCA) from the marine sediment records studied (a) ODP Site 975B, (b) 293G, (c) 302G, (d) 434G, (e) 304G, (f) 292G, and (g) 300G.

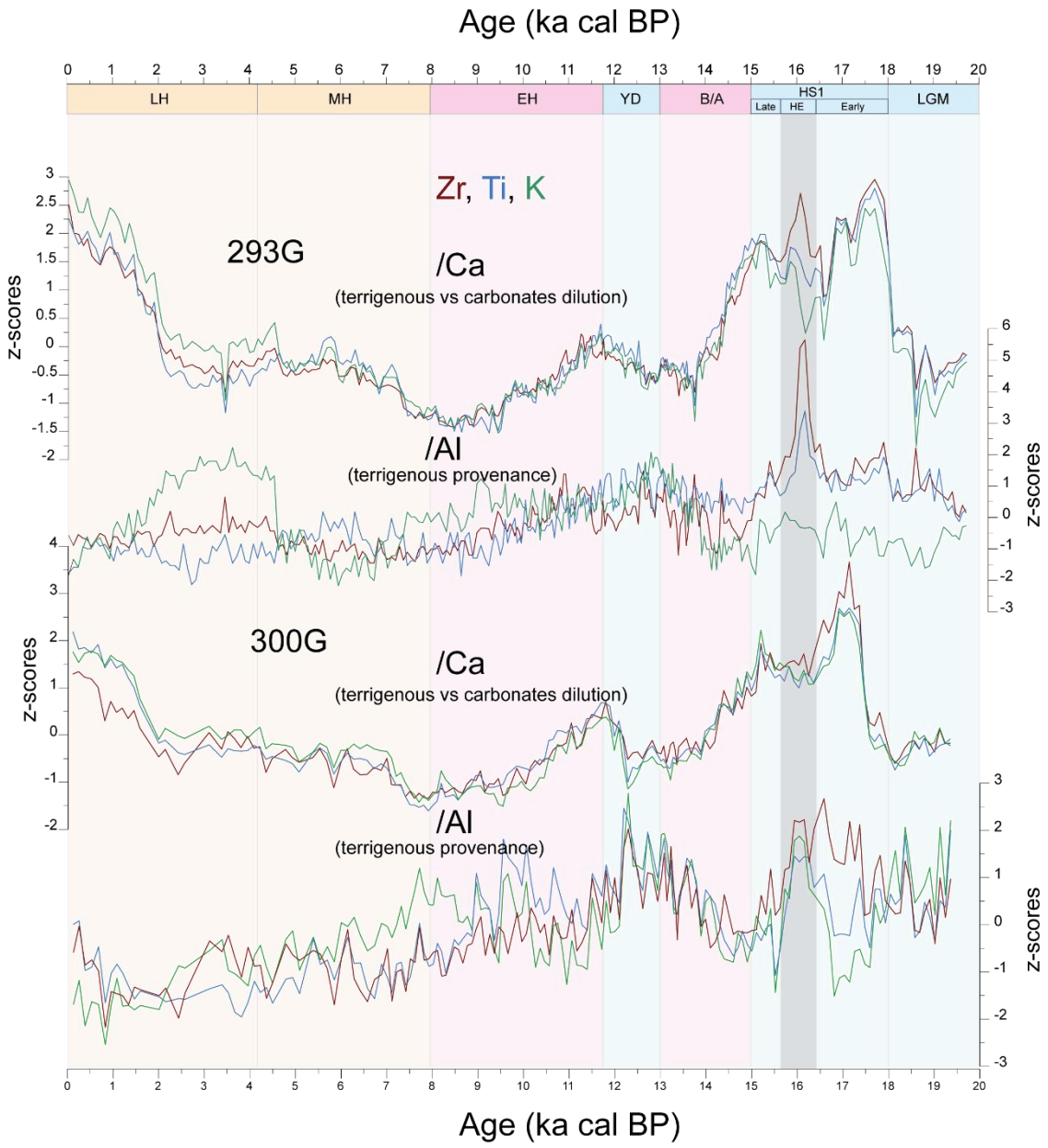

Figure Supplementary 7. Variation of the riverine-derived K, and the eolian-derived Zr and Ti elements, with respect to the detrital ('X'/Al) and the carbonate ('X'/Ca) fractions in marine cores 293G and 300G. All the ratios were normalized by subtracting the mean and dividing by the standard deviation in order to compare the variations. LGM: Last Glacial Maximum; HS1: Heinrich Stadial 1; HE1: Heinrich Event 1; B/A: Bölling-Alleröd; YD: Younger Dryas; EH: Early Holocene; MH: Middle Holocene. The gray bar indicates the interval of maximum eolian dust input recorded.

r \ p-value	**Silt/clay**	**MD99 >10 µm [%]**	**MD99 Ti/Ca**	**293G Ti/Ca**	**293G Zr/Al**	**293G K/Al**	**293G PC1**	**293G PC2**	**975B Ti/Ca**	**302G Ti/Ca**	**302G K/Al**	**302G Zr/Al**	**302G PC1**	**302G PC 2**	**434G Ti/Ca**	**434G PC1**	**434G PC 2**	**434G Zr/Al**	**434G K/Al**	**292G Ti/Ca**	**292G PC1**	**292G PC2**
Silt/clay		0	0	0	0	0.01	0	0	0	0	0.07	0	0	0	0	0	0.1	0	0.72	0	0.1	0
MD99 >10 µm [%]	0.89		0	0	0.01	0.01	0	0.01	0	0	0.05	0	0	0.04	0	0	0.5	0.1	0.48	0.3	0.6	0.1
MD99 Ti/Ca	0.57	0.57		0	0	0	0	0	0	0	0	0	0	0.07	0.77	0.97	0.8	1	0.74	0	0	0.6
293G Ti/Ca	0.54	0.45	0.63		0	0	0	0	0	0	0	0	0	0	0	0	0.2	0.2	0.33	0	0	0
293G Zr/Al	0.38	0.31	0.55	0.49		0.09	0	0	0	0	0.09	0	0	0	0.92	0.61	0.1	0.2	0.74	0.5	0.3	0
293G K/Al	-0.3	-0.31	-0.5	-0.5	-0.2		0	0.72	0	0	0	0.61	0	0.09	0.67	0.8	0	0	0.01	0.1	0.3	0
293G PC1	0.54	0.47	0.69	0.97	0.43	-0.5		0	0	0	0	0	0	0.02	0	0	0.3	0.3	0.02	0.1	0	1
293G PC2	0.47	0.32	0.33	0.48	0.83	-0	0.36		0	0	0.52	0	0	0	0.28	0.02	0	0	0.09	0	0	0
975B Ti/Ca	0.56	0.52	0.85	0.82	0.67	-0.6	0.83	0.48		0	0	0	0	0	0.3	0.08	0.4	1	0.67	0.1	0.1	0.4
302G Ti/Ca	0.6	0.55	0.74	0.9	0.52	-0.5	0.89	0.45	0.86		0	0	0	0	0	0	0.3	0.1	0.11	0	0	0
302G K/Al	-0.2	-0.23	-0.4	-0.5	-0.2	0.39	-0.5	-0.1	-0.5	-0.5		0	0	0.3	0.4	0.41	0.3	0.6	0.85	1	0.9	0.3
302G Zr/Al	0.44	0.38	0.47	0.37	0.44	-0.1	0.36	0.44	0.53	0.42	0.38		0	0	0.12	0.06	0	0	0.84	0	0	0
302G PC1	0.61	0.59	0.82	0.84	0.56	-0.6	0.86	0.43	0.86	0.96	-0.5	0.38		0.02	0	0	0.3	0.7	0	0.1	0.1	0.6
302G PC2	-0.4	-0.24	-0.2	-0.4	-0.4	-0.2	-0.3	-0.7	-0.4	-0.4	-0.1	-0.6	-0.3		0.37	0.03	0	0	0.02	0	0	0
434G Ti/Ca	0.63	0.52	-0.1	0.6	0.02	-0.1	0.53	0.2	0.19	0.7	-0.2	0.28	0.78	-0.2		0	0.2	0.9	0	0	0	0.3
434G PC1	0.67	0.49	-0	0.75	0.09	0.05	0.58	0.4	0.31	0.77	-0.2	0.34	0.69	-0.4	0.93		0.9	0.2	0.06	0	0	0
434G PC2	0.29	0.13	0.05	0.22	0.31	0.59	-0.2	0.74	0.16	0.2	0.17	0.42	-0.2	-0.8	-0.2	0.03		0	0	0	0	0
434G Zr/Al	0.5	0.32	0	0.25	0.22	0.7	-0.2	0.78	0	0.27	0.11	0.43	-0.1	-0.9	-0	0.22	0.9		0	0	0	0
434G K/Al	-0.1	-0.13	-0.1	-0.2	0.06	0.46	-0.4	0.31	-0.1	-0.3	0.04	-0	-0.6	-0.4	-0.6	-0.3	0.5	0.5		0.5	0.2	0.3
292G Ti/Ca	0.42	0.21	0.44	0.61	0.13	0.35	0.37	0.53	0.34	0.6	0.01	0.53	0.32	-0.6	0.42	0.51	0.5	0.6	-0.1		0	0
292G PC1	0.3	0.1	0.43	0.58	0.19	0.19	0.38	0.46	0.34	0.59	-0	0.47	0.31	-0.5	0.4	0.48	0.4	0.4	-0.2	0.9		0
292G PC2	0.58	0.36	0.1	0.42	0.4	0.6	-0	0.82	0.18	0.49	0.21	0.59	0.12	-0.8	0.23	0.45	0.8	0.9	0.2	0.7	0.7	

Table S1. Correlations among Ti/Ca, K/Al and Zr/Al ratios, PC1 and PC2, of the selected cores from the Algero-Balearic and Alboran Sea basins with the silt/clay ratio and UP10 from core MD99-2343 located in the Minorca contouritic drift (Frigola et al., 2008), and the Ti/Ca ratio in core U1385 from the western Iberian margin (Hodell et al., 2015), spanning from the Last Glacial Maximum (LGM) to the Organic Rich Layer (ORL1) demise. Gray shadow indicates cores that not cover the entire interval.

r \ p-value	MD99 Silt/clay	MD99 >10 µm [%]	MD99 Ti/Ca	293G Ti/Ca	293G Zr/Al	293G K/Al	293G PC 1	293G PC 2	975B Ti/Ca	302G Ti/Ca	302G K/Al	302G Zr/Al	302G PC1	302G PC 2	434G Ti/Ca	434G PC 1	434G PC 2	434 Zr/Al	434 K/Al	292G Ti/Ca	292G PC1	292G PC2
Silt/clay		0	0.09	0	0	0.09	0	0	0	0	0.06	0.62	0	0.98	0.23	0.93	0.01	0.12	0.52	0	0	0.3
MD99 >10 µm [%]	0.52		0	0	0.13	0.49	0	0.01	0.03	0	0	0.82	0	0.06	0	0.01	0	0.07	0.02	0	0	0.3
MD99 Ti/Ca	-0.22	-0.4		0	0.13	0	0	0.81	0	0	0	0.07	0	0.36	0	0	0.87	0	0	0	0	0
293G Ti/Ca	-0.53	-0.6	0.81		0.49	0	0	0.01	0.05	0	0	0.69	0	0.01	0	0	0.02	0	0	0	0	0
293G Zr/Al	-0.37	-0.2	-0.2	0.09		0	0.26	0	0.14	0.65	0.81	0.76	0.29	0.35	0.38	0.01	0	0.22	0	0.5	0.5	0.1
293G K/Al	-0.22	0.09	-0.5	-0.4	0.75		0.02	0	0	0.01	0	0.67	0.03	0	0	0	0	0	0	0	0	0
293G PC1	-0.55	-0.62	0.76	0.98	0.15	-0.3		0	0.1	0	0	0.71	0	0.02	0	0	0	0	0	0	0	0
293G PC2	0.61	0.35	-0	-0.3	-0.7	-0.7	-0.4		0.01	0.02	0.91	0.92	0.01	0.05	0.86	0.02	0	0.63	0.01	0	0	0.1
975B Ti/Ca	-0.4	0.32	-0.5	-0.3	0.22	0.48	-0.2	-0.4		0.01	0	0.16	0.02	0.88	0	0	0.4	0.39	0	0	0	0
302G Ti/Ca	-0.46	-0.59	0.83	0.95	0.06	-0.3	0.93	-0.3	-0.4		0	0.45	0	0.05	0	0	0.01	0	0	0	0	0
302G K/Al	0.25	0.68	-0.8	-0.8	0.03	0.51	-0.8	0.01	0.64	-0.8		0.07	0	0.01	0	0	0.05	0	0	0	0	0
302G Zr/Al	0.07	0.03	-0.2	-0.1	0.04	0.06	-0.1	-0	0.21	-0.1	0.24		0.51	0	0.5	0.5	0.99	0.62	0.23	0.5	0.6	0.4
302G PC1	-0.48	-0.62	0.77	0.96	0.14	-0.3	0.95	-0.4	-0.3	0.96	-0.8	-0.1		0.07	0	0	0	0	0	0	0	0
302G PC2	0	0.25	-0.1	-0.3	0.12	0.37	-0.3	-0.3	0.02	-0.3	0.33	-0.4	-0.2		0	0	0.61	0.05	0.01	0	0	0.5
434G Ti/Ca	-0.16	-0.53	0.84	0.83	-0.1	-0.6	0.8	0.02	-0.6	0.84	-0.9	-0.1	0.8	-0.4		0	0.15	0	0	0	0	0
434G PC1	-0.01	-0.32	0.78	0.66	-0.4	-0.8	0.62	0.3	-0.5	0.66	-0.8	-0.1	0.6	-0.4	0.9		0.13	0	0	0	0	0
434G PC2	0.34	0.57	-0	-0.3	-0.6	-0.4	-0.4	0.67	0.13	-0.3	0.25	0	-0.4	-0.1	-0.2	0.2		0.52	0.2	0	0	0.6
434G Zr/Al	0.2	0.23	-0.6	-0.7	0.16	0.42	-0.6	0.06	0.13	-0.6	0.42	-0.1	-0.6	0.25	-0.6	-0.5	0.08		0	0	0	0
434G K/Al	-0.08	0.29	-0.7	-0.6	0.37	0.7	-0.5	-0.3	0.59	-0.6	0.69	0.16	-0.5	0.32	-0.8	-0.8	-0.2	0.61		0	0	0
292G Ti/Ca	-0.37	-0.57	0.81	0.92	0.08	-0.4	0.92	-0.3	-0.4	0.93	-0.8	-0.1	0.92	-0.3	0.91	0.72	-0.4	-0.6	-0.6		0	0
292G PC1	-0.37	-0.6	0.78	0.91	0.08	-0.4	0.92	-0.3	-0.4	0.91	-0.8	-0.1	0.91	-0.3	0.9	0.72	-0.4	-0.6	-0.6	1		0
292G PC2	0.14	-0.13	0.45	0.33	-0.3	-0.5	0.3	0.22	-0.4	0.42	-0.4	0.11	0.35	-0.1	0.53	0.52	-0.1	-0.4	-0.5	0.5	0.5	

Table S2. Correlations among Ti/Ca, K/Al and Zr/Al ratios, PC1 and PC2, of the selected cores from the Algero-Balearic and Alboran Sea basins with the silt/clay ratio and UP10 from core MD99-2343 located in the Minorca contouritic drift (Frigola et al., 2008), and the Ti/Ca ratio in core U1385 from the western Iberian margin (Hodell et al., 2015), spanning from the ORL1 demise to the present.

III

VEGETATION AND GEOCHEMICAL RESPONSES TO HOLOCENE RAPID CLIMATE CHANGE IN THE SIERRA NEVADA (SOUTHEASTERN IBERIA): THE LAGUNA HONDERA RECORD

III. Vegetation and geochemical responses to Holocene rapid climate change in the Sierra Nevada (southeastern Iberia): the Laguna Hondera record

Jose M. Mesa-Fernández[1,2], Gonzalo Jiménez-Moreno[1], Marta Rodrigo-Gámiz[2], Antonio García-Alix[1,2], Francisco J. Jiménez-Espejo[2,3], Francisca Martínez-Ruiz[2], R. Scott Anderson[4], Jon Camuera[1], and María J. Ramos-Román[1]

[1]Departamento de Estratigrafía y Paleontología, Universidad de Granada (UGR), Avda. Fuente Nueva s/n, 18002, Granada, Spain

[2]Instituto Andaluz de Ciencias de la Tierra (IACT), CSIC-UGR, Avenida de las Palmeras 4, 18100, Armilla, Granada, Spain

[3]Department of Biogeochemistry (JAMSTEC), Yokosuka, Japan

[4]School of Earth and Sustainability, Northern Arizona University, Flagstaff, AZ, USA

Correspondence: Jose Manuel Mesa-Fernández (jmesa@iact.ugr-csic.es)

Published in *Climate of the Past 14, 1687–1706.*

DOI: 10.5194/cp-14-1687-2018

Impact Factor: 3.47

Abstract

High-altitude peat bogs and lacustrine records are very sensitive to climate changes and atmospheric dust input. Recent studies have shown a close relationship between regional climate aridity and enhanced eolian input to lake sediments. However, changes in regional-scale dust fluxes due to climate variability at short scales and how alpine environments were impacted by climatic- and human-induced environmental changes are not completely understood. Here we present a multi-proxy (palynological, geochemical and magnetic susceptibility) lake sediment record of climate variability in the Sierra Nevada (southeastern Iberian Peninsula) over the Holocene. Magnetic susceptibility and geochemical proxies obtained from the high mountain lake record of Laguna Hondera evidence humid conditions during the early Holocene, while a trend towards more arid conditions is recognized since ~ 7000 cal yr BP, with enhanced Saharan eolian dust deposition until the present. This trend towards enhanced arid conditions was modulated by millennial-scale climate variability. Relative humid conditions occurred during the Iberian Roman Humid Period (2600–1450 cal yr BP) and predominantly arid conditions occurred during the Dark Ages and the Medieval Climate Anomaly (1450–650 cal yr BP). The Little Ice Age (650–150 cal yr BP) is characterized in the Laguna Hondera record by an increase in runoff and a minimum in eolian input. In addition, we further suggest that human impact in the area is noticed through the record of *Olea* cultivation, *Pinus* reforestation and Pb pollution during the Industrial Period (150 cal yr BP–present). Furthermore, we estimated that the correlation between Zr and Ca concentrations stands for Saharan dust input to the Sierra Nevada lake records. These assumptions support that present-day biochemical observations, pointing to eolian input as the main inorganic nutrient source for oligotrophic mountain lakes, are comparable to the past record of eolian supply to these high-altitude lakes.

1. Introduction

The southern Iberian Peninsula has been the location for a number of recent studies detailing past vegetation and former climate of the region (Carrión et al., 2001, 2003, 2007, 2010; Carrión, 2002; Jiménez-Espejo et al., 2008; Martín-Puertas et al., 2008, 2010; Combourieu Nebout et al., 2009; Fletcher et al., 2010; Nieto-Moreno et al., 2011, 2015; Rodrigo-Gámiz et al., 2011; Moreno et al., 2012; Jiménez-Moreno et al., 2015). Some of these studies have also documented that the western Mediterranean area has been very sensitive to short-term climatic fluctuations throughout the Holocene (e.g. Fletcher and Sánchez-Goñi, 2008; Combourieu Nebout et al., 2009; Fletcher et al., 2010; Jiménez-Moreno et al., 2013). However, a subset of recent studies has attempted to determine how Mediterranean alpine environments have been affected by Holocene climate change through the study of sedimentary records from high-elevation wetlands in the Sierra Nevada (Anderson et al., 2011; García-Alix et al., 2012, 2013; Jiménez-Moreno and Anderson, 2012; Jiménez-Moreno et al., 2013; Jiménez-Espejo et al., 2014; Ramos-Román et al., 2016; García-Alix et al., 2017). These alpine lake and bog records show minimal anthropic influence because they are usually at a higher elevation than major regional late Holocene human landscape modification. This allows for a potentially clearer climatic signal to be determined from these sites. Even though human impact is less important at high elevations, the impacts of human activities has also been reconstructed from these late Holocene sedimentary records (Anderson et al., 2011; García-Alix et al., 2012, 2013, 2017, 2018).

Several studies have highlighted the role of atmospheric mineral dust deposition in marine (Pulido-Villena et al., 2008a) and terrestrial (Morales-Baquero et al., 1999; Ballantyne et al., 2011) ecosystem fertilization through major micronutrients supply. Similar results have been described in the Sierra Nevada alpine lakes, where Saharan dust is especially important in conditioning plankton communities from oligotrophic lakes (Morales-Baquero et al., 2006a, b; Mladenov et al., 2008; Pulido-Villena et al., 2008b; Reche et al., 2009). Although this eolian signal has been occasionally recorded in the sedimentary sequences from the Sierra Nevada lakes (Jiménez-Espejo et al., 2014; García-Alix et al., 2017), the record of inorganic nutrients in Saharan dust input in past lake geochemistry has remained elusive. This study investigates a multi-proxy sediment core record from Laguna Hondera (LH), located in the Sierra Nevada range with two main goals: (1) identifying and characterizing climatic variability during the Holocene, with a focus on

vegetation changes, eolian input and runoff sediments variations, and (2) understanding the Saharan dust influence on past lake sedimentation and geochemistry.

2. Study area

The Sierra Nevada is the highest mountain range in the southern Iberian Peninsula. Bedrock of the high elevations of the Sierra Nevada is mostly composed of metamorphic rocks, principally mica schists (Castillo Martín, 2009). During the late Pleistocene, the Sierra Nevada was one of the southernmost mountains to support alpine glaciers and its last advance was recorded during the Little Ice Age (LIA; Palma et al., 2017; Oliva et al., 2018). Subsequently to the melting of ice at the end of the Last Glacial Maximum, wetlands and small lakes formed in the glacial cirque basins, which occur between 2451 and 3227 m a.s.l. (Schulte, 2002; Castillo Martín, 2009; Palma et al., 2017). Several alpine wetland and lakes have been studied in this area during the last few years, as shown in Fig. 1.

2.1 Regional climate and vegetation

A mediterranean climate characterizes southern Iberia, with a marked seasonal variation between warm and dry summers and cool and humid winters (e.g. Lionello et al., 2006). Overprinting this general climate is the influence of the North Atlantic Oscillation (NAO) (Trigo et al., 2004; Trouet et al., 2009). Southern Iberia is also characterized by strong altitudinal contrasts, which in turn control the precipitation patterns, with mean annual values ranging from <400 to >1400 $mmyr^{-1}$ in the southeast desert lowlands and the southwest highland, respectively (Jiménez-Moreno et al., 2013 and references therein).

As with most mountainous regions, species and species groupings in the Sierra Nevada are distributed with respect to elevation, depending on the temperature and rainfall gradients (e.g. El Aallali et al., 1998; Valle, 2003). Above 2800 m a.s.l. the cryoromediterranean flora occurs as tundra-like open grassland. The oromediterranean belt (1900–2800 m a.s.l.) mostly includes dwarf *Juniperus* (juniper), xerophytic shrublands and pasturelands and *Pinus sylvestris* and *P. nigra*. The supramediterranean belt (~ 1400–1900 m a.s.l.) is characterized by mixed deciduous and evergreen forest species (i.e. evergreen and deciduous *Quercus*, with *Pinus* spp. and others). Mesomediterranean vegetation (600–1400 m a.s.l.) includes sclerophyllous shrublands

and evergreen *Quercus* woodlands. The natural vegetation has been strongly altered by human activities and cultivation in recent centuries, increasing significantly the abundance of *Olea* (olive), due to cultivation at lower altitudes (Anderson et al., 2011, and references therein), and *Pinus* due to reforestation primarily at higher elevations (Valbuena-Carabaña, 2010).

2.2 Laguna Hondera

LH (2899 m a.s.l.; 37°02.88^0 N, 3°17.66^0 W, lake surface: 0.0053 km^2; maximum depth: 0.8m; Morales-Baquero et al., 1999; Fig. 1) is a small and shallow lake located at the lowest elevation of a set of lakes locally named Cañada de Siete Lagunas, a glacial valley between two of the highest peaks of the mountain range in the Iberian Peninsula: Alcazaba (3366 m a.s.l.) and Mulhacén (3479 m a.s.l.). LH has a large catchment area of 1.546 km^2, which is much larger than previously studied sites in the region (Laguna de Río Seco, LdRS, 0.099 km^2; Borreguil de la Caldera, BdlC, 0.62 km^2; Morales-Baquero et al., 1999; Ramos-Román et al., 2016; Fig. 1 for locations). The lake was reduced to a little pond in the deepest area of the basin when cored in September 2012, with a maximum depth of only a few centimetres. LH presently occurs in the cryoromediterranean vegetation belt (2800 m a.s.l.) (El Aallali et al., 1998; Valle et al., 2003). The bedrock in the LH basin consists of Paleozoic and Precambrian mica schist with disthene and staurolite of the lower part of the Caldera Formation (Díaz de Federico et al., 1980).

3. Methods

3.1 Core sampling, lithology and chronology

Six sediment cores were recovered from LH with a Livingstone piston corer in September 2012. LH 12-03 (83 cm) was selected for a multi-proxy study because it was the longest core. Cores were wrapped with tin foil and plastic film and transported to Universidad de Granada, where they were stored at 4 °C.

Core LH 12-03 was split longitudinally and the sediments were described. Magnetic susceptibility was measured every 0.5 cm with a Bartington MS2E meter in SI units

($\times 10^{-4}$) (Fig. 2). The sediment cores were subsampled every 1 cm for several analyses, including pollen and geochemistry.

The age model was built using seven AMS radiocarbon dates from vegetal remains (Table 1; Fig. 2) by means of Clam software (Blaauw, 2010; version 2.2), which used the IntCal13 curve for radiocarbon age calibration (Reimer et al., 2013). A smooth spline approach was chosen (Fig. 2). The sediment accumulation rate (SAR) was calculated with the average rate from the Clam smooth spline output (Fig. 2).

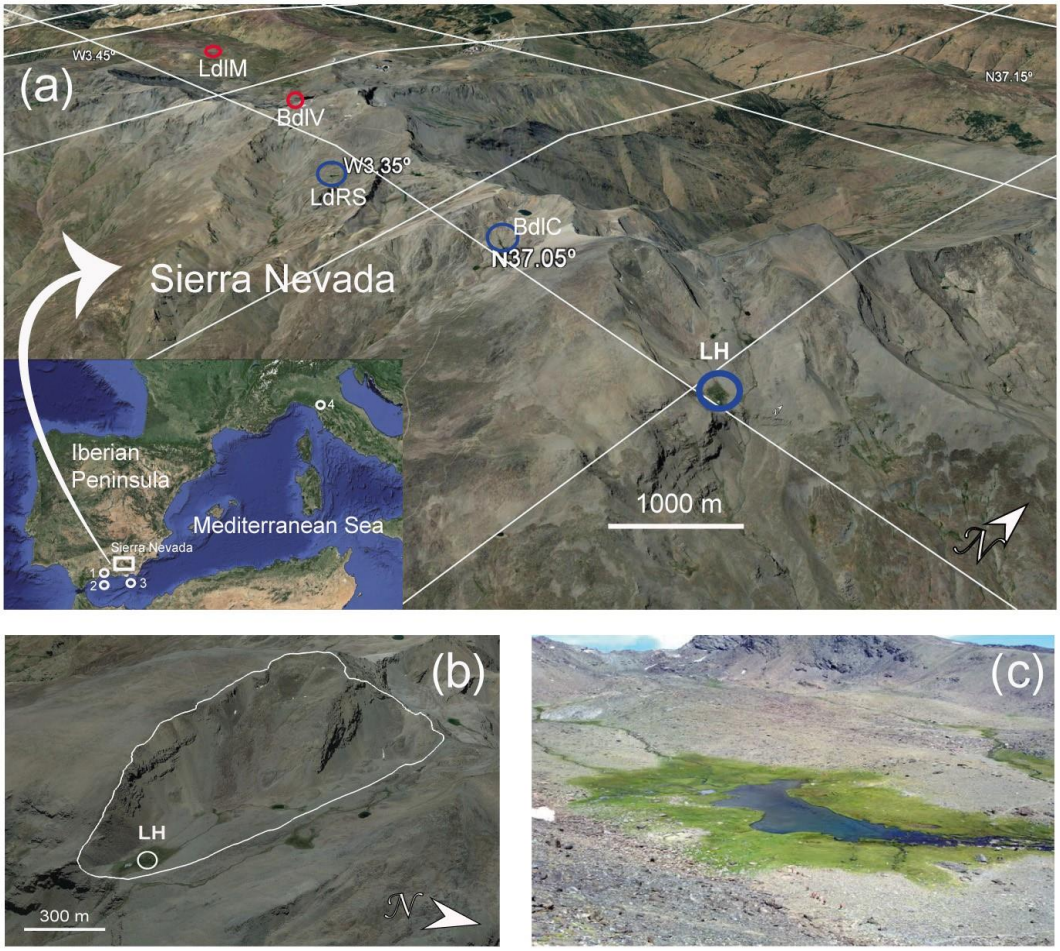

Figure 1. (a) Location of the Laguna Hondera (LH) in the Sierra Nevada, southern Iberian Peninsula, along with other nearby records mentioned in the text. (1) El Refugio Cave stalagmite record (Walczak et al., 2015); (2) ODP 976 pollen record (Combourieu Nebout et al., 2009); (3) MD95-2043 pollen record (Fletcher and Sánchez-Goñi, 2008); (4) CC26, Corchia Cave stalagmite record (Zanchetta et al., 2007; Regattieri et al., 2014). Sierra Nevada north-facing sites are encircled in red, south-facing sites are encircled in blue. LH: Laguna Hondera, the current study, is shown in bold. LdLM: Laguna de la Mula (Jiménez-Moreno et al., 2013); BdLV: Borreguil de la Virgen (García-Alix et al., 2012; Jiménez-Moreno and Anderson, 2012); LdRS: Laguna de Río Seco (Anderson et al., 2011; García-Alix et al., 2013; Jiménez-Espejo et al., 2014); BdlC: Borreguil de la Caldera (Ramos-Román et al., 2016; García-Alix et al., 2017). (b) Regional satellite photo of LH. The white line indicates the catchment area. (c) Photo of Laguna Hondera in September 2012, when the core was taken. Photo taken by Gonzalo Jiménez-Moreno.

Table 1. Age data for LH 12-03. All ages were calibrated using IntCal13 curve (Reimer et al., 2013) with Clam program (Blaauw, 2010; version 2.2).

Lab Number	Depth (cm)	Dating Method	Age (14C yr BP±1σ)	Calibrated age (cal yr BP) 2σ ranges
	0	Present	2012 CE	-63
Poz-72421	7	14C	40±40	29-139
D-AMS 008539	22	14C	1112±32	935-1078
D-AMS 008540	39	14C	2675±30	2750-2809
BETA-411994	44	14C	3350±30	3550-3643
BETA-411995	55.5	14C	5480±30	6261-6318
Poz-72423	57.5	14C	5510±50	6266-6405
Poz-72424	62	14C	6450±50	7272-7433
Poz-72425	74	14C	8620±70	9479-9778

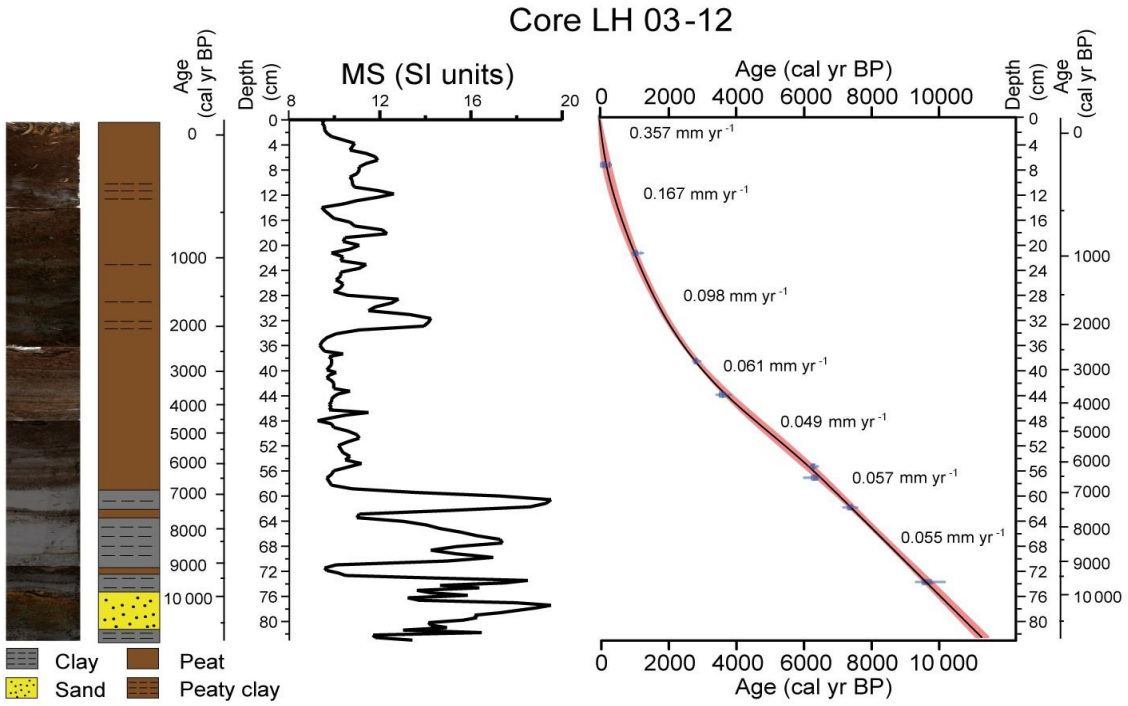

Figure 2. Photo of core LH 12-03, along with the lithology, magnetic susceptibility (MS, in SI units) profile and age–depth model. Sediment accumulation rates (SARs in mm yr $^{-1}$) are shown between individual radiocarbon ages; the red shadow represents the plus–minus range (see details in text for method of construction).

3.2 Pollen

Pollen analysis was performed on 1 cm^3 of sample collected at regular 1 cm interval throughout the first 62 cm of the core. Older sediments (from 62 to 82 cm depth) were barren in pollen, and only one interval at 73 cm could be studied (Fig. 2). Pollen extraction included HCl and HF treatment, sieving, and the addition of Lycopodium spores for calculation of pollen concentration (modified from Faegri and Iversen, 1989). Sieving was done using a 10µm nylon sieve. The resulting pollen residue was suspended in glycerine and mounted on microscope slides. Slides were analysed at 400× magnification, counting a minimum of 300 pollen grains. An overview of pollen taxa with abundances >1% for core LH 12-03 is plotted using the Tilia software (Grimm, 1993) in Fig. 3. Terrestrial pollen percentages, including *Pinus* (see discussion below) were calculated based on the total pollen sum, excluding the aquatic and wetland pollen (Cyperaceae, Ranunculaceae and Typha), since they record a more local environmental signal.

Percentages for aquatics and wetland pollen plotted in Fig. 3 were calculated based on the total pollen sum. The pollen zonation was delimitated visually by a cluster analysis constrained by age of taxa abundance >1% using CONISS software (Grimm, 1987) (Fig. 3). *Olea* was differentiated from other Oleaceae, such as *Phillyrea*, because *Olea* present a thicker endexine and higher size of reticulum in polar vision than *Phillyrea* (Beug, 2004).

3.3 Geochemical analyses

X-ray fluorescence (XRF) Avaatech core scanner®, located at the University of Barcelona, was used to measure light and heavy elements in the LH 12-03 core. An X-ray current of 650µA, a 10s count time and 10kV X-ray voltage were used for measuring light elements, whereas 1700µA X-ray current, 35s count time and 30kV X-ray voltage were used for heavy elements. Sampling interval for these analyses was every 0.5 cm. For our study only three elements (K, Ca and Ti) were considered to have enough counts to be representative.

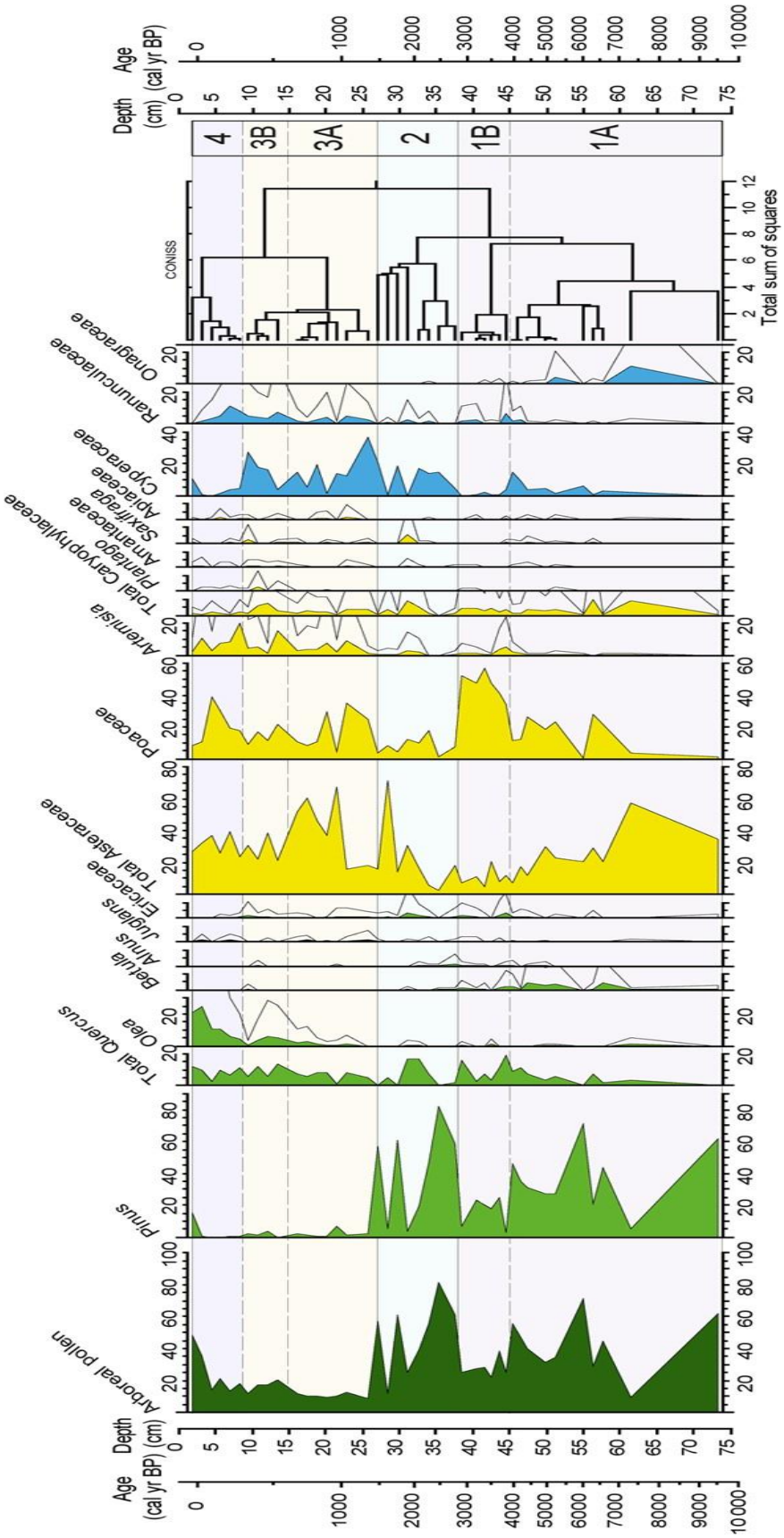

Figure 3. Pollen percentage diagram of the LH 12-03 record showing major selected taxa. Major tree species are shown in green, shrubs and herbs are shown in yellow, and wetland and aquatic types are in blue. Pollen was graphed with the Tilia program (Grimm, 1993) and zoned using the CONISS cluster analysis program (Grimm, 1987).

Inductively coupled plasma–optical emission spectrometry (ICP-OES; PerkinElmer optima 8300) was used for major element analysis on discrete samples every 2 cm. Prior to analysis, the samples were dried in an oven and digested with HNO_3 and HF. Blanks and international standards were used for quality control; the analytical accuracy was higher than ±2.79% and 1.89% for 50ppm elemental concentrations of Al and Ca, respectively, and better than ±0.44% for 5ppm elemental concentrations of K.

Trace element analysis was performed with inductively coupled plasma mass spectrometry (ICP-MS; PerkinElmer Sciex Elan 5000). Samples were measured in triplicate through spectrometry using Re and Rh as internal standards. The instrumental error is 2% for elemental concentrations of 50 ppm (Bea, 1996). Both ICP-OES and ICP-MS analyses were performed at the Centre for Scientific Instrumentation (CIC), University of Granada, Spain.

3.4 Mineralogical analyses

Morphological and compositional analyses were performed using scanning electron microscopy (SEM) with an AURIGA model microscope (Carl Zeiss SMT) coupled with energy-dispersive X-ray microanalysis (EDX) and electron backscatter diffraction (EBSD) mode, also at the CIC (University of Granada, Spain). Mineral grains were analysed to determine provenance, in particular those of eolian origin.

3.5 Statistical analysis

R-mode principal components analysis (PCA) was run on the geochemical dataset using the PAST software (Hammer et al., 2001). PCA identifies hypothetical variables (components) accounting for as much as possible of the variance in multivariate data (Davis, 1986; Harper, 1999). The elements used in the PCA were standardized by subtracting the mean and dividing by the standard deviation (Davis, 1986). Pb was not included in the PCA due to its anthropogenic origin from mining and industrial pollution during the latest Holocene in this area (García-Alix et al., 2013).

4. Results

4.1 Lithology and magnetic susceptibility

The LH 12-03 sediment core consists primarily of peat in the upper ~ 60 cm, with mostly sand and clay layers below (Fig. 2). Positive MS peaks coincide with the grey clay intervals between 58 and 72 cm. Peat intervals coincide with relatively low MS values. For example, a minimum in MS occurs at 36–48 cm depth, related with a peaty interval with root remains. Near the bottom of the core, between 76 and 80 cm, a sandy oxidized interval occurs.

4.2 Chronology and sedimentation rate

The age model of LH 12-03 documents that the record spans the last 10800 cal yr BP (Table 1; Fig. 2). SARs were calculated using the average rate from the Clam smooth spline output (Fig. 2). The SAR below ~ 39 cm is very constant, varying between 0.049 and 0.061 mm yr^{-1}. The SAR increases exponentially to 0.098 mm yr^{-1} at 22 cm, 0.167 mm yr^{-1} at ~ 9 cm and 0.357 mm yr^{-1} at the core top. Accordingly, with the model age and the SAR, resolution of pollen analysis varies between ~ 40 yr $sample^{-1}$ in the top of the core and ~ 120 yr $sample^{-1}$ in the lower part. The resolution of the geochemical analysis on discrete samples varies between 100 and 400 yr $sample^{-1}$, but the geochemical XRF core scanning resolution ranges between 15 and 100 yr $sample^{-1}$, providing higher resolution than geochemical data on discrete samples. The MS analysis resolution varies between 15 and 100 yr $sample^{-1}$.

4.3 Pollen

A total of 50 distinct pollen taxa were recognized, but only those with abundance higher than 1% are included in the pollen diagram (Fig. 3). Four pollen zones for the LH 12-03 record are identified, using variation in pollen species plotted in Fig. 3 and a cluster analysis run through the CONISS software (Grimm, 1987).

Zone LH-1 (core bottom–2600 cal yr BP) is subdivided into two subzones. Subzone LH-1A (bottom–4000 cal yr BP) is defined by the alternation between arboreal pollen (AP) and herbs. AP is composed primarily of *Pinus*, but also *Quercus*. During the interval from ~ 9500 to ~ 7000 cal yr BP only two samples were analysed, due to the low preservation

of pollen in this interval. Pollen in this period is dominated by an alternation between Asteraceae (3%–60%) and *Pinus* (5%–60%) (Fig. 3). The highest occurrence of Onagraceae (~ 10%) is identified in this subzone, and Caryophyllaceae reach high values (~ 10%) as well. Only minor amounts of graminoids (Poaceae and Cyperaceae) occur during this period.

Between ~ 7000 and ~ 4000, *Pinus* pollen varies from 70% to ~ 55%, with a minimum (~ 30%) at 5000 cal yr BP. *Quercus* species increase from ~ 2% to ~ 10%. The highest percentages of *Betula* (~ 5%) in the record occurs at this time. Asteraceae pollen decreases (~ 5%–30%), but Poaceae increase from <5% at the opening of the subzone to >25%. Cyperaceae occur in high percentages (15%).

The subzone LH-1B (~ 4000–2600 cal yr BP) is defined primarily by a great increase in Poaceae pollen (to ~ 60%) (Fig. 3). Other important herbs and shrubs include Asteraceae (5%–15%) and Caryophyllaceae (~ 5%). Other pollen types that increase for the first time in this zone include Ericaceae (~ 3%), *Artemisia* (~ 3%) and Ranunculaceae (~ 2%–6%). *Pinus* (~ 3%–25%) and Cyperaceae (0%–14%) record a minimum in this zone, and Onagraceae disappear altogether (Fig. 3).

Zone LH-2 (~ 2600–1450 cal yr BP) pollen assemblages show high variability. *Pinus* pollen varies between ~ 80% to ~ 3% from the onset to the end of the zone. Aquatic pollen such as Cyperaceae (~ 15%) increases. On the other hand, an increase in herbs such as Asteraceae (~ 5%–70%) occurs along the zone, and Poaceae pollen varies between ~ 7 and 12%.

Zone LH-3 (~ 1450–150 cal yr BP) is subdivided in two subzones. Subzone 3A (~ 1450–600 cal yr BP) is characterized by an increase in herbaceous pollen, led by Poaceae (~ 35% maximum during this zone), Asteraceae (~ 60% maximum during this zone after ~ 1000 cal yr BP) and *Artemisia* (~ 10%), with the resulting decrease in AP. From this subzone to the present, *Quercus* pollen is the major component of AP instead of *Pinus*. Cyperaceae also show a decrease, and Ranunculaceae reach ~ 5%. Subzone 3B (~ 600–150 cal yr BP) documents an increase in *Olea* (~ 6%), Poaceae (20%), Caryophyllaceae (7%) and *Artemisia* (~ 2%–20%). *Pinus* (~ 2%) and Asteraceae (~ 20%) decrease in this period. Aquatic and wetland pollen show a rise (Cyperaceae ~ 30%, Ranunculaceae ~ 10%).

Zone LH-4 (~ 150 cal yr BP-present) depicts a further increase in *Olea* (~ 25%), Poaceae (~ 40%) and *Artemisia* (~ 10%).

4.4 Sediment composition

The XRF-scanning method relies on determining the relative variations on elements composition. Nevertheless, due to the presence of major variations in organic matter or carbonates it is necessary to normalize the measured count in order to obtain an environmentally relevant signal (Löwemark et al., 2011). Aluminium and titanium normalizations are commonly used to discern possible fluctuations in the lithogenic fraction (enrichment or depletion of specific elements), particularly in the terrigenous aluminosilicate sediment fraction (Van der Weijden, 2002; Calvert and Pedersen 2007; Martínez-Ruiz et al., 2015). For this study, the XRF data were normalized to Ti since the Al counts obtained were very low. Poor detection of Al can be related to either low Al content, or high organic and water contents that increase radiation absorption and affect the intensity of this light element, among other possibilities (e.g. Tjallingii et al., 2007).

Since data spacing is different between the analyses on discrete samples and the XRF scanner, a linear interpolation was performed with the purpose of equalizing the space of the different time series (150–300 years). Afterwards, the mobile average was worked out along the time series (taking into account the five nearest points) in order to easily identify trends by means of smoothing out data irregularities. The obtained data were compared, and both XRF-scanner and discrete sample data showed a good correlation. Consequently, the geochemical proxies displayed higher time resolution than the discrete samples (Table 2). Discrete sample and XRF data results are described together in order to simplify this section (Fig. 4).

Table 2. Simulation of proxy correlation: (A) regular interpolation of 300 years sampling spacing, (B) regular interpolation of 300 years sampling spacing and five data points moving average, (C) regular interpolation of 150 years sampling spacing, (D) regular interpolation of 150 years sampling spacing and five data point moving average.

	Simulation							
Correlation	A		B		C		D	
Ca/Ca (XRF)	0.63	p<0.01	0.50	p<0.01	0.57	p<0.01	0.54	p<0.01
K/K (XRF)	0.53	p<0.01	0.64	p<0.01	0.56	p<0.01	0.65	p<0.01

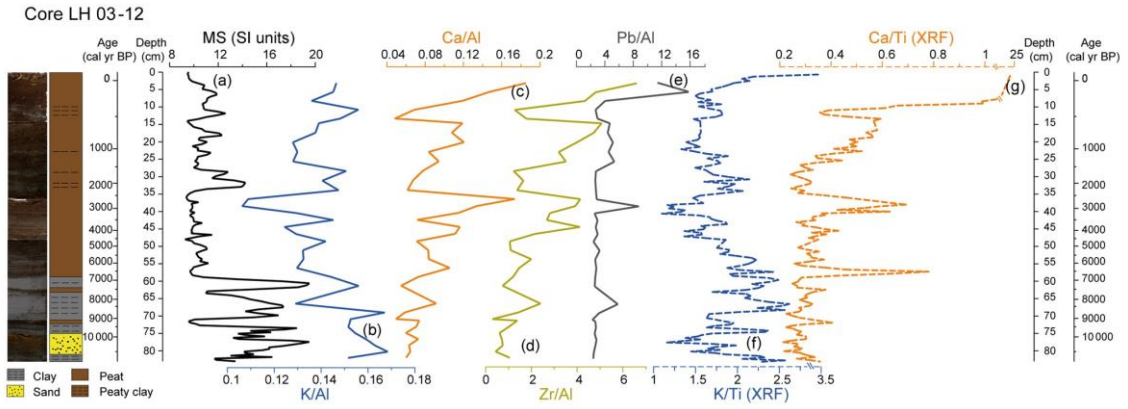

Figure 4. Detailed geochemical diagram of the LH 12-03 record showing the selected proxies: (a) MS; (b) K/Al; (c) Ca/Al; (d) Zr/Al; (e) Pb/Al; (f) K/Ti (XRF); (g) Ca/Ti (XRF) (MS in SI units, Zr/Al and Pb/Al scale $\times 10^{-4}$ and XRF in counts).

The lower part of the core is typified by maximum values of K/Al and K/Ti ratios, coinciding with the lowest values in Ca/Al, Ca/Ti and Zr/Al ratios. Pb/Al data show a stable pattern during this interval. Nevertheless, between 10000 and 9000 cal yr BP and ~ 8200 cal yr BP the trends were reversed, with relatively low K/Al, low K/Ti and slightly increasing Zr/Al, Ca/Al and Ca/Ti ratios. A positive peak in Pb/Al ratio at ~ 8200 cal yr BP is also observed.

Between ~ 7000 and 4000 cal yr BP a decreasing trend in K/Al and K/Ti ratios occurs along with an increasing trend in Zr/Al, Ca/Al and Ca/Ti ratios. The Pb/Al ratio remains constant throughout this interval.

From ~ 4000 to ~ 2600 cal yr BP an increase in Zr/Al, Ca/Al and Ca/Ti ratios is documented. A maximum in eolian proxies occurs at ~ 2600 cal yr BP. A K/Al and K/Ti minima occurs between ~ 3000 and ~ 2600 cal yr BP. The Pb/Al ratio shows a positive peak at ~ 2800 cal yr BP.

The interval between ~ 2600 and ~ 1450 cal yr BP is characterized by low Ca/Al, Ca/Ti and Zr/Al ratios, with relatively high K/Al and K/Ti ratios. The Pb/Al ratio shows a flat pattern, increasing at ~ 1500 cal yr BP.

The period between ~ 1450 and ~ 650 cal yr BP depicts higher ratios of Zr/Al, Ca/Al and Ca/Ti and decreasing ratios of K/Al and K/Ti. A somewhat higher Pb/Al ratio is also registered during this interval.

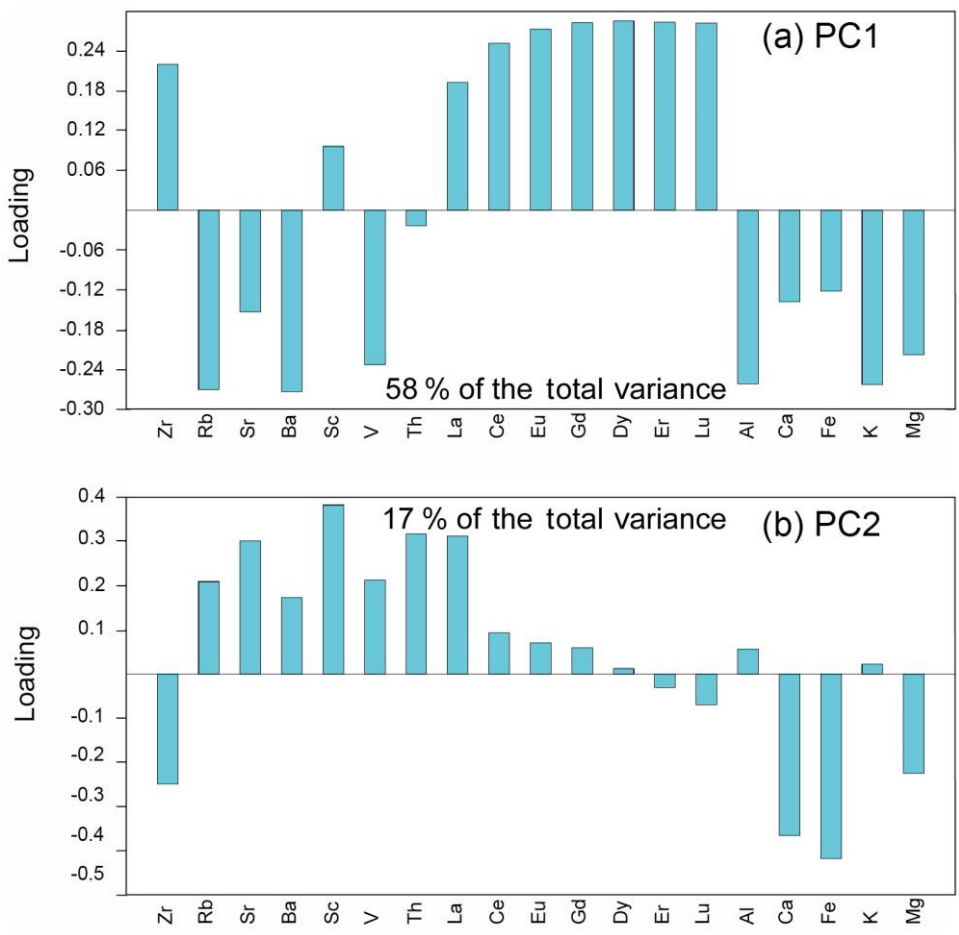

Figure 5. Principal component analysis (PCA) loadings from selected geochemical elements. (a) PC1, which describes 58% of total variance; (b) PC2, which describes 17% of total variance.

From ~ 650 to ~ 150 low values of Zr/Al and Ca/Ti ratios and minimum values Ca/Al ratio occur. Higher K/Al and K/Ti values are also observed. The Pb/Al ratio decreases during this interval. From ~ 150 to the present, an increase in Zr/Al, Ca/Al, Ca/Ti and K/Ti and a Pb/Al maximum occur. Lower K/Al ratio is recorded during this period.

Several studies have demonstrated that PCA of geochemical data can elucidate the importance of different geochemical components driving the environmental responses in marine and lacustrine records (Bahr et al., 2014; Yuan, 2017). We performed a PCA of the LH geochemical data, which yielded two significant components (Fig. 5). The first principal component (PC1) describes 58% of the total variance. The main negative loadings for PC1 are Rb, Ba, Al, K, Ca, Mg and Sr, while large positive loadings correspond to Zr and rare earth elements (REEs). The second principal component (PC2) explains 17% of the total variance. The main negative loading for PC2 are Fe, Ca, Zr, Mg and Lu. Positive loads correspond to Al, K, Ba, Sr and other elements.

SEM analyses show an alternation between a lithology rich in rock fragments and another rich in organic remains. Also, diatom frustules, rich in silica, are particularly abundant since ~ 6300 cal yr BP to the present. Other minerals such as zircon, rounded quartz and monazite were also identified (Fig. 6).

5. Discussion

Pollen and geochemical proxies have been widely used for reconstructing vegetation changes and environmental and climate variations in southern Iberia (e.g. Carrión, 2002; Sánchez-Goñi and Fletcher, 2008; Anderson et al., 2011; Nieto-Moreno et al., 2011; Jiménez-Moreno and Anderson, 2012; Moreno et al., 2012; Fletcher and Zielhofer, 2013; Jiménez-Espejo et al., 2014; Ramos-Román et al., 2016). Variations in the occurrences of arboreal taxa such as *Pinus* and other mesic species (e.g, *Betula, Quercus*), indicating relative humid and warm conditions, and xerophytic species (e.g. Poaceae, Asteraceae, Amaranthaceae, *Artemisia*), representing aridity, have been useful for reconstructing relative humidity changes in southern Iberia (e.g. Carrión et al., 2001, 2007, 2010; Anderson et al., 2011; Jiménez-Moreno and Anderson, 2012; Jiménez-Moreno et al., 2013, 2015; Ramos-Román et al., 2016, 2018a, b). *Pinus* reach percentages over 70% in our record. This bisaccate pollen grain is favoured by wind transport and has a larger dispersal area than other tree species, and sometimes might be overrepresented (Poska and Pidek, 2010; Pérez-Díaz et al., 2016). Nevertheless, LH is located at 2899 m a.s.l., only 99 m above the treeline and the upper boundary of the oromediterranean belt (1900–2800 m a.s.l.), where *Pinus sylvestris* is the main tree species (El Aallali et al., 1998; Valle, 2003). Therefore, this apparently anomalous high concentration of *Pinus* may be caused by an upward migration of the oromediterranean belt and treeline towards higher elevations and around the LH during warmer and more humid periods, which could have been overstated due to its high pollen production and dispersal. Therefore, *Pinus* seems to be mostly recording a regional climatic signal, without allocthonous influence.

Over 75% of the total geochemical data variance is explained by the PC1 and PC2 (Fig. 5). We interpret the results of PC1 as resulting from certain sorting between heavy minerals (positive loading; Zr and REE) vs. clay minerals and feldspars (negative loadings; K, Al and Ca). The drainage basin is mainly composed of mica schist and consequently enhanced in K-rich minerals such as mica and feldspar (Díaz de Federico et al., 1980). This sorting between heavy minerals (enriched in Zr and REE) and clays

and feldspars (enriched in K and Al) (Fig. 5a) was probably linked to physical weathering within the basin and to resulting runoff until final deposition in the lake.

On the other hand, we interpret the results of PC2 as differentiating autochthonous elements (positive loadings) vs. Saharan allochthonous input (negative loadings). In the first case, due to the abundance of mica schist within the LH drainage basin (Díaz de Federico et al., 1980), the K/Al and K/Ti ratios are interpreted as detrital products, and thus a proxy of runoff. In the second case, PC2 negative loading grouped elements (Zr, Ca, Mg and Fe; see Fig. 5b) that are coherent with Saharan input composition (dolomite, iron oxides and heavy minerals) (Ávila, 1997; Morales-Baquero et al., 2006b; Moreno et al., 2006; Pulido-Villena et al., 2007). In addition, Ca shows a strong positive correlation with Zr since 6300 cal yr BP ($r = 0.57$; $p<0.05$), supporting an eolian origin of the Ca in LH sediments. Although we cannot exclude other nearby Ca sources or changes in the source of African dust (Moreno et al., 2006), the 85% of dust reaching southern Iberia derives from the Sahara (Morales-Baquero and Pérez-Martínez, 2016; Jiménez et al., 2018). For instance, enrichment in heavy minerals such as zircon and palygorskite has previously been used as an eolian proxy in the western Mediterranean (e.g. Combourieu Nebout et al., 2002; Rodrigo-Gámiz et al., 2011, 2015). High concentrations of Ca in other lacustrine systems is usually associated with biogenic sources when anti-correlated with terrigenous elements (Yuan, 2017). Nevertheless, elevated Ca in the LH record is linked with detrital elements, as shown by PC1, where Ca is associated with K and Al (Fig. 5a). Therefore, Ca/Al and Ca/Ti ratios are used in the LH record as Saharan eolian input proxies.

Elemental ratio variations, such as the ratios K/Al and K/Ti indicating fluvial input and the ratios Zr/Al or Zr/Th indicating aridity and eolian input, have been previously interpreted in Alboran Sea marine records as well as in southern Iberia lake records (Martín-Puertas et al., 2010; Nieto-Moreno et al., 2011, 2015; Rodrigo-Gámiz et al., 2011; Jiménez-Espejo et al., 2014; Martínez-Ruiz et al., 2015; García-Alix et al., 2017, 2018). Thus, the integration of both palynological data and geochemical ratios used as detrital input from LH have allowed the reconstruction of the palaeoclimate and palaeoenvironmental history in the Sierra Nevada during the Holocene.

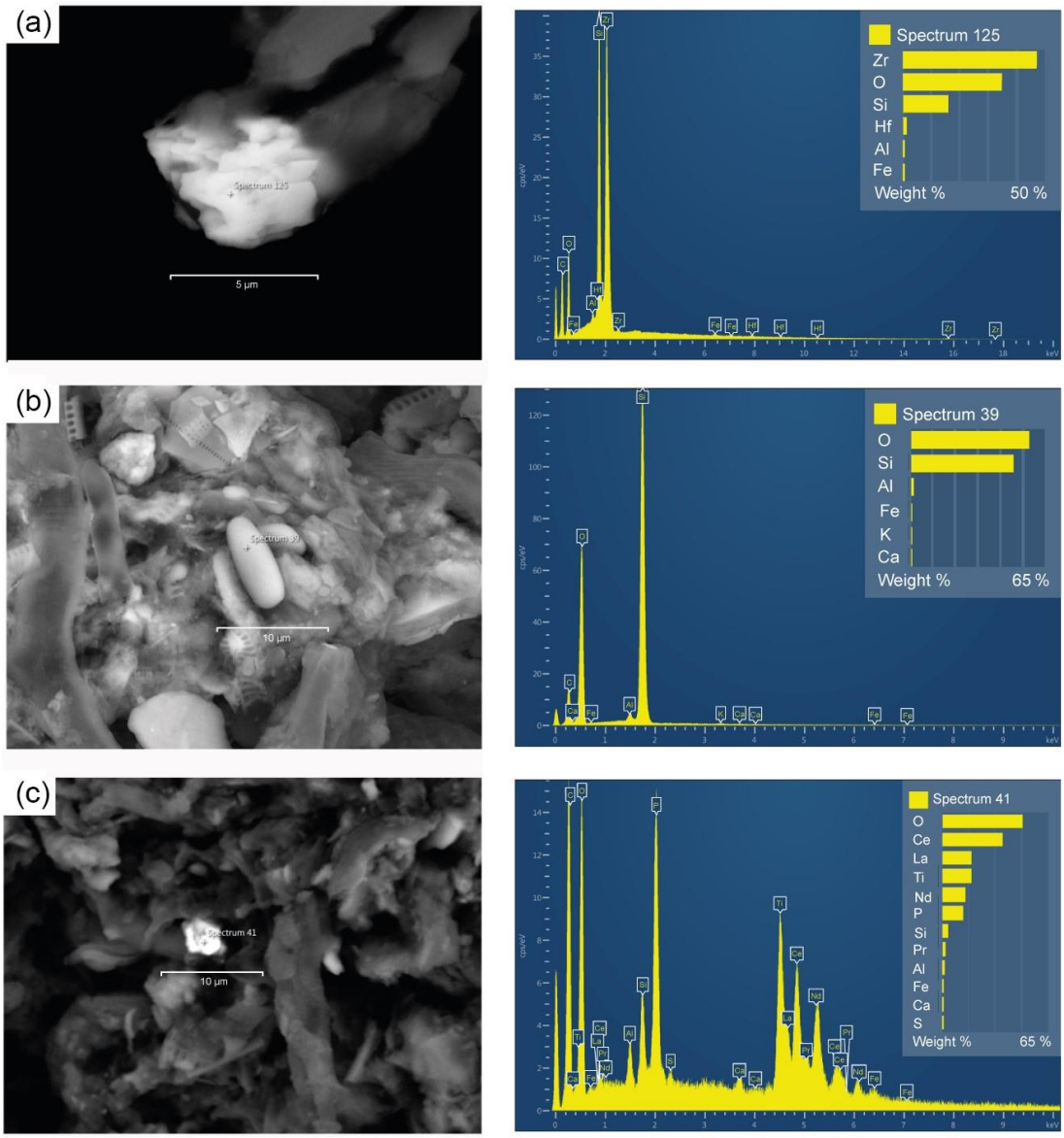

Figure 6. Electron backscatter diffraction microphotographs of the Laguna Hondera record with clearer colours representing heavier minerals. The dendrograms represent the elemental composition of each mineral. (a) Zircon, with high Zr content; (b) rounded quartz related with eolian transport; (c) monazite, with high REE content.

5.1 Holocene palaeoclimate and palaeoenvironmental history

5.1.1 Early and mid-Holocene humid conditions (10 800–7000 cal yr BP)

The wettest conditions are recorded during the early Holocene in the Sierra Nevada. This is shown in the LH record by the highest K/Al ratio and MS values, and the low values in Zr/Al, Ca/Al and Ca/Ti ratios, suggesting that runoff dominated over eolian processes at this time (zone LH-1; Fig. 7) and agreeing with previous studies in the area (Anderson

et al., 2011; Jiménez-Moreno and Anderson, 2012; García-Alix et al., 2012; Jiménez-Espejo et al., 2014).

Unfortunately, the pollen record from LH during this interval is insufficient to confirm this interpretation, due to the high detrital sediment composition and low organic content, as shown by the low MS values and low pollen preservation.

An early Holocene humid stage is noticed in other nearby sites, such as the south-facing Laguna de Río Seco (LdRS; Fig. 1) (Anderson et al., 2011), when the highest lake level of the Holocene occurred. This is also coeval with the dominance of arboreal species such as *Pinus* as well as aquatic and wetland plants (Anderson et al., 2011). Low eolian input, noted by geochemical ratios, is also recorded in LdRS during this interval (Jiménez-Espejo et al., 2014). Further indications of elevated humidity come from the north-facing Borreguil de la Virgen (BdlV) (see Fig. 1), which is dominated by an AP assemblage and a high occurrence of aquatic algae *Pediastrum* along with a higher lake level (Jiménez-Moreno and Anderson, 2012).

Although the preponderance of evidence accumulated for the early Holocene suggests overall humid conditions, at least three relatively arid periods are identified with the geochemical data in the LH record (Fig. 7). The first arid period occurred between ~ 9600 and 9000 cal yr BP, the second occurred ~ 8200 cal yr BP and the third around 7500 cal yr BP.

The first arid event is characterized in LH by a decrease in K/Al and K/Ti ratios and MS, resulting from the lower runoff input with the concomitant change to a more peaty composition. This event could be correlated with a dryness event recorded in the Siles Lake record (Carrion, 2002) at ~ 9300 cal yr BP noticed by an increase in *Pseudoschizaea*, which was coeval with a minor decrease in arboreal pollen also recorded in several sites in northern Iberia (Iriarte-Chiapusso et al., 2016). At marine site ODP 976 (Fig. 1; Combourieu-Nebout et al., 2009) a decrease in deciduous *Quercus* occurred between 9500 and 9200 cal yr BP, indicating a rapid excursion towards arid conditions (Fig. 7). The speleothem record of Corchia Cave also shows dryer conditions during this interval (Fig. 7; Regattieri et al., 2014) In addition, a decrease in fluvial input in the Southern Alps and an aridification phase in southeastern France and southeastern Iberia have been similarly recorded (Jalut et al., 2000).

The second dry event recorded at ~ 8200 cal yr BP is depicted in the LH record by a negative peak in K/Ti and K/Al ratios, and by the onset of a trend toward peatier lithology, as evidenced by the MS profile. This event is not recognized in LH record as clearly as the 9500 cal yr BP and the 7500 cal yr BP dry events. A decrease in *Pinus* percentage is observed in the nearby LdRS (Anderson et al., 2011), while a forest decrease is recorded in the Alboran Sea sites MD95-2043 and ODP 976. In several records from northwestern Iberia, a decrease in arboreal pollen also occurred at this time (Iriarte-Chiapusso et al., 2016).

The 8.2 ka event was the most rapid climate change towards cooler conditions occurred during the Holocene. It was defined in Greenland ice cores by minimum values of $\delta^{18}O$ and affected the North Atlantic basin and the Mediterranean area (Alley et al., 1997; Rasmussen et al., 2007; Wiersma et al., 2011). Recent simulations point to a freshwater input in the North Atlantic which could slow down the North Atlantic Deep Water (NADW) formation, preventing the heat transport over the Northern Hemisphere (Wiersma et al., 2010, 2011; Young et al., 2013).

Another dry event is recorded in LH at ~ 7500 cal yr BP, evidenced by the higher peat content in the sediment, as well as by the lower MS values and a relative minimum in the K/Ti ratio. A relative AP minimum also occurred in LH at this time. This short-lived event is depicted as sharper than the 8200 cal yr BP event in several sites in southern Iberia and the Alboran Sea: in the Padul record, located at 725 m a.s.l. in the lower part of the Sierra Nevada, a decrease in both evergreen and deciduous *Quercus* is interpreted as a dry and cold event (Ramos-Román, 2018; Ramos-Román et al., 2018a); forest expansion in Guadiana valley during the early to mid-Holocene is interrupted by a xeric shrublands development between 7850 and 7390 cal yr BP (Fletcher et al., 2007); in the Alboran Sea a decrease in deciduous *Quercus* is registered at site MD95-2043; at site 300G a decrease in winter and summer temperatures is also recorded during this interval (Jiménez-Espejo et al., 2008); in Pergusa lake (southern Italy) a trend toward arid conditions began at ~ 7500 cal yr BP (Magny et al., 2012); in Corchia Cave an arid excursion occurred at ~ 7500 cal yr BP within an overall humid period between 8300 cal yr BP and 7200 cal yr BP (Fig. 7; Regattieri et al., 2014).

Importantly, these arid events recorded in LH at 9600 to 9000 and 8200 cal yr BP are coeval with the ice-rafted debris events 6 and 5 defined by Bond et al. (1997) for the North Atlantic.

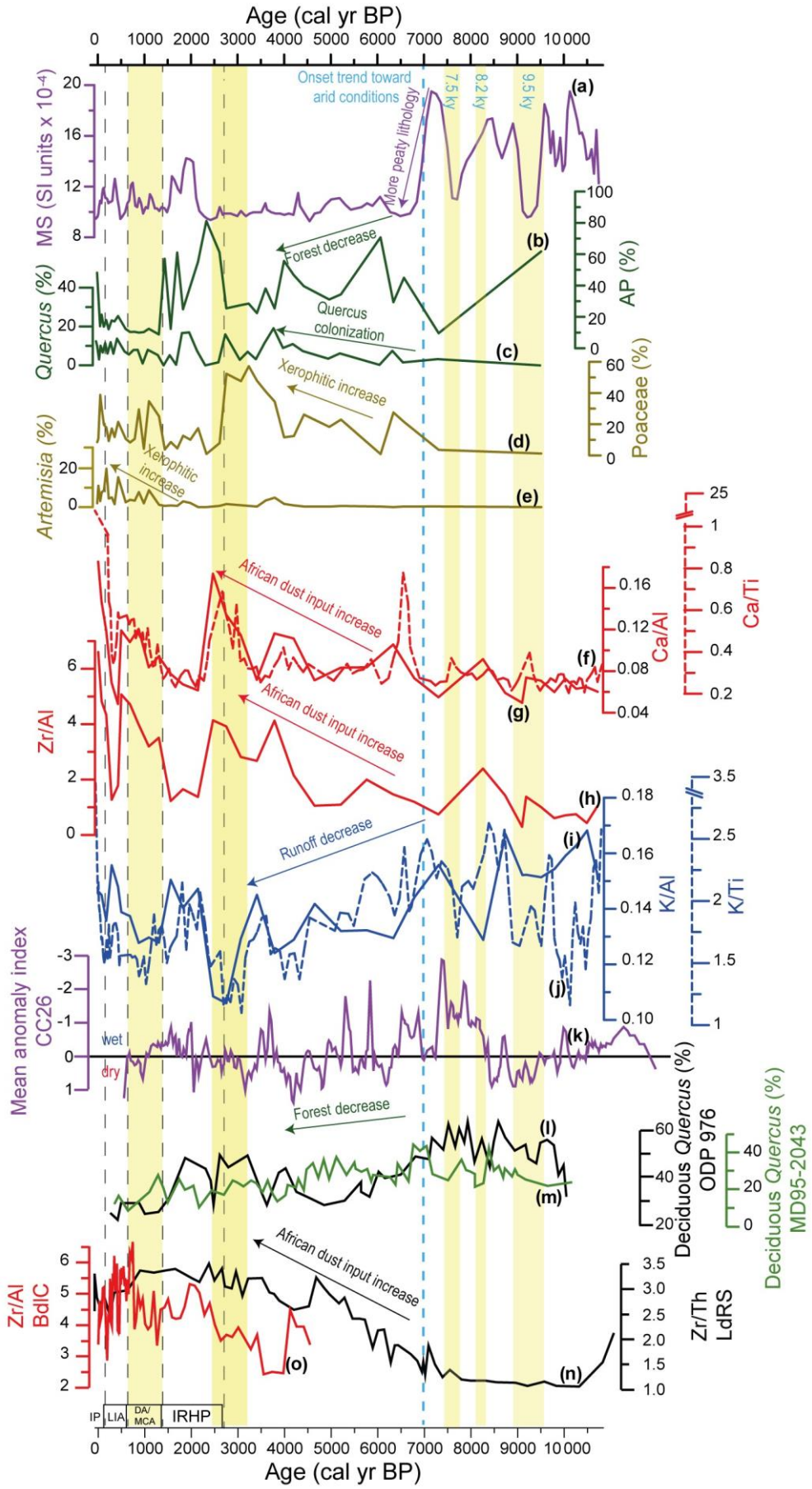
Age (cal yr BP)
0 1000 2000 3000 4000 5000 6000 7000 8000 9000 10000
Onset trend toward arid conditions
7.5 ky
8.2 ky
9.5 ky
(a)
MS (SI units x 10⁻⁴)
20 16 12 8
More peaty lithology
100 80 60 40 20 0
AP (%)
Forest decrease
(b)
Quercus (%)
40 20 0
Quercus colonization
(c)
60 40 20 0
Poaceae (%)
Xerophitic increase
(d)
Artemisia (%)
20 0
Xerophitic increase
(e)
25 1 0.8 0.6 0.4 0.2
Ca/Ti
African dust input increase
0.16 0.12 0.08 0.04
Ca/Al
(f)
(g)
Zr/Al
6 4 2 0
African dust input increase
(h)
Runoff decrease
(i)
3.5 2.5 2 1.5 1
K/Ti
0.18 0.16 0.14 0.12 0.10
K/Al
(j)
(k)
Mean anomaly index CC26
-3 -2 -1 0 1
wet
dry
Forest decrease
(l)
(m)
60 40 20
Deciduous Quercus (%) ODP 976
40 20 0
Deciduous Quercus (%) MD95-2043
Zr/Al BdIC
6 5 4 3 2
African dust input increase
(o)
(n)
3.5 3.0 2.5 2.0 1.5 1.0
Zr/Th LdRS
IP
LIA
DA/ MCA
IRHP
0 1000 2000 3000 4000 5000 6000 7000 8000 9000 10000
Age (cal yr BP)

5.1.2 Middle and late Holocene (~7000–2600 cal yr BP)

The middle and late Holocene in the southern Iberian Peninsula is characterized by a trend towards more arid conditions (Jalut et al., 2009; Anderson et al., 2011; Rodrigo-Gámiz et al., 2011; Jiménez-Moreno and Anderson, 2012; Jiménez-Espejo et al., 2014). In the LH record an abrupt decrease in the MS values indicates a lithological change to more peaty sedimentation at ~ 7000 cal yr BP. Similarly, a decrease in the K/Al and K/Ti ratios points to a transition to less humidity and runoff (Fig. 7). The *Quercus* percentage increases at this time, partially replacing the *Pinus*, which make up most of the AP during the record. A progressive increasing trend in eolian input from the Sahara (Zr/Al, Ca/Al and Ca/Ti ratios) is observed around 5500–6500 cal yr BP (Fig. 7), also pointing to an increase in aridity in the area. This change coincides with regional increases in the Zr/Th ratio (equivalent to Zr/Al ratio) and *Artemisia* pollen, with decreases in *Betula* and *Pinus* in the LdRS record (Anderson et al., 2011; Jiménez-Espejo et al., 2014) and in *Pinus* in the BdlV record (Jiménez-Moreno and Anderson, 2012). Rodrigo-Gámiz et al. (2011) and Jiménez-Espejo et al. (2014) observed similar geochemical patterns in western Mediterranean marine records and in LdRS, with a decline in fluvial input and a decline in surface runoff, respectively. The same pattern is noticed in marine pollen records MD95-2043 and ODP 976 (Fletcher and Sanchez Goñi, 2008; Combourieu Nebout et al., 2009; Fig. 7). Contemporaneously, aridity is also suggested from speleothem data around the Mediterranean area: at El Refugio cave, a hiatus in the speleothem growing rate occurred between 7300 and 6100 cal yr BP (Walczak et al., 2015), which is coeval with a drop in $\delta^{18}O$ in Soreq (Israel) and Corchia (Italy; CC26; Figs. 1 and 7) caves at 7000 cal yr BP (Bar-Matthews et al., 2000; Zanchetta et al., 2007; Regattieri et al., 2014). Also

Figure 7. Comparison between the MS data (in SI units $\times 10^{-4}$), the most important pollen taxa and geochemical proxies from Laguna Hondera (LH) record, with nearby paleoclimate records. (a) LH magnetic susceptibility (MS) record; (b) arboreal pollen (AP) percentage from LH; (c) *Quercus* percentage from LH; (d) Poaceae percentage from LH; (e) *Artemisia* percentage from LH; (f) Ca/Ti (XRF) ratio from LH in dashed line; (g) Ca/Al ratio from LH; (h) Zr/Al ratio from LH; (i) K/Al ratio from LH; (j) K/Ti (XRF) ratio from LH in dashed line; (k) mean anomaly index from CC26 record (Corchia cave; Regattieri et al., 2014); (l) deciduous *Quercus* from ODP 976 record (Alboran Sea; Combourieu-Nebout et al., 2009); (m) deciduous *Quercus* from MD95-2043 record (Alboran Sea; Fletcher and Sanchez-Goñi, 2008); (n) Zr/Th ratio from Laguna de Río Seco (LdRS) (Jiménez-Espejo et al., 2014; García-Alix et al., 2018); (o) Zr/Al ratio from Borreguil de la Caldera (BdlC) (García-Alix et al., 2017; 2018). Yellow bands indicate more arid intervals. Dark dashed lines are used for separating the different current era periods: IRHP: Iberian Roman Humid Period; DA: Dark Ages; MCA: Medieval Climate Anomaly; LIA: Little Ice Age; IP: Industrial Period. Blue dashed line indicates the onset of the trend toward arid conditions.

at ~ 7000 cal yr BP a decreasing trend in the deciduous/sclerophyllous pollen ratio occurred in southeastern France and Iberia (Jalut et al., 2000) and at continental sites around the Mediterranean Sea (Jalut et al., 2009). In addition, very low lake levels were recorded in the Sahara–Sahel Belt (Liu et al., 2007) and in the Southern Alps (Magny et al., 2002).

Enhanced arid conditions are observed in the LH record between 4000 and 2500 cal yr BP, interpreted through a decline in AP and a Poaceae maximum. Also, a surface runoff minimum and an increase in eolian input proxies took place between 3500 and 2500 cal yr BP (zone LH-3). In Corchia Cave an arid interval was recorded at ~ 3100 cal yr BP (Regattieri et al., 2014), coeval with another one observed globally and described by Mayewski et al. (2004) between 3500 and 2500 cal yr BP. Nevertheless, this period is not climatically stable; fluctuations are observed in K/Ti, K/Al, Ca/Ti, Ca/Al and Zr/Al ratios. Furthermore, peaks in *Quercus* are recorded in LH, LdlM and ODP 976 sites at ~ 3900 cal yr BP and ~ 3100 cal yr BP, when AP in LH decreases (Combourieu Nebout et al., 2009; Jiménez-Moreno et al., 2013). This fact is a priori contradictory, but could be explained by altitudinal displacements of the tree taxa such as *Quercus* in the oromediterranean belt due to the climatic variability that occurred along this interval (Carrión, 2002). During warmer periods, this species would be displaced towards higher elevation and the influence of *Quercus* pollen in the Sierra Nevada would be larger; this could explain relative higher *Quercus* percentages in LdlM, LH and also in the ODP 976 record. The same relationship between *Quercus* and *Pinus* is observed when comparing the BdlC and Padul records, located nearby to each other but with a large altitude difference (BdlC ~ 2992 m a.s.l.; Padul ~ 725 m a.s.l.; Ramos-Román, 2018), where it is also likely linked to movements in the oromediterranean belt (Ramos-Román, 2018). These altitudinal displacements of the tree taxa have been previously related to temperature changes in other southern Iberian records, suggesting an ecological niche competition between *Pinus* and *Quercus* species at middle altitudes (see Carrión et al., 2002 for a revision).

5.1.3 Iberian Roman Humid Period (IRHP; ~2600–1450 cal yr BP)

Because there is no consensus in the literature about the chronology for the main climatic stages during the last 2000 years (Muñoz-Sobrino et al., 2014; Helama et al., 2017), here

we follow the chronology proposed by Moreno et al. (2012): Dark Ages (DA, 1450–1050 cal yr BP); Medieval Climate Anomaly (MCA, 1050–650 cal yr BP); and LIA (650–150 cal yr BP). Another climatic stage precedes the DA – the Iberian Roman Humid Period (IRHP, 2600– 1600 cal yr BP), originally described by Martín-Puertas et al. (2008). However, in the LH record we have established different IRHP limits (2600–1450), based according to the pollen zonation (Fig. 3) and coinciding with the DA onset defined by Moreno et al. (2012).

The IRHP has been described as the wettest period in the western Mediterranean from proxies determined both in marine and lacustrine records during the late Holocene (Reed et al., 2001; Fletcher and Sanchez-Goñi 2008; Combourieu Nebout et al., 2009; Martín-Puertas et al., 2009; Nieto-Moreno et al., 2013; Sánchez-López et al., 2016). A relative maximum in AP occurred in the LH record during this time, also indicating forest development and relative high humidity during the late Holocene in the area (zone LH4; Fig. 7). This is further supported by high K/Al and K/Ti ratios and MS values, indicating high detrital input in the drainage basin, a minimum in Poaceae and low Saharan eolian input (low Ca/Al, Ca/Ti and Zr/Al ratios) (Fig. 7). Fluvial elemental ratios have also shown an increase in river runoff in Alboran Sea marine records (Nieto-Moreno et al., 2011; Rodrigo-Gámiz et al., 2011). This humid period seems to be correlated with a solar maximum (Solanki et al., 2004) and persistent negative NAO conditions (Olsen et al., 2012), which could have triggered general humid conditions in the Mediterranean. However, in the LH record fluctuation in AP between 2300 and 1800 cal yr BP occurred, pointing to arid conditions at that time. This arid event also seems to show up in BdlC, with a decrease in AP between 2400 and 1900 cal yr BP (Ramos-Román et al., 2016) and in Zoñar Lake, with highly chemically concentrated water and gypsum deposition between 2140 and 1800 cal yr BP (Martín-Puertas et al., 2009). In Corchia Cave a rapid excursion towards arid condition is recoded at ~ 2000 cal yr BP (Regattieri et al., 2014) (Fig. 7). As we explained in Sect. 5, the apparently anomalous percentages of *Pinus* at this time could be justified by upward migrations of the oromediterranean forest species triggered by higher temperatures and/or the high pollen production and dispersal of *Pinus*. Nevertheless, we cannot exclude others factors that could influence the pollen transport such as the wind energy, mostly controlled by the NAO in the southern Iberia. A persistent negative NAO phase, as occurred during the IRWP (Sánchez-López et al., 2016), would have triggered more humid conditions and higher westerlies influence over southern

Europe. The higher occurrence of *Pinus* in the surrounding area due to the favorable climatic conditions, along with the higher wind energy over the Sierra Nevada and the characteristics of bisaccate pollen, could have overstated the percentages of *Pinus* in our record.

5.1.4 Dark Ages and Medieval Climate Anomaly (DA, MCA; 1450–650 cal yr BP)

Predominantly arid conditions, depicted by high abundance of herbaceous and xerophytic species and an AP minimum in the LH record, are shown for both DA and MCA (zone LH-5; Fig. 7). This is further supported in this record by an increase in Saharan eolian input Ca/Al, Ca/Ti and Zr/Al ratios, and by a decrease in surface runoff, indicated by the K/Al and K/Ti ratios (zone LH-5; Fig. 7). These results from LH agree with climate estimations of overall aridity modulated by a persistent positive NAO phase during this period (Trouet et al., 2009; Olsen et al., 2012), also previously noted by Ramos-Román et al. (2016) in the area (Fig. 7).

Generally arid climate conditions during the DA and the MCA have also been previously described in the LdlM and BdlC records, shown by a decrease in mesophytes and a rise of xerophytic vegetation during that time (Jiménez-Moreno et al., 2013; Ramos-Román et al., 2016). Several pollen records in south and central Iberian Peninsula also indicate aridity during the DA and MCA, for example grassland expanded at Cañada de la Cruz, while in Siles Lake a lower occurrence of woodlands occurred (Carrión, 2002). Also, in Cimera Lake, low lake level and higher occurrence of xerophytes were recorded (Sánchez-López et al., 2016). Arid conditions were depicted in Zoñar Lake by an increase in *Pistacia* and heliophytes (i.e. Chenopodiaceae) and lower lake level (Martín-Puertas et al., 2010). Similar climatic conditions were noticed in the marine records MD95-2043 and ODP 976 in the Alboran Sea through decreases in forestation (Fletcher and Sánchez-Goñi, 2008; Combourieu Nebout et al., 2009; Fig. 7). Arid conditions in Basa de la Mora (northern Iberian Peninsula) occurred during this time, characterized by maximum values of *Artemisia*, and a lower development of deciduous *Quercus* and aquatic species such as *Potamogeton*, also indicating low lake water levels (Moreno et al., 2012). Arid conditions were also documented by geochemical data in marine records from the Alboran Sea (Nieto-Moreno et al., 2013, 2015), in the Gulf of Lion and south of Sicily (Jalut et al., 2009). Aridity has also been interpreted for central Europe using lake-level reconstructions (Magny, 2004) and in speleothems records in central Italy (Regattieri et

al., 2014). Nevertheless, wetter conditions were recorded during the DA in some records from northern Iberian Peninsula (Sánchez-López et al., 2016). Humid conditions depicted by higher lake level and less salinity occurred in Arreo Lake (Corella et al., 2013). In Sanabria Lake, the dominance of planktonic diatom *Aulacoseira subborealis* is interpreted as relative humid conditions at that time (Jambrina-Enríquez et al., 2014). This heterogeneity in the climate during the DA is due to the existence of a north–south humidity gradient in the Iberian Peninsula (Sánchez-López et al., 2016). Nonetheless, this gradient seems to be more diffuse during the MCA, which is characterized as an overall arid period in the entire Iberian Peninsula (Morellón et al., 2012; Sánchez-López et al., 2016).

5.1.5 Little Ice Age (LIA; 650–150 cal yr BP)

The LIA is interpreted as an overall humid period in the LH record. This is indicated by higher AP values than during the MCA, low Saharan dust input (low Ca/Al, Ca/Ti and Zr/Al ratios), a decrease in herbs (Poaceae) and high values in the K/Al and K/Ti ratios indicating enhanced runoff (zone LH-6A; Fig. 7). An increase in fluvially derived proxies has been previously documented in other Iberian terrestrial records such as Basa de la Mora Lake (Moreno et al., 2012), Zoñar Lake (Martín-Puertas et al., 2010) or Cimera Lake (Sánchez-López et al., 2016) and marine records from the Alboran Sea basin (Nieto-Moreno et al., 2011, 2015). Lake-level reconstructions in Estanya Lake, in the Pre-Pyrenees (northeastern Spain), have shown high water levels during this period (Morellón et al., 2009, 2011), supporting our humid climate inferences. Nevertheless, fluctuations in *Artemisia* during the LIA suggest an unstable period in the Sierra Nevada (Fig. 8), in agreement with the high variability in *Pinus*, *Artemisia* and water availability deduced from recent high-resolution studies in the neighbouring BdlC and BdlV records (Ramos-Román et al., 2016; García-Alix et al.,

2017). The same pattern occurred in several Iberian records (Oliva et al., 2018), revealing that the LIA was not a climatically stable period and many oscillations at a short timescale occurred.

A persistently negative NAO phase, although with high variability, occurred during this period (Trouet et al., 2009), which could explain the overall humid conditions observed in southern Europe. As in the early Holocene arid events, solar variability has been

hypothesized as the main forcing of this climatic event (Bond et al., 2001; Mayewski et al., 2004; Fletcher et al., 2013; Ramos-Román et al., 2016).

5.2 Industrial Period (IP; 150 cal yr BP–present)

The IP is characterized by a sharp increase in the Pb/Al ratio in the LH record (Fig. 8), suggesting more mining, fossil fuel burning or other human industrial activities (García-Alix et al., 2013, 2017). This is coeval with a rise in AP, which is also related to human activities such as *Olea* commercial cultivation at lower elevations around the Sierra Nevada or *Pinus* reforestation in the area (Figs. 7 and 8; Valbuena-Carabaña et al., 2010; Anderson et al., 2011). The same pattern has also been observed in other records from the Sierra Nevada (Jiménez-Moreno and Anderson, 2012; García-Alix et al., 2013; Ramos-Román et al., 2016), in Zoñar Lake and in the Alboran Sea records (Martín-Puertas et al., 2010). In addition, a progressively increasing trend in Zr/Al and Ca/Al ratios is observed during the last two centuries, which could be related to increasing local aridity and/or anthropogenic desertification, but also with a change in the origin and/or composition of the dust reaching the lake (Jiménez-Espejo et al., 2014), likely related to the beginning of extensive agriculture and the concomitant desertification in the Sahel region (Mulitza et al., 2010).

5.3 Significance of the eolian record from Laguna Hondera

Saharan dust influence over current alpine lake ecosystems is widely known (Morales-Baquero et al., 2006a, b; Pulido-Villena et al., 2008b; Mladenov et al., 2011, Jiménez et al., 2018). The most representative elements of Saharan dust in LH record are Fe, Zr and Ca, as shown by the PC2 loading (Fig. 5), where Ca and Fe directly affect the alpine lake biogeochemistry in this region (Pulido-Villena et al., 2006, 2008b, Jiménez et al., 2018). Zirconium is transported in heavy minerals in eolian dust (Govin et al., 2012) and has largely been used in the Iberian Peninsula and the western Mediterranean as an indicator of eolian Saharan input (Moreno et al., 2006; Nieto-Moreno et al., 2011; Rodrigo-Gámiz et al., 2011; Jiménez-Espejo et al., 2014; Martínez-Ruiz et al., 2015, and references therein). High Zr content has also been identified in present aerosols at high elevations in the Sierra Nevada (García-Alix et al., 2017). Considering the low weatherable base cation reserves in the LH bedrock catchment area, calcium is suggested to be carried by

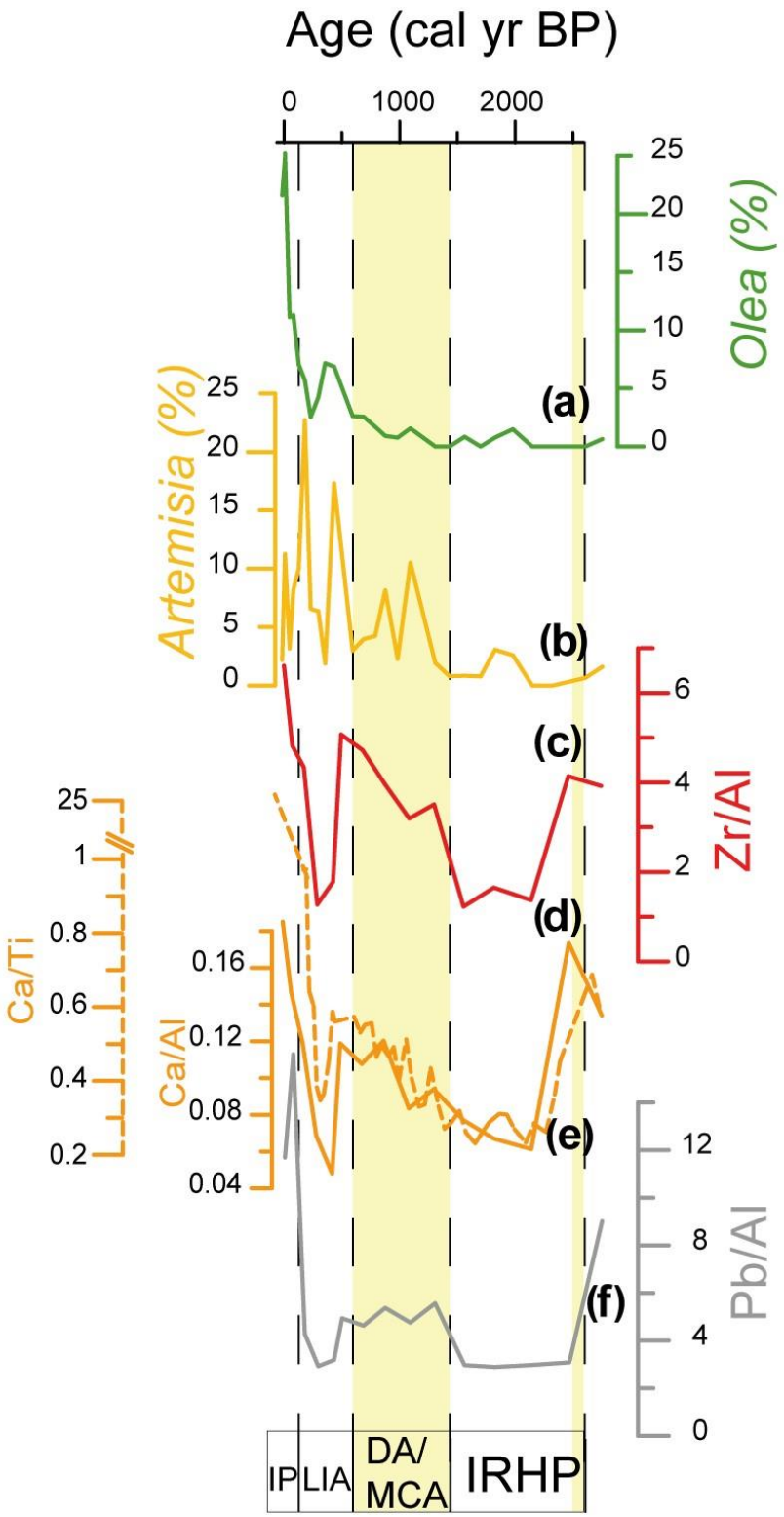

Figure 8. Comparison of geochemical proxies with pollen taxa, related to anthropogenic impact for the last ~ 2600 cal yr BP. (a) *Olea* percentage from LH; (b) *Artemisia* percentage from LH record; (c) Zr/Al ratio from LH; (d) Ca/Al ratio from LH; (e) Ca/Ti (XRF) ratio from LH in dashed line; (f) Pb/Al ratio from LH. Yellow bands indicate more arid intervals. Dark dashed lines are used for separating the different current era periods: IRHP: Iberian Roman Humid Period; DA: Dark Ages; MCA: Medieval Climate Anomaly; LIA: Little Ice Age; IP: Industrial Period.

atmospheric input of Saharan dust into alpine lakes in the Sierra Nevada (Pulido-Villena et al., 2006, see discussion; Morales-Baquero et al., 2013). This is the first time that the Ca signal is properly recorded in a long record from the Sierra Nevada. This could be explained by higher evaporation rates at this site promoting annual lake desiccation that could prevent Ca water column dissolution and using or recycling by organism, preserving better the original eolian signal. These elements have an essential role as nutrients, becoming winnowed and recycled rapidly in the oligotrophic alpine lake ecosystem (Morales-Baquero et al., 2006b). This phenomenon has also been observed in other high-elevation lakes where the phytoplankton is supported by a small and continually recycled nutrient pool (e.g. Sawatzky et al., 2006).

The SEM observations further confirm the presence of Saharan dust in the lake sediments from LH and the occurrence of Zircon, the main source of eolian Zr, which is relatively abundant (Fig. 6a). Quartz with rounded morphologies (eolian erosion) are also frequent (Fig. 6b) in the uppermost part of the record as well as REE rich minerals, such as monazite, which is typical of the Saharan–Sahel Corridor area (Moreno et al., 2006) (Fig. 6c). In addition, the fact that the highest correlation between Ca and Zr occurred after ~ 6300 cal yr BP, (r = 0.57, p<0.005), along with the SEM observation and the low availability of Ca in these ecosystems, could suggest that the beginning of Saharan dust arrivals to the lake, including both elements, took place at this time, giving rise to the present way of nutrient inputs in these alpine lakes (Morales-Baquero et al., 2006b; Pulido-Villena et al., 2006). The onset of Saharan dust input into southern Iberia occurred prior to the end of the African Humid Period (AHP; ~ 5500 cal yr BP; deMenocal et al., 2000), as previously noticed in the nearby LdRS (Jiménez-Espejo et al., 2014) and in the Alboran Sea (Rodrigo-Gámiz et al., 2011). This could suggest a progressive climatic deterioration in northern Africa, which culminated with the AHP demise and the massive Saharan dust input recorded in all records in the Sierra Nevada at ~ 3500 cal yr BP (Fig. 7).

6 Conclusions

The multi-proxy paleoclimate analysis from LH has allowed the reconstruction of the vegetation and climate evolution in the Sierra Nevada and southern Iberia during the Holocene, and the possible factors that have triggered paleoenvironmental changes.

Climate during the early Holocene was predominantly humid, with two relatively arid periods between 10000 and 9000 and at ~ 7500 cal yr BP, resulting in less detrital inputs and a change to more peaty lithology. The onset of an arid trend took place around 7000 cal yr BP, decreasing the runoff input in the area. A significant increase in eolian-derived elements occurred between 6300 and 5500 cal yr BP, coinciding with the AHP demise. An arid interval is recorded between 4000 and 2500 cal yr BP, with a vegetation assemblage dominated by xerophytes.

Relative humid conditions occurred in the area between 2500 and 1450 cal yr BP, interrupting the late Holocene aridification trend. This humid interval was characterized by expansion of forest vegetation, high runoff input, and a more clayey lithology. However, during the DA and the MCA (1450–650 cal yr BP) there was enhanced eolian input and an expansion of xerophytes, indicating increased arid conditions. In contrast, the LIA (650–150 cal yr BP) was characterized by predominant humid conditions as indicated by high runoff and low eolian input. The IP (150 cal yr BP–present) is characterized in the LH record by the highest values of the Pb/Al ratio, probably indicating fossil fuel burning by enhanced mining and metallurgy industry. The increase in human activities at this time in this area can also be deduced by the expansion of *Olea* cultivation at lower elevations and *Pinus* reforestation in the area.

Importantly, the LH record shows a unique and exceptional Ca signal derived from eolian input (high Ca–Zr correlation) during the past ~ 6300 years in the Sierra Nevada. The good preservation of the Ca record might have been favoured by the high evaporation and the low lake depth, which could have prevented Ca column water dissolution and its re-use by organisms. Our record indicates that present-day inorganic nutrient input from Sahara was established 6300 years ago and lasted until the present, with variations depending on the prevailing climate.

IV

STABLE HYDROGEN AND CARBON ISOTOPE RECORDS OF PLANT WAX *N*-ALKANES FROM THE ALBORAN SEA BASIN (WESTERNMOST MEDITERRANEAN) INDICATE PRECIPITATION AND SEDIMENT DYNAMICS DURING THE LAST DEGLACIATION

IV. Stable hydrogen and carbon isotope records of plant wax *n*-alkanes from the Alboran Sea basin (westernmost Mediterranean) indicate precipitation and sediment dynamics during the last deglaciation

Jose Manuel Mesa-Fernández[1], Marta Rodrigo-Gámiz[2], Francisca Martínez-Ruiz[1], Antonio García-Alix[1,2], Marcel T. J. van der Meer[3]

[1] Instituto Andaluz de Ciencias de la Tierra (IACT), CSIC-UGR, Avenida de las Palmeras 4, 18100, Armilla, Granada, Spain

[2] Departamento de Estratigrafía y Paleontología, Universidad de Granada (UGR), Avda. Fuente Nueva s/n, 18071, Granada, Spain

[3] Department of Marine Microbiology and Biogeochemistry, Royal Netherlands Institute for Sea Research (NIOZ), Den Burg, Texel, The Netherlands

Correspondence to: Jose Manuel Mesa-Fernández (jmesa@ugr.com)

Under review in *Palaeogeography, Palaeoclimatology, Palaeoecology*

Impact factor: 3.32

Abstract

Leaf wax derived *n*-alkane stable carbon ($\delta^{13}C_{wax}$) and hydrogen ($\delta^{2}H_{wax}$) isotope records from marine records from in the westernmost Mediterranean (Alboran Sea basin) have been studied to reconstruct hydrological conditions and sediment input for the last 20 ka in this region. Despite the close proximity between the two sites, the sediment cores are located in different Alboran Sea basins, and terrestrial derived-organic matter in the cores come from different catchment areas. The Fuengirola and Guadalhorce rivers influence the western Alboran site, while the Andarax river influences the eastern Alboran site. The $\delta^{13}C_{wax}$ profiles suggest that long-chain *n*-alkanes at both locations are mainly supplied by the aforementioned rivers, and therefore, reflected differences in the vegetation of their catchment areas as well as in sediment transport dynamics. In both records, short-term variability in the $\delta^{13}C_{wax}$ signal responds to humidity changes, while long-term variability suggests changes in the organic matter source as a consequence of sea level variations. Prior to the sea level rise triggered by the melt water pulse between 11.5-8.8 cal ka BP, the $\delta^{13}C_{wax}$ values suggest that the *n*-alkanes were mainly derived from vegetation close to the coast, and transported through the canyons by rivers or by wave action. After 11.2 cal ka BP, the sea level rise promoted the transport of terrestrial organic matter as dense sediment fluxes directly deposited in the canyon during periods of enhanced precipitation. During these humid periods, the coastal and the riparian vegetation was mixed with high-altitude vegetation adapted to more arid conditions. In the western Alboran site, a higher $\delta^{13}C_{wax}$ values suggest drier conditions reflecting major input of terrestrial organic matter derived by the Guadalhorce river, whose catchment basin comprises high-altitude vegetation. Despite these dissimilarities of the $\delta^{13}C_{wax}$ values between western and eastern Alboran records, the $\delta^{2}H_{wax}$ values depicted similar trends at both sites, suggesting that the $\delta^{2}H_{wax}$ rather responds to regional factors. More negative $\delta^{2}H_{wax}$ values were recorded during periods of enhanced winter precipitation pointing to a higher precipitation amount effect and/or an isotopically-depleted Atlantic moisture source. In contrast, during periods of relatively lower winter precipitation, the higher $\delta^{2}H_{wax}$ values point to a higher contribution from a moisture source with a relatively high $\delta^{2}H$ signature such as the Mediterranean Sea.

1. Introduction

The Mediterranean region is located between the tropical and mid-latitude climate belts, and its climate is sensitive to high and low latitude dynamics, but there are differences between the eastern and the western basins (Trigo et al., 2002; Lionello et al., 2006; Lionello et al., 2012). While the climate in the eastern Mediterranean basin is highly influenced by internal Mediterranean climate dynamics and the African and Asian Monsoon, the western Mediterranean basin is highly dependent on North Atlantic climate dynamics (Lionello et al., 2006). Recent studies have also highlighted the role of the western Mediterranean Sea as source for precipitation at both short-term (Celle-Jeanton et al., 2001; Goodess and Jones, 2002; Araguas-Araguas and Díaz-Tejeiro, 2005; Martín-Vide et al., 2005; Gimeno et al., 2010) and long-term time scales (Schirrmacher et al., 2020; García-Alix et al., 2021; Toney et al., 2020). This Mediterranean-derived precipitation is primarily registered in the western Mediterranean region during the warm season and can be occasionally torrential (Romero et al., 1998; Gimeno et al., 2010).

The interplay between North Atlantic and Mediterranean climate dynamics, which drives the present-day climate in the western Mediterranean, have also controlled the precipitation and the vegetation in southern Iberia and northern Africa during the last 20 ka (Cacho et al., 2001; Zielhofer et al., 2019; García-Alix et al., 2021). This high-low latitude teleconnection has been related to the Atlantic Meridional Overturning Circulation (AMOC), which has influenced the Hadley and Farrel cell position and the intensity of the westerlies and thus the moisture transport to the Mediterranean area (Jackson et al., 2015; Sánchez-Goñi et al., 2020). Periods of enhanced meltwater input in the North Atlantic during the last 20 ka, such as the Heinrich Stadial 1 (HS1; 18-15 cal ka BP) or the Younger Dryas (YD; 13-11.7 cal ka BP) were related to AMOC reduction or collapse, colder sea surface temperatures (SST), less atmospheric moisture and enhanced westerlies, promoting cold and arid conditions in the southwestern Mediterranean (Brauer et al., 2008; Brayshaw et al., 2009; Fletcher et al., 2010; Jackson et al., 2015). Conversely, during periods of enhanced AMOC, greater heat transport to the North Atlantic and the warmer SST promoted more humid westerlies entering in the southwestern Mediterranean area (Brayshaw et al., 2009, 2010).

Nonetheless, how the Mediterranean Sea moisture pool has affected past precipitation dynamics and vegetation changes in the region remains unknown. The stable isotopic composition of precipitation can be a useful tool for discerning moisture sources and

precipitation dynamics in the Mediterranean area, since the negative water budget in the Mediterranean Sea results in isotopically-enriched moisture, while Atlantic-derived precipitation has a lower stable hydrogen and oxygen isotopic composition (Celle-Jeanton et al., 2001; Araguás-Araguás and Díaz-Tejeiro, 2005; Moreno et al., 2014).

Recently, an increasing number of studies have explored the past relationships between precipitation patterns and the hydrogen, oxygen and carbon stable isotope values at mid-latitudes deduced from speleothems, ostracods, and specific organic compounds such as long-chained *n*-alkanes (Roberts et al., 2008; Krklec and Domínguez-Villar, 2014; Moreno et al., 2014; Zielhofer et al., 2017; Pérez-Mejías et al., 2020; Schirrmacher et al., 2020; Cheddadi et al., 2021;). However, most of these studies have been performed on continental records (Schäfer et al., 2018; Cheddadi et al., 2021; García-Alix et al., 2021) or have just covered a short-time interval (Schirrmacher et al., 2020). There is an often ignored issue when these terrestrial-derived proxies are studied in marine sediments, since the influence of the sedimentary evolution of the basin can severely affect the source of the organic matter in the record (Bliedtner et al., 2020), especially when eustatic changes occurred.

The Alboran Sea basin is located in the westernmost Mediterranean and connected to the Atlantic by the Gibraltar Strait, being sensible to the interplay between past Mediterranean and Atlantic dynamics (Cacho et al., 1999). The high sedimentation rates of this basin (Comas et al., 1999) comprise sediment derived from riverine discharge and eolian dust pulses from the African margin (Fabres et al., 2002; Palanques et al., 2005). Thus, the Alboran Sea basin is the perfect location to assess the potential effects of marine dynamics in the sedimentary accumulation and evolution of the terrestrial organic matter signal. Therefore, with the aim to improve the knowledge of past precipitation patterns since the Last Glacial Maximum (LGM) in the westernmost Mediterranean and to evaluate how the sedimentary dynamics affect terrestrial derived proxy records in marine sediments, we study the stable carbon and hydrogen isotope values ($\delta^{13}C$ and $\delta^{2}H$) of long-chained *n*-alkanes in two marine sediment records from the Alboran Sea. Despite their close proximity, these sediment records are influenced by different local oceanographic configurations and sedimentary conditions (Rodrigo-Gámiz et al., 2014). We will focus on the impact of the deglacial transgression on the sedimentary long chained *n*-alkanes and the reconstruction of changes in the precipitation moisture sources.

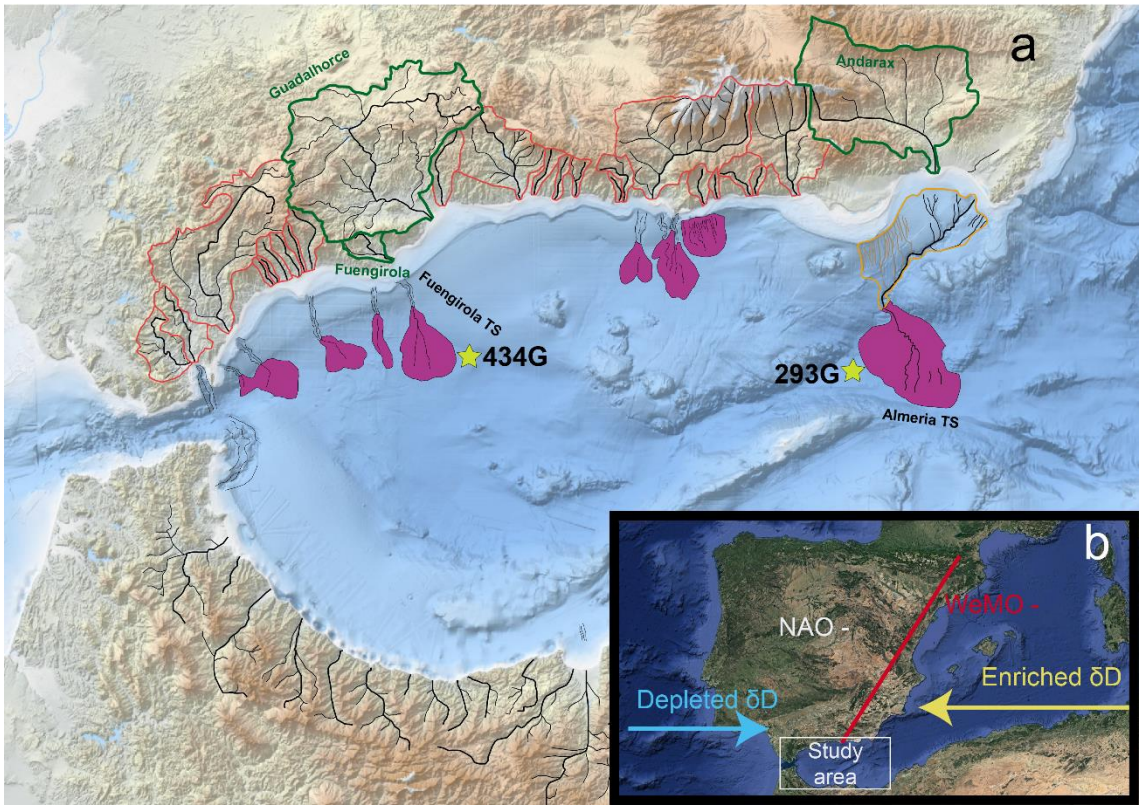

Figure 1. (a) Map showing the location of the studied marine sediment cores, the main rivers around the Alboran Sea and the Turbidite Systems (TSs); (b) Map showing the main atmospheric modes controlling the winter precipitation in the Iberian Peninsula. Catchment basins of the main rivers supplying sediment to the studied records are shown as green polygons. Catchment basins of other rivers from southern Iberia are shown as red polygons. Orange polygon indicate the area influencing the Almeria TS and brown lines indicate gullies (Liquete et al., 2005; Ercilla et al., 2016).

2. Long-chained *n*-alkanes as paleoenvironmental proxies

Long-chained *n*-alkanes are found in leaf-waxes of vascular plants and serve as a protection against dehydration, creating longer and more hydrophobic chains during more arid or hotter conditions (e.g., Eglinton and Hamilton, 1967; Eglinton and Eglinton, 2008). An increasing number of studies have highlighted the potential of these plant-wax derived biomarkers as useful tools for reconstructing vegetation and hydrological changes over different timescales (e.g., Pagani et al., 2006; Niedermeyer et al., 2010; Sachs, et al., 2009; Jaeschke et al., 2020), since they are relatively resistant to degradation and diagenesis, allowing a good preservation in fossil records, i.e. lakes, paleosols or marine environments (e.g., Eglinton and Eglinton, 2008). In general, long-chained *n*-alkanes (C_{27}-C_{33}) usually derive from the leaf-wax of terrestrial plants, which are transported to the marine environments by riverine runoff or eolian inputs (Schefuß et al., 2003; Diefendorf and Freimuth, 2017).

The $\delta^{13}C$ values of *n*-alkanes is controlled by the relation between the ambient and the intracellular CO_2 concentration (Freeman and Hayes, 1992). In order to prevent the dehydration, the plant close their stomata thereby limiting the pool of CO_2 available for biosynthesis, increasing the values of $\delta^{13}C$ *n*-alkanes; so, the carbon isotopic composition of the *n*-alkanes is heavier in dry and/or warm environments (Diefendorf et al., 2010; Pretince et al., 2010; Wang et al., 2018). The $\delta^{13}C$ in *n*-alkanes can be also indicative of the plant photosynthetic pathway, since the isotopic fractionation during carbon fixation differ between C_3, C_4 and crassulacean acid metabolism (CAM) plants (Schefuß et al., 2003, 2005; Bi et al., 2005; Castañeda et al., 2009; Diefendorf et al., 2011; Jaeschke et al., 2020). Also, within the C_3 plants can be differences in the leaf $\delta^{13}C$ depending on the plant functional type (Diefendorf et al., 2010). Therefore, the $\delta^{13}C$ signature of leaf-waxes preserved in the sedimentary record can be used for reconstructing vegetation changes (e.g. Schefuß et al., 2003, 2005; Castañeda et al., 2009).

Additionally, the hydrogen isotopic composition of the *n*-alkanes registers the signal of the water source used by these organisms during growth (e.g., Sasche et al., 2012), that is ultimately related to the isotopic composition of precipitation after a significant biological fractionation effect (Sachse et al., 2012). Several environmental factors can influence the isotopic signature of precipitation, being especially important temperature, evapotranspiration, precipitation amount and moisture source (Dansgaard, 1964). Among them, precipitation amount and moisture source have been the main control on precipitation isotopic patterns from the last glacial cycle in southern Iberia (Toney et al., 2020; García-Alix et al. 2021). Recent studies by Toney et al. (2020), Schirrmacher et al. (2020) and García-Alix et al. (2021) have also demonstrated that the $\delta^{2}H$ signature of present-day precipitation in southern Iberia has a high correlation with the $\delta^{2}H$ recorded in sedimentary *n*-alkanes, and thus, can be used to reconstruct past precipitation patterns in this area.

3. Study area

The Alboran Sea is the westernmost basin of the Mediterranean Sea and it is located between South Iberia and North Africa (Fig. 1). The oceanography in the western Mediterranean can be synthetized in three main water masses: on the surface the relatively fresh Atlantic Water mixes with the Mediterranean water to form the Modified Atlantic Water (MAW), which occupies the upper 200 m and flows eastward (Millot et al., 1999).

The MAW forms two anticyclonic gyres during its path eastward, the quasi-permanent Western Alboran Gyre (WAG) and the seasonal Eastern Alboran Gyre (EAG) (Heburn and La Violette, 1990). The intermediate waters are composed by different water masses from different origins flowing westward, from these, the Levantine Intermediate Water (LIW), which is formed in the Levantine basin, is the most relevant (Millot et al., 2013). The deepest part of the basin is filled by the Western Mediterranean Deep Water (WMDW), which is formed in the Gulf of Lions and the Liguro-Provençal basin during winter (MEDOC group, 1970). The Mediterranean waters flowing out the Alboran Sea through the Gibraltar Strait called Mediterranean Outflow Water (MOW), and is composed by 80% LIW and 20% WMDW (Kinder and Parrilla, 1987).

The Alboran basin is surrounded by young relatively massifs and presents high sedimentation rates (Comas et al., 1999). The sedimentation is mostly composed of a mixture of allochthonous terrigenous inputs and autochthonous carbonates. The lithogenic fraction represents around the 70% of the sediment in the Alboran basin, which mainly derived from riverine discharge, eolian dust pulses from Morocco, Mauritania, Mali, Niger and Algeria and coastal erosion (Fabrés et al., 2002; Martínez-Ruiz et al., 2015; Rodrigo-Gámiz et al., 2015). The torrential character of the rivers surrounding the Alboran Sea implies that most of the sediment load arriving from the continent occurs during late fall and winter, mainly as flood events (Fernández-Salas et al., 2003; Liquete et al., 2005; Palanques et al., 2005; Puig et al., 2017). The torrential precipitation in these rivers basins promotes the formation of dense fluxes, such as hyperpycnal fluxes which are able to bypass a narrow continental shelf (Bouma et al., 2004). Once on the shelf break the sediment reaches the canyon head and is channelized by turbidite systems (TSs) and transported into the deep Alboran basin (Palanques et al., 2005; Ercilla et al., 2016; Puig et al., 2017). The TSs in the Alboran Sea are mostly located in the southern Iberian margin (Ercilla et al., 2016, 2019).

In particular, the Almería TS is the largest one in the Alboran Sea with three tributary systems incising the shelf break (Fig. 1) (García et al., 2006). It is fed by the Andarax river, whose basin covers 2160.5 km^2, and a maximum elevation of 2481 m above sea level (masl) (Liquete et al., 2005). The Andarax river sediment load is 5.7 kg/s, being the highest in the Alboran basin. The Fuengirola TS is the second largest TS in the Alboran Sea. The Fuengirola River, which has a basin area of 129.5 km^2 and a maximum elevation of 993 masl., is the closest to the canyon head, which is incised in the shelf break (Fig. 1)

(Ercilla et al., 2016). Due to the disconnection between the river mouth and the canyon head, the Fuengirola TS is likely also influenced by the Guadalhorce River, the third major river regarding to the sediment load, after the Andarax and Adra rivers. The Guadalhorce river catchment area has a basin area of 3180.9 km^2, a maximum elevation of 1703 masl. Due to the coastal morphology, there is a dominant S-SW littoral drift (Fernández-Salas et al., 2003), suggesting a significant influence of the Guadalhorce sediments in the Fuengirola TS. In general, the sedimentation in the whole basin results from a complex interaction between hemipelagic sedimentation, high-density sediment flows and the influence of deep currents.

3.1 Precipitation patterns and vegetation in the catchment basins of studied records

The present precipitation patterns in the Iberian Peninsula are mainly controlled by the influence of the North Atlantic Oscillation (NAO) and the entrance of Atlantic storm track during wintertime (Trigo et al., 2004). Nonetheless, in the eastern and southeastern coast of Iberia the annual precipitation is also influenced by the Western Mediterranean Oscillation and the cyclonic precipitation also has a significant contribution to the annual precipitation (Trigo et al., 2002; Martín-Vide and López-Bustins et al., 2006; Gonzalez-Hidalgo et al., 2009; Serrano-Notivoli et al., 2018). Additionally, the orography also plays an important role reducing the arrival of Atlantic fronts to the eastern Iberia (Martín-Vide and López-Bustins et al., 2006). During spring and summer, this convective precipitation and cyclonic rains of Mediterranean origin are controlled by the strong diurnal fluctuation of inland surface temperatures, also influencing some regions far from the coast (Romero et al., 1998; Celle-Jeanton et al., 2001).

The high variability in the source and amount of precipitation in southern Iberia exhibit a decrease in the Atlantic moisture influence and precipitation amount eastward (Fig. 1) (Celle-Jeanton et al., 2001; Gimeno et al., 2010) while the coastal areas are more influenced by Mediterranean moisture source (Romero et al., 1998). These differences in the source and amount of precipitation would have impacted on past vegetation in the riverine catchment basins flowing into the Alboran Sea.

The Guadalhorce river catchment area, located in the western part of the Alboran Sea, registers a mean annual precipitation of 497.5 mm/ yr. The vegetation in the catchment basin encompasses the thermo- and mesomediterranean vegetational belts, corresponding

to a climate arid to sub-humid in this catchment basin (Valle et al., 2007). No detailed data from the Fuengirola river catchment basin are available, but the annual mean precipitation estimated from 1970 to 2000 is between 600 and 800 mm/yr (https://www.juntadeandalucia.es/medioambiente). Vegetation surrounding the Fuengirola river basin belongs to the termomediterranean belt composed by *Quercus suber*; *Myrto communis* and *Querceto suberis S.* and dry-sub-humid of holm oak, with *Smilaco mauritanicae, Querceto rotundifoliae S, Cystus malacitanus* (Valle et al., 2007).

The Andarax catchment area, located in the south-easternmost part of the Iberian Peninsula, presents mean annual precipitation in the river basin around 318.9 mm/yr, and the vegetation is therefore the typical from a sub-desertic climate, being mainly composed by xerophytes, i. e. *Pistacia lentiscus* (Valle et al., 2007).

Furthermore, riparian vegetation generally occurs in the rivers shore and mouths, is more expanded in the Gualhorce and Fuengirola rivers than in the Andarax river (sub-humid *vs* semi-arid) (Valle et al., 2007).

4. Methods

4.1 Samples description and chronology

Two marine sediment records (cores 293G and 434G) from the eastern and western Alboran Sea basins, respectively, have been studied here. These were recovered during the oceanographic cruises Training Through Research (TTR) 12 and 17, respectively, onboard of the *RV* Prof Logachev (Comas and Ivanov, 2003).

Core 293G was collected in the east Alboran Sea basin (lat. 36º10.414N, long. 2º45.280W; depth 1840 m below sea level (mbsl); length 402 cm) close to the lobe of the Almeria TS, while core 434G was recovered in the west Alboran Sea basin (lat. 36º12.313N, long. 4º18.735W; depth 1108 mbsl; length 252.5 cm), close to the lobe of the Fuengirola TS. The lithology of both sediment records consists in loose mostly detrital sediment composed mainly of clays, with minor amounts of quartz, feldspar and other accessory minerals, and biogenic carbonates.

The chronologies of these records have been previously published by Rodrigo-Gámiz et al. (2011, 2014), and both have been updated using the R-package rbacon 2.4.2 software (Blaauw and Christen, 2011) with the Marine20 calibration curve (Heaton et al., 2020),

which resulted in similar calibrated ages. The record of eastern Alboran (core 293G) covered the last 19.78 cal ka BP, while the record from western Alboran (core 434G) registered the last 13.64 cal ka BP (Rodrigo-Gámiz et al. 2011, 2014).

4.2 Lipid extraction and biomarker analysis

Lipid extraction of freeze-dried sediment samples from cores 293G and 434G was previously performed by Rodrigo-Gámiz et al. (2014). Within the apolar fraction of each sediment core, we have selected a total of 66 samples from core 293G and 56 from core 434G from key climatic periods in order to analyse the *n*-alkane relative abundance and stable carbon and hydrogen isotope composition.

The apolar fraction was re-dissolved in 100 μl of *n*-hexane. Analysis of *n*-alkanes was performed on a Hewlett Packard 6890 Gas Chromatograph (GC) equipped with flame ionization detector (FID) using a fused silica column CP Sil-5 (25 m × 0.32 mm internal diameter, 0.12 μm film thickness), an on-column injector and He as mobile phase. We have calculated different *n*-alkanes based indices as:

The carbon preference index (CPI) of the long-chain *n*-alkanes according with Killops and Killops (2004):

$$CPI = 1/2 \times [(C_{25}+C_{27}+C_{29}+C_{31}) / (C_{26}+C_{28}+C_{30}+C_{32}) + (C_{27}+C_{29}+C_{31}+C_{33}) / (C_{26}+C_{28}+C_{30}+C_{32})] \quad (1)$$

The Average Chain Length (ACL) for the *n*-alkane range C_{27} to C_{33}, following Schefuß et al. (2003):

$$ACL = (25xC_{25}+27xC_{27}+29xC_{29}+31xC_{31}+33xC_{33}) / (C_{25}+C_{27}+C_{29}+C_{31}+C_{33}) \quad (2)$$

Compound–specific carbon isotope analyses of *n*-alkanes ($\delta^{13}C$) were performed in duplicate on a Thermo Trace GC (1310) coupled with a Thermo Delta-V advantage

isotope ratio mass spectrometer (IRMS) via a GC-isolink II and conflo IV (number of samples analysed for $\delta^{13}C$: 42 for core 293G and 46 for core 434G; Tables S1 and S2). Compounds were oxidized to CO_2 in a Thermo Combustion Reactor at 1000 °C, the reactor was oxidized daily for at least 15 minutes and every analytical run was followed by 2 minutes seed oxidation. An in house developed GC standard was analysed daily to assess the chromatographic performance, this standard was combined with two perdeuterated *n*-alkanes with a certified, 'Europa flour', isotopic composition standard to check the functioning of the isotope ratio monitoring mass spectrometer. Samples were measured only if the difference of the *n*-alkanes between online and given values was less than 0.5 ‰. Duplicates of each sample were measured when possible.

The hydrogen isotopic composition of *n*-alkanes (δ^2H) was determined using a Thermo Trace GC (1310) coupled with a Thermo Electron Delta V irMS via a GC-isolink II and conflo IV (number of samples analysed for δ^2H: 22 for core 293G and 27 for core 434G; Tables S1 and S2). Compounds were pyrolyzed at 1450 ºC in an empty ceramic tube, which was pre-activated with hexane. H_2 gas with a predetermined stable isotopic composition was used as monitoring gas. Mix B (Schimmelmann, Indiana University) was used to check machine functioning at the beginning of every day. Samples were only analysed if the average deviation of Mix B from the off-line determined values was 5 ‰ or less for hydrogen isotopic analyses. Analyses were done in duplicate when possible and squalene standard was co-injected with every sample. Samples without duplicates are indicate in Tables 1 and 2

Values of $\delta^{13}C$ and δ^2H were expressed with respect to the Vienna Pee Dee Belemnite (VPDB) and Vienna Standard Mean Ocean Water (VSMOW) standards, respectively. The δ^2H values were corrected for the potential influence of sea ice volume on the marine water isotopic composition following Niedermeyer et al. (2010).

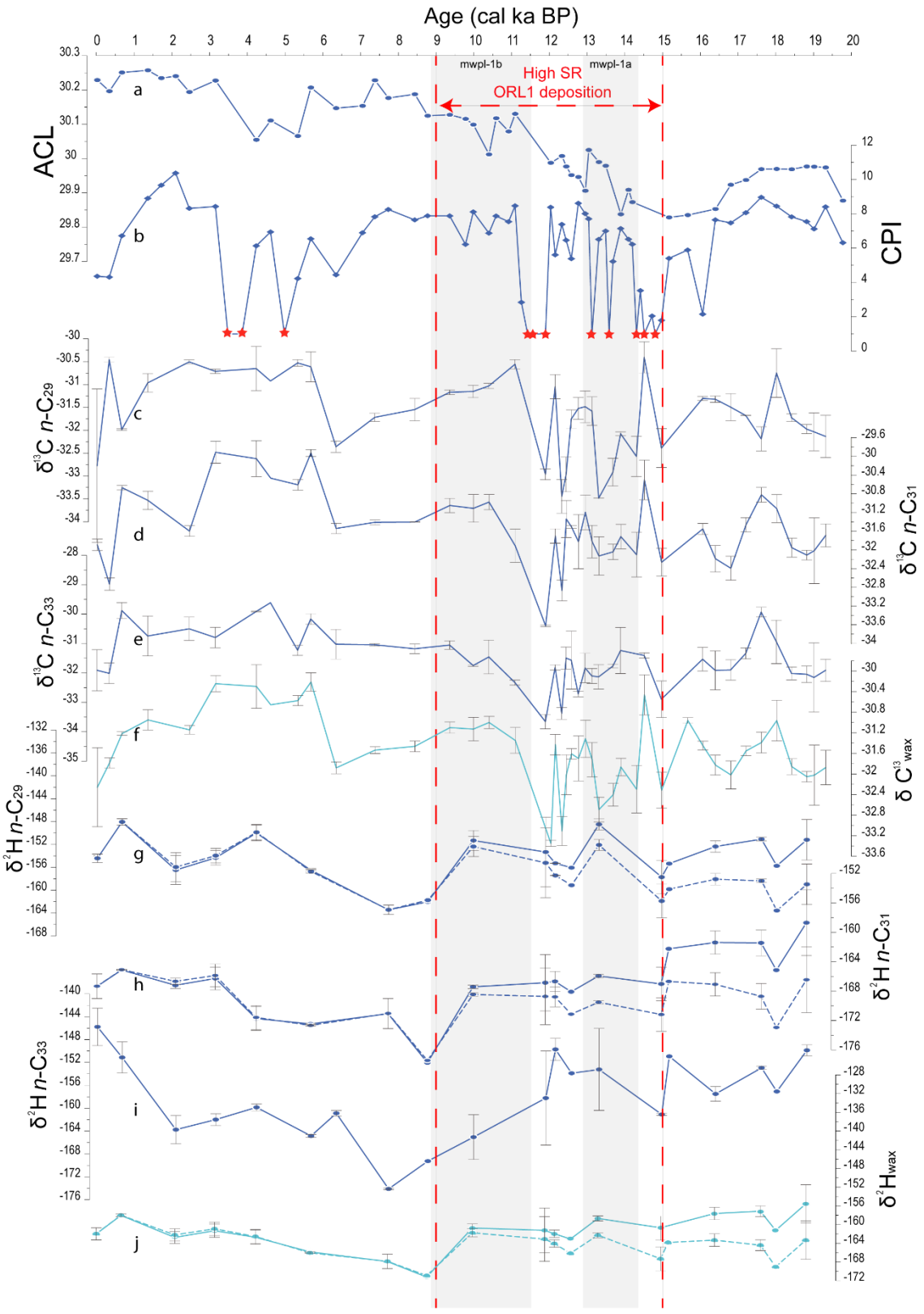

Figure 2. *n*-alkanes distribution and isotopic signature from core 293G: (a) Carbon Preference Index (CPI); (b) Average Chain Length (ACL); $\delta^{13}C$ from homologue (c) C_{29}; (d) C_{31} and (e) C_{33}; (f) $\delta^{13}C_{wax}$; $\delta^{2}H$ (ice volume corrected) from homologue (g) C_{29}; (h) C_{31} and (i) C_{33}; (j) $\delta^{2}H_{wax}$.

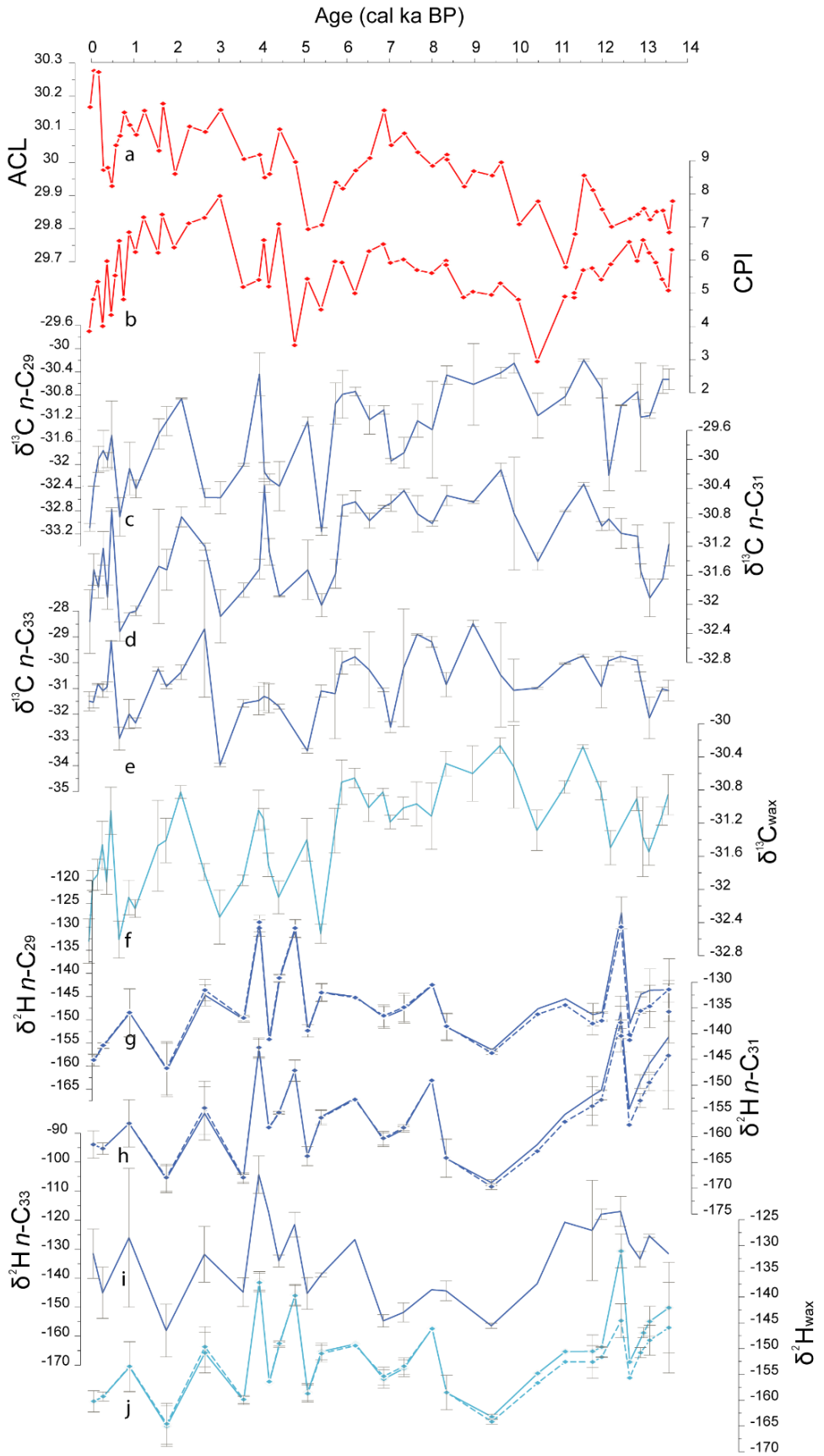

Figure 3. *n*-alkanes distribution and isotopic signature from core 434G: (a) Carbon Preference Index (CPI); (b) Average Chain Length (ACL); $\delta^{13}C$ from homologue (c) C_{29}; (d) C_{31} and (e) C_{33}; (f) $\delta^{13}C_{wax}$; $\delta^{2}H$ (ice volume corrected) from homologue (g) C_{29}; (h) C_{31} and (i) C_{33}; (j) $\delta^{2}H_{wax}$.

5. Results

The ACL for each marine core, 293G and 434G, show similar values, with the *n*-C_{31} alkanes being the most abundant homologue of the long-chain *n*-alkanes throughout the records, except for the interval between 16.5 to 14.5 cal ka BP in core 293G (Table S1). The ACL in core 293G ranges from 29.4 to 30.3 with an average value of 30 (Table S1), recording the lowest values between 15.0 and 14.0 cal ka BP and the highest values in the most recent samples (Fig. 2). The ACL in core 434G ranges from 29.6 to 30.3 with an average of 30 (Table S2), with the lowest values between 12 and 10 cal ka BP and the highest values during the Late Holocene (Fig. 3).

The CPI of the long-chain *n*-alkanes gives information about the maturity/degradation of the organic matter (Bray and Evans, 1961). The strong odd-over-even *n*-alkane distribution is the typical of vascular terrestrial plants, as also deduced by the CPI values. High CPI values are typical of terrestrial plant origin, while CPI values ~1 or lower indicate a bacterial degradation or algal source (Gelpi et al., 1970; Cranwell et al., 1987). CPI values in core 293G ranges between 1.8 and 10.3 and in core 434G between 2.9 and 7.9. Samples with CPI values <1 or presenting an unresolved complex mixture (UCM) in the *n*-alkane distribution were excluded of the $\delta^{13}C$ and $\delta^{2}H$ analyses (Tables S1 and S2 since they could indicate a mix of organic matter sources, bacterial activity, and/or high degradation of the carbon chains (Jeng et al., 2006; Castañeda et al., 2011). Several samples with a CPI between 2 and 3, pointing to relatively high amounts of even *n*-alkanes, showed relatively high $\delta^{2}H$ values for all *n*-alkanes (Table S1), suggesting that the even *n*-alkanes were potentially produced during microbial induced degradation or recycling processes of the odd-carbon numbered *n*-alkanes taking place in the sediment (Sachse et al., 2004; Häggi et al., 2021). These samples, which only occurred in the 293G sediment core, have shown an enrichment of ~10 ‰ with respect to the adjacent analyzed samples, supporting that these enriched values are not from fresh organic matter but likely from reworked and older sediments (Sachse et al., 2004; Häggi et al., 2021). Therefore, these samples have not been considered for paleoclimate interpretation.

The $\delta^{13}C$ and hydrogen $\delta^{2}H$ isotopic values for the C_{29}, C_{31} and C_{33} homologues in cores 293G and 434G are shown in Table S1 and S2., respectively. The weighted mean averages, referred hereafter as $\delta^{13}C_{wax}$ and $\delta^{2}H_{wax}$, were calculated for the two more abundant homologues, *n*-C_{29} and *n*-C_{31} alkanes using their relative abundances (Sachse et al., 2003). The $\delta^{13}C_{wax}$ values in core 293G range between -33.3 ‰ during the Bölling-

Alleröd period (B-A) and -30.2‰ during the Middle-Late Holocene (Fig. 2), and in core 434G vary between -32.6 ‰ at 5.5 cal ka BP and -30.3 ‰ at around 10 cal ka BP (Fig. 3). The δ^2H_{wax} values in core 293G range between -130.7 ‰ during the Last Glacial Maximum (LGM) and -170.91 ‰ during the Early Holocene (Fig. 2), while in core 434G vary between -136.9 ‰ at around 4.2 ka cal BP and -165.1 ‰ at 1.7 ka cal BP (Fig. 3).

6. Discussion

6.1 *n*-alkane source and preservation in the studied records

The sedimentary long chain *n*-alkanes in marine records mainly come from eolian inputs of eroded leaf-waxes, especially in marine environments with low sedimentation rates, and from riverine runoff from catchment soil-derived leaf-waxes washed into the surrounding marine area (Schefuß et al., 2003; Diefendorf and Freimuth, 2017; Liu et al., 2020). In the case of the studied records in the Alboran Sea, which is a narrow basin surrounded by rivers and with an important influence of the North African eolian dust, the proper identification of the source of the *n*-alkanes is of paramount importance for performing accurate paleoclimatic and paleohydrological interpretations (Kusch et al., 2010; Bliedtner et al., 2020; Liu et al., 2020). Several *n*-alkane indices can be used to constrain the source.

The ACL ranging between 29.4 and 30.3 and the CPI values > 1, point to terrestrial vascular plants as principal source of these *n*-alkanes (Bush and McInerney, 2013). In general CPI profiles in both Alboran records during the Holocene are similar (Figs. 2 and 3). In the eastern Alboran, the 293G sediment core depicted an interval with low CPI reaching values of 1.8 and with UCMs in the *n*-alkane distribution between 15 and 11 cal ka BP (Table S1; Fig. 2), suggesting a higher bacterial activity and degraded organic matter (e.g., Wang et al., 2014). The isotopic composition of these samples with low CPI is characterized by exceptional positive δ^2H_{wax} values, suggesting an addition of older, degraded and/or reworked terrestrial organic matter (Häggi et al., 2021). These samples are not included for the climatic reconstruction. This interval corresponds to the Organic Rich Layer 1 (ORL1) deposition, a period characterized by extraordinary organic matter preservation between 15.0 and 9.0 cal ka BP caused by reduced bottom waters ventilation and an increase in the sedimentation rate (Cacho et al., 2002; Mesa-Fernández et al., 2022). Flooding events in the Alboran Sea shelf have been described during the

transgression boosted by the melt-water pulses 1a (mwp-1a; 14.5-12.8 cal ka BP) and 1b (mwp-1b; 11.5-8.8 cal ka BP) and likely forced the sedimentation rate increase (Standford et al., 2011; Lambeck et al., 2014; Mesa-Fernández et al., 2022). The organic matter accumulated in soils between 35 and 15 cal ka BP when the continental shelf was exposed, was rapidly eroded by wave ravinement and transported basinward, resulting in older and more mature organic matter in the deep basin sediments (Catuneanu, 2006). Also, the sea level rise during the transgression could destabilize the shelf break and promote the occurrence of turbidites in the nearby TS (Catuneanu, 2006), explaining the low CPI values and the occurrence of UCM during this period (Fig. 2). Note that the cores do not show any direct sedimentary evidence of turbidites (not erosive surfaces or intervals of reworked foraminifera) and they have solid age models (Rodrigo-Gámiz et al., 2011, 2014), suggesting that turbidites mainly affected the cores by supplying older or more degraded terrestrial organic matter.

Although less extreme, a second period with low CPI values and significant UCMs in the *n*-alkane distribution is recognized in both western and eastern Alboran sites between 5.5 and 3.5 cal ka BP (Figs. 2 and 3). It is worth to note that although both cores recorded this decrease in CPI to 3.43 and 4.42, respectively, only the core 293G shows significant UCMs, pointing that the Almeria TS, which is larger than the Fuengirola TS, might be more susceptible to receive reworked or degraded terrestrial organic matter than the latter from the shelf, highlighting the differences between the two records settings despite their nearby location (Fig.1). During this low CPI time period, an increase in a terrigenous input proxy, the K/Al ratio suggested important input of detrital mica and K-feldspar-rich sediments likely from the surrounding continental areas (Martínez-Ruiz et al., 2003; Rodrigo-Gámiz et al., 2011). This interval further coincided with the onset of human landscape modification and fires during the Middle-Late Holocene in southern Iberia (Carrión et al., 2010; García-Alix et al., 2013; Schirrmascher et al., 2019). The anthropic deforestation along with a dry period, could have boosted the effective erosion and the supply of more mature or reworked organic matter to the marine settings. The influence of changes in the *n*-alkane sources during these two intervals (from 15 to 11 cal ka BP and from 5.5 to 3.5 cal ka BP) with the presence of UCMs and low CPI values will be explained in detail in the next section.

Regarding the photosynthetic pathway of the vegetation growing in the catchment basins, previous studies have suggested that C_3 plants dominated in central and southern Iberia

during the deglaciation and the Holocene (Jiménez-Espejo et al., 2014; Schäfer et al., 2018). Nevertheless, the terrestrial record from lake Tislit in Morocco, which nowadays is dominated by C_3 vegetation, recorded an interval of increase C_4 vegetation during the HS1 as response of pervasive arid conditions during the AMOC collapse (Lynch-Stieglitz, 2017; Cheddadi et al., 2021). In the Alboran Sea this period was characterized by a large amount of Saharan eolian input (Rodrigo-Gámiz et al., 2011), which might could have influenced the sedimentary *n*-alkane record.

Nonetheless, in the eastern Alboran sites, $\delta^{13}C$ values ranging between -30.9 ‰ and -33.1 ‰ during the HS1 and the YD, while the $\delta^{13}C$ average values for C_3 and C_4 plants are – around -34.7 ‰ for C_{29} (-35.2 ‰ for C_{31}) and-21.4 ‰ for C_{29} (-21.7 ‰ for C_{31}) respectively (Castañeda et al., 2009), suggesting negligible influence of *n*-alkanes from C_4 plants covering the North Africa margin (Fig. 4). Thus, the studied Alboran Sea records were more influenced by the organic matter input from southern Iberia than from North Africa supporting present-day observations that points to riverine input as the main factor controlling the sedimentation in the basin with minor influence of Saharan eolian input (Fabrés et al., 2002). Therefore, the negligible mixture between C_3 and C_4 vegetation will make the interpretation of $\delta^{13}C$ and $\delta^{2}H$ isotopic values of long-chain *n*-alkanes in the studied records easier, since the isotope fractionation caused by different plant functional type can be neglected (Bi et al., 2005; Wang et al., 2013).

6.2 Main controls on stable carbon isotope records in the Alboran Sea basins

Since our records are only influenced by C_3 plants, changes in the $\delta^{13}C$ signature are supposed to respond to changes in the water availability (Zech et al., 2007) or changes in the source of the *n*-alkanes. The latter can be important due to shelf flooding that occurred during the transgression during the time period studied, as suggested above.

Nearby continental Iberian records have related the $\delta^{13}C$ *n*-alkane variations in bulk organic matter to hydric stress under arid conditions (i.e. García-Alix et al., 2012, 2014, 2017; Toney et al., 2020), presenting the opposite pattern to the studied records at long-term time scales, i.e. the $\delta^{13}C$ values during the deglaciation are more negative than during the Early Holocene (Fig. 4). However, when higher frequency patterns are compared between the $\delta^{13}C$ signature from the eastern Alboran Sea with pollen records from nearby continental and marine areas, i.e. Padul wetland from the southern Iberia, lake Tislit from

the northern Africa, and the Alboran MD95-2043 record, a coherent evolution during the deglaciation is observed, with more positive $\delta^{13}C$ values and more arid conditions and drought adapted vegetation during the HS1 and YD and more negative $\delta^{13}C$ values pointing to more humid adapted vegetation during the B-A (Fig. 4; Fletcher et al., 2010; Camuera et al., 2021; Cheddadi et al., 2021).

After 11.8 cal ka BP, an abrupt increase in the $\delta^{13}C$ values from -33 to -31 ‰ is observed in the eastern Alboran site (Fig. 4), which would suggest more arid conditions, and thus, more hydric stress. Nonetheless, the pollen records pointed to more humid conditions in the western Mediterranean during the Early Holocene (Fletcher et al., 2010; Camuera et al., 2021; Cheddadi et al., 2021) as response of a reactivation of the AMOC, higher SST and atmospheric moisture in the North Atlantic, and weaker and more humid westerlies (Brayshaw et al., 2010; Fletcher et al., 2010; Ng et al., 2018). Therefore, this change in the $\delta^{13}C_{wax}$ signature might not be related to hydric stress, but to changes in the source of the *n*-alkanes, thus in the type of vegetation in the catchments (Diefendorf et al., 2010).

6.2.1 Sea-level transgression controls on stable carbon isotope record during the deglaciation and Early Holocene Melt water pulse-1b in the eastern Alboran Sea

We propose that during the deglaciation, the leaf wax derived *n*-alkanes recorded in the eastern Alboran site derived from the emerged continental shelf, which is relatively flat, and because of the closeness to the sea, plants should have been adapted to more humid conditions, and thus, more depleted $\delta^{13}C_{wax}$ than inland. Although the climate was mostly arid during the LGM and the HS1, before the shelf flooding (~15 cal ka BP), the connection of the coastline to the continental slope would have promoted the direct deposition of terrestrial material including leaf wax *n*-alkanes eroded by runoff of the Andarax river and several coastal creeks into the deeper part of the basin (Fig. 5a). In addition, the predominantly Mediterranean sourced precipitation during this period (García-Alix et al., 2021) point to a greater influence of spring/fall rainfall and thus, enhanced convective or cyclonic processes on the coast (Romero et al., 1999; Trigo et al., 2002) that could have promoted the wash of the coastal vegetation *n*-alkanes.

After the onset of the shelf flooding during the B-A, the coastline retreated more inland promoting the disconnection between the Andarax mouth with the canyon head, and thus the leaf wax *n*-alkanes started to deposit on the submerged shelf instead of been directly

transported to the deep basin. Nevertheless, the deposition occurred above the storm wave base, which nowadays in the zone reaches 30-35 m water depth (Bárcenas et al., 2015). Therefore, *n*-alkanes derived from coastal vegetation deposited on the inner shelf were still susceptible to being transported basinward by the wave action (Fig. 5b).

A key-time period regarding to the sedimentation of *n*-alkanes in the Alboran Sea occurred during the transition from the YD to the Early Holocene. This interval was coeval with the mwp-1b (11.5-8.8 cal ka BP) (Stanford et al., 2011; Lambeck et al., 2014), and with high sedimentation rates in the eastern Alboran basin, which would have promoted the ORL1b deposition (Mesa-Fernández et al., 2021). Interestingly, the YD-Early Holocene transition from more negative to more positive $\delta^{13}C_{wax}$ values in the eastern Alboran record is preceded by some UCMs in the apolar fractions between 11.8 and 11.2 cal ka BP, fitting with a rapid sea-level increase and the input of more mature or reworked OM into the basin (Fig. 4).

After 11.2 cal ka BP the storm wave base would be located above the shelf break, and then part of the shelf was unaffected by the wave action. The coastal vegetation would now be deposited in the shoreface or the inner shelf and not transported directly through the canyon into the deep basin (Fig. 5c, d). At this time, terrestrial organic matter would reach the canyon head and mainly be transported to the basin during events of enhanced precipitation, since these events were able to promote hyperpicnal fluxes capable to bypass the shelf, as occur at present-day during winter (Palanques et al., 2005; Puig et al., 2017). These events of enhanced precipitation could have led to washing the whole Andarax river basin and mixing the isotopic depleted coastal vegetation signal with the isotopically more enriched vegetation of higher altitudes (thermo- *vs* mesomediterranean), imprinting a more positive $\delta^{13}C$ value in the 293G record after 11.8 cal ka BP.

In summary, we propose that the change to more positive $\delta^{13}C_{wax}$ values in the YD-Early Holocene transition, did not respond to changes towards more humid conditions that would reduce the hydric stress of the plants, but responded to a change in the sedimentary conditions as a consequence of the sea-level transgression that changed the *n*-alkane source (plant type input).

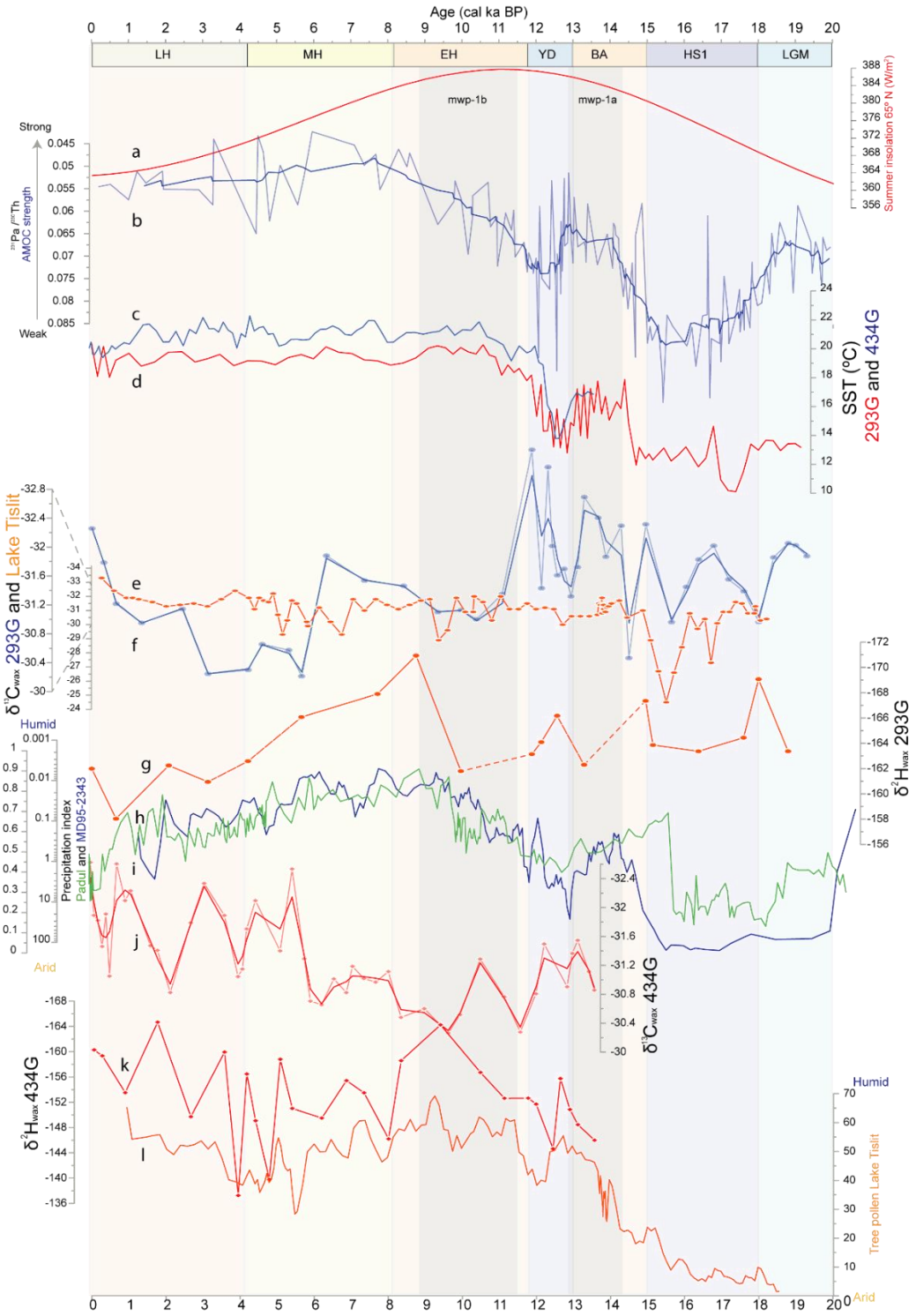

Figure 4. Age profile of (a) Summer insolation at 65ºN (Laskar 2004); (b) $^{231}Pa/^{230}Th$, individual points (transparent) and composite (opaque) indicating Atlantic Meridional Overturning Circulation (AMOC) strength (reverse axis) (Ng et al., 2018); Sea Surface Temperature (STT) from cores (c) 434G and (d) 293G (Rodrigo-Gámiz et al., 2014); (e) $\delta^{13}C_{wax}$ from Lake Tislit (core GC27; Cheddadi et al., 2021); (f) $\delta^{13}C_{wax}$ from core 293G (single point and 3 after applying an smooth of 3 points); (g) $\delta^{2}H_{wax}$ (ice volume corrected) from core 293G; (h) Precipitation Index from core MD95-2343 (Fletcher et al., 2010; (i) Pollen precipitation index from Padul wetland (Padul-15-05; Camuera et al., 2019) (reversed axis); (j) $\delta^{13}C_{wax}$ from core 434G (single point and after applying an smooth of 3 points); (k) $\delta^{2}H_{wax}$ (ice volume corrected) from core 434G; (l) Tree pollen percentage from Lake Tislit (core GC27; Cheddadi et al., 2021).

6.2.2 Changes in the n-alkane pool due to climate variability control the stable carbon isotope records during the Holocene

After the change in the sedimentary regime occurring at the Early Holocene, between 11.8 and 11.2 cal ka BP, the eastern Alboran record showed a trend to more negative $\delta^{13}C_{wax}$ values during the Early-Middle Holocene (Fig. 4). Conversely, in the western Alboran Sea basin, an opposite trend is observed, showing more positive values during the Early Holocene and more negative values of $\delta^{13}C_{wax}$ during the end of the African Humid Period during the Middle Holocene (Alley et al., 1997; Bond et al., 1997; Magny et al., 2007; Fletcher et al., 2010).

In other southern Iberian and northern Africa records the Early Holocene has been recorded as the wettest period over the last 35 ka (García-Alix et al., 2021; Ramos Román et al., 2018; Zielhofer et al., 2017), since the winter insolation minima over the North Atlantic promoted higher SST in the North Atlantic and promoted more humid and weaker westerlies into the Mediterranean area increasing the amount of rainfall (Fletcher et al., 2010; Moreno et al., 2014; Tzedakis et al., 2018). The unexpected trend shown by $\delta^{13}C_{wax}$ in the western Alboran record highlighted the complexity of using the $\delta^{13}C_{wax}$ from marine sediments as proxy for environmental changes registered in terrestrial areas due to the potential mixture of the *n*-alkane sources. This a priori incongruence can be explained by two hypotheses, not exclusive to each other, involving the relative contributions of the Fuengirola and Guadalhorce rivers to the organic matter supplied to the western record.

It is important to note, that the vegetation belts have migrated in the southern Iberian Peninsula over the last 20 ka (Combourieu-Nebout et al., 2009; Camuera et al., 2019). Nonetheless, the size, the maximum altitude and the closeness to the sea of the Fuengirola and Guadalhorce catchment basins are constraining factors for these migrations. The vegetation in Fuengirola catchment basin would always be more humid-adapted and would have warmer and more stable climate conditions (as the thermo-mediterranean vegetation belt nowadays; Valle et al., 2007), than those of the Guadalhorce catchment basin, which would be more adapted to aridity and colder conditions in summer and winter (Fig. 1).

The first hypothesis is related to the effect of the transgression on the sediment source arriving into the deep basin: the western Alboran record would be more influenced by the Fuengirola river and the sub-humid thermomediterranean vegetation of its catchment

basin before the mwp-1b. The sediment trapped in the shelf would be transported basinward by the wave action during storms, channelizing by the canyon located in the shelf break (Barcenas et al., 2015). Afterwards, the combined effect of the disconnection of the storm wave-base level with the canyon head at ~11.2 cal ka BP and the precipitation increase during the Early Holocene, would have promoted much more contribution from the Guadalhorce river than from the Fuengirola river in the 434G sedimentation. Since the catchment basin of the Guadalhorce river covers both, sub-humid thermomediterranean and the sub-arid mesomediterranean belts, the $\delta^{13}C_{wax}$ values of the *n*-alkane pool should be more positive than that of the Fuengirola *n*-alkane pool in this scenario of more humid conditions (Fig.6c).

The second hypothesis would be related to the moisture source and the rainfall season: Although the riverine discharge nowadays occurred in winter, the torrential rains with high erosive potential occurred during cyclonic rains of Mediterranean origin in spring or fall (Esteban-Parra et al., 1998; Romero et al., 1998; Gimeno et al., 2010). In this regard, the opposite pattern depicted by the $\delta^{13}C_{wax}$ in the 434G core with respect to others nearby records, showing higher (lower) values during wet (dry) periods, could be related to shifts in the rainfall season that affected the *n*-alkane pool. During wet periods of Atlantic predominant moisture source and enhanced winter precipitation, larger rivers such as Guadalhorce could have played a major role supplying sediment to the 434G site. However, during dry periods, a decrease in the winter precipitation would have promoted a higher influence of spring-fall precipitation, which usually occurs as cyclonic and torrential rains. Therefore, the influence of sediment eroded from the Fuengirola basin during arid periods would be greater due to its closeness to the sea. This would also affect the organic matter delivery from each catchment basin. As in the first hypothesis, a mix of vegetation from the thermo- and mesomediterranean belt would be expected when the influence from the Guadalhorce was greater, and the other way around, higher contribution of thermomediterranean and coastal vegetation when the influence of Fuengirola basin was larger. Therefore, more positive $\delta^{13}C_{wax}$ in the 434G record during the Early Holocene would represent higher influence of the Guadalhorce river, not more arid conditions (Fig. 5c).

Later on, around 6.5 cal ka BP an abrupt change occurred in the $\delta^{13}C_{wax}$ values in both Alboran records although with different responses (Fig 4): In the eastern Alboran record, the stable carbon isotopes support a change to more arid conditions, while in the western

Alboran record points to more influence of the Fuengirola river. This change suggests less precipitation amount, coeval with the onset of an aridification trend in several lacustrine records in southern Iberia and North Africa (Fig. 4), showing an increase in xerophytic species while the trees are decreasing (Carrión et al., 2010; Anderson et al., 2011; García-Alix et al., 2012; 2017; Jiménez-Moreno et al., 2013; Zielhofer et al., 2017; Ramos -Román et al., 2018; Cheddadi et al., 2021). These arid conditions in the south-western Mediterranean are coeval with an interval of strengthened AMOC, thus decreasing the entrance of the Atlantic storm track into the Mediterranean (Brayshaw et al., 2010; Zielhofer et a., 2017; Tzedakis et al., 2018). This is in agreement with the establishment of the current atmospheric dynamic in the western Mediterranean after ~5.5 cal ka BP (Fletcher et al., 2013; Toney et al., 2020; García-Alix et al., 2021).

During the Late Holocene the eastern Alboran record showed anomalously more humid conditions, likely related to the increasing anthropogenic changes in the land use, as it can be observed in the chalcolithic settlement of Los Millares, located in the Andarax catchment basin and very close to the river (Molina Gonzalez et al., 2004) (Fig. 4). On the other hand, the western Alboran record showed different phases of Guadalhorce and Fuengirola rivers influence (Fig. 4). The Guadalhorce river dominates during humid periods, such as the Iberian Roman Humid Period (2.6-1.4 cal ka BP) and in lesser magnitude during the Little Ice Age (0.65-0.15 cal ka BP), coinciding with negative NAO phase and enhanced winter precipitation (Fig. 4; Martín-Puertas et al., 2009, 2010; Fletcher et al., 2010; García-Alix et al., 2017; Ramos-Román et al., 2018; Toney et al., 2020). In the same way, periods with higher influence of the Fuengirola river were coeval with reduced winter precipitation intervals, such as the Dark Ages and the Medieval Climate Anomaly (1.4-0.65 cal ka BP), suggesting a positive NAO phase, and an advance of xerophytic and semi-desertic taxa in southern Iberia (Moreno et al., 2012; Jiménez-Moreno et al., 2013; Ramos-Román et al., 2016, 2018; Mesa-Fernández et al., 2018). The strong similarities, although with opposite trend, between the pollen records (Ramos-Román et al., 2016, 2018; Mesa-Fernández et al., 2018; Camuera et a., 2019) and the $\delta^{13}C_{wax}$ signature of the western Alboran record (Fig. 4) points to a climatic control driving its evolution. However, this climatic control on the $\delta^{13}C_{wax}$ values did not respond to changes in the humidity conditions, but to changes in the *n*-alkane source area.

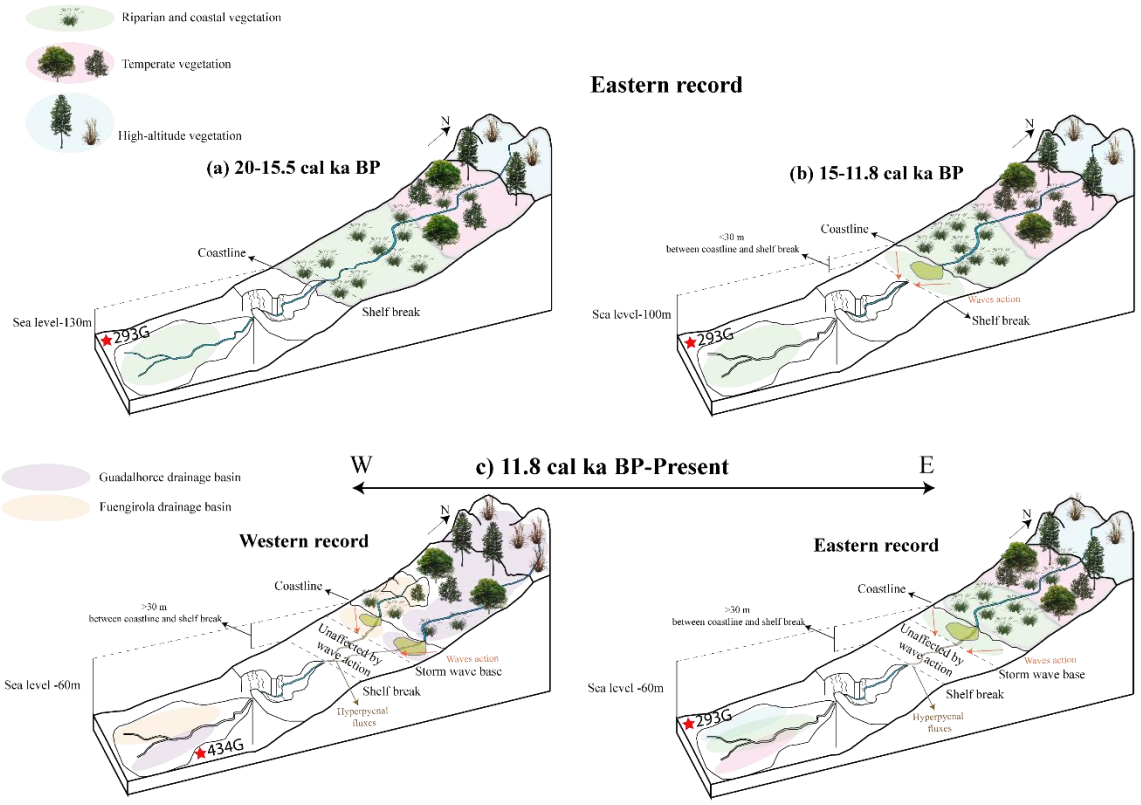

Figure 5. Theoretical sedimentary model in the western and eastern Alboran records for the last 20 ka. (a) From 20 to 15.5 cal ka BP in the eastern Alboran record: River connected to the canyon head, high influence of coastal and riparian vegetation in the deep basin sediments; (b) From 15.5 to 11.8 cal ka BP in the eastern Alboran record: River mouth disconnected to the canyon head but the shelf is above the storm wave-base level, high influence of coastal and riparian vegetation in the deep basin sediments; (c) From 11.8 cal ka BP to Present-day. Western Alboran record: During enhanced winter precipitation periods, the Guadalhorce river has higher influence in the sediment core, and thus a mix of more positive $\delta^{13}C$ values. During reduced winter precipitation periods and more precipitation in fall/spring, higher influence of the Fuengirola river, thus more coastal vegetation. Eastern Alboran record: River mouth disconnected to the canyon head, part of the shelf is below the storm wave-base level. Fresh terrestrial organic matter reaches the basin during high precipitation events which wash the whole basin. *n*-alkanes mix of coastal and high-altitude vegetation

6.3 δ^2H record as paleohydrological proxy since the LGM

The resolution of the δ^2H_{wax} from the 293G record, located in the eastern Alboran basin, is relatively low, which prevent a detailed interpretation from the LGM to the B-A (Fig. 6). Nevertheless, the δ^2H_{wax} values of the *n*-alkanes during the deglaciation in the eastern Alboran Sea site were much higher during the HS1 than during the B-A (Fig. 4). The HS1 is characterized by arid conditions in the southwestern Mediterranean, as shown by nearby pollen records (Fletcher and Sánchez-Goñi, 2008; Combourieu-Nebout et al.,

2009; Camuera et al., 2019; Cheddadi et al., 2021) and the $\delta^{13}C$ values from the 293G, located in the eastern Alboran (Fig. 4). The AMOC weakening in the North Atlantic, triggered by the meltwater discharge, also resulted in colder SST and less humid westerlies, triggering a decrease in the amount of winter precipitation in the southern Iberia (Brayshaw et al., 2010; Jackson et al., 2015). Nevertheless, the release of isotopically-depleted meltwater into the Atlantic and the Mediterranean during the Heinrich event 1 depleted the isotopic composition of the surface water, resulting in more negative values during the HS1 than during the LGM, even if the latter was less arid than the former (Sierro et al., 2005, 2020; Cheddadi et al., 2021; García-Alix et al., 2021).

The B-A is characterized by overall depleted δ^2H values, but an interval of relatively high values around 13.4 and 14.0 cal ka BP, can be recognized in the Alboran and in the south Spain and North Africa records, suggesting internal variability during this period (Fig. 6) (Cheddadi et al., 2021; García-Alix et al., 2021). The high values between 13.4 and 14 cal ka BP could be tentatively related to the Greenland Interstadial 1d, known as Older Dryas, which triggered arid conditions in the Mediterranean area (Lowe et al., 2008; Rasmusen et al., 2008; Dormoy et al., 2009; López-Sáez et al., 2020).

The transition to the YD is recorded in both eastern and western Alboran Sea sites as a two phased event, with depleted δ^2H_{wax} values at the onset and enriched δ^2H_{wax} values after 12.5 cal ka BP (Fig. 6). The depleted δ^2H_{wax} values between 13.5 and 12.5 cal ka BP coincided with the onset of the AMOC slowdown triggered by the meltwater discharge in the North Atlantic that could also have affected the Mediterranean (Fig. 4; McManus et al., 2004; Ng et al., 2018), and thus, δ^2H_{wax} values were more negative independent of an Atlantic or Mediterranean moisture source (García-Alix et al., 2021). Between 12.5 and 11.5 cal ka BP higher δ^2H_{wax} values are recorded in both basins (Fig. 6), suggesting a moisture source from the Mediterranean likely related to scarce winter precipitation triggered by the reduced AMOC, and higher influence of spring/late summer precipitation in the southwestern Mediterranean (Fletcher et al., 2010; Zielhofer et al., 2017; Ng et al., 2018; Camuera et al., 2021). Nevertheless, this δ^2H enrichment has not been recognized in the Padul wetland record in southern Iberia (Fig. 6; García-Alix et al., 2021), which could be related to a lower influence of the Mediterranean cyclonic precipitation inland. Other records in the Alboran Sea and the western Iberian margin have recognized overall dry condition during the YD interrupted by one or more humid sub-phases (Fletcher et al., 2013; Naughton et al., 2016, 2019).

The Early Holocene shows an abrupt shift to lower δ^2H_{wax} values in the western Alboran Sea record at around 10 cal ka BP and in the eastern Alboran Sea record at around 9 cal ka BP, consistent with a greater influence of the Atlantic moisture contribution (Fig. 6). The lower δ^2H_{wax} values during the Early Holocene compared with the B-A period suggest higher winter precipitation amounts in the former than in the latter, as shown by the nearby pollen (Combourieu-Nebout et al., 2009; Fletcher et al., 2010; Camuera et al., 2021; Cheddadi et al., 2021) (Fig. 4) and *n*-alkane δ^2H records (Fig. 6; García-Alix et al., 2021). Depleted δ^2H_{wax} values in the Alboran Sea records coincided with the minimum in winter insolation in the North Atlantic and the seasonality maximum, which resulted in a weaker AMOC, and an increase in the amount of Atlantic winter precipitation in the Mediterranean area (Fig. 6; Brayshaw et al., 2009; Zielhofer et al., 2017; Ng et al., 2018). This is supported by a recent study by Cheddadi et al. (2021) which has also related the occurrence of the African Humid Period with a southward displacement of the Atlantic storm track. Other *n*-alkane δ^2H records from two wetlands at different elevations recovered in southern Iberia, also documented a pervasive Atlantic moisture influence during this interval (Fig. 6; Toney et al., 2020; García-Alix et al., 2021).

The δ^2H_{wax} values of the western and eastern records fit with the humid conditions depicted by pollen records from southern Iberia and North Africa during the Early Holocene, but the $\delta^{13}C_{wax}$ values indicate enhanced aridity, contradicting regional climate reconstructions (Fig. 4). This would suggest that the δ^2H_{wax} is recording the regional variability meanwhile the $\delta^{13}C_{wax}$ is more sensitive to local changes. More depleted δ^2H_{wax} values in the eastern than in the western record are likely related to the higher altitude of the Andarax catchment basin and therefore, a stronger altitudinal effect in the δ^2H of the precipitation. On the other hand, the delayed response in the eastern Alboran record could be related to a higher influence of the Andarax catchment basin to the winter-early spring Mediterranean precipitation, as occurred nowadays (Martín-Vide and López-Bustins, 2006; Serrano-Notivoli et al., 2018).

The precipitation during the last part of the Middle Holocene in the Alboran Sea and surrounding continental areas is marked by a transition from prevalent Atlantic moisture source to more Mediterranean moisture contribution (Zielhofer et al., 2017; Toney et al., 2020; Cheddadi et al., 2021; García-Alix et al., 2021). This transition is punctuated by a see-saw event in the western Alboran record between 4.8 and 3.8 cal ka BP of Mediterranean-Atlantic-Mediterranean moisture source, which could be related to the

worldwide recognized event at 4.2 cal ka BP (Bini et al., 2019). This event has also been recorded by a decrease in humid pollen taxa in different western Mediterranean records (Fletcher et al., 2010; Jiménez-Moreno et al., 2015; Ramos-Román et al., 2016; Mesa-Fernández et al., 2018).

Despite the low resolution of both δ^2H_{wax} Alboran profiles, the different trends in the eastern and western Alboran records suggest that such differences during the Middle-Late Holocene could be related to the establishment of the present-day climate regime. Thus, the precipitation over the western Alboran Sea drainage basin would have been more influenced by NAO dynamics while the eastern Alboran Sea drainage basin would have been subjected to a more significant influence of the Western Mediterranean Oscillation (López-Bustins et al., 2006; Moreno et al., 2017; Serrano-Notivoli et al., 2018).

7. Conclusions

The study of stable carbon and hydrogen isotopes obtained from leaf wax long-chain *n*-alkanes along with other~~s~~ *n*-alkanes based proxies have allowed the reconstruction of the hydrological conditions and sediment input variations in the Alboran Sea over the last 20 ka.

Comparisons between the obtained proxy records and continental paleoclimatic records from the southern Iberia and northern Morocco suggest that $\delta^{13}C_{wax}$ values in the Alboran Sea are significantly influenced by changes in the *n*-alkanes source area and by the sedimentary processes at each site while the δ^2H_{wax} signature respond to regional variation in the precipitation patterns. The $\delta^{13}C_{wax}$ record supports the sedimentary *n*-alkanes in the Alboran Sea being mainly derived from C_3 plants likely from the southern Iberia. Nevertheless, the $\delta^{13}C_{wax}$ record along the last 20 ka at each core is different despite the close proximity of the records, suggesting that they are not responding to the same forcings. The occurrence of some intervals with low CPI values and UCMs between 15-11 cal ka BP during the rapid sea level rise triggered by the melt-water pulses 1a and 1b point to the erosion of older soils formed when the shelf was exposed and/or to the occurrence of turbidites triggered by the destabilization of the shelf break. These UCMs are recognized in the eastern record, likely due to the basin architecture which is more prone to receive sediment from the shelf.

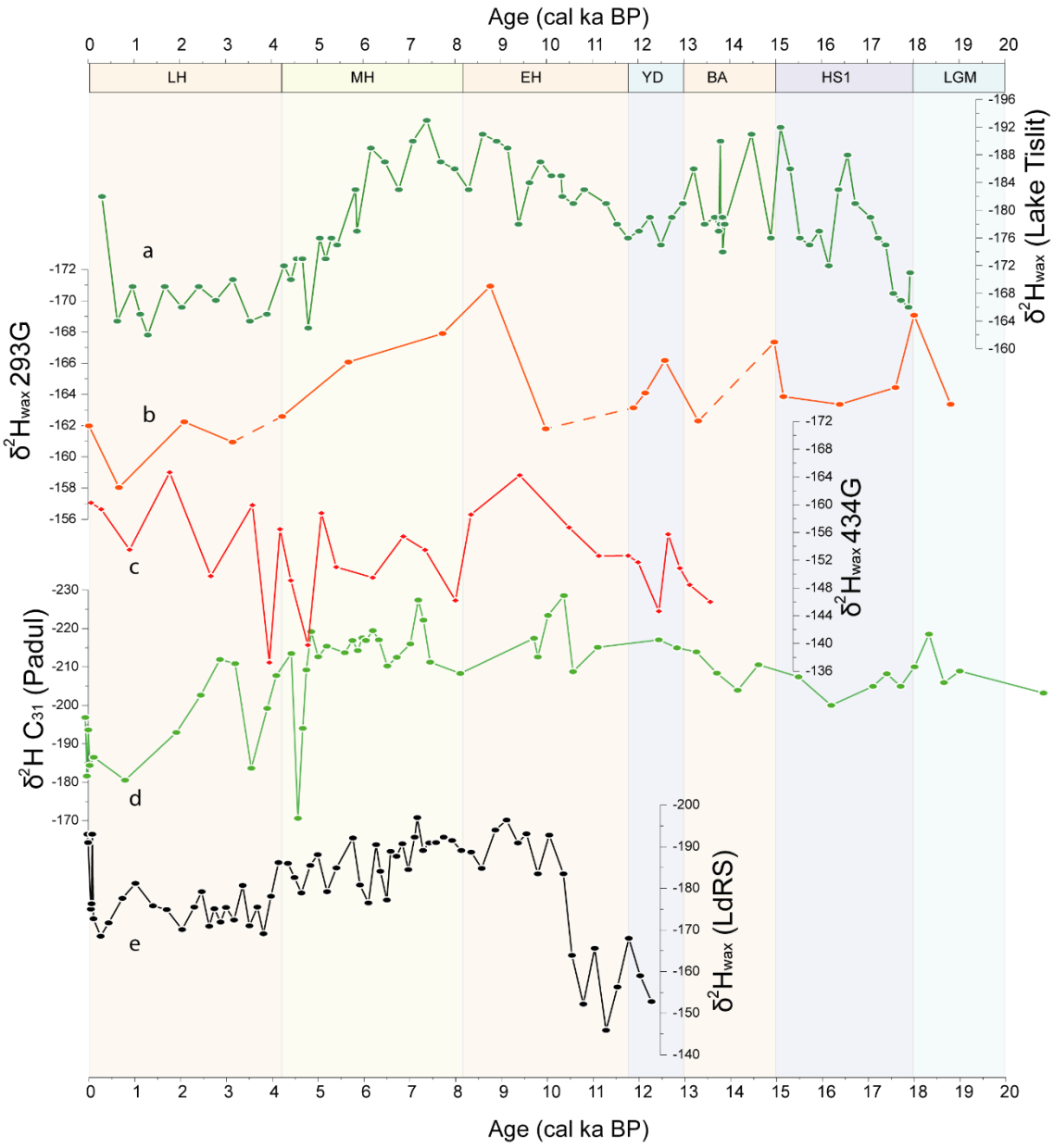

Figure 6. Comparison between δ^2H records from: (a) Lake Tislit (core GC27; Cheddadi et al., 2021); (b) Padul wetland (Padul-15-05; García-Alix et al., 2021); (c) western Alboran site, 434G sediment core; (d) eastern Alboran site, 293G sediment core, and (e) Laguna de Río Seco (LdRS; Toney et al., 2020).

Furthermore, in the eastern Alboran, a major change in the $\delta^{13}C_{wax}$ occurred at the onset of the mwp-1b, between 11.8-11.2 cal ka BP as response to the sea level transgression and likely a change in the plant type input. Prior to this interval deposition, the input of leaf wax *n*-alkanes into the eastern Alboran site mainly derived from coastal vegetation with low $\delta^{13}C_{wax}$ values. After 11.2 cal ka BP the disconnection of the storm wave base with the shelf break reduced the influence of the coastal vegetation and the *n*-alkanes

show more positive values, suggesting that the *n*-alkane source was the entire Andarax basin.

The western Alboran core is mainly influenced by two rivers, and thus the $\delta^{13}C_{wax}$ signal depends on the river supplying larger sediment input. During enhanced winter precipitation there was a greater influence of vegetation from the Guadalhorce river basin, which was more adapted to arid condition. On the other hand, during reduced winter precipitation, there was a major influence of vegetation from the Fuengirola river, whose drainage basin is smaller and closer to the coast, thus the vegetation was more adapted to humid conditions.

Conversely to the $\delta^{13}C_{wax}$, the $\delta^{2}H_{wax}$ signature at both Alboran sites shows a similar trend to other records located in the southern Iberia and northern Africa, suggesting similar precipitation pattern over the last 20 ka.

During the HS1, the melt water influx in the westernmost Mediterranean resulted in a highly depleted values of precipitation, even more depleted values than during the LGM. The YD record shows an early phase characterized by depleted $\delta^{2}H_{wax}$ values, likely related to other pulse of melt water. A late phase during the YD is characterized by more enriched $\delta^{2}H_{wax}$ values likely as the result of reduced winter precipitation triggered by an AMOC reduction and the high influence of spring and summer precipitations.

The Early Holocene is characterized by the lowest $\delta^{2}H_{wax}$ values of the last 20 ka, consistent with a stronger AMOC and an enhanced Atlantic moisture influence over the western Mediterranean area. The Middle-Late Holocene is characterized by a transition from a pervasive Atlantic moisture source to more Mediterranean conditions, punctuated by a see-saw between 4.8 and 3.8 cal ka BP of Mediterranean-Atlantic-Mediterranean moisture sources. After 3.8 cal ka BP the eastern Alboran record points to more influence of Mediterranean precipitation while the western record indicates higher influence from Atlantic precipitation, thus suggesting the establishment of the present-day climatic conditions.

Supplement to:

Stable hydrogen and carbon isotope records of plant wax *n*-alkanes from the Alboran Sea basin (westernmost Mediterranean) indicate precipitation and sediment dynamics during the last deglaciation

Jose Manuel Mesa-Fernández[1], Marta Rodrigo-Gámiz[2], Francisca Martínez-Ruiz[1], Antonio García-Alix[1,2], Marcel T. J. van der Meer[3]

[1] Instituto Andaluz de Ciencias de la Tierra (IACT), CSIC-UGR, Avenida de las Palmeras 4, 18100, Armilla, Granada, Spain

[2] Departamento de Estratigrafía y Paleontología, Universidad de Granada (UGR), Avda. Fuente Nueva s/n, 18071, Granada, Spain

[3] Department of Marine Microbiology and Biogeochemistry, Royal Netherlands Institute for Sea Research (NIOZ), Den Burg, Texel, The Netherlands

Correspondence to: Jose Manuel Mesa-Fernández (jmesa@ugr.com)

SAMPLE ID	293G 1 0-1.5	293G 1 6-7.5	293G 1 12-13.5	293G 1 24-25.5	293G 1 30-31.5	293G 1 36-37.5	293G 1 42-43.5	293G 1 54-55.5	293G 2 1.5-3	293G 2 7.5-9
DEPTH (cm)	0.75	6.75	12.75	24.75	30.75	36.75	42.75	54.75	60.25	66.25
Age (cal ka BP)	0.025	0.346	0.679	1.366	1.723	2.103	2.466	3.158	3.488	3.865
ACL	30.2	30.2	30.3	30.3	30.2	30.2	30.2	30.2		
CPI	4.4	4.3	6.7	8.9	9.7	10.4	8.3	8.4	UCM	UCM
δC C27	-30.4	-29	-28.9	-29.4			-29.3	-29.1		
Stdev C27	0.4	0.1	0	0.4			0.1	0.3		
δC C29	-32.8	-30.5	-32	-31			-30.5	-30.7		
Stdev C29	1.7	0.1	0	0.2			0	0		
δC C31	-31.9	-32.7	-30.7	-30.9			-31.6	-29.9		
Stdev C31	0.1	0.1	0	0.2			0.1	0.2		
δC C33	-31.9	-32	-29.9	-30.7			-30.5	-30.8		
Stdev C33	0.7	0.4	0.3	0.7			0.4	0.3		
δD C27	-148		-132.7			-151.4				
Stdev δD C27	2.9		1.8			3.8		10.2		
δD C29	-154.4		-148.1			-156.5		-154.3		
δD C29 Ice corrected	-154.4		-148.1			-156		-154		
Stdev δD C29	0.7		0.6			2.5		1.3		
δD C31	-167.4		-165.1			-167.2		-166.3		
dD C31 Ice corrected	-167.4		-165.1			-166.7		-165.9		
Stdev δD C31	1.7		0.1			0.4		1.5		
δD C33	-145.8		-151.1			-163.8		-162		
Stdev δD C33	3.3		2.7			2.5		1		

293G 3 45-46.5	293G 3 33-34.5	293G 3 27-28.5	293G 3 15-16.5	293G 3 9-10.5	293G 3 3-4.5	293G 2 49.5-51	293G 2 37.5-39	293G 2 31.5-33	293G 2 25.5-27	293G 2 19.5-21	293G 2 13.5-15
162.25	150.25	144.25	132.25	126.25	120.25	108.25	96.25	90.25	84.25	78.25	72.25
9.364	8.779	8.438	7.738	7.381	7.054	6.353	5.684	5.338	4.986	4.618	4.24
30.1	30.1	30.1	30.2	30.2	30.2	30.1	30.2	30.1		30.1	30.1
6.2	7.9	7.9	8.3	7.8	6.9	4.4	6.5	4.2	UCM	6.9	6.1
-29.2		-29.1		-28.9		-29.2	-29.2	-28.8		-28.5	-29
0.4		0.2		0		0.1	0.1	0.1		n.d.	0.2
-31.2		-31.5		-31.7		-32.4	-30.6	-30.5		-30.9	-30.7
0.1		0.2		0.1		0.1	0.3	0.1		n.d.	0.5
-31.1		-31.4		-31.4		-31.5	-29.9	-30.6		-30.5	-30.1
0.2		0		0.1		0.1	0.1	0.1		n.d.	0.4
-31.1		-31.2		-31		-31	-30.2	-31.2		-29.6	-29.9
0.1		0.2		0		0.5	0.2	0.2		n.d.	0
	-158		-158.9				-156.1				-147
	n.d.		0.6			9.6	5.8				2.8
	-162		-163.4			-136.8	-156.5				-150
	-161.8		-163.4			-137	-156.8				-149.9
	n.d.		0.8			2.4	0.3				1.4
	-177.8		-171.1			-159.7	-172.5				-171.7
	-177.5		-171.1			-159.9	-172.7				-171.6
	n.d.		2			2	0.1				1.6
	-169.3		-174.1			-160.9	-164.9				-159.9
	n.d.		0.1			0.5	0.3				0.6

293G 5 15-16.5	293G 5 12-13.5	293G 5 9-10.5	293G 5 0-1.5	293G 4 52.5-54	293G 4 46.5-48	293G 4 40.5-42	293G 4 34.5-36	293G 4 22.5-24	293G 4 16.5-18	293G 4 4.5-6	293G 3 57-58
247.75	244.75	241.75	232.75	227.75	221.75	215.75	209.75	197.75	191.75	179.75	174
12.159	12.039	11.902	11.566	11.429	11.264	11.096	10.925	10.594	10.403	9.989	9.783
30	29.8	30				29.5	30.1	30.1	30.1	30	30.1
7.4	5.6	8.4	UCM	UCM	UCM	2.8	8.5	7.5	7.9	6.9	8.1
-29.6		-30.5				-29.1		-29.7		-29.5	
0.2		0				0		0.1		0.4	
-31		-33				-30.6		-31		-31.2	
0.3		0.1				0.1		0.1		0.1	
-31.7		-33.6				-31.9		-31		-31.1	
0.2		0				0.4		0.2		0.3	
-31.8		-33.7				-32.3		-31.5		-31.7	
0.1		0.2				0.1		0.6		0	
-152.3		xxx				-123.4					
0.3		21.9				3.7				9.1	
-155.3		-153.3				-131				-151.3	
-157.4		-155.2				-132.4				-152.4	
0		6.1				1.3				1.7	
-166.7		-166.9				-150.9				-167.4	
-168.8		-168.8				-152.4				-168.5	
1.4		3.8				5				0.2	
-149.7		-158.2				-138.3				-165.1	
1.9		8.2				8.5				3.9	

293G 6 10.5-12	293G 6 4.5-6	293G 6 1.5-3	293G 5 57-58	293G 5 51-52.5	293G 5 45-46.5	293G 5 42-43.5	293G 5 39-40.5	293G 5 33-34.5	293G 5 27-28.5	293G 5 22.5-24	293G 5 19.5-21
301.25	295.25	292.25	289.5	283.75	277.75	274.75	271.75	265.75	259.75	255.25	252.25
13.895	13.689	13.587	13.495	13.314	13.135	13.046	12.955	12.772	12.587	12.45	12.335
29.9	29.8	29.7		30	30		30	29.9	29.9	30	30
6.5	7.1	5.2	UCM	7	6.5	UCM	7.7	8	8.6	5.4	6.5
-30.3	-31.1			-30.5	-29.8		-30.1	-29.9	-30.1	-31.6	-32.4
0.4	0.5			0.3	0.3		0.2	0.2	0.3	2.2	1
-32.1	-32.9			-33.5	-31.6		-31.5	-31.5	-31.8	-33	-33.4
0	0.3			0	0.3		0.3	0.2	0.2	0.4	0.4
-31.7	-32			-32.1	-31.8		-31.2	-31.8	-31.5	-31.3	-32.9
0.3	0.2			0.4	0.3		0.4	0.6	0	0.4	0.2
-31.2	-31.8			-32.1	-32.1		-31.8	-32.7	-31.6	-31.5	-33.4
0.8	0.1			0.4	0.3		0.5	0.1	1	0.4	0.2
				-142.8					-146.8		
				4					n.d.		
				-148.5					-156.1		
				-152.1					-159.2		
				1					n.d.		
				-165.9					-168.1		
				-169.5					-171.2		
				0.2					n.d.		
				-148.2					-153.9		
				7.2					n.d.		

293G 7 1.5-3	293G 6 55.5-57	293G 6 49.5-51	293G 6 42-43.5	293G 6 39-40.5	293G 6 36-37.5	293G 6 34.5-36	293G 6 28.5-30	293G 6 25.5-27	293G 6 22.5-24	293G 6 19.5-21	293G 6 16.5-18
351.25	346.25	340.25	332.75	329.75	326.75	325.25	319.25	316.25	313.25	310.25	307.25
16.402	16.067	15.669	15.174	14.975	14.809	14.726	14.519	14.416	14.311	14.203	14.1
29.9	29.9	29.6	29.8	29.8	29.4		29.5		29.6		29.9
7.5	7.6	2.1	5.9	5.4	1.8	UCM	2	UCM	3.5	UCM	6.2
-30.1	-29.9	-28.8	-32.5	-31.4			-29.4		-30.4		
0.3	0.2	0.1	0.5	0.5			0.3		0.3		
-31.3	-31.3	-30.7	-34.3	-32.4			-30.4		-32.6		
0.1	0	0.1	0.2	0.4			0.3		0.4		
-32.2	-31.6	-31.1	-33.9	-32.3			-30.5		-32.1		
0.3	0.1	0	0.6	0.3			0.4		0.5		
-31.9	-31.5	-31.3	-33.1	-32.9			-31.4		-31.4		
0.7	0.4	0.2	0.3	0.6			0.1		3		
-150.8		-133.1	-137.1	-142.7			-124.4				
3.3		n.d.	n.d.	1.3			0.1				
-152.4		-133.9	-155.4	-157.7			-126.3				
-158.1		-139.6	-159.8	-161.9			-130				
1		n.d.	n.d.	2.9			0.4				
-161.4		-144.3	-162.2	-167			-136.5				
-167.1		-150	-166.7	-171.2			-140.3				
1.6		n.d.	n.d.	2.3			1.4				
-157.5		-139.5	-150.9	-161.1			-120				
1.3		n.d.	n.d.	0.2			1.7				

293G 7 7.5-9	293G 7 13.5-15	293G 7 19.5-21	293G 7 25.5-27	293G 7 31.5-33	293G 7 37.5-39	293G 7 40.5-42	293G 7 46.5-48
357.25	363.25	369.25	375.25	381.25	387.25	390.25	396.25
16.809	17.211	17.619	18.024	18.423	18.821	19.018	19.323
29.9	30	30	30	30	30	30	29.9
8.1	9	8.5	7.8	7.5	7.1	8.4	6.3
-30.1	-29.8	-29.8	-30	-30.8	-30.9	-31	-30.7
0.3	0.1	0.3	0.1	0.1	0.2	0.4	0.1
-31.5	-31.7	-32.2	-30.7	-31.7	-32	-32	-32.1
0.3	0	0.3	0.5	0.1	0.1	0.4	0.5
-32.4	-31.5	-30.8	-31.1	-32	-32.1	-32	-31.7
0.3	0.2	0.2	0.3	0.2	0.1	0.7	0.2
-31.9	-31.3	-29.9	-30.9	-32	-32	-32.2	-31.9
0.3	0.2	0.2	0.7	0.2	0.3	1.2	0.4
		-144.8	-152.2				
		0.3	n.d.		11		
		-151.1	-155.7		-151.2		
		-158.4	-163.6		-159		
		0.3	n.d.		3.5		
		-161.4	-165.1		-158.7		
		-168.7	-173		-166.5		
		1.8	n.d.		4.5		
		-152.9	-157.1		-149.9		
		0.3	n.d.		1		

Table S1. Average Chain Length (ACL), Carbon Preference Index (CPI), carbon and hydrogen isotope ratios of C_{27} – C_{33} *n*-alkanes from core 293G, n.d. denotes when concentrations were too low for duplicate isotope measurements. UCM: Unresolved Complex Mixture

SAMPLE ID	434G-0 0-1,5	434G-0 3-4,5	434G-0 6-7,5	434G-0 9-10,5	434G-0 12-13,5	434G-0 15-16,5	434G-0 18-19,5	434G-0 21-22,5	434G-0 24-25,5	434G-0 27-28,5
DEPTH (cm)	0.75	3.75	6.75	9.75	12.75	15.8	18.8	21.8	24.8	27.75
Age (cal ka BP)	-0.04	0.058	0.17	0.28	0.38	0.48	0.57	0.67	0.77	0.899
ACL	30.2	30.3	30.3	30	30	29.9	30	30.1	30.1	30.1
CPI	3.9	4.8	5.3	4	6	4.3	5.5	6.6	4.8	6.8
Stdev δC C27	0.1	0.4	0.2	0.1	0.4	0.3		0.2		0.5
δC C29	-33.1	-32.4	-31.9	-31.8	-31.9	-31.5		-32.9		-32.1
Stdev δC C29	0.1	0	0.2	0.3	0.1	0.6		0.3		0.5
δC C31	-32.2	-31.5	-31.8	-31.2	-31.9	-30.7		-32.4		-32.1
Stdev δC C31	0.4	0.2	0.2	0.2	0.2	0		0.1		0
δC C33	-31.5	-31.5	-30.8	-31.1	-30.9	-29.1		-32.9		-32
Stdev δC C33	0.4	0.2	0	0.3	0.2	0		0.4		0.6
δD C27		-140.7		-129.3						
Stdev δD C27		1.3		2.3						
δD C29		-158.7		-155.5						-148.5
δD C29 Ice corrected		-158.7		-155.5						-148.5
Stdev δD C29		1.3		0.6						5.2
δD C31		-161.5		-162.3						-157.4
dD C31 Ice corrected		-161.5		-162.3						-157.4
Stdev δD C31		2.6		1.1						4.6
δD C33		-131.4		-144.9						-126
Stdev δD C33		8.5		8.9						23.9

434G-2 0-1,5	434G-1 51-52,5	434G-1 48-49,5	434G-1 39-40,5	434G-1 27-28,5	434G-1 21-22,5	434G-1 15-16,5	434G-1 9-10,5	434G-1 4,5-6	434G-1 3-4,5	434G-0 33-34,5	434G-0 30-31,5
90.75	87.8	84.75	75.75	63.8	57.75	51.8	45.8	41.3	39.8	33.8	30.8
4.18	4.07	3.948	3.579	3.03	2.67	2.3	1.96	1.68	1.58	1.24	1.05
30	29.9	30	30	30.2	30.1	30.1	30	30.2	30	30.2	30.1
5.2	6.6	5.4	5.2	7.9	7.3	7.1	6.4	7.4	6.2	7.3	6.2
0	0.4	0.2	0	0.1	0.5	0.1			0.3		0.5
-32.3	-32.1	-30.4	-32	-32.6	-32.6	-30.9			-31.5		-32.4
0.1	0.2	0.4	0	0.3	0.2	0			0.3		0.2
-31.3	-30.4	-31.5	-31.8	-32.2	-31.2	-30.8			-31.5		-32.1
0.2	0.1	0.1	0.1	0.4	0	0.1			0.8		0.1
-31.4	-31.3	-31.5	-31.6	-34	-28.7	-30.4			-30.2		-32.3
0.6	0.5	0.6	0.1	0.1	2.7	0.3			0.1		0.2
-139.5			-145.4								
n.d.		20	5.5								
-154.4		-129.2	-149.9		-144.7						
-154.2		-130.2	-149.6		-143.6						
n.d.		1.8	0.6		2.3						
-158.3		-142.9	-168.2		-155.4						
-158.2		-142.7	-167.9		-154.4						
n.d.		1.8	0.9		5.2						
-117.2		-104.2	-144.7		-131.7						
n.d.		6.5	5		9.6						

434G-3 13,5-15	434G-3 7,5-9	434G-3 1,5-3	434G-2 54-56	434G-2 48-49,5-	434G-2 42-43,5	434G-2 36-37,5	434G-2 33-34,5	434G-2 27-28,5	434G-2 21-22,5	434G-2 15-16,5	434G-2 6-7,5
160.3	154.3	148.3	145	138.8	132.8	126.8	123.8	117.8	111.8	105.8	96.75
7.661	7.345	7.038	6.87	6.534	6.203	5.9	5.737	5.407	5.084	4.788	4.417
30	30.1	30	30.2	30	30	29.9	29.9	29.8	29.8	30	30.1
5.7	6	5.9	6.5	6.3	5	5.9	6	4.5	5.4	3.4	7.1
0.1	0.3	0	0.1	0	0.2	0.4	0.6	0	0.1		0.2
-31.2	-31.8	-31.9	-31.1	-31.2	-30.7	-30.8	-30.9	-33.2	-31.3		-32.4
0.3	0.3	0	0.1	0.2	0.1	0.4	0.4	0.1	0.1		0.4
-30.8	-30.4	-30.6	-30.7	-30.8	-30.6	-30.6	-31.6	-32	-31.5		-31.9
0.2	0	0.1	0	0.1	0.2	0.1	0.2	0.2	0.4		0
-28.9	-30.2	-32.5	-31.1	-30.3	-29.8	-30	-31.2	-31.1	-33.4		-31.7
0	2.3	0.2	0.1	1.5	0.3	0.4	1.8	0.2	0.1		0.1
	-149.5		-151.8		-161.1			-135.5	-149	-127.8	-135.7
	0.6		0.1		n.d.			0.3	2.3	4.6	4.8
	-147.6		-149.4		-145			-144	-152.3	-130.3	-141.1
	-147.3		-149.1		-145.2			-144.2	-152.4	-130.3	-141
	3		2.4		n.d.			1.9	1.4	1.9	0.8
	-158.5		-160.6		-152.5			-156.1	-163.7	-147.2	-155.4
	-158.2		-160.3		-152.8			-156.3	-163.8	-147.1	-155.3
	0.6		1.3		n.d.			1.4	1.9	2.1	0.3
	-151.7		-154.6		-126.6			-138.8	-145.2	-121.4	-134
	3.3		2.1		n.d.			0.8	5.5	4.3	2

434G-4 18-19,5	434G-4 15-16,5	434G-4 12-13,5	434G-4 9-10,5	434G-4 0-1,5	434G-3 49,5-51	434G-3 43,5-45	434G-3 40,5-42	434G-3 34,5-36	434G-3 31,5-33	434G-3 25,5-27	434G-3 19,5-21
220.3	217.3	214.3	211.3	202.3	196.3	190.3	187.3	181.3	178.3	172.3	166.3
11.78	11.57	11.35	11.13	10.49	10.04	9.621	9.409	8.976	8.754	8.346	8.007
29.9	30	29.8	29.7	29.9	29.8	30	30	30	29.9	30	30
5.8	5.7	4.9	4.9	2.9	4.8	5.3	5	5	4.9	6	5.6
0.1	0.2		0	0.3	0.3	0.3		0.4		0.9	0
-30.7	-30.2		-30.8	-31.2	-30.3	-30.4		-30.6		-30.5	-31.4
0.2	0		0.2	0.4	0.2	0.1		0.7		0.2	0.8
-30.9	-30.3		-30.7	-31.4	-30.7	-30.1		-30.6		-30.5	-30.9
0.1	0		0	0.1	0.8	0.1		0		0.1	0
-30.9	-29.7		-30	-31	-31.1	-30.5		-28.5		-30.8	-29.2
0.8	0.1		0	0	1.2	2		0.1		0.5	0.2
-141.3			-132.3	-137.7			-154.1			-129.7	-136.1
2.6			n.d.	n.d.			0.2			1.1	n.d.
-148.8			-145.4	-147.5			-156.4			-151.5	-142.5
-150.8			-146.9	-148.8			-157.2			-151.4	-142.5
2.4			n.d.	n.d.			0.3			2.9	n.d.
-152			-155.7	-161.5			-168.9			-164.2	-149
-154.1			-157.1	-162.8			-169.7			-164.1	-149.1
3.7			n.d.	n.d.			0.6			3.7	n.d.
-123.4			-120.6	-141.8			-156.3			-144.3	-143.9
17.3			n.d.	n.d.			0.9			3.4	n.d.

434G-4 49,5-51	434G-4 48-49,5	434G-4 45-46,5	434G-4 42-43,5	434G-4 39-40,5	434G-4 36-37,5	434G-4 33-34,5	434G-4 30-31,5	434G-4 24-25,5	434G-4 21-22,5
252	250.3	247.3	244.3	241.3	238.3	235.3	232.3	226.3	223.3
13.7	13.57	13.42	13.27	13.12	12.97	12.83	12.65	12.21	11.99
30	29.8	29.8	29.8	29.8	29.9	29.8	29.8	29.8	29.9
6	5.1	5.4	5.9	6.2	6.6	6	6.6	5.9	5.4
	0.2	0		0	0	0.2	0.1	0.3	1.5
	-30.5	-30.5		-31.2	-31.2	-30.7	-31	-32.2	-31
	0.2	0.2		0	0.9	0.1	0	0.3	0.3
	-31.2	-31.7		-31.9	-31.5	-31.1	-31	-30.8	-31.7
	0.3	0		0.3	0.1	0.2	0.2	0.2	1.1
	-31.1	-31		-32.1	-30.5	-29.9	-29.8	-29.9	-31.8
	0.4	0.1		0.8	0.2	0.2	0.2	0.2	0.7
		-130.3		-135.5	-140.1		-143.7	-116.4	-132.5
		1.6		7.9	3		n.d.	5.2	2.2
		-143.5		-143.6	-144.4		-150.7	-126.9	-148.3
		-148.3		-147.1	-148.1		-153.2	-153.5	-150.2
		6.7		4.6	0.5		n.d.	3.5	0.1
		-140.7		-145.8	-149.3		-154.6	-135.8	-150.9
		-144.3		-149.5	-153		-157.7	-137.8	-152.8
		10.4		1.6	1.3		n.d.	3.2	0
		-131.4		-125.3	-133.3		-127.9	-116.9	-117.8
				0.5	2.7		n.d.	5.2	1.8

Table S2. Average Chain Length (ACL), Carbon Preference Index (CPI), carbon and hydrogen isotope ratios of C_{27} – C_{33} *n*-alkanes from core 434G, n.d. denotes when concentrations were too low for duplicate isotope measurements. UCM: Unresolved Complex Mixture

V

INTEGRATED DISCUSSION ON MARINE AND CONTINENTAL RECORDS

V. Integrated discussion on marine and continental records

In this PhD diverse sediment records from continental and marine realms have been studied using multiple approaches in order to characterize paleoclimate responses since the end of the LGM in the western Mediterranean. Following this main goal, in this chapter, results and conclusions from previous chapters are integrated and compared with other available sedimentary records in the western Mediterranean area in order to get new insights into climate teleconnections between high and low latitudes and also into the reconstruction of the anthropogenic impact in this region.

1. Sub-orbital scale paleoenvironmental evolution in the western Mediterranean area

1.1 The early deglaciation

The transition between the late LGM and the HS1 in the western Mediterranean is characterized by reduced WMDW formation as supported by the relatively low Ti/Ca values registered in the studied records. This reduced WMDW formation could be tentatively related to the mwp-19 ka (~ 19 cal ka BP; Huang and Tian, 2008; Clark et al., 2009; Álvarez-Solas et al., 2011) and the onset of the retreat of the glacial in the Mediterranean region (Ivy-Ochs, 2008; Palacios et al., 2020). The mwp-19 ka and the glacial retreat released freshwater input in the Gulf of Lions reducing the surface salinity and thus the WMDW formation.

The HS1 is characterized by a great advance of the sea ice sheet, extremely low SST and the input of IRD in the North Atlantic Sea (Heinrich et al., 1988; Eynaud et al., 2009; Toucanne et al., 2021). In the western Mediterranean, arid and cold conditions have been documented at this time (Kageyama et al., 2005; Combourieu-Nebout et al., 2009; Sierro et al., 2020; Rodrigo-Gámiz et al., 2011; Camuera et al., 2021). The Ti/Ca ratio in the studied marine records indicates an increase of the WMDW formation and well-ventilated seafloor. The relatively enriched δ^2H_{wax} in the Alboran area also suggests lesser influence of Atlantic winter precipitation and higher influence of precipitation derived of Mediterranean moisture. Less influence of δ^2H_{wax} depleted precipitation has been also recognized in the southern Iberia and North Morocco (Cheddadi et al., 2021; García-Alix et al., 2021).

The HE1 is characterized by a $\delta^{18}O$ depletion in surface waters pointing to a melt water influx in the Mediterranean, which is recognizable along the different western Mediterranean sub-basins (Sierro et al., 2005; Cacho et al., 2006; Jiménez-Espejo et al., 2007; Rodrigo-Gámiz et al., 2011; Ausín et al., 2015a; Alonso et al., 2021). The input of less dense waters in the western Mediterranean prevented surface water sink in the Gulf of Lions and thus reduced the formation of the WMDW (Sierro et al., 2005; Frigola et al., 2007). The time period at ~ 17-16 cal ka BP is characterized by different Ti/Ca ratios in the Algero-Balearic basin and the Alboran basin, which has been explained by a shallowing of the Bernoulli aspiration depth of WMDW in the Alboran basin as result of the reduced density gradient in the Gibraltar Strait (Mesa-Fernández et al., 2022). This led to decreasing seafloor oxygenation, which resulted in enhanced organic matter preservation, as shown by the TOC content in the Alboran Sea basins, and the development of the pre-ORL1 interval (Rodrigo-Gámiz et al., 2011; Pérez-Asensio et al., 2020; Mesa-Fernández et al., 2022). In addition, the freshening of the Mediterranean surface water could have reduced the oxygen isotopic differences between Mediterranean and Atlantic surface waters, and thus, in the isotopic $\delta^{2}H_{wax}$ composition of the precipitation, as also recognized in other records in northeast and southeast Iberia (Pérez-Mejías et al., 2020; García-Alix et al., 2021).

1.2 ORL1 in the Alboran Sea basins: onset, demise, and possible causes

Despite ORLs have been sometimes referred as the western expression of the sapropels (Murat, 1999), they differ in time and in driving mechanisms (Rogerson et al., 2008; Rohling et al., 2015). Recently, Casanova-Arenillas et al. (2022) recognized three types of ORLs based on sedimentological and ichnological features, which likely indicated different processes involving its deposition. Among the ORLs, the most recent one, ORL1, (15-9 cal ka BP) has been the most extensively studied while older ORLs are still poorly known. ORL1 comprises the B-A period, the YD and almost the whole Early Holocene (e.g., Cacho et al., 2001; Rodrigo-Gamiz, 2011; Pérez-Asensio et al., 2020). Its onset has been related to the freshwater input derived from the melting of the Alps and Pyrenees glaciers and the mwp-1a and 1b in the North Atlantic (Lambeck et al., 2014), which prevented the surface water sink in the Gulf of Lions (Rogerson et al., 2008; Rohling et al., 2015). The ORL1 demise has been related to a reactivation of the WMDW promoting the reventilation of the seafloor (Jiménez-Espejo et al., 2007; Pérez-Asensio

et al., 2020). Nevertheless, all the works invoking a reactivation of WMDW as the trigger for the ORL1 demise are based on an increase of the grain size upper than 10 μm in a record recovered in the Minorca drift (Frigola et al., 2007, 2008). However, the increase in this fraction has not been recorded in other contourites (Alonso et al., 2021) or hemipelagic sediments (Mesa-Fernández et al., 2022) in the Alboran Sea basins nor by redox elements (Rodrigo-Gámiz et al., 2011).

The analysis of redox-sensitive elements has demonstrated that during the ORL1 oxygen condition were highly variable. In the studied records, two phases have identified within the ORL1 in agreement with previous works (Martrat et al., 2014; Pérez-Asensio et al., 2020), and redox conditions have been characterized in each sub-phase. The obtained results support that the occurrence of the ORL1 is associated with a sharp increase in the SR in the Alboran Sea basin. The sub-phase 1a (15-11.7 cal ka BP) is characterized by a sharp increase of the Mo/Al and U/Al ratios and low values of the Mn/Al ratio. The end of the ORL1a was triggered by a reactivation of the WMDW during the YD as supported by changes in bottom water oxygenation proxies. Conversely, the ORL1b is characterized by low Mo/Al values, relatively high U/Al values and increasing Mn/Al values, suggesting less reduced conditions in the bottom waters. The demise of the ORL1b at around 9 cal ka BP also characterized by a decrease in the Sr/Ca values and a sharp decrease in the SR. As was hypothesized in *Chapter II*, this sudden increase in both, the Sr/Ca ratio and SR, could be related to: (1) the shelf flooding during the transgression which triggered the remobilization basinward of the loose sediments and the destabilization of the shelf break and (2) the overall humid conditions dominant during the B-A and the Early Holocene. The first idea is based on the leaf wax derived *n*-alkanes distribution (with UCMs) obtained during the interval with high SR, indicating degraded, mixed or reworked organic matter. The second hypothesis is based on the $\delta^{13}C_{wax}$ of core 293G pointing to a change in the vegetation source, likely triggered by the sea level rise and by the coastline migration. The WMDW slowdown along with the increase of the SR prevented the organic matter to be oxidized resulting in the onset of the ORL1 (15-9 cal ka BP) deposition. In addition, an increase in productivity with respect to the HS1 is also recorded in the Alboran Sea basin (Ausín et al., 2015a; Bazzicalupo et al., 2018; Wang et al., 2019). An enhanced flux of organic matter along with more stagnated water column could have increased the effective transport of the organic matter from the surface to the seafloor, since there was less piracy of the organic particles by the currents.

The B-A period (15-13 cal ka BP) was characterized by overall humid condition, as also supported by a sharp decrease in the Ti/Ca ratio and depleted δ^2H_{wax} values. The reactivation of the AMOC promoted the northward transport of warm conditions and reduced the temperature gradient between low and high latitudes, retreating the winter ice sheet maximum expansion northward (McManus et al., 2004; Ng et al., 2018; Toucanne et al., 2021). Higher SST and lower temperature contrast resulted in more humid and weaker westerlies, which resulted in higher precipitation amount and a major influence of Atlantic precipitation. Cheddadi et al. (2021) pointed to a southward migration of the Atlantic storm track as south as 24ºN as one important factor causing the green Sahara during the AHP.

The end of the ORL1a occurred during the YD, characterized by dry and cold conditions as result of a freshwater input in the North Atlantic from glacial lakes (Fanning and Weaver, 1997; Teller et al., 2002; Magny and Begeot, 2004). The concomitant slowdown of the AMOC, triggered similar conditions to the HS1 but in a lesser magnitude. Colder temperatures, a southward advance of the winter sea ice sheet in the northern hemisphere and a higher temperature contrast between the Mediterranean and the North Atlantic could have promoted the input of dry and cold winds in the Gulf of Lions, triggering the WMDW formation that re-ventilated the seafloor and interrupted the ORL1a deposition, as suggested by the increasing Ti/Ca values in the different marine records. This re-ventilation marked the end of the more reduced seafloor conditions in the Alboran Sea basin, as supported by the Mo/Al ratio, which returned to background values. The lower SST in the North Atlantic likely provoked less humid westerlies resulting in less winter precipitation over the Mediterranean area and thus, a greater record of spring/autumn precipitation, which mainly is derived from the enriched δ^2H_{wax} Mediterranean Sea moisture. During this interval the mountain glaciers in the Mediterranean area advanced as result of the pervasive cold temperatures.

The sea level rise during the mwp-1a (14.5-12.8 cal ka BP) triggered by the melting of the alpine glaciers reduced the surface salinity in the Gulf of Lions and thus reduced the WMDW formation (Rogerson et al., 2008, 2012; Rohling et al., 2015). The rapid sea level rise during the mwp-1a along with the pervasive humid conditions increased the SR in the Alboran Sea basin and the input of carbonate material from the shelf. Likely, the shelf flood and the wave ravinement focused on the shelf edge increased the downward transport of sediment. This is supported by the increasing trend of the Sr/Ca ratio and the

input of reworked and/or degraded terrestrial organic matter. The variation of the redox geochemical proxies, U/Al, Mo/Al and Mn/Al ratios, supported the poor oxygen conditions in the seafloor of the Alboran Sea basin.

The ORL1b (11.7-9 cal ka BP) encompassed most of the Early Holocene (11.7-8.2 cal ka BP) and is characterized by sub-oxic ferruginous conditions, with low values of Mo/Al, moderate of U/Al and increasing values of Mn/Al ratios. This interval coincided with the maximum summer insolation in the north hemisphere that promoted the evaporation and resulted in more humid westerlies (Laskar et al., 2004; Brayshaw et al., 2010). The depleted δ^2H_{wax} values in the westernmost Mediterranean region suggest enhanced winter precipitation with an Atlantic moisture source (*Chapter 3;* Cheddadi et al., 2021; García-Alix et al., 2021). The warmer conditions occurred during this interval triggered the mwp-1b (11.5-8.8 cal ka BP), and glacier retreat in the Mediterranean area. The sea level rise during the mwp-1b likely triggered the disconnection of the storm wave base and the shelf slope resulting in a drastic change in the leaf wax *n*-alkanes distribution supplied into the Alboran basin, which previously was biased toward a kind of coastal vegetation. Nevertheless, the ORL1b is characterized by a still high SR and Sr/Ca ratio, suggesting shallow carbonate input likely controlled by the high fluvial input and with not influence of the wave ravinement as during the ORL1a deposition (Catuneanu, 2006). In contrast to the ORL1a in which the reduced ventilation of the deep basin had greater influence, the ORL1b seem to be more influenced by an increase of productivity in the Alboran Sea (Ausín et al., 2015a; Wang et al., 2019; Pérez-Asensio et al., 2020), with high SR. The demise of the ORL1b in the Alboran Sea basin coincided with a decrease of the productivity, the Sr/Ca ratio and SR, which could have promoted the oxidation of the organic matter.

1.3 The Holocene

The glaciers in Sierra Nevada retreated with the onset on the Early Holocene, forming diverse lakes and wetlands (Anderson et al., 2011; Palacios et al., 2020). The Early Holocene coincided with a summer solar maximum and a reactivation of the AMOC. The warmer temperatures in the North Atlantic promoted the evaporation which resulted more humid westerlies (Brayshaw et al., 2010). The overall warm SST increased the humidity carried by the westerlies and resulted in a more depleted δ^2H_{wax} values as result of higher precipitation amount and predominant Atlantic moisture source. This glacial retreat also

triggered the formation of high altitude lakes in Sierra Nevada in the southern face, while in the northern face these lakes and wetlands are dated younger. The early phases of these wetlands are characterized by a predominant clayey lithology as result of the pervasive humid condition and the enhanced erosion of their catchment basins. The high input of clay sediments into the LH resulted in a low preservation of the pollen grains, but when preserved, the assemblages were mainly composed by *Pinus* pollen, suggesting humid conditions. During the Early Holocene, it is observed a marked difference in the climate response between the alpine wetland records and the marine records from the western Mediterranean basins. For instance, the centennial scale climate variability recorded in the LH record, depicted by the K/Al ratio as arid conditions, is not recorded in the marine sediment records.

The Middle Holocene is characterized by a trend towards more arid conditions. A reduction in winter precipitation in the surrounding western Mediterranean area is indicated by $\delta^{13}C_{wax}$ record of the 434G, which points to a higher contribution of *n*-alkanes from the Fuengirola river catchment basin to the western Alboran site. At around 6.3-4.5 cal ka BP there was an increase in the Saharan eolian input, showed by a marked increased trend in the Ca/Al and Zr/Al ratios in the LH record. Due to the absence of carbonates in the Sierra Nevada range, the increase in Ca did seem to be related to winds transport, although there are carbonates in the Granadian basin. The Zr is largely enriched in the Saharan dust, and its increase was triggered by the desertification of the Sahara-Sahel belt (de Menocal et al., 2000). The increase in aridity conditions was clearly recognized in some others Sierra Nevada wetland records (Jiménez-Espejo et al., 2014; Ramos-Román et al., 2016; García-Alix et al., 2017), though it is less evident in the western Mediterranean marine records. Particularly, in cores 434G, 292G, 293G, and 302G, characterized by SRs greater than 16 cam/ka, the increase in the Zr/Al ratio is not evident as it was during the HS1, likely due to the most arid conditions occurred at this time. Conversely, in cores 304G and 975B were the SR was lower, (14.4 cm/ka and 8.4 cm/ka respectively) this increase was more evident and depicted similar trends to those identified in Sierra Nevada records (Fig. 1). This could be due to differences in the SR, in those records where the SR were lower the eolian signal is less diluted than in those marine records with higher SR or higher influences of downslope or along-slope transport.

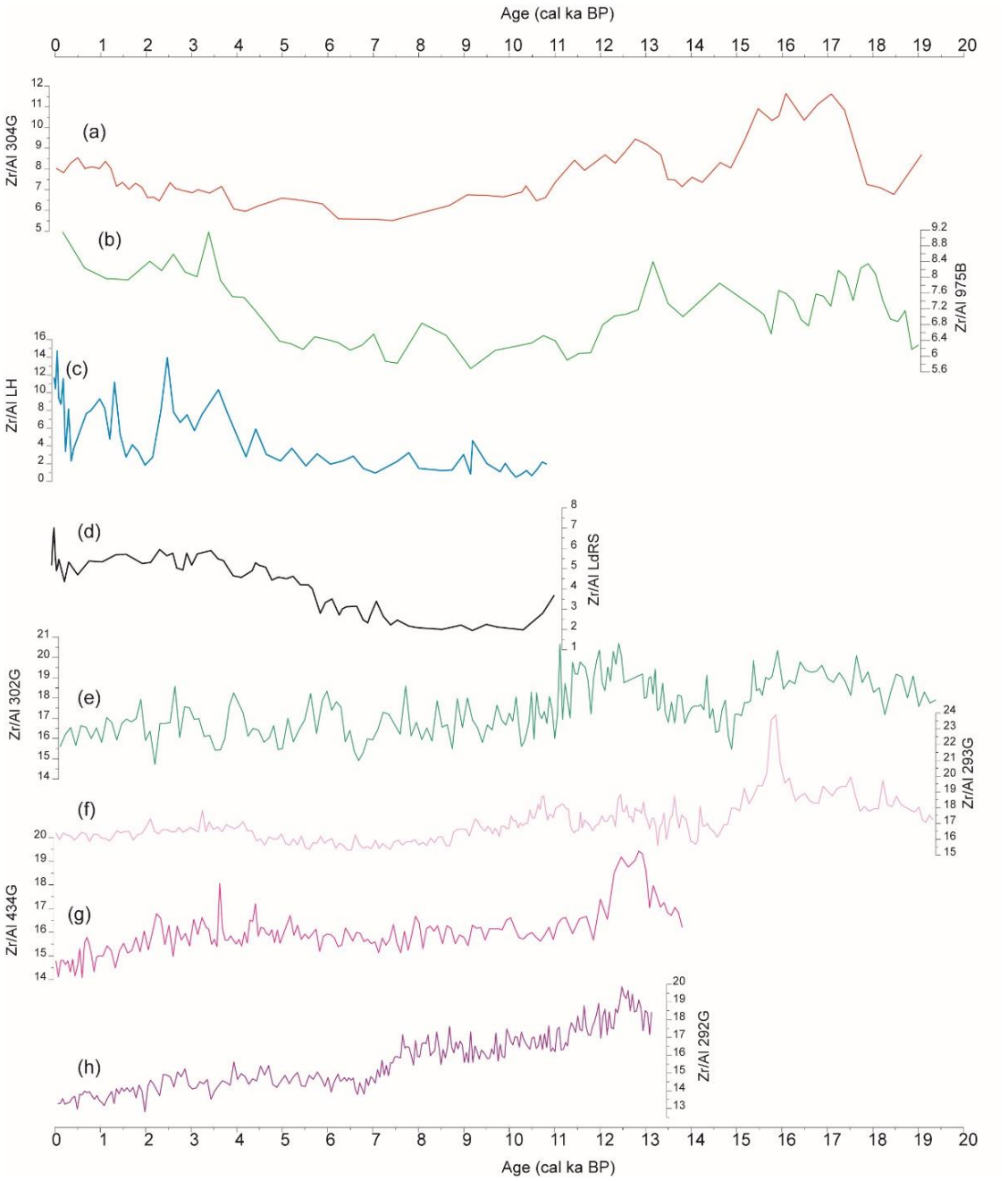

Figure 1. Comparison of Zr/Al ratio profiles from records: (a) 304G, (b) 975B, (c) LH (Mesa-Fermández et al., 2018), (d) LdRS (Anderson et al., 2011); (e) Zr/Al 302G; (f) 293G (Rodrigo-Gámiz et al., 2011); (g) 434G and (h) (292G).

The onset of the Late Holocene is marked by the cold and dry 4.2 ka event (Bini et al., 2019). Although, this event has been recognized in the north and south hemispheres, it seems not to have a great influence in the thermohaline circulation of the western Mediterranean Sea. Conversely, the δ^2H_{wax} record from the record 434G depicted a two-phased peak suggesting reduced precipitation from Atlantic source and higher influence from Mediterranean-sourced precipitation. This is also supported by other nearby records

from Morocco and southern Iberia pointing to a blocking of the westerlies in the meridional North Atlantic (Zielhofer et al., 2017). Pollen and geochemical records from LH pointed to more arid conditions shown by an increase in Poaceae pollen grains and in the Zr/Al ratio. A reduction in precipitation would be expected when the westerlies do not enter in the Mediterranean region. In addition, the reduced influence of the westerlies could have also promoted the southern wind from the Sahara-Sahel region, as supported by the Zr/Al ratio increase.

The IRHP (2.60-1.45 cal ka BP) is characterized by overall warm and humid conditions. A sharp increase in arboreal pollen and K/Al ratio was recorded in LH, resulting in a more clayey lithology. The eolian input in the wetland was severely reduced during this interval. A higher supply of organic matter from the Guadalhorce river drainage basin pointed by $\delta^{13}C_{wax}$ are also consistent with enhanced winter conditions and with a negative phase of the NAO (Martín-Puertas et al., 2009). A maximum in solar radiation could reduce the latitudinal gradient in the North Atlantic and weaken the westerlies displacing them to the Mediterranean area. The DA-MCA periods (1.45-0.65 cal ka BP) were characterized by overall arid conditions in the LH record, i.e. minimum values of arboreal pollen and runoff proxies along with an increase in the eolian input. A higher organic matter input from the Fuengirola river drainage basin is also recognized in the $\delta^{13}C_{wax}$ from record 434G, suggesting reduced precipitation. These intervals are also characterized by a positive NAO and a stronger AMOC than during the IRHP (Wanner et al., 2001). The LIA (0.65-0.15 cal ka BP) was characterized by humid conditions with an increase in arboreal pollen and runoff proxies in the LH record, along with a higher influence of the organic matter from the Guadalhorce river drainage basin in the $\delta^{13}C_{wax}$ from 434G record.

2. Climate teleconnection between high and middle latitudes during the deglaciation

As previously explained, the teleconnection between the Mediterranean region and the North Atlantic nowadays is based on the strength and position of the westerlies that control the humidity and temperature over the Mediterranean area and North Europe (i.e. Trigo et al., 2004). Nevertheless, during the last deglaciation, the SST and the position of the sea ice sheet could have also been influenced by the position of the convection cells and the humidity carried by the westerlies. In the literature there is certain consensus that during stadials periods there was an intensification of the westerlies (as during a positive

NAO phase) due to the temperature gradient between low and high latitudes (Brauer et al., 2008; Naughton et al.,2016, 2019; Li et al., 2019). There is also certain consensus that the southward advance of the sea ice sheet in the North Atlantic displaced southward the Farrel and Hadley cells, thus displacing southward the ITCZ and the westerly weather system (Walker et al., 2019). Hence, some authors have suggested a northward displacement of the westerlies and the storm track during stadials due to the higher temperature gradient (e.g., Brayshaw et al., 2009, 2010; Li et al., 2019), while others interpreted that there is a southward displacement (Bardají et al., 2009; Torner et al., 2019). However, there is a consensus that during high SST there was more near-surface atmospheric moisture content, thus more humid westerlies and vice versa (Held and Soden 2006; Brayshaw et al., 2010). The data obtained during this thesis suggest a minor influence of the Atlantic precipitation and overall arid conditions during the stadials. Nevertheless, it is difficult to assess if the reduced Atlantic moisture was triggered by the lower SST or by a northward displacement of the westerlies due to the higher temperature gradient between low and high latitudes.

On the other hand, the teleconnection between middle and high latitudes also influenced the formation of new WMDW. It depends on the heat loss of the surface water in the Gulf of Lions and by the salinity and temperature conditions of the subjacent intermediate water (Josey et al., 2011; Smith et al., 2008). The characteristic and intensity of the WMDW in the present exert a noticeable control on the thermohaline circulation in the western Mediterranean and influence the composition of the MOW, which in turn pump warm and salty waters to the North Atlantic. For this reason, reconstructing the WMDW dynamics under past climate scenarios have been a scope for paleoceanographers and paleoclimatologist over the last decades (Cacho et al., 2001; Sierro et al., 2005; Frigola et al., 2007, 2008, 2012; Bardají et al., 2009; Rodrigo-Gámiz et al., 2011; Ausín et al., 2015a). Apart from the characteristic of the LIW, the formation of the WMDW is related to heat loss of the surface waters under the influence of the winter dry winds as Tramuntana and Mistral (Smith et al., 2008; Schroeder et al., 2010; Canals et al., 2013), although less work has been focused on reconstructing these winds. In absence of these reconstructions, most of works that have attempted to link the deep-water formation with atmospheric processes have used a NAO-like dynamic for their explanation (Frigola et al., 2007; Bardají et al., 2009; Ausín et al., 2015b; Bazzicalupo et al., 2018; Torner et al., 2019), most of them based on the strong correlation found between the NAO and the

WMDW, as documented by Rixen et al. (2005). Nevertheless, these authors related the enhancement of WMDW formation to a positive (Frigola et al., 2007) either to a negative NAO-like phases (Bardají et al., 2009; Ausín et al., 2015b; Bazzicalupo et al., 2018), despite the work by Rixen et al. (2005) related the formation of WMDW with a positive NAO phase. More recent works analyzed the present-day relationship between the sea surface heat loss in the Mediterranean location of dense water formation and four main climatic modes, i.e., NAO, EAP, Scandinavian and East Atlantic/Western Russian (Josey et al., 2011; Papadopoulos et al., 2012). They concluded that for the Gulf of Lions the NAO only exert a minor influence in the surface heat loss, and that the main climatic mode dominating the heat loss in the area is the negative EA phase. As already explained, the EA is characterized by a low-pressure pole located in the western Ireland, but in its negative phase it changes to a positive pressure pole. The north hemisphere anticyclonic movement of the negative EA leads the southward movement of higher latitude cold and dry winds (Josey et al., 2011; Papadopoulos et al., 2012) (Fig. 2). If nowadays the heat loss in the Gulf of Lions is triggered by a high-pressure pole in the eastern North Atlantic, it seems unlikely that during the Holocene and the last deglaciation the heat loss depended on the westerlies position or strength. In addition, even if the westerlies were colder and drier than nowadays, they were likely warmer and more humid than those wind blowing from the North, so a southward migration of the westerlies seems an unlikely mechanism for explaining the increase of WMDW formation during stadials. We tentatively propose, that during phases of reduced or collapsed AMOC, the southward extension of the sea ice sheet during wintertime could create a pressure gradient between the cold eastern North Atlantic and the relatively warm Mediterranean. This could have led to an atmospheric situation similar to a negative EA phase, which promoted the northern cold and dry winds entering into the Gulf of Lions and favoring the WMDW formation. A higher pressure in the North Atlantic could have blocked the direct entrance of westerlies into the Mediterranean area, and a relatively warmer Mediterranean Sea could have also promoted the precipitation derived from Mediterranean moisture. This could also explain the more enriched δ^2H_{wax} values recorded during the HS1 and the YD in the western Mediterranean records (Cheddadi et al., 2021; García-Alix et al., 2021).

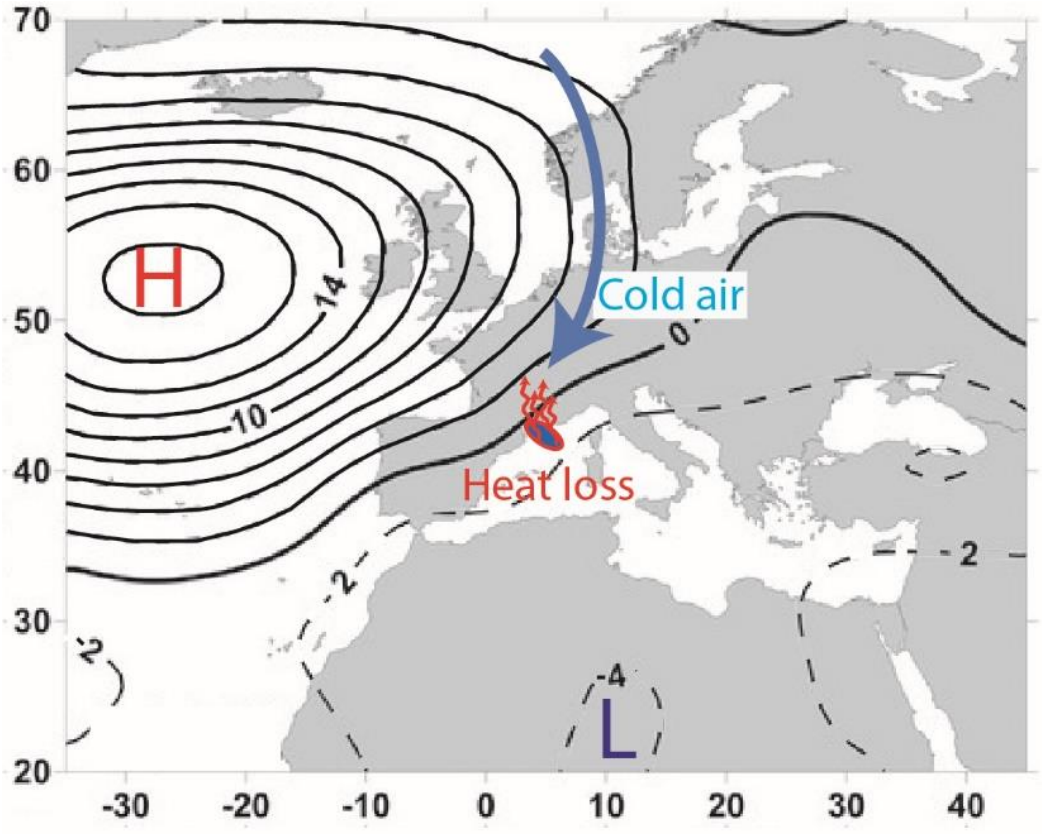

Figure 2. Negative EA phase (values are hypothetical). The anticyclonic gyre located in the eastern Atlantic promotes the southward migration of cold and dry winds into the Gulf of Lions, enhancing the surface water heat loss and triggering the WMDW formation. Modified from Papadopoulos et al. (2012).

3. Anthropic impact

The Iberian Peninsula has a large history of human occupation over the Quaternary (Finlayson et al., 2006), particularly during the Middle and Late Holocene when human activities significantly increased with the burning, pastoralism and mining of agrarian and metallurgical societies (Carrión et al., 2007, 2010). The human pressure in the Iberian Peninsula was heterogeneous but in the southeastern regions several important, such as the Millarian (Blanco-González et al., 2018) developed at this time. The metallurgical specialization of the Millarian society is hotly debated between archeologists (Lull et al. 2010; Murillo-Barroso et al. 2015, 2017). Diverse studies, including that from the nearby LdRS record in Sierra Nevada, have shown that mining and metallurgy activities commenced by ~4.5 cal ka BP in this area (García-Alix et al., 2013, and references therein), as shown by an enhanced Pb/Al ratio since this time. For the LH record, the first clear signal of lead pollution from mining and smeltering occurred around 2800 cal yr BP, coinciding with the Late Bronze Age (3.2-2.8 cal ka BP) and the Early Iron Age (2.8-

2.5 cal ka BP) (García-Alix et al., 2012. The same signal is also recorded in the nearby LdRS (García-Alix et al., 2013). Regarding the marine records 292G, 293G and 434G, these also show an increase in the Pb/Al ratio background levels between 3 and 2.5 cal ka BP (Fig. 3). The record 293G, which is located close to the Almeria TS and fed by the Andarax river, is the first one in registering such increase, likely because the Millarian society was settled close to this river.

The IRHP represents the most important lead pollution period prior to the IP mainly derived from mining activities (Settle and Patterson, 1980). However, only the record 292G shows an increase in the Pb/Al ratio while the LH, 293G and 292G records do not register enhanced pollution at this time. This could be due to a local effect, such as a higher catchment area in LH involving a high runoff input, supported by an increase in the K/Al and K/Ti ratios during this humid period that could have diluted the Pb signal transported by eolian input. In addition, a regional effect, such as a weaker dust mobilization due to the humid conditions prevailing at this time, or patchy pollution distribution, could explain this variability in the studied records. Differences could also be due to different sedimentation rates which can dilute the Pb signal. Apart from the 292G, other nearby continental records, such as the Zoñar Lake (Martín-Puertas et al., 2010) or the LdRS, also shown an increasing Pb/Al ratio during the IRHP.

Over the last 2 cal ka BP there was an unprecedented increase in the terrigenous input in the marine records from the Iberian margin (Cutmore et al., 2021; Mesa-Fernández et al., 2022). The increase of the use of soil due to the agriculture and mining along with the rise of settlement in Iberia and North Africa during by the Roman Empire could enhance the effective erosion and thus the terrigenous input into marine basins. Nevertheless, we cannot rule out that these variations could be also modulate by natural causes. The terrigenous input increase could bias the climatic signatures during this period, especially reconstructions based solely on elemental geochemical ratios.

An increasing trend in *Artemisia* pollen, which points to a climatic or anthropic aridification, coeval with another Pb/Al peak is recognized during the MCA. Increasing anthropic activities during this time are supported by the first appearance of coprophilous fungi such as *Sordiales* and *Sporormiella*, which occurred in BdlC (Ramos-Román et al., 2016) and in LdRS (Anderson et al., 2011), suggesting grazing activities at high altitudes in Sierra Nevada (Anderson et al., 2011; Jiménez-Moreno and Anderson, 2012; Ramos-Román et al., 2016). At around 0.6 cal ka BP there was a slight increase in *Olea europaea*

pollen grains with a sharp increase during the las 150 year (Jiménez-Moreno et al., 2013; Ramos-Román et al., 2016, 2019; Mesa-Fernández et al., 2018). This is evidenced by the onset of the cultivation of olives in the southern Iberian region and its extensive agriculture over the last 150 years. Nowadays, olive agriculture is one of the main economic activities developed in the southern Spain. This olive pollen increase in all the Sierra Nevada pollen records is undoubtedly the response to anthropic cultivation, though this signal is also superimposed to the climate variability record (Ramos-Román et al., 2019). The last 150 years are characterized as well by a sharp increase in the Pb/Al ratio in marine and continental records which is related to the increase in mining activities around the region and recently also to the use of leaded fuels. Moreover, there the increase in the Zr/Al ratio in all the Sierra Nevada records and in the marine records further support increasing local aridity and/or anthropogenic desertification, with a change in the origin and/or composition of the dust reaching this region (Jiménez-Espejo et al., 2014), likely related to the beginning of extensive agriculture and the concomitant desertification in the Sahel region (Mulitza et al., 2010). In general, the studied records evidence that the human impact is mostly remarkable during the last 2-3 millennia, suggesting increasing human activities in the southern Iberian region.

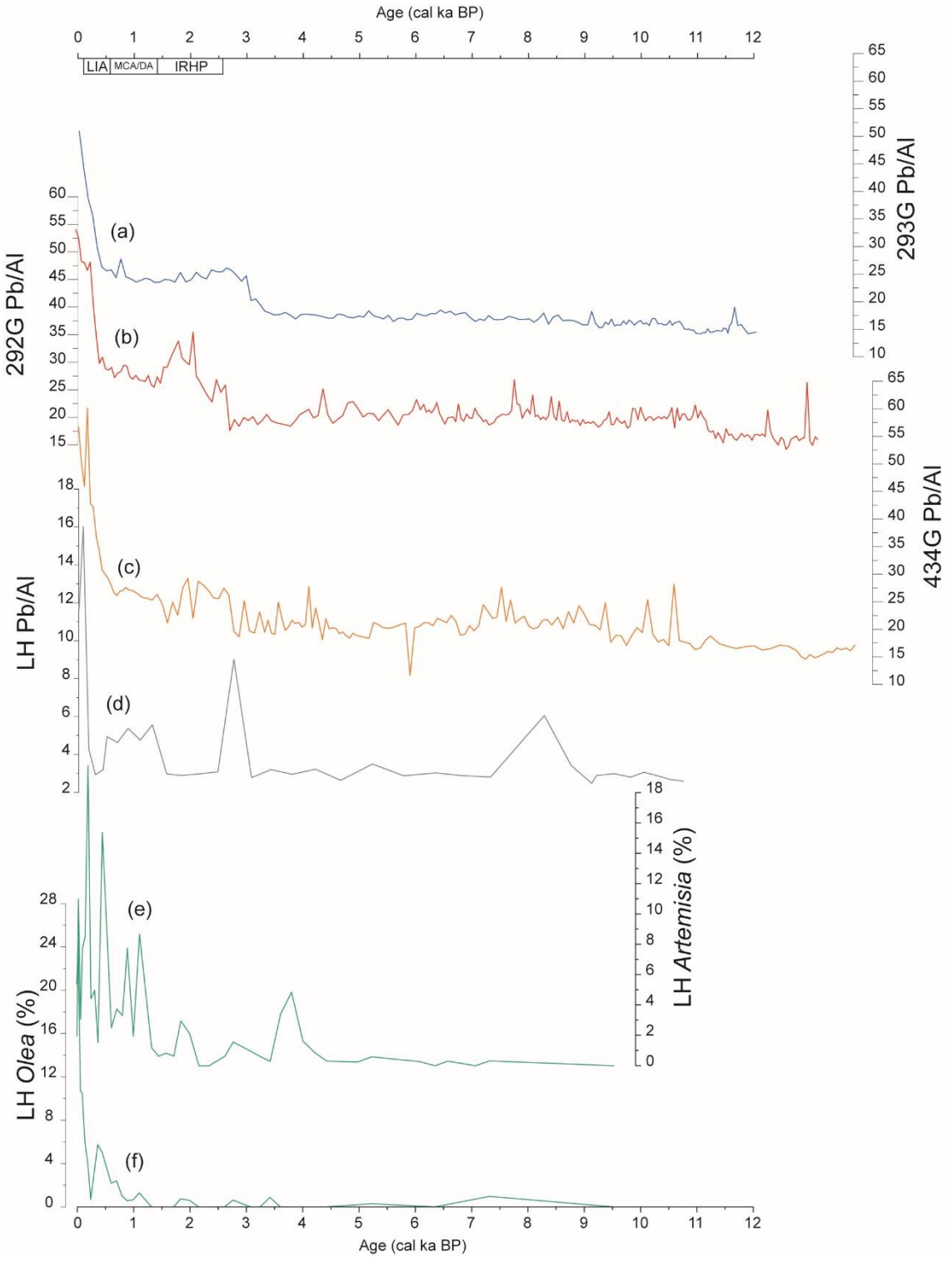

Figure 3. Comparison of Pb/Al ratio profiles from the cores: (a) 293G; (b) 292G; (c) 434G and (d) LH with pollen taxa related to anthropogenic impact from LH: (e) *Artemisia* and (f) *Olea*.

VI CONCLUSIONS / CONCLUSIONES

VI. Conclusions / Conclusiones

1. Conclusions

The high-resolution paleoclimate and paleoceanographic study carried out on seven marine sediment records and the comparison of continental and marine environments from the western Mediterranean has allowed us to obtaining the following conclusions:

- Regarding the paleoenvironmental information obtained from different major and trace elemental-based geochemical ratios, although the relative variations between terrigenous and carbonate fractions in hemipelagic environments are influenced by marine productivity, eolian and riverine inputs, shelf erosion, and sea level variations, it has been demonstrated that bottom currents also play a major control for this variation.

- In terms of paleoceanographic conditions, the reconstruction of the WMDW intensity and ventilation support overall well-ventilated conditions and intense WMDW formation during the HS1. This enhanced formation appears related to the arid and colder conditions and the higher influence of northern winds likely triggered by the southward advance of the sea ice sheets. During the HS1, the formation of WMDW and the Bernoulli aspiration through the Gibraltar Strait were significantly enhanced. During the HE1, the influx of meltwater from the Laurentide and Fennoscandian ice sheets reduced the density of the surface waters, decreasing the WMDW formation and reducing the density gradient at the Gibraltar Strait and thus, the Bernoulli aspiration depth. The shoaling of Bernoulli aspiration triggered a decrease in bottom waters oxygenation, as supported by the increase of the U/Al ratio.

- The study of redox-sensitive elemental proxies has allowed to differentiating two phases within the ORL1: ORL1a (15-11.7 cal ka BP), characterized by strong reducing conditions and by a sharp increase of the Mo/Al and U/Al ratios along with a decrease in the Mn/Al ratio. This sub-phase coincided with an increase in the SR in the deep basin, which can be explained by pervasive humid conditions over the continent and the wave ravinement over the shelf break in the early transgression. The demise of the ORL1a occurred during the YD with the reactivation of the WMDW and the end of the highly reducing bottom conditions as depicted by the Mo/Al ratio. The ORL1b (11.7-9 cal ka BP) is characterized by suboxic ferruginous conditions, with low values of the Mo/Al ratio, and increasing values of the Mn/Al ratio, supporting that this sub-phase occurred under more oxic conditions that the ORL1a. Our result suggests that the organic matter

preservation during the ORL1b was triggered by enhanced surface productivity and the high SR as a response to the pervasive humid conditions in the continent. In addition, both sub-phases coincided with the occurrence of the mwp-1a and 1b. The demise of the ORL1b seems to be related to the reduction of the SR in the deep basin rather than reactivation of the WMDW, as has been previously suggested.

- The alpine glacial retreat during the last deglaciation promoted the formation of diverse lakes. Among them, the formation of the Laguna Hondera (LH) wetland occurred during the Early Holocene, which is characterized by overall warm and humid conditions, interrupted by two arid periods between 9.5 and 9 cal ka BP and at ~8.2 cal ka BP. These two arid intervals are characterized by lower detrital input and the development of peaty lithology, coinciding with the Bonds events 6 and 5, which could have modified the humidity and/or the position of the westerlies. The Early Holocene in the studied LH record is also characterized by low preservation of the pollen grains, likely related to the formation of the bog. The onset of an aridity trend in the Sierra Nevada records occurred at ~7 cal ka BP, characterized by a gradual decrease in the runoff depicted by the K/Al and Rb/Al ratios along with the substitution of arboreal pollen by xerophytic pollen peaking ~4-2.5 cal ka BP. Moreover, a significant increase in eolian-derived elements occurred between 6.3 and 5.5 cal ka BP.

- In continental records, the Late Holocene has shown high climate variability. The IRHP is characterized by an increase in the runoff input and an expansion of the arboreal vegetation to higher altitudes. During the DA and the MCA there was a new advance in xerophytes and a reduction in runoff. The LIA is characterized by an increase in humidity depicted by a rise in the runoff input and by a slight increase of the arboreal pollen, which may be limited by the colder conditions. The IP is characterized by the highest anthropic influence as evidenced by the highest values of the Pb/Al ratio, probably indicating fossil fuel burning by enhanced mining and metallurgy industry. Regarding the pollen assemblage, a sharp increase in *Olea europaea* and *Pinus* coincided with the onset of the olive cultivation and the pine reforestation. The LH record shows a remarkable increase in the Ca signal derived from eolian input (high Ca-Zr correlation) during the past ~6.3 cal ka BP in Sierra Nevada. Nowadays, the input of Ca into the alpine lakes of Sierra Nevada controls the productivity in the lakes and induces the seasonal blooms of algae. In this regard, our record indicates that present-day inorganic nutrient input from Sahara

was established at 6.3cal ka BP and lasted until the present, with variations depending on the prevailing climate conditions.

- The study of stable carbon and hydrogen isotopes measured on leaf wax *n*-alkanes in two marine records from the eastern and western Alboran Sea basins highlights the complex interplay between climate and sedimentary processes. In the studied records, the $\delta^{13}C_{wax}$ seems to be mainly controlled by the source area of the *n*-alkanes and the $\delta^{2}H_{wax}$ signal by the regional precipitation patterns. The $\delta^{13}C_{wax}$ values have shown that *n*-alkanes derive from C_3 vegetation likely from southern Iberia. Despite the proximity of both cores, the $\delta^{13}C_{wax}$ profiles showed different evolutions in the eastern and western Alboran basins. In the 293G record, the $\delta^{13}C_{wax}$ profile showed mainly an influence of coastal vegetation more adapted to humidity prior to the mwp-1b, followed by more negative values indicating the landward vegetation. During the interval between 15 and 11 cal ka BP the occurrence of low CPI values and UCM in the *n*-alkanes have been related to the erosion of old soils developed in the shelf when it was exposed, or due to the occurrence of turbidites as a result of the destabilization of the shelf break. The UCM are only recognized in the eastern Alboran basin, core 293G, which is prone to receive more sediment from the shelf due to the architecture and size of the Almeria TS compared with Fuengirola TS which fed the 434G record. After 11.7 cal ka BP, there was a disconnection between the storm wave base and the shelf break reducing the influence of the coastal vegetation, and the *n*-alkanes showed a more positive signature, suggesting that during this phase the *n*-alkanes source was the whole Andarax basin. The western Alboran core is under the influence of two rivers catchments, Guadalhorce and Fuengirola, and therefore the *n*-alkane distribution could depend on the rivers that supply more sediment at each time period. During periods of enhanced winter precipitation, there was a major influence of the Guadalhorce river, which drainage basin encompasses vegetation from the thermo- and meso-mediterranean belts. Conversely, during periods of reduced winter precipitation or major spring/autumn precipitation, the Fuengirola river could have had a greater influence on the *n*-alkane record, supplying vegetation of the thermomediterranean belt. Thus, during more humid intervals the *n*-alkane record shows more arid vegetation because it was mainly supplied by the Guadalhorce river. Conversely, during more arid period the record show more humid vegetation because it was mainly supplied by the Fuengirola river.

- The δ^2H_{wax} profiles in both Alboran Sea records show a similar evolution to other records from northern Africa and southern Iberia, suggesting that δ^2H_{wax} recorded the source area and the amount of precipitation. During the HS1, the δ^2H_{wax} shows depleted values, likely as a response to the meltwater influx in the Mediterranean. Similarly, the first phase of the YD is similarly characterized by more depleted values, but the second phase is characterized by enhanced δ^2H_{wax} values, as result of an AMOC slowdown and more precipitation from Mediterranean source. The Early Holocene is characterized by the most depleted δ^2H_{wax} values of the whole record, as result of the insolation maxima, the enhancement of the AMOC and more humid westerlies. The Middle-Late Holocene is characterized by a transition from pervasive Atlantic moisture source to more Mediterranean conditions, punctuated by a see-saw between 4.8 and 3.8 cal ka BP of Mediterranean-Atlantic-Mediterranean moisture source. Later on, the opposite pattern is shown by the studied records, which suggests the establishment of the present-day climate conditions, in which the eastern Alboran basin is influenced by Mediterranean winter precipitation while the western Alboran basin has a higher influence from Atlantic precipitation.

- The comparison of marine and continental sediment records is usually complex, but the signal of anthropic activities and eolian input has been recognized and correlated in both kind of records. Regarding the eolian input, a correlation for the past 6 cal ka BP between the Zr/Al ratio of Sierra Nevada and the western Mediterranean basin records is recognized only when the marine records have a low SR. The eolian signal in records with relatively high SRs is likely diluted and thus, unrecognizable. Regarding to the anthropic activities signal, although the human settlements in southern Iberian were well developed since 5 cal ka BP. Nevertheless, the first clear signal in the studied sediment records is recognized around 3.8 cal ka BP in the continental records and between 3.5 and 2.5 cal ka BP in the marine records both of them depicted by an increase in the Pb/Al background values, likely related to enhanced metallurgy activities. In the studied marine sediment records, there was a sharp increase in terrigenous input at around 2 cal ka BP, likely related to increasing soil use for agrarian activities and desertification for livestock activities. This increase should be taken into account in studies aimed at reconstructing paleoclimate conditions during the last 2 ka based in inorganic geochemical proxies since the climatic signal could be masked by the anthropic impact. In particular, a significant anthropic impact is recorded during the last 150 years, with an increase of olive

cultivation and high values of the Pb/Al ratio, likely derived from the increase in the use of leaded fuels.

2. Conclusiones

El estudio paleoclimático y paleoceanográfico de alta resolución llevado a cabo en diversos registros de sedimentos marinos y lacustres, así como la comparación de ambos tipos de ambientes sedimentarios en el oeste del Mediterráneo, ha permitido obtener las siguientes conclusiones:

- Con respecto a la información paleoambiental obtenida a partir de diversos indicadores geoquímicos basados en las relaciones de elementos mayores y trazas, ha podido establecerse que aunque la variación relativa entre las fracciones terrígena y carbonatada en ambientes hemipelágicos está influenciada por la productividad marina, por los aportes fluviales y eólicos y por las variaciones del nivel del mar, las corrientes profundas también juegan un papel esencial en el control de dicha variación.

- En relación con las condiciones paleoceanográficas, la reconstrucción de la intensidad y la ventilación de las masas de agua profunda del oeste del Mediterráneo indica condiciones de buena ventilación y formación intensa de estas aguas durante el intervalo HS1. Esta mayor intensidad de formación de agua profunda parece estar relacionada con el avance hacia el sur de la capa de hielo durante este intervalo, en el que tanto la formación de agua profunda en el golfo de León como la aspiración de Bernoulli a través del estrecho de Gibraltar se acentuaron significativamente. Durante el HE1, la entrada masiva de agua de deshielo procedente de los casquetes Laurentino y Fenoescandinavo redujo el gradiente de densidad en el estrecho de Gibraltar, provocando una somerización de la profundidad de aspiración. La somerización de la aspiración de Bernoulli a través del estrecho de Gibraltar produjo una disminución en la oxigenación en la cuenca del mar de Alborán, como señalan los indicadores de oxigenación utilizados, en particular la relación U/Al.

- El estudio de los indicadores geoquímicos sensibles a las condiciones redox ha permitido diferenciar dos fases de formación de la ORL1. La ORL1a (15-11.7 cal ka BP) estuvo caracterizada por unas condiciones muy reductoras en el fondo de la cuenca, como indican los incrementos en las relaciones Mo/Al y U/Al y la disminución de la relación Mn/Al. Esta subfase coincide con un aumento en la tasa de sedimentación en la cuenca

como resultado de las condiciones húmedas imperantes durante este periodo y de la erosión superficial en el borde de la plataforma durante las primeras etapas de la transgresión. El final de la ORL1a tuvo lugar durante el YD, coincidiendo con la reactivación de la formación de agua profunda y el final de las condiciones reductoras en el fondo marino, como indica la relación Mo/Al. La ORL1b (11.7-9 cal ka BP) se caracteriza por condiciones subóxicas ferruginosas, como demuestran los valores menores de la relación Mo/Al y el incremento en la relación Mn/Al, que indican una mayor oxigenación del fondo durante esta subfase que durante la anterior. Los resultados obtenidos también indican que la mayor preservación de materia orgánica durante la ORL1b deriva fundamentalmente de una mayor productividad superficial y de una alta tasa de sedimentación como consecuencia de condiciones más húmedas en el continente. Además, ambas subfases coinciden con los pulsos de deshielo 1a y 1b. Así, el final de la ORL1b se relacionaría esencialmente con la reducción de la tasa de sedimentación en la cuenca profunda y no con la reactivación de la formación de agua profunda, como había sido sugerido en trabajos previos.

- En lo referente a ambientes continentales, la retirada de los glaciares alpinos durante la deglaciación del Holoceno temprano dio lugar a la formación de diversos lagos y humedales. En este periodo, el registro lacustre de Laguna Hondera (LH) se caracterizó por condiciones generalmente húmedas, interrumpidas por dos periodos áridos entre 9.5 y 9 cal ka BP y en torno a 8.2 cal ka BP. Estos dos periodos áridos se caracterizan por un bajo aporte detrítico y el desarrollo de turba, y coinciden con dos eventos Bond, 6 y 5, que pudieron influir en la humedad o posición de los vientos del oeste. En general, el Holoceno temprano en el registro de LH se caracteriza por una baja preservación de los granos de polen. El inicio de una tendencia hacia condiciones más áridas se produce en torno a 7 cal ka BP, coincidiendo con una disminución de la escorrentía superficial en la cuenca, como indican las relaciones K/Al y Rb/Al junto con la sustitución de especies arbóreas por xerofitas, que culminó entre 4 y 2.5 cal ka BP.

- En los registros continentales, el Holoceno tardío muestra una gran variabilidad climática. El IRHP se caracteriza por un incremento de la escorrentía y por la expansión de vegetación arbórea a mayor altitud. Durante los DA y la MCA tuvo lugar un nuevo avance de las xerofitas, coincidiendo con una disminución de la escorrentía. La LIA se caracteriza por un aumento de la humedad y de la escorrentía, así como por un ligero incremento de polen arbóreo, quizás limitado por las condiciones frías. El IP se

caracteriza por un gran impacto antrópico en el registro sedimentario, como indica el incremento significativo de la relación Pb/Al, en general derivado de la quema de combustibles fósiles y de actividades mineras y metalúrgicas. También se produjo un gran aumento del polen de *Olea europaea* y *Pinus*, coincidiendo con el inicio del cultivo extensivo del olivo en altitudes bajas y la reforestación de pino en Sierra Nevada. Actualmente, el aporte de Ca en los lagos alpinos de Serra Nevada controla la productividad, induciendo 'blooms' estacionales de algas. A este respecto, el registro analizado demuestra que el actual aporte de nutrientes inorgánicos procedentes del Sahara se estableció hace 6.3 cal ka BP y dura hasta hoy, con ligeras variaciones según las condiciones climáticas imperantes.

- El estudio de isótopos estables de carbono e hidrógeno medidos en *n*-alcanos derivados de la cera de hojas en dos registros marinos de las cuencas oriental y occidental del mar de Alborán demuestra la compleja interacción entre el clima y los procesos sedimentarios. En los registros estudiados, la señal del $\delta^{13}C_{wax}$ parece estar controlada principalmente por el área fuente de los *n*-alcanos y la señal del $\delta^{2}H_{wax}$ por los patrones regionales de precipitación. Los valores de $\delta^{13}C_{wax}$ indican que los *n*-alcanos provienen de plantas tipo C3 probablemente del sur de Iberia. A pesar de la proximidad de ambos registros, los perfiles del $\delta^{13}C_{wax}$ muestran tendencias diferentes en las cuencas oriental y occidental de Alborán. En el registro 293G, situado en la cuenca oriental, el perfil del $\delta^{13}C_{wax}$ parece estar principalmente influenciado por una vegetación costera más adaptada a la humedad antes del mwp-1b, mientras que los valores más negativos registrados después de este intervalo indican un aporte de vegetación más interior. Durante el intervalo entre 15 y 11 cal ka BP, los valores bajos de CPI y la aparición de UCM en los *n*-alcanos derivan de la erosión de antiguos suelos desarrollados en la plataforma cuando estuvo expuesta, o bien se deben al aporte de turbiditas como resultado de la desestabilización del borde del talud continental. La presencia de UCM en los *n*-alcanos solo se reconoce en la cuenca oriental de Alborán, en el registro 293G, el cual es más propenso a recibir sedimentos de la plataforma debido a la arquitectura y el tamaño del sistema turbidítico de Almería, en comparación con el sistema turbidítico de Fuengirola que alimentó el registro 434G. A partir de los 11.7 cal ka BP, se produjo una desconexión entre el nivel de base del oleaje de tormenta y el borde de la plataforma, lo que redujo la influencia de la vegetación costera y dio lugar a valores más positivos del $\delta^{13}C_{wax}$; esto sugiere que durante esta fase el área fuente de *n*-alcanos fue toda la cuenca del Andarax. El testigo de la cuenca

occidental de Alborán estuvo bajo la influencia de las cuencas de dos ríos, el Guadalhorce y el Fuengirola, por lo que la distribución de los *n*-alcanos podría depender de qué río aportara más sedimento en cada periodo. Durante los periodos de mayor precipitación invernal existiría una gran influencia del río Guadalhorce, cuya cuenca de drenaje engloba vegetación de los cinturones termomediterráneo y mesomediterráneo. Por el contrario, durante los periodos de menor precipitación invernal o de mayor precipitación primaveral/otoñal, el río Fuengirola podría haber tenido una mayor influencia en aporte de *n*-alcanos, con vegetación del cinturón termomediterráneo. Así, durante los intervalos más húmedos, el registro de *n*-alcanos muestra una vegetación más árida, debido a que fue abastecido principalmente por el río Guadalhorce; por el contrario, en los intervalos más áridos el registro indica una vegetación más húmeda debido a la mayor influencia del río Fuengirola.

- La señal del δ^2H_{wax} en ambos registros del mar de Alborán muestra una evolución similar a la de otros registros del norte de África y el sur de Iberia, lo que sugiere que el δ^2H_{wax} registra tanto la procedencia como la cantidad de precipitación. Durante el intervalo HS1, la señal del δ^2H_{wax} muestra valores bajos, probablemente como resultado de la entrada de agua de deshielo en el Mediterráneo. De manera similar, la primera fase del YD se caracteriza por valores más bajos del δ^2H_{wax}, pero la segunda fase se caracteriza por valores más positivos, como resultado de una desaceleración de la AMOC y un incremento en la precipitación de origen mediterráneo. El Holoceno temprano se caracteriza por presentar los valores del δ^2H_{wax} más bajos de todo el registro, como resultado de los máximos de insolación, el aumento de la AMOC y una mayor humedad de los vientos del oeste. El Holoceno medio-tardío se caracteriza por una transición de una fuente de humedad predominantemente atlántica a una más mediterránea, así como por una fluctuación importante en la fuente de humedad mediterránea-atlántica-mediterránea entre los 4.8 y 3.8 cal ka BP. Posteriormente, los registros estudiados muestran un patrón inverso, lo que sugiere el establecimiento de las condiciones climáticas actuales, en las que el este de Alborán está principalmente afectado por las precipitaciones invernales de origen mediterráneo mientras que la cuenca occidental tiene una mayor influencia de las precipitaciones atlánticas.

- La comparación climática entre registros de sedimentos marinos y continentales suele ser compleja, pero la señal de actividades antrópicas y de aporte eólico se reconocen y correlacionan en ambos tipos de registros. Existe una buena correlación durante los

últimos 6 cal ka del indicador Zr/Al entre los registros de Sierra Nevada y de las cuencas del oeste del Mediterráneo, pero sólo cuando los testigos marinos presentan una tasa de sedimentación baja. La señal eólica en los registros marinos con alta tasa de sedimentación probablemente se encuentre diluida, por lo que resulta irreconocible. Con respecto a la señal de impacto antrópico, aunque los asentamientos humanos en el sur de la Península Ibérica estaban plenamente desarrollados desde aproximadamente 5 cal ka BP, la primera señal clara en los registros estudiados se reconoce en torno a 3.8 cal ka BP en sedimentos continentales y entre 3.5 y 2.5 cal ka BP en sedimentos marinos, marcada en ambos casos por un aumento en los valores de la relación Pb/Al, probablemente relacionado con una mayor actividad metalúrgica. En los registros de sedimento marino, se reconoce un fuerte aumento en la entrada de terrígenos alrededor de 2 cal ka BP, probablemente relacionado con el uso de los suelos para actividades agrícolas y ganaderas. Este incremento debe tenerse en cuenta en estudios que tengan como objetivo reconstruir las condiciones paleoclimáticas durante los últimos dos milenios basados en indicadores geoquímicos inorgánicos, ya que la señal climática podría estar enmascarada por el impacto antrópico. Cabe también señalar que durante los últimos 150 años se registra un impacto antrópico muy significativo, con un aumento del polen de olivo por su cultivo extensivo y un incremento de la relación Pb/Al, probablemente debido al aumento del uso de combustibles con plomo.

VII FUTURE PERSPECTIVES

VII. Future perspectives

This PhD thesis is a step forward in the understanding of the evolution of past climate and oceanographic changes in the western Mediterranean region during the last 20 ka. However, many open questions still need to be addressed in the near future. In the short term, the work currently in progress will be summarized in upcoming manuscripts. In particular, the variability in oxygen conditions during the formation of alpine wetlands in Sierra Nevada will be analyzed, and geochemical records will be also integrated with pollen and *n*-alkanes records already published (Jiménez-Moreno and Anderson, 2012; García-Alix et al. 2012, 2017) in order to gain further insights into the formation and evolution of these wetlands.

In the middle term, it is also planned to integrate geochemical proxies from new sediment records from the Algero-Balearic and the Alboran basins recovered at shallower depths, in order to characterize the evolution of the Ti/Ca ratio and redox proxies at different depths, thus gaining new knowledge on the sedimentary and oceanographic evolution along the western Mediterranean basins. It is also planned to study and integrate pollen, dinoflagellates and geochemical proxies in marine sediment records recovered in both hemipelagic and contouritic environments, in order to elucidate the climatic variability and sedimentary processes in these two different marine environments.

Finally, in the long term, comparing the available records with north African records will allow to characterize the climatic variability at larger spatial scales and depict a more global picture of the westerlies influence and the Intertropical Convergence Zone over middle latitudes.

VIII AGRADECIMIENTOS

VIII. Agradecimientos

Una vez terminado este trabajo, solo queda la parte más importante: agradecer la ayuda de todos los que han colaborado de forma directa o indirecta en su realización. Son tantas las personas que me han brindado su ayuda a lo largo de estos años que probablemente me olvide de alguna, así que pido disculpas de antemano si me dejo algún nombre en el tintero.

En primer lugar, quiero expresar mi más profundo agradecimiento a mis directoras de tesis, Francisca Martínez Ruiz y Marta Rodrigo Gámiz, a quienes debo mi iniciación en el mundo de la ciencia. Quiero agradecer a ambas su comprensión, cariño y disponibilidad durante estos años. Muchas gracias, Paqui, por confiar en mí para esta tesis doctoral y por darme la oportunidad de dedicarme a este trabajo que tanto me apasiona. Muchas gracias, Marta, por estar siempre ahí cuando he necesitado ayuda, consejos científicos o simplemente un café o hablar de cualquier tema. Ha sido una gran suerte contar con vosotras como directoras.

Quiero también expresar mi agradecimiento a los doctores Gonzalo Jiménez Moreno, Antonio García-Alix y Francisco J. Jiménez Espejo por sus valiosos consejos y su ayuda incondicional. Muchas gracias a Gonzalo, que supervisó mi primer trabajo científico, por permitirme iniciar esta andadura. Muchas gracias a Nono por su paciencia, su apoyo y sus cervezas artesanas. Muchas gracias a Francis por compartir conmigo su experiencia científica. Gracias a los tres también por vuestra confianza más allá del plano profesional.

Muchas gracias también al resto de coautores de los artículos que se incluyen en esta tesis (Marcel T. J. van der Meer, Jon Camuera, María José Ramos Román, Alejandro López Avilés, Marga García, Francisco J. Sierro y R. Scott Anderson) por sus valiosas contribuciones científicas: sin ellos este trabajo no habría sido posible.

A nivel institucional, debo agradecer al Ministerio de Economía y Competitividad por la concesión de una ayuda del programa de Formación de Personal Investigador (BES-2016-077024) que ha permitido la realización de esta tesis. Este trabajo ha sido posible gracias a la financiación de los proyectos CGL2015-66830-R y PID2019-104624RB-I00 del Plan Estatal de Investigación Científica y Técnica y de Innovación (MCIN/AEI/ 10.13039/501100011033), de los proyectos CGL2017-92600-EXP (AEI), P18-RT-3804 y del Grupo de Investigación RNM-179 (Junta de Andalucía), cofinanciados con fondos de desarrollo regional (FEDER).

Quiero expresar mi agradecimiento a todo el personal del Instituto Andaluz de Ciencias de la Tierra (CSIC-UGR), centro donde se ha realizado esta tesis, en especial al personal de administración y servicios: Amparo, Ana, Carolina, Manolo, Alejandro, Juani, Meri, Antonio y muy particularmente a Eli por enseñarme tantas técnicas de laboratorio y poner un poco de orden en mi caos.

Quiero agradecer de forma muy especial al personal del Departamento de Estratigrafía y Paleontología de la Universidad de Granada por su cálida acogida. Muchas gracias a los directores de este departamento durante el desarrollo de esta tesis, Francisco J. Rodríguez Tovar y Ángel Puga, por proporcionarme un espacio de trabajo y por brindarme la oportunidad de impartir docencia en los grados de Geología y Biología, permitiéndome así completar mi formación en esta etapa predoctoral. Muchísimas gracias a Socorro Aranda y Nuria Alcalá por todas las facilidades en la resolución de temas burocráticas y por su amabilidad.

Muchas gracias a todo el personal del Royal Netherlands Institute for Sea Research (NIOZ, Países Bajos), donde realicé una estancia de tres meses en el año 2019, especialmente a Marcel y Jort por su inestimable ayuda en el trabajo de laboratorio. Además, quiero agradecer a Ruth, Gonçalo, Yanming, Gianlucca, Annalisa, Fons, Victor, Diana, Alejandro y el resto de compañeros su hospitalidad y simpatía durante el tiempo que permanecí en esta institución. Así mismo, quiero agradecer a la profesora Francesca Sangiorgi su cálida acogida en la Universidad de Utrecht y sus valiosas lecciones sobre dinoflagelados.

Muchísimas gracias a mis compañeros doctorandos del IACT por tantos buenos ratos, risas y cervezas. Mil gracias por todo lo compartido a Claudia, Laura, Rubén, Sara, Manu, Nicole, Adrián, Dimitris, Manolis, Marievi, Marga, Álvaro, Ceci, Erwin, Cerrillo, Yassamina, Yussef y Giorgi.

Muchísimas gracias también a los doctorandos del Departamento de Estratigrafía y Paleontología, en especial a mis compañeros de mi despacho okupado durante estos años: Jon, María José, Paola, Santi, Christian, Willy, Javi, Pablo y Nico. Ha sido un placer compartir todo este tiempo con vosotros, muchísimas gracias por las discusiones científicas, los cafés, las comidas en el despacho y comedores, los viernes sociales y tantas y tantas cervezas. Muchas gracias a Raef, que no es compañero de despacho, pero lo invade con frecuencia, por estar siempre ahí. Gracias también a Charo, Aurora, Álex, Erik, Noel, Dino, Olmo, Sergio, Juan Diego, y a los compañeros

de otros departamentos (Mada, Patri, Mapi, Luis, Ángela, Tato, Cristina…) por tantos buenos ratos compartidos.

Quiero agradecer también a mis colegas de Granada (amigos de toda la vida y compañeros que conocí en la carrera) por su apoyo incondicional: Rober, Carlos, Gersan, Álvaro, Jotade, Gea, Carlos, Casto, Aguayo, Javi Heavy, Inés, Juanan, Rocío, Raquel, Mario, Mada, Ceci, Natalia, Rita, Claudia, Blanca, Paloma, Lidia, Sofi y Michu, Bea, Lope, Juanpe, Celia, Gonzalo, Txia, Mariana, Tere, Ane, Julia, Alberto, Pedro, y a toda la peña que se me olvida. A mis compañeros de piso, Manu, Sergio, Bea, Katha, Casto y Manu. También a Mada y a Javi por su inestimable compañía durante la pandemia, que la hizo mucho más llevadera. Gracias también a Raef, Conchi, Antonio, el Mosca, Méndez, Salvi, Ana Mari, Canco, Estrella, Liverpool, Pagudo y Poi, ellos sabrán por qué.

A Raquel tengo que darle las gracias por todo el cariño, el apoyo y la comprensión que me ha dado durante estos años, especialmente en los momentos más difíciles, por su paciencia infinita y por ser tan buena persona. Muchas gracias por estar siempre a mi lado.

Por último, quiero dar las gracias a mi familia por estar siempre ahí y ser un pilar fundamental en mi vida: a mis tíos, primos y sobrinos, a los abuelos que se han ido y a mi abuela Carmela, que me ha dado tanto durante tanto tiempo. A mi hermano Rober, por todo lo que nos hemos peleado de chicos y por el apoyo que nos damos ahora. A mis padres, Fuensanta y Jose, no tengo suficientes palabras de agradecimiento por todo el cariño que me han dado desde que era un enano. Gracias por guiarme hasta convertirme en la persona que soy.

IX REFERENCES

IX. REFERENCES

Algeo, T.J., Tribovillard, N., 2009. Environmental analysis of paleoceanographic systems based on molybdenum-uranium covariation. Chem. Geol. 268, 211–225. https://doi.org/10.1016/j.chemgeo.2009.09.001

Algeo, T.J., Li, C., 2020. Redox classification and calibration of redox thresholds in sedimentary systems. Geochim. Cosmochim. Acta 287, 8–26. https://doi.org/10.1016/j.gca.2020.01.055

Algeo, T.J., Liu, J., 2020. A re-assessment of elemental proxies for paleoredox analysis. Chem. Geol. 540, 119549. https://doi.org/10.1016/j.chemgeo.2020.119549

Alley, R.B., Mayewski, P.A., Sowers, T., Stuiver, M., Taylor, K.C., Clark, P.U., 1997. Holocene climatic instability: A prominent, widespread event 8200 yr ago. Geology 25, 483–486. https://doi.org/10.1130/0091-7613(1997)025<0483

Alley, R.B., Anandakrishnan, S., Jung, P., Clough, A., 2001. Stochastic resonance in the north Atlantic: Further insights. Geophys. Monogr. Ser. 126, 57–68. https://doi.org/10.1029/GM126p0057

Alley, R.B., Ágústsdóttir, A.M., 2005. The 8k event: Cause and consequences of a major Holocene abrupt climate change. Quat. Sci. Rev. 24, 1123–1149. https://doi.org/10.1016/j.quascirev.2004.12.004

Alonso, B., Ercilla, G., 2003. Small turbidite systems in a complex tectonic setting (SW Mediterranean Sea): Morphology and growth patterns. Mar. Pet. Geol. 19, 1225–1240. https://doi.org/10.1016/S0264-8172(03)00036-9

Alonso, B., Juan, C., Ercilla, G., Cacho, I., López-González, N., Rodríquez-Tovar, F.J., Dorador, J., Francés, G., Casas, D., Vandorpe, T., Vázquez, J.T., 2021. Paleoceanographic and paleoclimatic variability in the Western Mediterranean during the last 25 cal. kyr BP. New insights from contourite drifts. Mar. Geol. 437. https://doi.org/10.1016/j.margeo.2021.106488

Álvarez-Solas, J., Montoya, M., Ritz, C., Ramstein, G., Charbit, S., Dumas, C., Nisancioglu, K., Dokken, T., Ganopolski, A., 2011. Heinrich event 1: An example

of dynamical ice-sheet reaction to oceanic changes. Clim. Past 7, 1297–1306. https://doi.org/10.5194/cp-7-1297-2011

Anderson, R.S., Jiménez-Moreno, G., Carrión, J.S., Pérez-Martínez, C., 2011. Postglacial history of alpine vegetation, fire, and climate from Laguna de Río Seco, Sierra Nevada, southern Spain. Quat. Sci. Rev. 30, 1615–1629. https://doi.org/10.1016/j.quascirev.2011.03.005

Andrade, A., Valdeolmillos, A., Ruíz-Zapata, B. 1994. Modern pollen spectra and contemporary vegetation in the Paramera Mountain range (Ávila, Spain), Rev. Palaeobot. Palyno., 82, 127-139, DOI:10.1016/0034-6667(94)90024-8

Aranbarri, J., González-Sampériz, P., Valero-Garcés, B., Moreno, A., Gil-Romera, G., Sevilla-Callejo, M., García-Prieto, E., Di Rita, F., Mata, M.P., Morellón, M., Magri, D., Rodríguez-Lázaro, J., Carrión, J.S., 2014. Rapid climatic changes and resilient vegetation during the Lateglacial and Holocene in a continental region of south-western Europe. Glob. Planet. Change 114, 50–65. https://doi.org/10.1016/j.gloplacha.2014.01.003

Ariztegui, D., Asioli, A., Lowe, J.J., Trincardi, F., Vigliotti, L., Tamburini, F., Chondrogianni, C., Accorsi, C.A., Bandini Mazzanti, M., Mercuri, A.M., Van Der Kaars, S., McKenzie, J.A., Oldfield, F., 2000. Palaeoclimate and the formation of sapropel S1: Inferences from Late Quaternary lacustrine and marine sequences in the central Mediterranean region. Palaeogeogr. Palaeoclimatol. Palaeoecol. 158, 215–240. https://doi.org/10.1016/S0031-0182(00)00051-1

Arz, H.W., Pätzold, J., Wefer, G., 1999. Climatic changes during the last deglaciation recorded in sediment cores from the northeastern Brazilian Continental Margin. Geo-Marine Lett. 19, 209–218. https://doi.org/10.1007/s003670050111

Andrade, A., Valdeolmillos, A., Ruíz-Zapata, B., 1994. Modern pollen spectra and contemporary vegetation in the Paramera Mountain range (Ávila, Spain), Rev. Palaeobot. Palyno., 82, 127-139, DOI:10.1016/0034-6667(94)90024-8

Ausín, B., Flores, J.A., Sierro, F.-J., Bárcena, M.-A., Hernández-Almeida, I., Francés, G., Gutiérrez-Arnillas, E., Martrat, B., Grimalt, J.O., Cacho, I., 2015a. Coccolithophore productivity and surface water dynamics in the Alboran Sea during the last 25kyr. Palaeogeogr. Palaeoclimatol. Palaeoecol. 418, 126–140. https://doi.org/10.1016/j.palaeo.2014.11.011

Ausín, Blanca, Flores, J.A., Sierro, F.J., Cacho, I., Hernández-Almeida, I., Martrat, B., Grimalt, J.O., 2015b. Atmospheric patterns driving Holocene productivity in the Alboran Sea (Western Mediterranean): A multiproxy approach. Holocene 25, 583–595. https://doi.org/10.1177/0959683614565952

Ausín, B., Hodell, D.A., Cutmore, A., Eglinton, T.I., 2020. The impact of abrupt deglacial climate variability on productivity and upwelling on the southwestern Iberian margin. Quat. Sci. Rev. 230, 106139. https://doi.org/10.1016/j.quascirev.2019.106139

Ávila, A., Queralt-Mitjans, I., Alarcón, M., 1997. Mineralogical composition of African dust delivered by red rains over northeastern Spain, J. Geophys. Res.-Atmos., 102, 21977-21996, DOI:10.1029/97JD00485.

Arrhenius, G., 1952. Sediment cores from the East Pacific. In: H. Pettersson (Ed.), Reports of the Swedish deep-sea expedition (1947–1948) (p. 227). Goteborg: Elanders Boktryckeri Aktiebolag.

Bahr, A., Jiménez-Espejo, F.J., Kolasinac, N., Grunert, P., Hernández-Molina, F.J., Röhl, U., Voelker, A.H.L., Escutia, C., Stow, D.A. V, Hodell, D., Alvarez-Zarikian, C.A., 2014. Deciphering bottom current velocity and paleoclimate signals from contourite deposits in the Gulf of Cádiz during the last 140 kyr: An inorganic geochemical approach. Geochemistry, Geophys. Geosystems 15, 3145–3160. https://doi.org/10.1002/2014GC005356

Bahr, A., Kaboth, S., Jiménez-Espejo, F.J., Sierro, F.J., Voelker, A.H.L., Lourens, L., Röhl, U., Reichart, G.J., Escutia, C., Hernández-Molina, F.J., Pross, J., Friedrich, O., 2015. Persistent monsoonal forcing of mediterranean outflow water dynamics during the late Pleistocene. Geology 43, 951–954. https://doi.org/10.1130/G37013.1

Baldini, L.M., McDermott, F., Baldini, J.U.L., Arias, P., Cueto, M., Fairchild, I.J., Hoffmann, D.L., Mattey, D.P., Müller, W., Nita, D.C., Ontañón, R., Garciá-Moncó, C., Richards, D.A., 2015. Regional temperature, atmospheric circulation, and sea-ice variability within the Younger Dryas Event constrained using a speleothem from northern Iberia. Earth Planet. Sci. Lett. 419, 101–110. https://doi.org/10.1016/j.epsl.2015.03.015

Ballantyne, A. P., Brahney, J., Fernandez, D., Lawrence, C. L., Saros, J., Neff, J. C., 2011. Biogeochemical response of alpine lakes to a recent increase in dust deposition in the Southwestern US, Biogeosciences, 8, 2689, DOI:10.5194/bg-8-2689-2011

Bárcena, M.A., Cacho, I., Abrantes, F., Sierro, F.J., Grimalt, J.O., Flores, J.A., 2001. Paleoproductivity variations related to climatic conditions in the Alboran Sea (western Mediterranean) during the last glacial-interglacial transition: The diatom record. Palaeogeogr. Palaeoclimatol. Palaeoecol. 167, 337–357. https://doi.org/10.1016/S0031-0182(00)00246-7

Bárcenas, P., Lobo, F.J., Macías, J., Fernández-Salas, L.M., López-González, N., Díaz del Río, V., 2015. Submarine deltaic geometries linked to steep , mountainous drainage basins in the northern shelf of the Alboran Sea : Filling the gaps in the spectrum of deltaic deposition. Geomorphology 232, 125–144. https://doi.org/10.1016/j.geomorph.2014.11.028

Bar-Matthews, M., Ayalon, A., Kaufman, A., 2000. Timing and hydrological conditions of sapropel events in the Eastern Mediterranean, as evident from speleothems, Soreq cave, Israel, Chem. Geol., 169, 145-156, DOI:10.1016/S0009-2541(99)00232-6

Bardají, T., Goy, J.L., Zazo, C., Hillaire-Marcel, C., Dabrio, C.J., Cabero, A., Ghaleb, B., Silva, P.G., Lario, J., 2009. Sea level and climate changes during OIS 5e in the Western Mediterranean. Geomorphology 104, 22–37. https://doi.org/10.1016/j.geomorph.2008.05.027

Bazzicalupo, P., Maiorano, P., Girone, A., Marino, M., Combourieu-Nebout, N., Incarbona, A., 2018. High-frequency climate fluctuations over the last deglaciation in the Alboran Sea, Western Mediterranean: Evidence from calcareous plankton assemblages. Palaeogeogr. Palaeoclimatol. Palaeoecol. 506, 226–241. https://doi.org/10.1016/J.PALAEO.2018.06.042

Bea, F., Montero, P., Stroh, A., Baasner, J., 1996. Microanalysis of minerals by an Excimer UV-LA-ICP-MS system. Chem. Geol. 133, 145–156. https://doi.org/10.1016/S0009-2541(96)00073-3

Berger, W.H., Jansen, E., 1994. Mid-Pleistocene climate shift: the Nansen connection. In: Johanessen, O.M., Muench, R.D., Overland, J.E. (Eds.), The Polar Oceans and Their Role in Shaping the Global Environment: the Nansen Centennial Volume, AGU Geophysical Monograph 84, 295-311.

Berner, R. A., 1971. Principles of chemical sedimentology. New York: McGraw-Hill.

Beug, H. J., 2004. Leitfaden der Pollenbestimmung für Mitteleuropa und angrenzende Gebiete, Fischer, Stuttgart.

Bi, X., Sheng, G., Liu, X., Li, C., Fu, J., 2005. Molecular and carbon and hydrogen isotopic composition of n-alkanes in plant leaf waxes. Org. Geochem. 36, 1405–1417. https://doi.org/10.1016/j.orggeochem.2005.06.001

Bini, M., Zanchetta, G., Persoiu, A., Cartier, R., Català, A., Cacho, I., Dean, J.R., Di Rita, F., Drysdale, R.N., Finnè, M., Isola, I., Jalali, B., Lirer, F., Magri, D., Masi, A., Marks, L., Mercuri, A.M., Peyron, O., Sadori, L., Sicre, M.-A., Welc, F., Zielhofer, C., Brisset, E., 2019. The 4.2 ka BP Event in the Mediterranean Region: an overview. Clim. Past 15, 555–577. https://doi.org/10.5194/cp-2018-147

Blaauw, M., 2010. Methods and code for "classical" age-modelling of radiocarbon sequences. Quat. Geochronol. 5, 512–518. https://doi.org/10.1016/j.quageo.2010.01.002

Blaauw, M., Christen, J.A., 2011. Flexible paleoclimate age-depth models using an autoregressive gamma process. Bayesian Anal. 6, 457–474. https://doi.org/10.1214/11-BA618

Blanco-González, A., Lillios, K.T., López-Sáez, J.A., Drake, B.L., 2018. Cultural, Demographic and Environmental Dynamics of the Copper and Early Bronze Age in Iberia (3300–1500 BC): Towards an Interregional Multiproxy Comparison at the Time of the 4.2 ky BP Event. J. World Prehistory 31, 1–79. https://doi.org/10.1007/s10963-018-9113-3

Bliedtner, M., Von Suchodoletz, H., Schäfer, I., Welte, C., Salazar, G., Sönke, S., Haas, M., Dubois, N., Zech, R., 2020. Age and origin of leaf wax n-Alkanes in fluvial sediment-paleosol sequences and implications for paleoenvironmental reconstructions. Hydrol. Earth Syst. Sci. 24, 2105–2120. https://doi.org/10.5194/hess-24-2105-2020

Blott, S.J., Pye, K., 2001. Gradistat: A grain size distribution and statistics package for the analysis of unconsolidated sediments. Earth Surf. Process. Landforms 26, 1237–1248. https://doi.org/10.1016/S0167-5648(08)70015-7

Bond, G., Heinricht, H., Broecker, W., Labeyrie, L., Mcmanus, J., Andrews, J., Huonll, S., Jantschik, R., Clasen, S., Simet, C., Tedesco, K., Klas, M., Bonanitt, G., Ivy, S., 1992. Evidence for massive discharges of icebergs into the North Atlantic ocean during the last glacial period. Nature 360, 245–249.

Bond, G., Broecker, W., Johnsentt, S., Mcmanus, J., Labeyrie, L., Jouzelll, J., Bonani, G., 1993. Correlations between climate records from North Atlantic sediments and Greenland ice 143–147.

Bond, G., Showers, W., Cheseby, M., Lotti, R., Almasi, P., DeMenocal, P., Priore, P., Cullen, H., Hajdas, I., Bonani, G., 1997. A pervasive Millennial-scale cycle in the North Atlantic Holocene Climate. Science 278, 1257–1266.

Bond, G., Kromer, B., Beer, J., Muscheler, R., Evans, M.N., Showers, W., Hoffmann, S., Lotti-bond, R., Hajdas, I., Bonani, G., 2001. Persistent Solar Influence on North Atlantic Climate During the Holocene. Science 294, 2130-2135. https://doi.org/10.1126/science.1065680

Bouimetarhan, I., Groeneveld, J., Dupont, L., Zonneveld, K., 2013. Low- to high-productivity pattern within Heinrich Stadial 1: Inferences from dinoflagellate cyst records off Senegal. Glob. Planet. Change 106, 64–76. https://doi.org/10.1016/j.gloplacha.2013.03.007

Bramlette, M. N., Bradley, W. H., 1940. Geology and biology of North Atlantic deep-sea cores between Newfoundland and Ireland. Part 1. Lithology and geologic interpretations. US Geological Survey Professional Paper, 196A, 1–34

Brauer, A., Haug, G.H., Dulski, P., Sigman, D.M., Negendank, J.F.W., 2008. An abrupt wind shift in western Europe at the onset of the Younger Dryas cold period. Nat. Geosci. 1, 520–523. https://doi.org/10.1038/ngeo263

Bray, E.E., Evans, E.D., 1961. Distribution of n-paraffins as a clue to recognition of source beds. Geochim. Cosmochim. Acta 22, 2–15. https://doi.org/10.1016/0016-7037(61)90069-2

Brayshaw, D., Woollings, T., Vellinga, M., 2009. Tropical and Extratropical Responses of the North Atlantic Atmospheric Circulation to a Sustained Weakening of the MOC. J. Clim. 22, 3146–3155. https://doi.org/10.1175/2008JCLI2594.1

Brayshaw, D.J., Hoskins, B., Black, E., 2010. Some physical drivers of changes in the winter storm tracks over the North Atlantic and Mediterranean during the Holocene. Philos. Trans. R. Soc. 368, 5185–5223. https://doi.org/10.1098/rsta.2010.0180

Buckley, M.W., Marshall, J., 2015. Reviews of Geophysics Observations, inferences, and mechanisms of the Atlantic Meridional Overturning Circulation: A review. Rev. Geophys. 54, 5–63. https://doi.org/10.1002/2015RG000493.Received

Bush, R.T., McInerney, F.A., 2013. Leaf wax n-alkane distributions in and across modern plants: Implications for paleoecology and chemotaxonomy. Geochim. Cosmochim. Acta 117, 161–179. https://doi.org/10.1016/j.gca.2013.04.016

Cacho, I., Grimalt, J.O., Pelejero, C., Canals, M., Sierro, F.J., Flores, J.A., Shackleton, N., 1999. Dansgaard-Oeschger and Heinrich event imprints in Alboran Sea paleotemperatures. Paleoceanography 14, 698–705. https://doi.org/10.1029/1999PA900044

Cacho, I., Grimalt, J.O., Canals, M., Sbaffi, L., Shackleton, N.J., Schönfeld, J., Zahn, R., 2001. Variability of the western Mediterranean Sea surface temperature during the last 25,000 years and its connection with the Northern Hemisphere climatic changes. Paleoceanography 16, 40–52. https://doi.org/10.1029/SP010

Cacho, I., Grimalt, J.O., Canals, M., 2002. Response of the Western Mediterranean Sea to rapid climatic variability during the last 50,000 years: A molecular biomarker approach. J. Mar. Syst. 33–34, 253–272. https://doi.org/10.1016/S0924-7963(02)00061-1

Cacho, I., Shackleton, N., Elderfield, H., Sierro, F.J., Grimalt, J.O., 2006. Glacial rapid variability in deep-water temperature and δ18O from the Western Mediterranean Sea. Quat. Sci. Rev. 25, 3294–3311. https://doi.org/10.1016/j.quascirev.2006.10.004

Calvert, S.E., Pedersen, T.F., 2007. Elemental Proxies for Palaeoclimatic and Palaeoceanographic Variability in Marine Sediments: Interpretation and Application, in: Developments in Marine Geology. Elsevier, Amsterdam, pp. 567–644. https://doi.org/10.1016/S1572-5480(07)01019-6

Camuera, J., Jiménez-moreno, G., Ramos-Román, M.J., García-Álix, A., Jiménez-Espejo, F.J., Toney, J.L., Anderson, R.S., 2021. Chronological control and centennial-scale climatic subdivisions of the Last Glacial Termination in the western

Mediterranean region. Quat. Sci. Rev. 255, 106814. https://doi.org/10.1016/j.quascirev.2021.106814

Camuera, J., Jiménez-Moreno, G., Ramos-Román, M.J., García-Alix, A., Toney, J.L., Anderson, R.S., Jiménez-Espejo, F., Bright, J., Webster, C., Yanes, Y., Carrión, J.S., 2019. Vegetation and climate changes during the last two glacial-interglacial cycles in the western Mediterranean: A new long pollen record from Padul (southern Iberian Peninsula). Quat. Sci. Rev. 205, 86–105. https://doi.org/10.1016/J.QUASCIREV.2018.12.013

Canals, M., Company, J.B., Martín, D., Sànchez-Vidal, A., Ramírez-Llodrà, E., 2013. Integrated study of Mediterranean deep canyons: Novel results and future challenges. Prog. Oceanogr. 118, 1–27. https://doi.org/10.1016/j.pocean.2013.09.004

Canfield, D.E., Thamdrup, B., 2009. Towards a consistent classification scheme for geochemical environments, or, why we wish the term “suboxic” would go away: Editorial. Geobiology 7, 385–392. https://doi.org/10.1111/j.1472-4669.2009.00214.x

Carrión, J. S., 2002. Patterns and processes of Late Quaternary environmental change in a montane region of southwestern Europe, Quaternary Sci. Rev., 21, 2047-2066, DOI:10.1016/S0277-3791(02)00010-0

Carrión, J. S., Munuera, M., Dupré, M., Andrade, A., 2001. Abrupt vegetation changes in the Segura mountains of southern Spain throughout the Holocene, J. Ecol., 89, 783-797, DOI:10.1046/j.0022-0477.2001.00601.x

Carrión, J. S., Sánchez-Gómez, P., Mota, J. F., Yll, E. I., Chaín, C., 2003. Fire and grazing are contigent on the Holocene vegetation dynamics of Sierra de Gádor, southern Spain, Holocene 13, 839-849, DOI:10.1191/0959683603hl662rp

Carrión, J. S., Fuentes, N., González-Sampériz, P., Sánchez Quirante, L., Finlayson, J. C., Fernández, S., Andrade, A., 2007. Holocene environmental change in a montane region of sourthern Europe with a long history of human settlement, Quaternary Sci. Rev., 26, 1455-1475, DOI:10.1016/j.quascirev.2007.03.013

Carrión, J.S., Fernández, S., González-Sampériz, P., Gil-Romera, G., Badal, E., Carrión-Marco, Y., López-Merino, L., López-Sáez, J.A., Fierro, E., Burjachs, F., 2010. Expected trends and surprises in the Lateglacial and Holocene vegetation history of

the Iberian Peninsula and Balearic Islands. Rev. Palaeobot. Palynol. 162, 458–475. https://doi.org/10.1016/j.revpalbo.2009.12.007

Cartier, R., Brisset, E., Guiter, F., Sylvestre, F., Tachikawa, K., Anthony, E.J., Paillès, C., Bruneton, H., Bard, E., Miramont, C., 2018. Multiproxy analyses of Lake Allos reveal synchronicity and divergence in geosystem dynamics during the Lateglacial/Holocene in the Alps. Quat. Sci. Rev. 186, 60–77. https://doi.org/10.1016/j.quascirev.2018.02.016

Casanova-Arenillas, S., Rodríguez-Tovar, F.J., Martínez-Ruiz, F., 2021. Ichnological analysis as a tool for assessing deep-sea circulation in the westernmost Mediterranean over the last Glacial Cycle. Palaeogeogr. Palaeoclimatol. Palaeoecol. 562, 110082. https://doi.org/10.1016/j.palaeo.2020.110082

Castañeda, I.S., Mulitza, S., Schefuß, E., Lopes dos Santos, R.A., Sinninghe Damste, J.S., Schouten, S., 2009. Wet phases in the Sahara/Sahel region and human migration patterns in North Africa. PNAs 106, 20159–20163.

Castañeda, I.S., Schouten, S., 2011. A review of molecular organic proxies for examining modern and ancient lacustrine environments. Quat. Sci. Rev. 30, 2851–2891. https://doi.org/10.1016/j.quascirev.2011.07.009

Castillo Martín, A., 2009. Lagunas de Sierra Nevada, Universidad de Granada, Granada.

Castro, S., Hernández-Molina, F.J., Weger, W., Jiménez-Espejo, F.J., Rodríguez-Tovar, F.J., Mena, A., Llave, E., Sierro, F.J., 2021. Contourite characterization and its discrimination from other deep-water deposits in the Gulf of Cadiz contourite depositional system. Sedimentology 68, 987–1027. https://doi.org/10.1111/sed.12813

Catuneanu, O., 2006. Principles of Sequence Stratigraphy.

Celle-Jeanton, H., Travi, Y., Blavoux, B., 2001. Isotopic typology of the precipitation in the Western Mediterranean region at three different time scales. Geophys. Res. Lett. 28, 1215–1218.

Cheddadi, R., Carré, M., Nourelbait, M., François, L., Rhoujjati, A., Manay, R., Ochoa, D., Schefuß, E., 2021. Early Holocene greening of the Sahara requires Mediterranean winter rainfall. Proc. Natl. Acad. Sci. 118, e2024898118. https://doi.org/10.1073/pnas.2024898118

Cisneros, M., Cacho, I., Frigola, J., Sanchez-Vidal, A., Calafat, A., Pedrosa-Pàmies, R., Rumín-Caparrós, A., Canals, M., 2019. Deep-water formation variability in the north-western Mediterranean Sea during the last 2500 yr: A proxy validation with present-day data. Glob. Planet. Change 177, 56–68. https://doi.org/10.1016/j.gloplacha.2019.03.012

Clark, P.U., Dyke, A.S., Shakun, J.D., Carlson, A.E., Clark, J., Wohlfarth, B., Mitrovica, J.X., Hostetler, S.W., McCabe, A.M., 2009. The Last Glacial Maximum. Science (80-.). 325, 710–714. https://doi.org/10.1126/science.1172873

Collins, M., Knutti, R., Arblaster, J., Dufresne, J.-L., Fichefet, T., Friedlingstein, P., Gao, X., Gutowski, W.J., Johns, T., Krinner, G., Shongwe, M., Tebaldi, C., Weaver, A.J., Wehner, M., Lucas, C., 2013. Long-term Climate Change: Projections, Commitments and Irreversibility, in: Intergovernmental Panel on Climate Change (Ed.), Climate Change 2013 - The Physical Science Basis. Cambridge University Press, Cambridge, pp. 1029–1136. https://doi.org/10.1017/CBO9781107415324.024

Colmenero-Hidalgo, E., Flores, J.-A., Sierro, F.J., Bárcena, M.Á., Löwemark, L., Schönfeld, J., Grimalt, J.O., 2004. Ocean surface water response to short-term climate changes revealed by coccolithophores from the Gulf of Cadiz (NE Atlantic) and Alboran Sea (W Mediterranean). Palaeogeogr. Palaeoclimatol. Palaeoecol. 205, 317–336. https://doi.org/10.1016/j.palaeo.2003.12.014

Comas, M., Zahn, R., Klaus, A., 1996. Setting: the Alboran Sea. Proc. Ocean Drill. Program, 161 Sci. Results 161.

Comas, M.C., Platt, J.P., Soto, J.I., Watts, A.B., 1999. The origin and tectonic history of the Alboran Basin: Insights from Leg 161 results. Proc. Ocean Drill. Progr. Sci. Results 161, 555–580. https://doi.org/10.2973/odp.proc.sr.161.262.1999

Comas, M., Pinheiro, L., Ivanov, M., 2009. Geo- marine research on the Mediterranean and European-Atlantic margins. International Conference and TTR-17 Post-cruise Meeting of the Training-through-Research Programme. Granada, Spain, 2–5 February 2009. In: Comas, M., Suzyumov, A. (Eds.), Deep-water Coral Mounds in the Alboran Sea: The Melilla Mound Field Revisited. IOC Workshop Report, NO. 220 (English). UNESCO, pp. 52.

Combourieu Nebout, N., Turon, J. L., Zahn, R., Capotondi, L., Londeix, L., Pahnke, K., 2002. Enhanced aridity and atmospheric high-pressure stability over the western

Mediterranean during the North Atlantic cold events of the past 50 ky, Geology, 30, 863-866, DOI:10.1130/0091-7613(2002)030<0863:EAAAHP>2.0.CO;2

Combourieu Nebout, N., Peyron, O., Dormoy, I., Desprat, S., Beaudouin, C., Kotthoff, U., Marret, F., 2009. Rapid climatic variability in the west Mediterranean during the last 25000 years from high resolution pollen data. Clim. Past 5, 503–521. https://doi.org/10.5194/cpd-5-671-2009

Comero, S., Locoro, G., Free, G., Vaccaro, S., De Capitani, L., Gawlik, B. M., 2011. Characterisation of Alpine lake sediments using multivariate statistical techniques, Chemometr. Intell. Lab., 107(1), 24-30, DOI:10.1016/j.chemolab.2011.01.002

Corella, J. P., Stefanova, V., El Anjoumi, A., Rico, E., Giralt, S., Moreno, A., Plata-Monter, A., Valero-Garcés, B. L., 2013. A 2500-year multi-proxy reconstruction of climate change and human activities in northern Spain: the Lake Arreo record, Palaeogeogr. Palaeoclimatol. Palaeoecol., 386, 555-568, DOI:10.1016/j.palaeo.2013.06.022

Cranwell, P.A., Eglinton, G., Robinson, N., 1987. Lipids of aquatic organisms as potential contributors to lacustrine sediments-II. Org. Geochem. 11, 513–527. https://doi.org/10.1016/0146-6380(87)90007-6

Cutmore, A., Ausín, B., Maslin, M., Eglinton, T., Hodell, D., Muschitiello, F., Menviel, L., Haghipour, N., Martrat, B., Margari, V., Tzedakis, P.C., 2021. Abrupt intrinsic and extrinsic responses of southwestern Iberian vegetation to millennial - scale variability over the past 28 ka 1–21. https://doi.org/10.1002/jqs.3392

Davis, J. C., and Sampson, R. J., 1986. Statistics and data analysis in geology, Willey, New York.

D'Agostino, R., Lionello, P., 2020. The atmospheric moisture budget in the Mediterranean: Mechanisms for seasonal changes in the Last Glacial Maximum and future warming scenario. Quat. Sci. Rev. 241, 106392. https://doi.org/10.1016/j.quascirev.2020.106392

Dansgaard, W., 1964. Stable isotopes in precipitation. Tellus 16, 436–468. https://doi.org/10.3402/tellusa.v16i4.8993

Dansgaard, W., Johnsen, S.J., Clausen, H.B., Dahl-Jensen, D., Gundestrup, N., Hammer, C.U., Oeschger, H., 1984. North Atlantic climatic oscillations revealed by deep

Greenland ice cores, in: Climate Processes and Climate Sensitivity. pp. 288–298. https://doi.org/10.1029/GM029p0288

de Lange, G.J., Thomson, J., Reitz, A., Slomp, C.P., Principato, M.S., Erba, E., Corselli, C., 2008. Synchronous basin-wide formation and redox-controlled preservation of a Mediterranean sapropel. Nat. Geosci. 1, 606. https://doi.org/10.1038/ngeo283

DeMenocal, P., Ortiz, J., Guilderson, T., Adkins, J., Sarnthein, M., Baker, L., Yarusinsky, M., 2000. Abrupt onset and termination of the African Humid Period: Rapid climate responses to gradual insolation forcing. Quat. Sci. Rev. 19, 347–361. https://doi.org/10.1016/S0277-3791(99)00081-5

Dennielou, B., Jégou, I., Droz, L., Jouet, G., Cattaneo, A., Berné, S., Aslanian, D., Loubrieu, B., Rabineau, M., Bermell, S., 2019b. Major modification of sediment routing by a large Mass Transport Deposit in the Gulf of Lions (Western Mediterranean). Mar. Geol. 411, 1–20. https://doi.org/10.1016/j.margeo.2019.01.011

Díaz de Federico, A., 1980. Estudio geológico del Complejo de Sierra Nevada en la transversal del Puerto de la Ragua (Cordillera Bética), Ph.D. thesis, Universidad de Granada, Granada.

Dickson, A.J., Leng, M.J., Maslin, M.A., Röhl, U., 2010. Oceanic, atmospheric and ice-sheet forcing of South East Atlantic Ocean productivity and South African monsoon intensity during MIS-12 to 10. Quat. Sci. Rev. 29, 3936–3947. https://doi.org/10.1016/j.quascirev.2010.09.014

Diefendorf, A.F., Mueller, K.E., Wing, S.L., Koch, P.L., Freeman, K.H., 2010. Global patterns in leaf 13C discrimination and implications for studies of past and future climate. Proc. Natl. Acad. Sci. U. S. A. 107, 5738–5743. https://doi.org/10.1073/pnas.0910513107

Diefendorf, A.F., Freeman, K.H., Wing, S.L., Graham, H. V., 2011. Production of n-alkyl lipids in living plants and implications for the geologic past. Geochim. Cosmochim. Acta 75, 7472–7485. https://doi.org/10.1016/j.gca.2011.09.028

Diefendorf, A.F., Freimuth, E.J., 2017. Extracting the most from terrestrial plant-derived n-alkyl lipids and their carbon isotopes from the sedimentary record: A review. Org. Geochem. 103, 1–21. https://doi.org/10.1016/j.orggeochem.2016.10.016

Dormoy, I., Peyron, O., Combourieu Nebout, N., Goring, S., Kotthoff, U., Magny, M., Pross, J., 2009. Terrestrial climate variability and seasonality changes in the Mediterranean region between 15 000 and 4000 years BP deduced from marine pollen records. Clima Past 5, 615–632.

Duhamel, M., Colin, C., Revel, M., Siani, G., Dapoigny, A., Douville, E., Wu, J., Zhao, Y., Liu, Z., Montagna, P., 2020. Variations in eastern Mediterranean hydrology during the last climatic cycle as inferred from neodymium isotopes in foraminifera. Quat. Sci. Rev. 237, 106306. https://doi.org/10.1016/j.quascirev.2020.106306

Dypvik, H., Harris, N.B., 2001. Geochemical facies analysis of fine-grained siliciclastics using Th/U, Zr/Rb and (Zr + Rb)/Sr ratios. Chem. Geol. 181, 131–146. https://doi.org/10.1016/S0009-2541(01)00278-9

Englebrecht, A. C., Sachs, J. P. 2005. Determination of sediment provenance at drift sites using hydrogen isotopes and unsaturation ratios in alkenones. Geochimica et Cosmochimica Acta, 69, 4253–4265. https://doi.org/10.1016/j.gca.2005.04.011

Eglinton G. and Hamilton R. J., 1967. Leafepicuticular waxes. Science 156, 1322–1335.

Eglinton, G., Calvin, M. 1967. Chemical fossils. Scientific American, 216, 32–43.

Eglinton, T.I., Eglinton, G., 2008. Molecular proxies for paleoclimatology. Earth Planet. Sci. Lett. 275, 1–16. https://doi.org/10.1016/j.epsl.2008.07.012

El Aallali, A., López Nieto, J. M., Pérez Raya, F., and Molero Mesa, J., 1998. Estudio de la vegetación forestal en la vertiente sur de Sierra Nevada (Alpujarra Alta granadina), Itinera Geobot., 11, 387-402

Ercilla, G., Alonso, B., Baraza, J., 1994. Post-Calabrian sequence stratigraphy of the northwestern Alboran Sea (southwestern Mediterranean). Mar. Geol. 120, 249–265. https://doi.org/10.1016/0025-3227(94)90061-2

Ercilla, G., Juan, C., Hernández-Molina, F.J., Bruno, M., Estrada, F., Alonso, B., Casas, D., Farran, M. l., Llave, E., García, M., Vázquez, J.T., D'Acremont, E., Gorini, C., Palomino, D., Valencia, J., El Moumni, B., Ammar, A., 2016. Significance of bottom currents in deep-sea morphodynamics: An example from the Alboran Sea. Mar. Geol. 378, 157–170. https://doi.org/10.1016/j.margeo.2015.09.007

Ercilla, G., Juan, C., Periáñez, R., Alonso, B., Abril, J.M., Estrada, F., Casas, D., Vázquez, J.T., D'Acremont, E., Gorini, C., El Moumni, B., Do Couto, D., Valencia, J., 2019.

Influence of alongslope processes on modern turbidite systems and canyons in the Alboran Sea (southwestern Mediterranean). Deep. Res. Part I Oceanogr. Res. Pap. 114, 1–16. https://doi.org/10.1016/j.dsr.2018.12.002

Esteban-Parra, M.J., Rodrigo, F.S., Castro-Diez, Y., 1998. Spatial and temporal patterns of precipitation in Spain for the period 1880-1992. Int. J. Climatol. 18, 1557–1574. https://doi.org/10.1002/(sici)1097-0088(19981130)18:14<1557::aid-joc328>3.0.co;2-j

Eynaud, F., De Abreu, L., Voelker, A., Schönfeld, J., Salgueiro, E., Turon, J.L., Penaud, A., Toucanne, S., Naughton, F., Sánchez Goñi, M.F., Malaizé, B., Cacho, I., 2009. Position of the Polar Front along the western Iberian margin during key cold episodes of the last 45 ka. Geochemistry, Geophys. Geosystems 10, Q07U05. https://doi.org/10.1029/2009GC002398

Fabres, J., Calafat, A., Sanchez-Vidal, A., Canals, M., Heussner, S., 2002. Composition and spatial variability of particle fluxes in the Western Alborán Gyre, Mediterranean Sea. J. Mar. Syst. 33–34, 431–456. https://doi.org/10.1016/S0924-7963(02)00070-2

Faegri, K., and Iversen, J., 1989. Textbook of Pollen Analysis, Wiley, New York.

Fanning, F., Weaver, A.J., 1997. Temporal-geographical meltwater influences on the North Atlantic conveyor: Implications for the Younger Dryas. Paleoceanography 12, 307–320.

Farquhar, G.D., O'Leary, M.H., Berry, J.A., 1982. On the relationship between carbon isotope discrimination and the intercellular carbon dioxide concentration in leaves. Aust. J. Plant Physiol. 9, 121–137.

Fernández-Salas, L.M., Lobo, F.J., Hernández-Molina, F.J., Somoza, L., Rodero, J., Díaz Del Río, V., Maldonado, A., 2003. High-resolution architecture of late Holocene highstand prodeltaic deposits from southern Spain: The imprint of high-frequency climatic and relative sea-level changes. Cont. Shelf Res. 23, 1037–1054. https://doi.org/10.1016/S0278-4343(03)00120-1

Filippidi, A., Triantaphyllou, M. V., De Lange, G.J., 2016. Eastern-Mediterranean ventilation variability during sapropel S1 formation, evaluated at two sites influenced by deep-water formation from Adriatic and Aegean Seas. Quat. Sci. Rev. 144, 95–106. https://doi.org/10.1016/j.quascirev.2016.05.024

Filippidi, A., De Lange, G.J., 2019. Eastern Mediterranean Deep Water Formation During Sapropel S1: A Reconstruction Using Geochemical Records Along a Bathymetric Transect in the Adriatic Outflow Region. Paleoceanogr. Paleoclimatology 34, 409–429. https://doi.org/10.1029/2018PA003459

Fink, H.G., Wienberg, C., De Pol-Holz, R., Wintersteller, P., Hebbeln, D., 2013. Cold-water coral growth in the Alboran Sea related to high productivity during the Late Pleistocene and Holocene. Mar. Geol. 339, 71–82. https://doi.org/10.1016/j.margeo.2013.04.009

Fischer, E.M., Beyerle, U., Schleussner, C.F., King, A.D., Knutti, R., 2018. Biased Estimates of Changes in Climate Extremes From Prescribed SST Simulations. Geophys. Res. Lett. 45, 8500–8509. https://doi.org/10.1029/2018GL079176

Fletcher, W. J., Boski, T., Moura, D., 2007. Palynological evidence for environmental and climatic change in the lower Guadiana valley, Portugal, during the last 13 000 years, Holocene, 17, 481-494, DOI:10.1177/0959683607077027

Fletcher, W.J., Sánchez Goñi, M.F., 2008. Orbital- and sub-orbital-scale climate impacts on vegetation of the western Mediterranean basin over the last 48,000 yr. Quat. Res. 70, 451–464. https://doi.org/10.1016/j.yqres.2008.07.002

Fletcher, W.J., Sanchez Goñi, M.F., Peyron, O., Dormoy, I., 2010. Abrupt climate changes of the last deglaciation detected in a Western Mediterranean forest record. Clim. Past 6, 245–264. https://doi.org/10.5194/cpd-5-203-2009

Fletcher, W.J., Zielhofer, C., 2013. Fragility of Western Mediterranean landscapes during Holocene Rapid Climate Changes. Catena 103, 16–29. https://doi.org/10.1016/j.catena.2011.05.001

Freeman, H., Hayes, J.M., 1992. Franctiontion of carbon isotopes by phytoplankton and estimates of ancient CO2 levels. Global Biogeochem. Cycles 6, 185–198.

Frigola, J., Moreno, A., Cacho, I., Canals, M., Sierro, F.J., Flores, J.A., Grimalt, J.O., Hodell, D.A., Curtis, J.H., 2007. Holocene climate variability in the western Mediterranean region from a deepwater sediment record. Paleoceanography 22, PA2209. https://doi.org/10.1029/2006PA001307

Frigola, J., Moreno, A., Cacho, I., Canals, M., Sierro, F.J., Flores, J.A., Grimalt, J.O., 2008. Evidence of abrupt changes in Western Mediterranean Deep Water circulation

during the last 50 kyr: A high-resolution marine record from the Balearic Sea. Quat. Int. 181, 88–104. https://doi.org/10.1016/j.quaint.2007.06.016

Frigola, J., Canals, M., Cacho, I., Moreno, A., Sierro, F.J., Flores, J.A., Berné, S., Jouet, G., Dennielou, B., Herrera, G., Pasqual, C., Grimalt, J.O., Galavazi, M., Schneider, R., 2012. A 500 kyr record of global sea-level oscillations in the Gulf of Lion, Mediterranean Sea: New insights into MIS 3 sea-level variability. Clim. Past 8, 1067–1077. https://doi.org/10.5194/cp-8-1067-2012

Finlayson, C., Giles Pacheco, F., Rodrı´guez-Vidal, J., Fa, D.A., Gutierrez Lo´ pez, J.M., Santiago Perez, A., Finlayson, G., Allue, E., Baena Preysler, J., Ca´ ceres, I., Carrio´ n, J.S., Ferna´ ndez Jalvo, Y., Gleed- Owen, C.P., Jime´ nez-Espejo, F.J., Lo´ pez, P., Lo´ pez Sa´ ez, J.A., Riquelme Cantal, J.A., Sa´ nchez Marco, A., Giles Guzman, F., Brown, K., Fuentes, N., Valarino, C.A., Villalpando, A., Stringer, C.B., Martinez-Ruiz, F., Sakamoto, T., 2006. Late survival of Neanderthals at the southernmost extreme of Europe. Nature, doi:10.1038/nature05195.

Gallego-Torres, D., Martínez-Ruiz, F., Paytan, A., Jiménez-Espejo, F.J., Ortega-Huertas, M., 2007. Pliocene-Holocene evolution of depositional conditions in the eastern Mediterranean: Role of anoxia vs. productivity at time of sapropel deposition. Palaeogeogr. Palaeoclimatol. Palaeoecol. 246, 242–239. https://doi.org/10.1016/j.palaeo.2006.10.008

García, M., Alonso, B., Ercilla, G., Gràcia, E., 2006. The tributary valley systems of the Almeria Canyon (Alboran Sea, SW Mediterranean): Sedimentary architecture. Mar. Geol. 226, 207–223. https://doi.org/10.1016/j.margeo.2005.10.002

García-Alix, A., Jiménez-Moreno, G., Anderson, R.S., Jiménez Espejo, F.J., Delgado Huertas, A., 2012. Holocene environmental change in southern Spain deduced from the isotopic record of a high-elevation wetland in Sierra Nevada. J. Paleolimnol. 48, 471–484. https://doi.org/10.1007/s10933-012-9625-2

García-Alix, A., Jiménez-Espejo, F.J., Lozano, J.A., Jiménez-Moreno, G., Martínez-Ruiz, F., García Sanjuán, L., Aranda Jiménez, G., García Alfonso, E., Ruiz-Puertas, G., Anderson, R.S., 2013. Anthropogenic impact and lead pollution throughout the Holocene in Southern Iberia. Sci. Total Environ. 449, 451–460. https://doi.org/10.1016/j.scitotenv.2013.01.081

García-Alix, A., Jiménez-Moreno, G., Jiménez-Espejo, F.J., García-García, F., Delgado Huertas, A., 2014. An environmental snapshot of the Bølling interstadial in Southern Iberia. Quat. Res. 81, 284–294. https://doi.org/10.1016/j.yqres.2014.01.009

García-Alix, A., Jiménez-Espejo, F.J., Toney, J.L., Jiménez-Moreno, G., Ramos-Román, M.J., Anderson, R.S., Ruano, P., Queralt, I., Delgado Huertas, A., Kuroda, J., 2017. Alpine bogs of southern Spain show human-induced environmental change superimposed on long-term natural variations. Sci. Rep. 7, 7439. https://doi.org/10.1038/s41598-017-07854-w

García-Alix, A., Jiménez-Espejo, F.J., Jiménez-Moreno, G., Toney, J.L., Ramos-Román, M.J., Camuera, J., Anderson, R.S., Delgado-Huertas, A., Martínez-Ruiz, F., Queralt, I., 2018. Holocene geochemical footprint from Semi-arid alpine wetlands in southern Spain. Sci. Data 5, 180024. https://doi.org/10.1038/sdata.2018.24

García-Alix, A., Camuera, J., Ramos-Román, M.J., Toney, J.L., Sachse, D., Schefuß, E., Jiménez-Moreno, G., Jiménez-Espejo, F.J., López-Avilés, A., Anderson, R.S., Yanes, Y., 2021. Paleohydrological dynamics in the Western Mediterranean during the last glacial cycle. Glob. Planet. Change 202, 103527. https://doi.org/10.1016/j.gloplacha.2021.103527

García-Lafuente, J., Naranjo, C., Sammartino, S., Sánchez-Garrido, J.C., Delgado, J., 2017. The Mediterranean outflow in the Strait of Gibraltar and its connection with upstream conditions in the Alborán Sea. Ocean Sci. 13, 195–207. https://doi.org/10.5194/os-13-195-2017

Gelpi, E., Schneider, H., Mann, J., Oró, J., 1970. Fatty acids of geochemical significance in microscopic algae. Phytochemistry 9, 603–613. https://doi.org/10.1016/S0031-9422(00)85701-5

Gimeno, L., Nieto, R., Trigo, R.M., Vicente-Serrano, S.M., López-Moreno, J.I., 2010. Where Does the Iberian Peninsula Moisture Come From? An Answer Based on a Lagrangian Approach. Am. Meteorol. Soc. 421–436. https://doi.org/10.1175/2009JHM1182.1

Goldberg, E. D.,1954. Marine geochemistry, I. Chemical scavengers of the sea. Journal of Geology, 62, 249–265.

Goldberg, E. D., Arrhenius, G. O. S., 1958. Chemistry of Pacific pelagic sediments. Geochimica et Cosmochimica Acta 13, 153–212.

González-Hidalgo, J.C., Lopez-Bustins, J.-A., Stepanek, P., Martín-Vide, J., de Luis, M., 2009. Monthly precipitation trends on the Mediterranean fringe of the Iberian Peninsula during the second-half of the twentieth century (1951–2000). Int. J. Climatol. 29, 1415–1429. https://doi.org/10.1002/joc

González Portilla, M., 1998. Primera Industrialización, Desequilibrios Territoriales Y Estado. Hist. Contemp. 17, 201–235.

Goodess, C.M., Jones, P.D., 2002. Links between circulation and changes in the characteristics of Iberian rainfall. Int. J. Climatol. 22, 1593–1615. https://doi.org/10.1002/joc.810

Govin, A., Holzwarth, U., Heslop, D., Ford Keeling, L., Zabel, M., Mulitza, S., Collins, J.A., Chiessi, C.M., 2012. Distribution of major elements in Atlantic surface sediments (36°N-49°S): Imprint of terrigenous input and continental weathering. Geochemistry, Geophys. Geosystems 13, Q01013. https://doi.org/10.1029/2011GC003785

GRID-Arendal, 2013. State of the Mediterranean Marine and Coastal Environment. https://www.grida.no/resources/5885

Grimm, E. C., 1987. CONISS: a Fortran 77 program for stratigraphically constrained cluster analysis by the method of incremental sum of squares, Comput. Geosci., 13, 13-35, DOI:10.1016/0098-3004(87)90022-7

Grimm, E., 1993. TILIA: a pollen program for analysis and display, Illinois State Museum, Springfield

Häggi, C., Pätzold, J., Bouillon, S., Schefuß, E., 2021. Impact of selective degradation on molecular isotope compositions in oxic and anoxic marine sediments. Org. Geochem. 153, 104192. https://doi.org/10.1016/j.orggeochem.2021.104192

Hammer, Ø., Harper, D.A.T., Ryan, P.D., 2001. PAST: Paleontological statistics software package for education and data analysis. Palaeontol. Electron. 4, 9.

Harper, D. A. T., 1999. Numerical Palaeobiology, John Wiley & Sons, Chichester.

Hays, J.D., Lozano, J.A., Shackleton, N.J., Irving, G., 1976. Reconstruction of the Atlantic and western Indian Ocean sectors of the 18.000 BP Antarctic Ocean. In: Cline, R.M., Hays, J.D. (Eds.), Investigation of Late Quaternary Paleoceanography and Paleoclimatology. Geological Society of America, Boulder, pp. 337e372.

Heaton, T.J., Köhler, P., Butzin, M., Bard, E., Reimer, R.W., Austin, W.E.N., Bronk Ramsey, C., Grootes, P.M., Hughen, K.A., Kromer, B., Reimer, P.J., Adkins, J., Burke, A., Cook, M.S., Olsen, J., Skinner, L.C., 2020. Marine20 - The Marine Radiocarbon Age Calibration Curve (0-55,000 cal BP). Radiocarbon 62, 779–820. https://doi.org/10.1017/RDC.2020.68

Heburn, G.W., La Violette, P.E., 1990. Variations in the Structure of the Anticyclonic Gyres. J. Geophys. Res. 95, 1599–1613.

Heinrich, H., 1988. Origin and consequences of cyclic ice rafting in the Northeast Atlantic Ocean during the past 130,000 years. Quat. Res. 29, 142–152. https://doi.org/10.1016/0033-5894(88)90057-9

Helama, S., Jones, P.D., Briffa, K.R., 2017. Dark Ages Cold Period: A literature review and directions for future research. Holocene 27, 1600–1606. https://doi.org/10.1177/0959683617693898

Held, I. M. Soden, B. J., 2006. Robust responses of the hydrological cycle to global warming. J. Clim. 19, 5686–5699. (doi:10.1175/JCLI3990.1)

Hemming, S.R., Biscaye, P.E., Broecker, W.S., Hemming, N.G., Klas, M., Hajdas, I., 1998. Provenance change coupled with increased clay flux during deglacial times in the western equatorial Atlantic. Palaeogeogr. Palaeoclimatol. Palaeoecol. 142, 217–230. https://doi.org/10.1016/S0031-0182(98)00069-8

Henrich, R., Cherubini, Y., Meggers, H., 2010. Climate and sea level induced turbidite activity in a canyon system offshore the hyperarid Western Sahara (Mauritania): The Timiris Canyon. Mar. Geol. 275, 178–198. https://doi.org/10.1016/j.margeo.2010.05.011

Hernández, A., Martin-Puertas, C., Moffa-Sánchez, P., Moreno-Chamarro, E., Ortega, P., Blockley, S., Cobb, K.M., Comas-Bru, L., Giralt, S., Goosse, H., Luterbacher, J., Martrat, B., Muscheler, R., Parnell, A., Pla-Rabes, S., Sjolte, J., Scaife, A.A., Swingedouw, D., Wise, E., Xu, G., 2020. Modes of climate variability: Synthesis and

review of proxy-based reconstructions through the Holocene. Earth-Science Rev. 209, 103286. https://doi.org/10.1016/j.earscirev.2020.103286

Hodell, D.A., Channeil, J.E.T., Curtis, J.H., Romero, O.E., Röhl, U., 2008. Onset of "Hudson Strait" Heinrich events in the eastern North Atlantic at the end of the middle Pleistocene transition (~640 ka)? Paleoceanography 23, 1–16. https://doi.org/10.1029/2008PA001591

Hodell, D., Crowhurst, S., Skinner, L., Tzedakis, P.C., Margari, V., Channell, J.E.T., Kamenov, G., MacLachlan, S., Rothwell, G., 2013. Response of Iberian Margin sediments to orbital and suborbital forcing over the past 420 ka. Paleoceanography 28, 185–199. https://doi.org/10.1002/palo.20017

Hodell, D., Lourens, L., Crowhurst, S., Konijnendijk, T., Tjallingii, R., Jiménez-Espejo, F., Skinner, L., Tzedakis, P.C., Members, S.S.P., 2015. A reference time scale for Site U1385 (Shackleton Site) on the SW Iberian Margin. Glob. Planet. Change 133, 49–64. https://doi.org/10.1016/j.gloplacha.2015.07.002

Hodell, D.A., Nicholl, J.A., Bontognali, T.R.R., Danino, S., Dorador, J., Dowdeswell, J.A., Einsle, J., Kuhlmann, H., Martrat, B., Mleneck-Vautravers, M.J., Rodríguez-Tovar, F.J., Röhl, U., 2017. Anatomy of Heinrich Layer 1 and its role in the last deglaciation. Paleoceanography 32, 284–303. https://doi.org/10.1002/2016PA003028

Huang, E., Tian, J., 2008. Melt-Water-Pulse (MWP) events and abrupt climate change of the last deglaciation. Chinese Sci. Bull. 53, 2867–2878. https://doi.org/10.1007/s11434-008-0206-8

Hughes, P. D., Gibbard, P. L., Ehlers, J., 2013. Timing of glaciation during the last glacial cycle: evaluating the concept of a global 'Last Glacial Maximum'(LGM). Earth-Science Reviews 125, 171-198.

Imbrie, J., Hays, J.D., Martinson, D.G., Mclntyre, A., Mix, A.C., Morley, J.J., Pisias, N.G., Prell and, W.L., Shackleton, N.J., 1984. The orbital theory of pleistocene climate: support from a revised chronology of the marine O180 record. In "Milankovitch and climate." Milankovitch Clim. 269–305.

IPCC, 2013. Climate change 2013: the physical science basis. In: Contribution of Working Group I to the Fifth Assessment Report of the Intergovernmental Panel on

Climate Change. Cambridge University Press, Cambridge, United Kingdom and New York, USA.

IPCC, 2018: Global warming of 1.5°C. An IPCC Special Report on the impacts of global warming of 1.5°C above pre-industrial levels and related global greenhouse gas emission pathways, in the context of strengthening the global response to the threat of climate change, sustainable development, and efforts to eradicate poverty [V. Masson-Delmotte, P. Zhai, H. O. Pörtner, D. Roberts, J. Skea, P.R. Shukla, A. Pirani, W. Moufouma-Okia, C. Péan, R. Pidcock, S. Connors, J. B. R. Matthews, Y. Chen, X. Zhou, M. I. Gomis, E. Lonnoy, T. Maycock, M. Tignor, T. Waterfield (eds.)].

IPCC, 2021. Climate Change 2021: The Physical Science Basis. Contribution of Working Group I to the Sixth Assessment Report of the Intergovernmental Panel on Climate Change [Masson-Delmotte, V., P. Zhai, A. Pirani, S.L. Connors, C. Péan, S. Berger, N. Caud, Y. Chen, L. Goldfarb, M.I. Gomis, M. Huang, K. Leitzell, E. Lonnoy, J.B.R. Matthews, T.K. Maycock, T. Waterfield, O. Yelekçi, R. Yu, and B. Zhou (eds.)]. Cambridge University Press.

Ivy-ochs, S., Kerschner, H., Schlu, C., 2007. Cosmogenic nuclides and the dating of Lateglacial and Early Holocene glacier variations : The Alpine perspective 165, 53–63. https://doi.org/10.1016/j.quaint.2006.12.008

Ivy-ochs, S., Kerschner, H., Reuther, A., Preusser, F., Heine, K., Maisch, M.A.X., Kubik, P.W., Schlu, C., 2008. Chronology of the last glacial cycle in the European Alps 23, 559–573. https://doi.org/10.1002/jqs.1202

Jackson, L.C., Kahana, R., Graham, T., Ringer, M.A., Woollings, T., Mecking, J. V., Wood, R.A., 2015. Global and European climate impacts of a slowdown of the AMOC in a high resolution GCM. Clim. Dyn. 45, 3299–3316. https://doi.org/10.1007/s00382-015-2540-2

Jacob, D., Kotova, L., Teichmann, C., Sobolowski, S.P., Vautard, R., Donnelly, C., Koutroulis, A.G., Grillakis, M.G., Tsanis, I.K., Damm, A., Sakalli, A., Vliet, M.T.H. Van, Centre, B., Ipsl, L., Uvsq, C.E.A.C., 2018. Earth's Future Climate Impacts in Europe Under +1.5∘C Global Warming Earth's Future. Earth's Futur. 6, 264–285. https://doi.org/10.1002/eft2.286

Jaeschke, A., Thienemann, M., Schefuß, E., Urban, J., Schäbitz, F., Wagner, B., Rethemeyer, J., 2020. Holocene Hydroclimate Variability and Vegetation Response

in the Ethiopian Highlands (Lake Dendi). Front. Earth Sci. 8, 585770. https://doi.org/10.3389/feart.2020.585770

Jalut, G., Esteban Amat, A., Bonnet, L., Gauquelin, T., ad Fontugne, M., 2000. Holocene climatic changes in the Western Mediterranean, from south-east France to south-east Spain, Palaeogeogr. Palaeocl., 160, 255-290, DOI:10.1016/S0031-0182(00)00075-4

Jalut, G., Dedoubat, J.J., Fontugne, M., Otto, T., 2009. Holocene circum-Mediterranean vegetation changes: Climate forcing and human impact. Quat. Int. 200, 4–18. https://doi.org/10.1016/j.quaint.2008.03.012

Jambrina-Enríquez, M., Rico, M., Moreno, A., Leira, M., Bernárdez, P., Prego, R., Recio, C., Valero-Garcés, B. L., 2014. Timing of deglaciation and postglacial environmental dynamics in NW Iberia: the Sanabria Lake record, Quaternary Sci. Rev., 94, 136-158, DOI:10.1016/j.quascirev.2014.04.018

Jeng, W.-L., 2006. Higher plant n-alkane average chain length as an indicator of petrogenic hydrocarbon contamination in marine sediments. Mar. Chem. 102, 242–251. https://doi.org/10.1016/j.marchem.2006.05.001

Jiménez, L., Rühland, K. M., Jeziorski, A., Smol, J. P., Pérez-Martínez, C., 2018. Climate change and Saharan dust drive recent cladoceran and primary production changes in remote alpine lakes of Sierra Nevada, Spain, Glob. Change Biol., 24, e139-e158, DOI:10.1111/gcb.13878

Jiménez-Amat, P., Zahn, R., 2015. Offset timing of climate oscillations during the last two glacial-interglacial transitions connected with large-scale freshwater perturbation. Paleoceanography 30, 768–788. https://doi.org/10.1002/2014PA002710

Jimenez-Espejo, F.J., Martinez-Ruiz, F., Sakamoto, T., Iijima, K., Gallego-Torres, D., Harada, N., 2007. Paleoenvironmental changes in the western Mediterranean since the last glacial maximum: High resolution multiproxy record from the Algero–Balearic basin. Palaeogeogr. Palaeoclimatol. Palaeoecol. 246, 292–306. https://doi.org/10.1016/j.palaeo.2006.10.005

Jiménez-Espejo, F.J., Martínez-Ruiz, F., Rogerson, M., González-Donoso, J.M., Romero, O.E., Linares, D., Sakamoto, T., Gallego-Torres, D., Rueda Ruiz, J.L., Ortega-Huertas, M., Perez Claros, J.A., 2008. Detrital input, productivity fluctuations, and

water mass circulation in the westernmost Mediterranean Sea since the Last Glacial Maximum. Geochemistry, Geophys. Geosystems 9, Q11U02. https://doi.org/10.1029/2008GC002096

Jiménez-Espejo, F.J., García-Alix, A., Jiménez-Moreno, G., Rodrigo-Gámiz, M., Anderson, R.S., Rodríguez-Tovar, F.J., Martínez-Ruiz, F., Giralt, S., Delgado Huertas, A., Pardo-Igúzquiza, E., 2014. Saharan aeolian input and effective humidity variations over western Europe during the Holocene from a high altitude record. Chem. Geol. 374–375, 1–12. https://doi.org/10.1016/j.chemgeo.2014.03.001

Jiménez-Moreno, G., Anderson, R.S., 2012. Holocene vegetation and climate change recorded in alpine bog sediments from the Borreguiles de la Virgen, Sierra Nevada, southern Spain. Quat. Res. 77, 44–53. https://doi.org/10.1016/j.yqres.2011.09.006

Jiménez-Moreno, G., García-Alix, A., Hernández-Corbalán, M.D., Anderson, R.S., Delgado-Huertas, A., 2013. Vegetation, fire, climate and human disturbance history in the southwestern Mediterranean area during the late Holocene. Quat. Res. 79, 110–122. https://doi.org/10.1016/j.yqres.2012.11.008

Jiménez-Moreno, G., Rodríguez-Ramírez, A., Pérez-Asensio, J.N., Carrión, J.S., López-Sáez, J.A., Villarías-Robles, J.J.R., Celestino-Pérez, S., Cerrillo-Cuenca, E., León, Á., Contreras, C., 2015. Impact of late-Holocene aridification trend, climate variability and geodynamic control on the environment from a coastal area in SW Spain. Holocene 25, 607–617. https://doi.org/10.1177/0959683614565955

Jiménez-Moreno, G., Anderson, R.S., Ramos-Román, M.J., Camuera, J., Mesa-Fernández, J.M., García-Alix, A., Jiménez-Espejo, F.J., Carrión, J.S., López-Avilés, A., 2020. The Holocene Cedrus pollen record from Sierra Nevada (S Spain), a proxy for climate change in N Africa. Quat. Sci. Rev. 242, 106468. https://doi.org/10.1016/j.quascirev.2020.106468

Josey, S.A., Somot, S., Tsimplis, M., 2011. Impacts of atmospheric modes of variability on Mediterranean Sea surface heat exchange. J. Geophys. Res. Ocean. 116, C02032. https://doi.org/10.1029/2010JC006685

Juan, C., Ercilla, G., Javier Hernández-Molina, F., Estrada, F., Alonso, B., Casas, D., García, M., Farran, M., Llave, E., Palomino, D., Vázquez, J.T., Medialdea, T., Gorini, C., D'Acremont, E., El Moumni, B., Ammar, A., 2016. Seismic evidence of current-controlled sedimentation in the Alboran Sea during the Pliocene and

Quaternary: Palaeoceanographic implications. Mar. Geol. 378, 292–311. https://doi.org/10.1016/j.margeo.2016.01.006

Jung, M., Ilmberger, J., Mangini, A., Emeis, K.-C., 1997. Why some Mediterranean sapropels survived burn-down (and others did not). Mar. Geol. 141, 51–60. https://doi.org/10.1016/S0025-3227(97)00031-5

Kaboth, S., Bahr, A., Reichart, G.J., Jacobs, B., Lourens, L.J., 2015. New insights into upper MOW variability over the last 150 kyr from IODP 339 Site U1386 in the Gulf of Cadiz. Mar. Geol. https://doi.org/10.1016/j.margeo.2015.08.014

Kageyama, M., Nebout, N.C., Sepulchre, P., Peyron, O., Krinner, G., Ramstein, G., Cazet, J.-P., 2005. The Last Glacial Maximum and Heinrich event 1 in terms of climate and vegetation around the Alboran Sea: a preliminary model-data comparison. Compt. Rendus Geosci.337,983–992.

Kenyon, N.H., Akhmetzhanov, A.M., Wheeler, A.J., van Weering, T.C.E., De Haas, H., Ivanov, M.K., 2003. Giant carbonate mud mounds in the southern Rockall Trough. Marine Geology 195, 5–30

Kinder, T.H., Parrilla, G., 1987. Yes, some of the Mediterranean outflow does come from great depth. J. Geophys. Res. 92, 2901–2906.

Krklec, K., Domínguez-Villar, D. 2014. Quantification of the impact of moisture source regions on the oxygen isotope composition of precipitation over Eagle Cave, central Spain. Geochim. Cosmochim. Acta 134, 39-54.

Kusch, S., Rethemeyer, J., Schefuß, E., Mollenhauer, G., 2010. Controls on the age of vascular plant biomarkers in Black Sea sediments. Geochim. Cosmochim. Acta 74, 7031–7047. https://doi.org/10.1016/j.gca.2010.09.005

Lambeck, K., Rouby, H., Purcell, A., Sun, Y., Sambridge, M., 2014. Sea level and global ice volumes from the Last Glacial Maximum to the Holocene. Proc. Natl. Acad. Sci. U. S. A. 111, 15296–15303. https://doi.org/10.1073/pnas.1411762111

Laskar, J., Robutel, P., Joutel, F., Gastineau, M., Correia, A.C.M., Levrard, B., 2004. A long-term numerical solution for the insolation quantities of the Earth. Astron. Astrophys. 428, 261–285. https://doi.org/10.1051/0004-6361:20041335

Lebreiro, S.M., Antón, L., Reguera, M.I., Marzocchi, A., 2018. Paleoceanographic and climatic implications of a new Mediterranean Outflow branch in the southern Gulf

of Cadiz. Quat. Sci. Rev. 197, 92–111. https://doi.org/10.1016/j.quascirev.2018.07.036

Li, Y., Song, Y., Yin, Q., Han, L., Wang, Y., 2019. Orbital and millennial northern mid-latitude westerlies over the last glacial period. Clim. Dyn. 53, 3315–3324. https://doi.org/10.1007/s00382-019-04704-5

Lionello, P., Sanna, A., 2005. Mediterranean wave climate variability and its links with NAO and Indian Monsoon. Clim. Dyn. 25, 611–623. https://doi.org/10.1007/s00382-005-0025-4

Lionello, P., Malanotte-Rizzoli, P., Boscolo, R., Alpert, P., Artale, V., Li, L., Luterbacher, J., May, W., Trigo, R., Tsimplis, M., Ulbrich, M., Xoplaki, E., 2006. The Mediterranean Climate: An Overview of the Main Characteristics and Issues, in: The Mediterranean Climate: An Overview of the Main Characteristics and Issues.

Lionello, P., Abrantes, F., Congedi, L., Dulac, F., Gacic, M., Goodess, C., Hoff, H., Kutiel, H., Planton, S., Reale, M., Struglia, M.V., Toreti, A., Tsimplis, M., Ulbrich, U., Xoplaki, E., 2012. Introduction: Mediterranean Climate — Background Information. https://doi.org/10.1016/B978-0-12-416042-2.00012-4

Lionello, P., Scarascia, L., 2018. The relation between climate change in the Mediterranean region and global warming. Reg. Environ. Chang. 18, 1481–1493.

Liquete, C., Arnau, P., Canals, M., Colas, S., 2005. Mediterranean river systems of Andalusia, southern Spain, and associated deltas: A source to sink approach. Mar. Geol. 222–223, 471–495. https://doi.org/10.1016/j.margeo.2005.06.033

Liu, Z., Wang, Y., Gallimore, R., Gasse, F., Johnson, T., deMenocal, P., Adkins, J., Notaro, M., Prentice, I. C., Kutzbach, J., Jacob, R., Behling, P., Wang, L., Ong, E., 2007. Simulating the transient evolution and abrupt change of Northern Africa atmosphere–ocean–terrestrial ecosystem in the Holocene. Quaternary Sci. Rev., 26, 1818-1837, DOI:10.1016/j.quascirev.2007.03.002

Liu, X., Rendle-Bühring, R., Henrich, R., 2016. Climate and sea-level controls on turbidity current activity on the Tanzanian upper slope during the last deglaciation and the Holocene. Quat. Sci. Rev. 133, 15–27. https://doi.org/10.1016/j.quascirev.2015.12.002

Liu, X., Rendle-Bühring, R., Kuhlmann, H., Li, A., 2017. Two phases of the Holocene East African Humid Period: Inferred from a high-resolution geochemical record off Tanzania. Earth Planet. Sci. Lett. 460, 123–134. https://doi.org/10.1016/j.epsl.2016.12.016

Liu, J., Algeo, T.J., 2020. Beyond redox: Control of trace-metal enrichment in anoxic marine facies by watermass chemistry and sedimentation rate. Geochim. Cosmochim. Acta 287, 296–317. https://doi.org/10.1016/j.gca.2020.02.037

Liu, J., An, Z., 2020. Leaf wax n-alkane carbon isotope values vary among major terrestrial plant groups: Different responses to precipitation amount and temperature, and implications for paleoenvironmental reconstruction. Earth-Science Rev. 202, 103081. https://doi.org/10.1016/j.earscirev.2020.103081

Lobo, F.J., Fernández-Salas, L.M., Moreno, I., Sanz, J.L., Maldonado, A., 2006. The sea-floor morphology of a Mediterranean shelf fed by small rivers, northern Alboran Sea margin. Cont. Shelf Res. 26, 2607–2628. https://doi.org/10.1016/j.csr.2006.08.006

Lombo Tombo, S., Dennielou, B., Berné, S., Bassetti, M.-A., Toucanne, S., Jorry, S.J., Jouet, G., Fontanier, C., 2015. Sea-level control on turbidite activity in the Rhone canyon and the upper fan during the Last Glacial Maximum and Early deglacial. Sediment. Geol. 323, 148–166. https://doi.org/10.1016/j.sedgeo.2015.04.009

López-Avilés, A., García-Álix, A., Jiménez-Moreno, G., Anderson, R.S., Toney, J.L., Mesa-Fernández, J.M., Jiménez-Espejo, F.J., 2021. Latest Holocene paleoenvironmental and paleoclimate reconstruction from an alpine bog in the Western Mediterranean region: The Borreguil de los Lavaderos de la Reina record (Sierra Nevada). Palaeogeogr. Palaeoclimatol. Palaeoecol. 573, 110434. https://doi.org/10.1016/j.palaeo.2021.110434

López-Avilés, A., Jiménez-Moreno, G., García-Alix, A., García-garcía, F., Camuera, J., Anderson, R.S., Sanjurjo-Sánchez, J., Arce Chamorro, C., Carrión, J.S., 2022. Catena Post-glacial evolution of alpine environments in the western Mediterranean region : The Laguna Seca record. Catena 211, 106033. https://doi.org/10.1016/j.catena.2022.106033

López-González, N., Alonso, B., Juan, C., Ercilla, G., Bozzano, G., Cacho, I., Casas, D., Palomino, D., Vázquez, J.-T., Estrada, F., Bárcenas, P., D'Acremont, E., Gorini, C., El Moumni, B., López-González, N., Alonso, B., Juan, C., Ercilla, G., Bozzano, G.,

Cacho, I., Casas, D., Palomino, D., Vázquez, J.-T., Estrada, F., Bárcenas, P., D'Acremont, E., Gorini, C., Moumni, B. El, 2019. 133,000 Years of Sedimentary Record in a Contourite Drift in the Western Alboran Sea: Sediment Sources and Paleocurrent Reconstruction. Geosciences 9, 345. https://doi.org/10.3390/geosciences9080345

López-Sáez, J.A., Carrasco, R.M., Turu, V., Ruiz-Zapata, B., Gil-García, M.J., Luelmo-Lautenschlaeger, R., Pérez-Díaz, S., Alba-Sánchez, F., Abel-Schaad, D., Ros, X., Pedraza, J., 2020. Late Glacial-early holocene vegetation and environmental changes in the western Iberian Central System inferred from a key site: The Navamuño record, Béjar range (Spain). Quat. Sci. Rev. 230, 106167. https://doi.org/10.1016/j.quascirev.2020.106167

Lowe, J.J., Rasmussen, S.O., Björck, S., Hoek, W.Z., Steffensen, J.P., Walker, M.J.C., Yu, Z.C., Group, the I., 2008. Synchronisation of palaeoenvironmental events in the North Atlantic region during the Last Termination: a revised protocol recommended by the INTIMATE group. Quat. Sci. Rev. 27, 6–17. https://doi.org/10.1016/j.quascirev.2007.09.016

Löwemark, L., Chen, H.-F., Yang, T.-N., Kylander, M., Yu, E.-F., Hsu, Y.-W., Lee, T.-Q., Song, S.-R., Jarvis, S., 2011. Normalizing XRF-scanner data: a cautionary note on the interpretation of high-resolution records from organic-rich lakes, J. Asian Earth Sci., 40, 1250-1256, DOI:10.1016/j.jseaes.2010.06.002

Lull, V., Micó, R., Rihuete Herrada, C., & Risch, R. (2015a). Transition and conflict at the end of the 3rd millennium BC in south Iberia. In H. Meller, H. W. Arz, R. Jung, & R. Risch (Eds.), 2200 BC – A climatic breakdown as a cause for the collapse of the old world? (pp. 365–408). Halle: Landesmuseum für VorgeschichteLynch-Stieglitz, J., 2017. The Atlantic Meridional Overturning Circulation and Abrupt Climate Change. Ann. Rev. Mar. Sci. 9, 83–104. https://doi.org/10.1146/annurev-marine-010816-060415

Magny, M., Miramont, C., Sivan, O., 2002. Assessment of the impact of climate and anthropogenic factors on Holocene Mediterranean vegetation in Europe on the basis of palaeohydrological records, Palaeogeogr. Palaeocl., 186, 47-59, DOI:10.1016/S0031-0182(02)00442-X

Magny, M., Bégeot, C., 2004. Hydrological changes in the European midlatitudes associated with freshwater outbursts from Lake Agassiz during the Younger Dryas event and the early Holocene. Quat. Res. https://doi.org/10.1016/j.yqres.2003.12.003

Magny, M., de Beaulieu, J.-L., Drescher-Schneider, R., Vannière, B., Walter-Simonnet, A.-V., Miras, Y., Millet, L., Bossuet, G., Peyron, O., Brugiapaglia, E., Leroux, A., 2007. Holocene climate changes in the central Mediterranean as recorded by lake-level fluctuations at Lake Accesa (Tuscany, Italy). Quat. Sci. Rev. 26, 1736–1758. https://doi.org/10.1016/j.quascirev.2007.04.014

Magny, M., Peyron, O., Sadori, L., Ortu, E., Zanchetta, G., Vannière, B., Tinner, W., 2012. Contrasting patterns of precipitation seasonality during the Holocene in the south- and north-central Mediterranean, J. Quat. Sci., 27, 290-296, DOI:10.1002/jqs.1543

Magny, M., Combourieu-Nebout, N., de Beaulieu, J.L., Bout-Roumazeilles, V., Colombaroli, D., Desprat, S., Francke, A., Joannin, S., Ortu, E., Peyron, O., Revel, M., Sadori, L., Siani, G., Sicre, M.A., Samartin, S., Simonneau, A., Tinner, W., Vannière, B., Wagner, B., Zanchetta, G., Anselmetti, F., Brugiapaglia, E., Chapron, E., Debret, M., Desmet, M., Didier, J., Essallami, L., Galop, D., Gilli, A., Haas, J.N., Kallel, N., Millet, L., Stock, A., Turon, J.L., Wirth, S., 2013. North–south palaeohydrological contrasts in the central Mediterranean during the Holocene: tentative synthesis and working hypotheses. Clim. Past 9, 2043–2071. https://doi.org/10.5194/cp-9-2043-2013

Manzano, S., Carrión, J.S., López-Merino, L., Jiménez-Moreno, G., Toney, J.L., Amstrong, H., Anderson, R.S., García-Alix, A., Pérez, J.L.G., Sánchez-Mata, D., 2019. A palaeoecological approach to understanding the past and present of Sierra Nevada, a Southwestern European biodiversity hotspot. Glob. Planet. Change 175, 238–250. https://doi.org/10.1016/j.gloplacha.2019.02.006

Marret, F., Scourse, J., Kennedy, H., Ufkes, E., Jansen, J.H.F., 2008. Marine production in the Congo-influenced SE Atlantic over the past 30,000 years: A novel dinoflagellate-cyst based transfer function approach. Mar. Micropaleontol. 68, 198–222. https://doi.org/10.1016/j.marmicro.2008.01.004

Martín-Puertas, C., Valero-Garcés, B. L., Mata, M. P., González-Sampériz, P., Bao, R., Moreno, A., Stefanova, V., 2008. Arid and humid phases in southern Spain during

the last 4000 years: the Zonar Lake record, Cordoba, Holocene, 18, 907-921, DOI:10.1177/0959683608093533

Martín-Puertas, C., Valero-Garcés, B.L., Brauer, A., Mata, M.P., Delgado-Huertas, A., Dulski, P., 2009. The Iberian-Roman Humid Period (2600-1600 cal yr BP) in the Zoñar Lake varve record (Andalucía, southern Spain). Quat. Res. 71, 108–120. https://doi.org/10.1016/j.yqres.2008.10.004

Martín-Puertas, C., Jiménez-Espejo, F., Martínez-Ruiz, F., Nieto-Moreno, V., Rodrigo, M., Mata, M.P., Valero-Garcés, B.L., 2010. Late Holocene climate variability in the southwestern Mediterranean region: An integrated marine and terrestrial geochemical approach. Clim. Past 6, 807–816. https://doi.org/10.5194/cp-6-807-2010

Martín, J., Miquel, J.C., Khripounoff, A., 2010. Impact of open sea deep convection on sediment remobilization in the western Mediterranean. Geophys. Res. Lett. 37, 1–6. https://doi.org/10.1029/2010GL043704

Martín, P., Sabatés, A., Lloret, J., Martin-Vide, J., 2012. Climate modulation of fish populations: The role of the Western Mediterranean Oscillation (WeMO) in sardine (Sardina pilchardus) and anchovy (Engraulis encrasicolus) production in the north-western Mediterranean. Clim. Change 110, 925–939. https://doi.org/10.1007/s10584-011-0091-z

Martin-Vide, J., Lopez-Bustins, J.-A., 2006. The Western Mediterranean oscillation and rainfall in the Iberian Peninsula. Int. J. Climatol. 26, 1455–1475. https://doi.org/10.1002/joc.1388

Martínez-Asensio, A., Marcos, M., Tsimplis, M.N., Gomis, D., Josey, S., Jordà, G., 2014. Impact of the atmospheric climate modes on Mediterranean sea level variability. Glob. Planet. Change 118, 1–15. https://doi.org/10.1016/j.gloplacha.2014.03.007

Martínez-Ruiz, F., Paytan, A., Kastner, M., González-Donoso, J.M., Linares, D., Bernasconi, S.M., Jimenez-Espejo, F.J., 2003. A comparative study of the geochemical and mineralogical characteristics of the S1 sapropel in the western and eastern Mediterranean. Palaeogeogr. Palaeoclimatol. Palaeoecol. 190, 23–37.

Martínez-Ruiz, F., Kastner, M., Gallego-Torres, D., Rodrigo-Gámiz, M., Nieto-Moreno, V., Ortega-Huertas, M., 2015. Paleoclimate and paleoceanography over the past

20,000yr in the Mediterranean Sea Basins as indicated by sediment elemental proxies. Quat. Sci. Rev. 107, 25–46. https://doi.org/10.1016/j.quascirev.2014.09.018

Martrat, B., Grimalt, J.O., Lopez-Martinez, C., Cacho, I., Sierro, F.J., Flores, J.A., Zahn, R., Canals, M., Curtis, J.H., Hodell, D.A., 2004. Abrupt temperature changes in the Western Mediterranean over the past 250,000 years. Science 306, 1762–1765. https://doi.org/10.1126/science.1101706

Martrat, B., Grimalt, J.O., Shackleton, N., De Abreu, L., Hutterli, M.A., Stocker, T.F., 2007. Four Climate Cycles of Recurring Deep and Surface Water Destabilizations on the Iberian Margin. Science 317, 502–507. https://doi.org/10.5040/9780755621101.0007

Martrat, B., Jimenez-amat, P., Zahn, R., Grimalt, J.O., 2014. Similarities and dissimilarities between the last two deglaciations and interglaciations in the North Atlantic region. Quat. Sci. Rev. 99, 122–134. https://doi.org/10.1016/j.quascirev.2014.06.016

Masqué, P., Fabres, J., Canals, M., Sanchez-Cabeza, J.A., Sanchez-Vidal, A., Cacho, I., Calafat, A.M., Bruach, J.M., 2003. Accumulation rates of major constituents of hemipelagic sediments in the deep Alboran Sea: A centennial perspective of sedimentary dynamics. Mar. Geol. 193, 207–233. https://doi.org/10.1016/S0025-3227(02)00593-5

Masson-Delmotte, V., Schulz, M., Abe-Ouchi, A., Beer, J., Ganopolski, A., González Rouco, J.F., Jansen, E., Lambeck, K., Luterbacher, J., Naish, T., Osborn, T., Otto-Bliesner, B., Quinn, T., Ramesh, R., Rojas, M., Shao, X., Timmermann, A., 2013. Information from Paleoclimate Archives, in: Intergovernmental Panel on Climate Change (Ed.), Climate Change 2013 - The Physical Science Basis. Cambridge University Press, Cambridge, pp. 383–464. https://doi.org/10.1017/CBO9781107415324.013

Mayewski, P.A., Rohling, E.E., Stager, J.C., Karlén, W., Maasch, K.A., Meeker, L.D., Meyerson, E.A., Gasse, F., van Kreveld, S., Holmgren, K., Lee-Thorp, J., Rosqvist, G., Rack, F., Staubwasser, M., Schneider, R.R., Steig, E.J., 2004. Holocene climate variability. Quat. Res. 62, 243–255. https://doi.org/10.1016/j.yqres.2004.07.001

McCave, I.N., Hall, I.R., 2006. Size sorting in marine muds: Processes, pitfalls, and prospects for paleoflow-speed proxies. Geochemistry, Geophys. Geosystems 7, Q10N05. https://doi.org/10.1029/2006GC001284

McCave, I.N., Manighetti, B., Robinson, S.G., 1995. Sortable silt and fine sediment size/composition slicing: Parameters for palaeocurrent speed and palaeoceanography. Paleoceanography 10, 593–610. https://doi.org/10.1029/94PA03039

McManus, J., Francois, R., Gherardi, J.-M., Keigwin, L., Brown-Leger, S., 2004. Collapse and rapid resumption of Atlantic meridional circualtion linked to deglacial climate changes. Nature 428, 834–837.

MEDOC Group, 1970. Observation of Formation of Deep Water in the Mediterranean Sea, 1969. Nature 227, 1037–1040.

Melki, T., Kallel, N., Jorissen, F.J., Guichard, F., Dennielou, B., Berné, S., Labeyrie, L., Fontugne, M., 2009. Abrupt climate change, sea surface salinity and paleoproductivity in the western Mediterranean Sea (Gulf of Lion) during the last 28 kyr. Palaeogeogr. Palaeoclimatol. Palaeoecol. 279, 96–113. https://doi.org/10.1016/j.palaeo.2009.05.005

Mesa-Fernández, J.M., Jiménez-Moreno, G., Rodrigo-Gámiz, M., García-Alix, A., Jiménez-Espejo, F.J., Martínez-Ruiz, F., Anderson, R.S., Camuera, J., Ramos-Román, M.J., 2018. Vegetation and geochemical responses to Holocene rapid climate change in the Sierra Nevada (southeastern Iberia): the Laguna Hondera record. Clim. Past 14, 1687–1706. https://doi.org/https://doi.org/10.5194/cp-14-1687-2018

Mesa-Fernández, J.M., Martínez-Ruiz, F., Rodrigo-Gámiz, M., Jiménez-Espejo, F.J., García, M., Sierro, F.J., 2022. Paleocirculation and paleoclimate conditions in the western Mediterranean basins over the last deglaciation: New insights from sediment composition variations. Glob. Planet. Change 209, 103732. https://doi.org/10.1016/j.gloplacha.2021.103732

Miebach, A., Niestrath, P., Roeser, P., Litt, T., 2016. Impacts of climate and humans on the vegetation in northwestern Turkey: Palynological insights from Lake Iznik since the Last Glacial. Clim. Past 12, 575–593. https://doi.org/10.5194/cp-12-575-2016

Milankovitch, M., 1941. Canon of insolation and the ice-age problem. Royal Serbian Sciences Special Publication. Section of Mathematical and Natural Sciences 33, 633

Millot, C., 1987. Circulation in the Hydrodynamics General circulation Mediterranean Sea Mesoscale phenomena. Oceanol. Acta 10, 143–149.

Millot, C., 1999. Circulation in the Western Mediterranean Sea. J. Mar. Syst. 20, 423–442. https://doi.org/10.1016/S0924-7963(98)00078-5

Millot, C., 2009. Another description of the Mediterranean Sea outflow. Prog. Oceanogr. 82, 101–124. https://doi.org/10.1016/j.pocean.2009.04.016

Millot, C., 2013. Levantine Intermediate Water characteristics: an astounding general misunderstanding! Sci. Mar. 77, 217–232. https://doi.org/10.3989/scimar.03518.13A

Miramontes, E., Garreau, P., Caillaud, M., Jouet, G., Pellen, R., Hernández-Molina, F.J., Clare, M.A., Cattaneo, A., 2019. Contourite distribution and bottom currents in the NW Mediterranean Sea: Coupling seafloor geomorphology and hydrodynamic modelling. Geomorphology 333, 43–60. https://doi.org/10.1016/j.geomorph.2019.02.030

Mladenov, N., Pulido-Villena, E., Morales-Baquero, R., Ortega-Retuerta, E., Sommaruga, R., Reche, I., 2008. Spatiotemporal drivers of dissolved organic matter in high alpine lakes: Role of Saharan dust inputs and bacterial activity, J. Geophys. Res.-Biogeo., 113, DOI:10.1029/2008JG000699

Mladenov, N., Sommaruga, R., Morales-Baquero, R., Laurion, I., Camarero, L., Diéguez,M. C., Camacho, A., Delgado, A., Torres, O., Chen, Z., Felip, M., Reche, I., 2011. Dust inputs and bacteria influence dissolved organic matter in clear alpine lakes, Nat. Commun. 2, 405, DOI:10.1038/ncomms1411

Molina González, F., Camara Serrano, J.A., Capel Martínez, J., Nájera Colino, T., Sáez Pérez, L., 2004. Los Millares y la periodización de la prehistoria reciente del sureste. In: Pellicer Catalán, M., Arribas, A. (Eds.), II -III Simposios de prehistoria Cueva de Nerja. Fundación Cueva de Nerja, Nerja. 142-158.

Morales-Baquero, R., Carrillo, P., Reche, I., Sánchez-Castillo, P., 1999. Nitrogen-phosphorus relationship in high mountain lakes: effects of the size of catchment basins, Can. J. Fish. Aquat. Sci., 56, 1809-1817, DOI:10.1139/cjfas-56-10-1809

Morales-Baquero, R., Pulido-Villena, E., Reche, I., 2006a. Atmospheric inputs of phosphorus and nitrogen to the southwest Mediterranean region: Biogeochemical responses of high mountain lakes, Limnol. Oceanogr., 51, 830-837, DOI:10.4319/lo.2006.51.2.0830

Morales-Baquero R., Pulido-Villena, E., Romera, O., Ortega-Retuerta, E., Conde-Porcuna, J. M., Pérez-Martinez, C., and Reche, I., 2006b. Significance of atmospheric deposition to freswater ecosystems in the southern Iberian Peninsula, Limnetica, 25, 171-180

Morales-Baquero, R., Pulido-Villena, E., Reche, I., 2013. Chemical signature of Saharan dust on dry and wet atmospheric deposition in the south-western Mediterranean region, Tellus B, 65, DOI:10.3402/tellusb.v65i0.18720

Morales-Baquero, R., Pérez-Martínez C., 2016. Saharan versus local influence on atmospheric aerosol deposition in the southern Iberian Peninsula: Significance for N and P inputs, Global Biogeochem. Cycles, 30, 501-513, DOI:10.1002/2015GB005254

Morellón, M., Valero-Garcés, B., Vegas-Vilarrúbia, T., González-Sampériz, P., Romero, Ó., Delgado-Huertas, A., Mata, P., Moreno, A., Rico, M., Corella, J.P., 2009. Lateglacial and Holocene palaeohydrology in the western Mediterranean region: The Lake Estanya record (NE Spain). Quat. Sci. Rev. 28, 2582–2599. https://doi.org/10.1016/j.quascirev.2009.05.014

Morellón, M., Valero-Garcés, B., González-Sampériz, P., Vegas-Vilarrúbia, T., Rubio, E., Rieradevall, M., Delgado-Huertas, A., Mata, P., Romero, O., Engstrom, D. R., López-Vicente, M., Navas, A., Soto, J., 2011. Climate changes and human activities recorded in the sediments of Lake Estanya (NE Spain) during the Medieval Warm Period and Little Ice Age, J. Paleolimnol., 46, 423-452, DOI:10.1007/s10933-009-9346-3

Morellón, M., Pérez-Sanz, A., Corella, J. P., Büntgen, U., Catalán, J., González-Samprizé, P., González-Trueba, J. J., López-Sáez, J. A., Moreno, A., Pla, S., Saz-Sánchez, M. Á., Scussolini, P., Serrano, E., Steinhilber, F., Stefanova, V., Vegas-Vilarrúbia, T., Saz-Sánchez, M. A., 2012: A multi-proxy perspective on millennium-long climate variability in the Southern Pyrenees, Clim. Past, DOI:10.5194/cpd-7-3049-2011

Moreno, A., Stoll, H., Jiménez-Sánchez, M., Cacho, I., Valero-Garcés, B., Ito, E., Edwards, R.L., 2010. A speleothem record of glacial (25-11.6 kyr BP) rapid climatic changes from northern Iberian Peninsula. Glob. Planet. Change 71, 218–231. https://doi.org/10.1016/j.gloplacha.2009.10.002

Moreno, A., Pérez, A., Frigola, J., Nieto-Moreno, V., Rodrigo-Gámiz, M., Martrat, B., González-Sampériz, P., Morellón, M., Martín-Puertas, C., Corella, J.P., Belmonte, Á., Sancho, C., Cacho, I., Herrera, G., Canals, M., Grimalt, J.O., Jiménez-Espejo, F., Martínez-Ruiz, F., Vegas-Vilarrúbia, T., Valero-Garcés, B.L., 2012. The Medieval Climate Anomaly in the Iberian Peninsula reconstructed from marine and lake records. Quat. Sci. Rev. 43, 16–32. https://doi.org/10.1016/j.quascirev.2012.04.007

Moreno, A., Pérez-Mejías, C., Bartolomé, M., Sancho, C., Cacho, I., Stoll, H., Delgado-Huertas, A., Hellstrom, J., Edwards, R.L., Cheng, H., 2017. New speleothem data from Molinos and Ejulve caves reveal Holocene hydrological variability in northeast Iberia. Quat. Res. 88, 223–233. https://doi.org/10.1017/qua.2017.39

Moreno, A., Sancho, C., Bartolome, M., Oliva-Urcia, B., Delgado-Huertas, A., Estrela, M.J., Corell, D., López-Moreno, J.I., Cacho, I., 2014. Climate controls on rainfall isotopes and their effects on cave drip water and speleothem growth: the case of Molinos cave (Teruel, NE Spain). Clim. Dyn. 43, 221–241. https://doi.org/10.1007/s00382-014-2140-6

Moreno, T., Querol, X., Castillo, S., Alastuey, A., Cuevas, E., Herrmann, L., Mounkaila, M., Elvira, J., Gibbons, W., 2006. Geochemical variations in aeolian mineral particles from the Sahara-Sahel Dust Corridor. Chemosphere 65, 261–270. https://doi.org/10.1016/j.chemosphere.2006.02.052

Mulitza, S., Heslop, D., Pittauerova, D., Fischer, H. W., Meyer, I., Stuut, J.-B., Zabel, M., Mollenhauer, G., Collins, J.A., Kuhnert, H., Schulz, M., 2010. Increase in African dust flux at the onset of commercial agriculture in the Sahel region, Nature, 466, 226-228, DOI:10.1038/nature09213

Muñoz-Sobrino, C., García-Moreiras, I., Castro, Y., Carreño, N. M., de Blas, E., Rodríguez, C. F., Judd, A., García-Gil, S., 2014. Climate and anthropogenic factors influencing an estuarine ecosystem from NW Iberia: new high resolution multiproxy analyses from San Simón Bay (Ría de Vigo), Quaternary Sci. Rev., 93, 11-33, DOI:10.1016/j.quascirev.2014.03.021

Murat, A., 1999. 41. Pliocene-Pleistocene occurrence of sapropels in the Western Mediterranean Sea and their relation to Eastern Mediterranean Sapropels, in: Proceedings of the Ocean Drilling Program, Scientific Results. pp. 519–527. https://doi.org/10.2973/odp.proc.sr.161.244.1999

Murillo-Barroso, M., Martino´n-Torres, M., Camalich-Massieu, M. D., Martín-Socas, D., Molina-González, F., 2017. Early metallurgy in SE Iberia. The workshop of Las Pilas (Moja´car, Almerı´a, Spain). Archaeological and Anthropological Sciences. https://doi.org/10.1007/s12520-016-0451-8.

Murillo-Barroso, M., Montero-Ruiz, I., Aranda Jiménez, G., 2015. An insight into the organisation of metal production in the Argaric society. Journal of Archaeological Science: Reports, 2, 141–155. https://doi.org/10.1016/j.jasrep.2015.01.010

Murray, R.W., Leinen, M., 1993. Chemical transport to the seafloor of the equatorial Pacific Ocean across a latitudinal transect at 135ºW: tracking sedimentary major, trace, and rare earth element fluxes at the Equator and the Intertropical Convergence Zone. Geochim. Cosmochim. Acta 57, 4141-4163.

Naranjo, C., García Lafuente, J., Sánchez Garrido, J.C., Sánchez Román, A., Delgado Cabello, J., 2012. The western alboran gyre helps ventilate the Western Mediterranean Deep Water through Gibraltar. Deep. Res. Part I Oceanogr. Res. Pap. 63, 157–163. https://doi.org/10.1016/j.dsr.2011.10.003

Naughton, F., Sanchez Goñi, M.F., Rodrigues, T., Salgueiro, E., Costas, S., Desprat, S., Duprat, J., Michel, E., Rossignol, L., Zaragosi, S., Voelker, A.H.L., Abrantes, F., 2016. Climate variability across the last deglaciation in NW Iberia and its margin. Quat. Int. 414, 9–22. https://doi.org/10.1016/j.quaint.2015.08.073

Naughton, F., Costas, S., Gomes, S.D., Desprat, S., Rodrigues, T., Sanchez Goñi, M.F., Renssen, H., Trigo, R., Bronk-Ramsey, C., Oliveira, D., Salgueiro, E., Voelker, A.H.L., Abrantes, F., 2019. Coupled ocean and atmospheric changes during Greenland stadial 1 in southwestern Europe. Quat. Sci. Rev. 212, 108–120. https://doi.org/10.1016/j.quascirev.2019.03.033

Ng, H.C., Robinson, L.F., McManus, J.F., Mohamed, K.J., Jacobel, A.W., Ivanovic, R.F., Gregoire, L.J., Chen, T., 2018. Coherent deglacial changes in western Atlantic Ocean circulation. Nat. Commun. 9, 2947. https://doi.org/10.1038/s41467-018-05312-3

Nichols, M.D., Xuan, C., Crowhurst, S., Hodell, D.A., Richter, C., Acton, G.D., Wilson, P.A., 2020. Climate-Induced Variability in Mediterranean Outflow to the North Atlantic Ocean During the Late Pleistocene. Paleoceanogr. Paleoclimatology 35, e2020PA003947. https://doi.org/10.1029/2020PA003947

Niedermeyer, E.M., Schefuß, E., Sessions, A.L., Mulitza, S., Mollenhauer, G., Schulz, M., Wefer, G., 2010. Orbital- and millennial-scale changes in the hydrologic cycle and vegetation in the western African Sahel: Insights from individual plant wax δD and δ13C. Quat. Sci. Rev. 29, 2996–3005. https://doi.org/10.1016/j.quascirev.2010.06.039

Nieto-Moreno, V., Martínez-Ruiz, F., Giralt, S., Jiménez-Espejo, F., Gallego-Torres, D., Rodrigo-Gámiz, M., García-Orellana, J., Ortega-Huertas, M., De Lange, G.J., 2011. Tracking climate variability in the western Mediterranean during the Late Holocene: A multiproxy approach. Clim. Past 7, 1395–1414. https://doi.org/10.5194/cp-7-1395-2011

Nieto-Moreno, V., Martínez-Ruiz, F., Willmott, V., García-Orellana, J., Masqué, P., Damsté, J. S., 2013: Climate conditions in the westernmost Mediterranean over the last two millennia: An integrated biomarker approach, Org. Geochem., 55, 1-10. DOI:10.1177/0959683613484613

Nieto-Moreno, V., Martínez-Ruiz, F., Gallego-Torres, D., Giralt, S., García-Orellana, J., Masqué, P., Sinninghe Damsté, J. S., Ortega-Huertas, M., 2015. Palaeoclimate and palaeoceanographic conditions in the westernmost Mediterranean over the last millennium: an integrated organic and inorganic approach, J. Geol. Soc. London , 172, 264-271, DOI: 10.1144/jgs2013-105

O'Leary, M.H., 1988. Carbon Isotopes in Photosynthesis. Bioscience 38, 328–336. https://doi.org/10.2307/1310735

O'Leary, M.H., 1995. Environmental effects on carbon isotope fractionation in terrestrial plants. In: Wada, E., Yokoyama, T., Minagawa, M., Ando, T., Fry, B.D. (Eds.), Stable Isotopes in the Biosphere. Kyoto University Press, Japan, pp. 79–91.

Oldfield, F., Asioli, A., Accorsi, C.A., Mercuri, A.M., Juggins, S., Langone, L., Rolph, T., Trincardi, F., Wolff, G., Gibbs, Z., Vigliotti, L., Frignani, M., van der Post, K., Branch, N., 2003. A high resolution late Holocene palaeo environmental record from

the central Adriatic Sea. Quat. Sci. Rev. 22, 319–342. https://doi.org/10.1016/S0277-3791(02)00088-4

Oliva, M., Gómez-Ortiz, A., 2012. Late-Holocene environmental dynamics and climate variability in a Mediterranean high mountain environment (Sierra Nevada, Spain) inferred from lake sediments and historical sources. Holocene 22, 915–927. https://doi.org/10.1177/0959683611434235

Oliva, M., Ruiz-Fernández, J., Barriendos, M., Benito, G., Cuadrat, J.M., Domínguez-Castro, F., García-Ruiz, J.M., Giralt, S., Gómez-Ortiz, A., Hernández, A., López-Costas, O., López-Moreno, J.I., López-Sáez, J.A., Martínez-Cortizas, A., Moreno, A., Prohom, M., Saz, M.A., Serrano, E., Tejedor, E., Trigo, R., Valero-Garcés, B., Vicente-Serrano, S.M., 2018. The Little Ice Age in Iberian mountains. Earth-Science Rev. 177, 175–208. https://doi.org/10.1016/j.earscirev.2017.11.010

Olsen, J., Anderson, N. J., Knudsen, M. F., 2012. Variability of the North Atlantic Oscillation over the past 5,200 years, Nat. Geosci., 5, 808-812, DOI:10.1038/ngeo1589

Oppo, D.W., McManus, J.F., Cullen, J.L., 2003. Deepwater variability in the Holocene epoch. Nature 422, 277–277. https://doi.org/10.1038/422277b

Pagani, M., Pedentchouk, N., Huber, M., Sluijs, A., Schouten, S., Brinkhuis, H., Sinninghe Damsté, J.S., Dickens, G.R., Scientists, E., 2006. Arctic hydrology during global warming at the Palaeocene / Eocene thermal maximum. Nat. Lett. 442, 671–675. https://doi.org/10.1038/nature05043

Palacios, D., Oliva, M., Gómez-Ortiz, A., Andrés, N., Fernández-Fernández, J.M., Schimmelpfennig, I., Léanni, L., Team, A.S.T.E.R., 2020. Climate sensitivity and geomorphological response of cirque glaciers from the late glacial to the Holocene, Sierra Nevada, Spain. Quat. Sci. Rev. 248. https://doi.org/10.1016/j.quascirev.2020.106617

Palanques, A., El Khatab, M., Puig, P., Masqué, P., Sánchez-Cabeza, J.A., Isla, E., 2005. Downward particle fluxes in the Guadiaro submarine canyon depositional system (north-western Alboran Sea), a river flood dominated system. Mar. Geol. 220, 23–40. https://doi.org/10.1016/j.margeo.2005.07.004

Palma, P., Oliva, M., García-Hernández, C., Gómez Ortiz, A., Ruiz-Fernández, J., Salvador-Franch, F., Catarineu, M., 2017. Spatial characterization of glacial and periglacial landforms in the highlands of Sierra Nevada (Spain). Sci. Total Environ. 584–585, 1256–1267. https://doi.org/10.1016/j.scitotenv.2017.01.196

Papadopoulos, Vassilis, P., Josey, S.A., Bartzokas, A., Somot, S., Ruiz, S., Drakopolou, P., 2012. Large-Scale Atmospheric Circulation Favoring Deep- and Intermediate-Water Formation in the Mediterranean Sea. Am. Meteorol. Soc. 6079–6091. https://doi.org/10.1175/JCLI-D-11-00657.1

Pérez-Asensio, J.N., Frigola, J., Pena, L.D., Sierro, F.J., Reguera, M.I., Rodríguez-tovar, F.J., Dorador, J., Asioli, A., Kuhlmann, J., Huhn, K., Cacho, I., 2020. Changes in western Mediterranean thermohaline circulation in association with a deglacial Organic Rich Layer formation in the Alboran Sea. Quat. Sci. Rev. 228, 106075. https://doi.org/10.1016/j.quascirev.2019.106075

Pérez-Folgado, M., Sierro, F.J., Flores, J.A., Cacho, I., Grimalt, J.O., Zahn, R., Shackleton, N., 2003. Western Mediterranean planktonic foraminifera events and millennial climatic variability during the last 70 kyr. Mar. Micropaleontol. 48, 49–70. https://doi.org/10.1016/S0377-8398(02)00160-3

Pérez-Mejías, C., Moreno, A., Bernal-Wormull, J., Cacho, I., Osácar, M.C., Edwards, R.L., Cheng, H., 2020. Oldest Dryas hydroclimate reorganization in the eastern Iberian Peninsula after the iceberg discharges of Heinrich Event 1. Quat. Res. 101, 67–83. https://doi.org/10.1017/qua.2020.112

Peters, H., Johns, W.E., Bower, A.S., Fratantoni, D.M., 2005. Mixing and entrainment in the Red Sea outflow plume. Part I: plume structure. Journal of Physical Oceanography 35, 569–583

Prentice, I.C., Harrison, S.P., Bartlein, P.J., 2011. Global vegetation and terrestrial carbon cycle changes after the last ice age. New Phytol. 189, 988–998.

Poska, A., Pidek, I. A., 2010.: Pollen dispersal and deposition characteristics of *Abies alba*, *Fagus sylvatica* and *Pinus sylvestris*, Roztocze region (SE Poland). Veg. Hist. Archaeobot., 19, 91-101, DOI:10.1007/s00334-009-0230-x

Puig, P., Durán, R., Muñoz, A., Elvira, E., Guillén, J., 2017. Submarine canyon-head morphologies and inferred sediment transport processes in the Alías-Almanzora

canyon system (SW Mediterranean): On the role of the sediment supply. Mar. Geol. 393, 21–34. https://doi.org/10.1016/j.margeo.2017.02.009

Pulido-Villena, E., Reche, I., and Morales-Baquero, R., 2006. Significance of atmospheric inputs of calcium over the southwestern Mediterranean region: High mountain lakes as tools for detection, Global Biogeochem. Cy., 20, GB2012, DOI:10.1029/2005GB002662

Pulido-Villena, E., Wagener, T., and Guieu, C., 2008a. Bacterial response to dust pulses in the western Mediterranean: Implications for carbon cycling in the oligotrophic ocean, Global Biogeochem. Cy., 22, DOI:10.1029/2007GB003091

Pulido-Villena, E., Reche, I., and Morales-Baquero, R., 2008b. Evidence of an atmospheric forcing on bacterioplankton and phytoplankton dynamics in a high mountain lake, Aquat. sci., 70, 1-9, DOI:10.1007/s00027-007-0944-8

Ramos-Román, M. J.: Holocene paleoenvironmental change, cli- mate and human impact in Sierra Nevada, Southern Iberian Peninsula, PhD Thesis, Universidad de Granada, Granada, Spain, 2018.

Ramos-Román, M.J., Jiménez-Moreno, G., Anderson, R.S., García-Alix, A., Toney, J.L., Jiménez-Espejo, F.J., Carrión, J.S., 2016. Centennial-scale vegetation and North Atlantic Oscillation changes during the Late Holocene in the southern Iberia. Quat. Sci. Rev. 143, 84–95. https://doi.org/10.1016/j.quascirev.2016.05.007

Ramos-Román, M.J., Jiménez-Moreno, G., Camuera, J., García-Alix, A., Anderson, R.S., Jiménez-Espejo, F.J., Carrión, J.S., 2018a. Holocene climate aridification trend and human impact interrupted by millennial- and centennial-scale climate fluctuations from a new sedimentary record from Padul (Sierra Nevada, southern Iberian Peninsula). Clim. Past 14, 117–137. https://doi.org/10.5194/cp-14-117-2018

Ramos-Román, M.J., Jiménez-Moreno, G., Camuera, J., García-Alix, A., Scott Anderson, R., Jiménez-Espejo, F.J., Sachse, D., Toney, J.L., Carrión, J.S., Webster, C., Yanes, Y., 2018b. Millennial-scale cyclical environment and climate variability during the Holocene in the western Mediterranean region deduced from a new multi-proxy analysis from the Padul record (Sierra Nevada, Spain). Glob. Planet. Change 168, 35–53. https://doi.org/10.1016/j.gloplacha.2018.06.003

Ramos-Román, M.J., Jiménez-Moreno, G., Anderson, R.S., García-Alix, A., Camuera, J., Mesa-Fernández, J.M., Manzano, S., 2019. Climate controlled historic olive tree occurrences and olive oil production in southern Spain. Glob. Planet. Change 182, 102996. https://doi.org/10.1016/j.gloplacha.2019.102996

Rasmussen, S.O., Seierstad, I.K., Andersen, K.K., Bigler, M., Dahl-Jensen, D., Johnsen, S.J., 2008. Synchronization of the NGRIP, GRIP, and GISP2 ice cores across MIS 2 and palaeoclimatic implications. Quat. Sci. Rev. 27, 18–28. https://doi.org/10.1016/j.quascirev.2007.01.016

Reche, I., Ortega-Retuerta, E., Romera, O., Villena, E. P., Baquero, R. M., Casamayor, E. O., 2009.: Effect of Saharan dust inputs on bacterial activity and community composition in Mediterranean lakes and reservoirs, Limnol. Oceanogr., 54, 869-879, DOI:10.4319/lo.2009.54.3.0869

Reed, J. M., Stevenson, A. C., Juggins, S., 2001.: A multi-proxy record of Holocene climatic change in southwestern Spain: the Laguna de Medina, Cádiz, Holocene, 11, 707-719, DOI:10.1191/09596830195735

Regattieri, E., Zanchetta, G., Drysdale, R. N., Isola, I., Hellstrom, J. C., Dallai, L., 2014. Lateglacial to holocene trace element record (Ba, Mg, Sr) from Corchia cave (Apuan Alps, central Italy): paleoenvironmental implications, J. Quat. Sci., 29, 381-392, DOI:10.1002/jqs.2712

Rehault, J.P., Boillot, G., Mauffret, A., 1984. The Western Mediterranean Basin geological evolution. Mar. Geol. 55, 447–477. https://doi.org/10.1016/0025-3227(84)90081-1

Reimer, P. J., Bard, E., Bayliss, A., Beck, J. W., Blackwell, P. G., Bronk Ramsey, C., Buck, C. E., Cheng, H., Edwards, R. L., Friedrich, M., Grootes, P. M., Guilderson, T. P., Haflidason, H., Hajdas, I., Hatté, C., Heaton, T. J., Hoffmann, D. L., Hogg, A. G., Hughen, K. A., Kaiser, K. F., Kromer, B., Manning, S. W., Niu, M., Reimer, R. W., Richards, D. A., Scott, M., Southon, J. R., Staff, R. A., Turney, C. S. M., van der Plicht, J., 2013. IntCal13 and Marine13 radiocarbon age calibration curves 0-50,000 years cal BP, Radiocarbon, 55, 1869-1887, DOI:10.2458/azu_js_rc.55.16947

Reitz, A., Lange, G.J. De, 2006. Abundant Sr-rich aragonite in eastern Mediterranean sapropel S1: Diagenetic vs. detrital/biogenic origin. Palaeogeogr. Palaeoclimatol. Palaeoecol. 235, 135–148. https://doi.org/10.1016/j.palaeo.2005.10.024

Repschläger, J., Weinelt, M., Kinkel, H., Andersen, N., Garbe-Schönberg, D., Schwab, C., 2015. Response of the subtropical North Atlantic surface hydrography on deglacial and Holocene AMOC changes. Paleoceanography 30, 456–476. https://doi.org/10.1002/2014PA002637

Repschläger, J., Zhao, N., Rand, D., Lisiecki, L., Muglia, J., Mulitza, S., Schmittner, A., Cartapanis, O., Bauch, H.A., Schiebel, R., Haug, G.H., 2021. Active North Atlantic deepwater formation during Heinrich Stadial 1. Quat. Sci. Rev. 270. https://doi.org/10.1016/j.quascirev.2021.107145

Revel, M., Ducassou, E., Skonieczny, C., Colin, C., Bastian, L., Bosch, D., Migeon, S., Mascle, J., 2015. 20,000 years of Nile River dynamics and environmental changes in the Nile catchment area as inferred from Nile upper continental slope sediments. Quat. Sci. Rev. https://doi.org/10.1016/j.quascirev.2015.10.030

Révillon, S., Jouet, G., Bayon, G., Rabineau, M., Dennielou, B., Hémond, C., Berné, S., 2011. The provenance of sediments in the Gulf of Lions, western Mediterranean Sea, Geochem. Geophy. Geosy., 12, Q08006, DOI:10.1029/2011GC003523

Reyment, R.A., Davis, J.C., 1988. Statistics and Data Analysis in Geology. Biometrics 44, 918. https://doi.org/10.2307/2531613

Rixen, M., Beckers, J.M., Levitus, S., Antonov, J., Boyer, T., Maillard, C., Fichaut, M., Balopoulos, E., Iona, S., Dooley, H., Garcia, M.J., Manca, B., Giorgetti, A., Manzella, G., Mikhailov, N., Pinardi, N., Zavatarelli, M., 2005. The Western Mediterranean Deep Water: A proxy for climate change. Geophys. Res. Lett. 32, 1–4. https://doi.org/10.1029/2005GL022702

Roberts, N., Jones, M.D., Benkaddour, A., Eastwood, W.J., Filippi, M.L., Frogley, M.R., Lamb, H.F., Leng, M.J., Reed, J.M., Stein, M., Stevens, L., Valero-Garcés, B., Zanchetta, G., 2008. Stable isotope records of Late Quaternary climate and hydrology from Mediterranean lakes: the ISOMED synthesis. Quat. Sci. Rev. 27, 2426–2441. https://doi.org/10.1016/j.quascirev.2008.09.005

Rodrigo-Gámiz, M., Martínez-Ruiz, F., Jiménez-Espejo, F.J., Gallego-Torres, D., Nieto-Moreno, V., Romero, O., Ariztegui, D., 2011. Impact of climate variability in the western Mediterranean during the last 20,000 years: Oceanic and atmospheric responses. Quat. Sci. Rev. 30, 2018–2034. https://doi.org/10.1016/j.quascirev.2011.05.011

Rodrigo-Gámiz, M., Martínez-Ruiz, F., Rampen, S.W., Schouten, S., Sinninghe Damsté, J.S., 2014a. Sea surface temperature variations in the western Mediterranean Sea over the last 20 kyr: A dual-organic proxy (UK′37 and LDI) approach. Paleoceanography 29, 87–98. https://doi.org/10.1002/2013PA002466.Received

Rodrigo-Gámiz, M., Martínez-Ruiz, F., Rodríguez-Tovar, F.J., Jiménez-Espejo, F.J., Pardo-Igúzquiza, E., 2014b. Millennial- to centennial-scale climate periodicities and forcing mechanisms in the westernmost Mediterranean for the past 20,000 yr. Quat. Res. 81, 78–93. https://doi.org/10.1016/j.yqres.2013.10.009

Rodrigo-Gámiz, M., Martínez-Ruiz, F., Chiaradia, M., Jiménez-Espejo, F.J., Ariztegui, D., 2015. Radiogenic isotopes for deciphering terrigenous input provenance in the western Mediterranean. Chem. Geol. 410, 237–250. https://doi.org/10.1016/j.chemgeo.2015.06.004

Rogerson, M., Rohling, E.J., Weaver, P.P.E., Murray, J.W., 2005. Glacial to interglacial changes in the settling depth of the Mediterranean Outflow plume. Paleoceanography 20, PA3007. https://doi.org/10.1029/2004PA001106

Rogerson, M., Rohlin, E.J., Weaver, P.P.E., 2006. Promotion of meridional overturning by Mediterranean-derived salt during the last deglaciation. Paleoceanography 21, 1–8. https://doi.org/10.1029/2006PA001306

Rogerson, M., Cacho, I., Jiménez-Espejo, F., Reguera, M.I., Sierro, F.J., Martínez-Ruiz, F., Frigola, J., Canals, M., 2008. A dynamic explanation for the origin of the western Mediterranean organic-rich layers. Geochemistry, Geophys. Geosystems 9, Q07U01. https://doi.org/10.1029/2007GC001936

Rogerson, M., Colmenero-Hidalgo, E., Levine, R.C., Rohling, E.J., Voelker, A.H.L., Bigg, G.R., Schönfeld, J., Cacho, I., Sierro, F.J., Löwemark, L., Reguera, M.I., De Abreu, L., Garrick, K., 2010. Enhanced Mediterranean-Atlantic exchange during Atlantic freshening phases. Geochemistry, Geophys. Geosystems 11, Q08013. https://doi.org/10.1029/2009GC002931

Rogerson, M., Rohling, E.J., Bigg, G.R., Ramirez, J., 2012. Paleoceanography of the Atlantic-Mediterranean exchange: Overview and first quantitative assessment of climatic forcing. Rev. Geophys. 50, RG2003. https://doi.org/10.1029/2011RG000376

Rohling, E.J., Den Dulk, M., Pujol, C., Vergnaud-Grazzini, C., 1995. Abrupt hydrographic change in the Alboran Sea (western Mediterranean) around 8000 yrs BP. Deep. Res. Part I 42, 1609–1619. https://doi.org/10.1016/0967-0637(95)00069-I

Rohling, E.J., Marino, G., Grant, K.M., 2015. Mediterranean climate and oceanography, and the periodic development of anoxic events (sapropels). Earth-Science Rev. 143, 62–97. https://doi.org/10.1016/j.earscirev.2015.01.008

Romero, R., Sumner, G., Ramis, C., Genove, A., 1999. A classification of the atmospheric circulation patterns producing significant daily rainfall in the spanish Mediterranean area. Int. J. Climatol. 19, 765–785.

Ruddiman, W.F., Thomson, J.S., 2001. The case for human causes of increased atmospheric CH4 over the last 5000 years. Quat. Sci. Rev. 20, 1769–1777. https://doi.org/10.1016/S0277-3791(01)00067-1

Sachs, J.P., Sachse, D., Smittenberg, R.H., Zhang, Z., Battisti, D.S., Golubic, S., 2009. Southward movement of the Pacific intertropical convergence zone AD 1400-1850. Nat. Geosci. 2, 519–525. https://doi.org/10.1038/ngeo554

Sachse, D., Radke, J., Gleixner, G., 2004. Hydrogen isotope ratios of recent lacustrine sedimentary n-alkanes record modern climate variability. Geochim. Cosmochim. Acta 68, 4877–4889. https://doi.org/10.1016/j.gca.2004.06.004

Sachse, D., Billault, I., Bowen, G.J., Chikaraishi, Y., Dawson, T.E., Feakins, S.J., Freeman, K.H., Magill, C.R., Mcinerney, F.A., van der Meer, M.T.J., Polissar, P., Robins, R.J., Sachs, J.P., Schmidt, H.-L., Sessions, A.L., White, J.W.C., West, J.B., Kahmen, A., 2012. Molecular Paleohydrology : Interpreting the Hydrogen-Isotopic Composition of Lipid Biomarkers from Photosynthesizing Organisms. Annu. Rev. Earth Planet. Sci. 40, 221–249. https://doi.org/10.1146/annurev-earth-042711-105535

Sánchez-Goñi, M.F., Fourcade, T., Salonen, S., Lesven, J., Frigola, J., Swingedouw, D., Sierro, F.J., 2020. Muted cooling and drying of NW Mediterranean in response to the strongest last glacial North American ice surges. GSA Bull. 133, 451–460. https://doi.org/10.1130/B35736.1/5074327/b35736.pdf

Sánchez Goñi, M.F., Desprat, S., Fletcher, W.J., Morales-Molino, C., Naughton, F., Oliveira, D., Urrego, D.H., Zorzi, C., 2018. Pollen from the Deep-Sea: A Breakthrough in the Mystery of the Ice Ages. Front. Plant Sci. 9, 38. https://doi.org/10.3389/fpls.2018.00038

Sánchez-López, G., Hernández, A., Pla-Rabes, S., Trigo, R.M., Toro, M., Granados, I., Sáez, A., Masqué, P., Pueyo, J.J., Rubio-Inglés, M.J., Giralt, S., 2016. Climate reconstruction for the last two millennia in central Iberia: The role of East Atlantic (EA), North Atlantic Oscillation (NAO) and their interplay over the Iberian Peninsula. Quat. Sci. Rev. 149, 135–150. https://doi.org/10.1016/j.quascirev.2016.07.021

Sanchez-Vidal, A., Calafat, A., Canals, M., Fabres, J., 2004. Particle fluxes in the Almeria-Oran Front: Control by coastal upwelling and sea surface circulation. J. Mar. Syst. https://doi.org/10.1016/j.jmarsys.2004.01.010

Sanchez-Vidal, A., Calafat, A., Canals, M., Frigola, J., Fabres, J., 2005. Particle fluxes and organic carbon balance across the Eastern Alboran Sea (SW Mediterranean Sea). Cont. Shelf Res. 25, 609–628. https://doi.org/10.1016/j.csr.2004.11.004

Sawatzky, C. L., Wurtsbaugh, W. A., Luecke, C., 2006.: The spatial and temporal dynamics of deep chlorophyll layers in high-mountain lakes: effects of nutrients, grazing, and herbivore recycling as growth determinants, J. Plankton Res., 28, 65–86, DOI:10.1093/plankt/fbi101

Schäfer, I.K., Bliedtner, M., Wolf, D., Kolb, T., Zech, J., Faust, D., Zech, R., 2018. A δ13C and δ2H leaf wax record from the Late Quaternary loess-paleosoil sequence El Paraíso, Central Spain. Palaeogeogr. Palaeoclimatol. Palaeoecol. 507, 52–59. https://doi.org/10.1016/j.palaeo.2018.06.039

Schefuß, E., Volker, R., Stuut, J.-B.W., Jansen, J.H.F., Sinninghe Damsté, S.J., 2003. Carbon isotope analyses of n -alkanes in dust from the lower atmosphere over the central eastern Atlantic. Geochim. Cosmochim. Acta 67, 1757–1767. https://doi.org/10.1016/S0016-7037(02)01414-X

Schefuß, E., Schouten, S., Schneider, R.R., 2005. Climatic controls on central African hydrology during the past 20,000 years. Nature 437, 1003–1006. https://doi.org/10.1038/nature03945

Scheuvens, D., Schütz, L., Kandler, K., Ebert, M., Weinbruch, S., 2013. Bulk composition of northern African dust and its source sediments - A compilation. Earth-Science Rev. 116, 170–194. https://doi.org/10.1016/j.earscirev.2012.08.005

Schirrmacher, J., Weinelt, M., Blanz, T., Andersen, N., Salgueiro, E., Schneider, R.R., 2019. Multi-decadal climate variability in southern Iberia during the mid- to late-Holocene. Clim. Past 15, 617–634. https://doi.org/10.5194/cp-2018-158

Schirrmacher, J., Andersen, N., Schneider, R.R., Weinelt, M., 2020a. Fossil leaf wax hydrogen isotopes reveal variability of Atlantic and Mediterranean climate forcing on the southeast Iberian Peninsula between 6000 to 3000 cal. BP. PLoS One 15, e0243662. https://doi.org/10.1371/journal.pone.0243662

Schirrmacher, J., Kneisel, J., Knitter, D., Hamer, W., Hinz, M., Schneider, R.R., Weinelt, M., 2020b. Spatial patterns of temperature, precipitation, and settlement dynamics on the Iberian Peninsula during the Chalcolithic and the Bronze Age. Quat. Sci. Rev. 233, 106220. https://doi.org/10.1016/j.quascirev.2020.106220

Schroeder, K., 2018. Current Systems in the Mediterranean Sea ☆, Encyclopedia of Ocean Sciences, 3rd Edition. Elsevier Inc. https://doi.org/10.1016/B978-0-12-409548-9.11296-5

Schroeder, K., Josey, S.A., Herrmann, M., Grignon, L., Gasparini, G.P., Bryden, H.L., 2010. Abrupt warming and salting of the Western Mediterranean Deep Water after 2005: Atmospheric forcings and lateral advection. J. Geophys. Res. Ocean. 115, C08029. https://doi.org/10.1029/2009JC005749

Schroeder, K., Ribotti, A., Borghini, M., Sorgente, R., Perilli, A., Gasparini, G.P., 2008. An extensive western Mediterranean deep water renewal between 2004 and 2006. Geophys. Res. Lett. 35. https://doi.org/10.1029/2008GL035146

Schulte, L., 2002. Climatic and human influence on river systems and glacier fluctuations in southeast Spain since the Last Glacial Maximum. Quat. Int. 93–94, 85–100. https://doi.org/10.1016/S1040-6182(02)00008-3

Serrano-Notivoli, R., Martín-Vide, J., Saz, M.A., Longares, L.A., Beguería, S., Sarricolea, P., Meseguer-Ruiz, O., de Luis, M., 2018. Spatio-temporal variability of daily precipitation concentration in Spain based on a high-resolution gridded data set. Int. J. Climatol. 38, e518–e530. https://doi.org/10.1002/joc.5387

Settle D. M., Patterson C. C., 1980. Lead in Albacore: guide to lead pollution in Americans, Science, 207, 1167-76, DOI:10.1126/science.6986654

Shackleton, N.J., 2000. The 100,000-year ice-age cycle identified and found to lag temperature, carbon dioxide, and orbital eccentricity. Science (80-.). 289, 1897–1902. https://doi.org/10.1126/science.289.5486.1897

Simoneit, B. R. T. (2002) Biomass burning – a review of organic tracers for smoke from incomplete combustion. Applied Geochemistry, 68, 129–62

Sierro, F.J., Hodell, D.A., Curtis, J.H., Flores, J.A., Reguera, I., Colmenero-Hidalgo, E., Bárcena, M.A., Grimalt, J.O., Cacho, I., Frigola, J., Canals, M., 2005. Impact of iceberg melting on Mediterranean thermohaline circulation during Heinrich events. Paleoceanography 20, PA2019. https://doi.org/10.1029/2004PA001051

Sierro, F.J., Hodell, D.A., Andersen, N., Azibeiro, L.A., Jiménez-Espejo, F.J., Bahr, A., Flores, J.A., Ausin, B., Rogerson, M., Lozano-Luz, R., Lebreiro, S.M., Hernández-Molina, F.J., 2020. Mediterranean Overflow over the last 250 ky: Freshwater forcing from the tropics to the Ice Sheets. Paleoceanogr. Paleoclimatology 35, e2020PA003931. https://doi.org/10.1029/2020PA003931

Skinner, L.C., Freeman, E., Hodell, D., Waelbroeck, C., Vazquez Riveiros, N., Scrivner, A.E., 2021. Atlantic Ocean Ventilation Changes Across the Last Deglaciation and Their Carbon Cycle Implications. Paleoceanogr. Paleoclimatology 36. https://doi.org/10.1029/2020PA004074

Smith, R.O., Bryden, H.L., Stansfield, K., 2008. Observations of new western Mediterranean deep water formation using Argo floats 2004-2006. Ocean Sci. 4, 133–149. https://doi.org/10.5194/os-4-133-2008

Smol, J.P., Birks, H., Last, W., 2002. Tracking Environmental Change Usin Lake Sediments.

Solanki, S. K., Usoskin, I. G., Kromer, B., Schüssler, M., Beer, J., 2004. Unusual activity of the Sun during recent decades compared to the previous 11,000 years, Nature, 431, 1084-1087, DOI:10.1038/nature02995

Stanford, J.D., Hemingway, R., Rohling, E.J., Challenor, P.G., Medina-elizalde, M., Lester, A.J., 2011. Sea-level probability for the last deglaciation: A statistical

analysis of far-field records. Glob. Planet. Change 79, 193–203. https://doi.org/10.1016/j.gloplacha.2010.11.002

Steinke, S., Mohtadi, M., Prange, M., Varma, V., Pittauerova, D., Fischer, H.W., 2014. Mid- to Late-Holocene Australian-Indonesian summer monsoon variability. Quat. Sci. Rev. 93, 142–154. https://doi.org/10.1016/j.quascirev.2014.04.006

Stommel, H., Bryden, H., Mangelsdorf, P., 1973. Does some of the Mediterranean outflow come from great depth? Pure Appl. Geophys. 105, 879–889. https://doi.org/10.1007/BF00875837

Stuut, J.B.W., Temmesfeld, F., De Deckker, P., 2014. A 550ka record of aeolian activity near north west cape, australia: Inferences from grain-size distributions and bulk chemistry of SE indian ocean deep-sea sediments. Quat. Sci. Rev. 83, 83–94. https://doi.org/10.1016/j.quascirev.2013.11.003

Tachikawa, K., Cartapanis, O., Vidal, L., Beaufort, L., Barlyaeva, T., Bard, E., 2011. The precession phase of hydrological variability in the Western Pacific Warm Pool during the past 400 ka. Quat. Sci. Rev. 30, 3716–3727. https://doi.org/10.1016/j.quascirev.2011.09.016

Teller, J.T., Leverington, D.W., Mann, J.D., 2002. Freshwater outbursts to the oceans from glacial Lake Agassiz and their role in climate change during the last deglaciation. Quat. Sci. Rev. 21, 879–887. https://doi.org/10.1016/S0277-3791(01)00145-7

Thomson, J., Nixon, S., Summerhayes, C.P., Schönfeld, J., Zahn, R., Grootes, P., 1999. Implications for sedimentation changes on the Iberian margin over the last two glacial/interglacial transitions from (230Th(excess))0 systematics. Earth Planet. Sci. Lett. 165, 255–270. https://doi.org/10.1016/S0012-821X(98)00265-9

Thomson, J., Crudeli, D., de Lange, G.J., Slomp, C.P., Erba, E., Corselli, C., Calvert, S.E., 2004. Florisphaera profunda and the origin and diagenesis of carbonate phases in eastern Mediterranean sapropel units. Paleoceanography 19, n/a-n/a. https://doi.org/10.1029/2003PA000976

Tierney, J.E., DeMenocal, P.B., 2013. Abrupt shifts in Horn of Africa hydroclimate since the last glacial maximum. Science 342, 843–846. https://doi.org/10.1126/science.1240411

Tinner, W., Theurillat, J.P., 2003. Uppermost Limit, Extent, and Fluctuations of the Timberline and Treeline Ecocline in the Swiss Central Alps during the Past 11,500 Years. Arctic, Antarct. Alp. Res. 35, 158–169. https://doi.org/10.1657/1523-0430(2003)035[0158:ULEAFO]2.0.CO;2

Tinner, W., Kaltenrieder, P., 2005. Rapid responses of high-mountain vegetation to early Holocene environmental changes in the Swiss Alps. J. Ecol. 93, 936–947. https://doi.org/10.1111/j.1365-2745.2005.01023.x

Tintoré, J., La Violette, P.E., Blade, I., Cruzado, A., 1988. A Study of an Intense Density Front in the Eastern Alboran Sea: The Almeria-Oran Front. J. Phys. Oceanogr. 18, 1384–1397. https://doi.org/10.1175/1520-0485(1988)018<1384:ASOAID>2.0.CO;2

Tintoré, J., Gomis, D., Alonso, S., Parrilla, G., 1991. Mesoscale Dynamics and Vertical Montion in the Alborán Sea. J. Phys. Oceanogr. 21, 811–823.

Tjallingii, R., Röhl, U., Kölling, M., Bickert, T., 2007. Influence of the water content on X-ray fluorescence core- scanning measurements in soft marine sediments. Geochemistry, Geophys. Geosystems 8, Q02004. https://doi.org/10.1029/2006GC001393

Toney, J.L., García-Alix, A., Jiménez-Moreno, G., Anderson, R.S., Moossen, H., Seki, O., 2020. New insights into Holocene hydrology and temperature from lipid biomarkers in western Mediterranean alpine wetlands. Quat. Sci. Rev. 240, 106395. https://doi.org/10.1016/j.quascirev.2020.106395

Torner, J., Cacho, I., Moreno, A., Sierro, F.J., Martrat, B., Rodriguez-Lazaro, J., Frigola, J., Arnau, P., Belmonte, Á., Hellstrom, J., Cheng, H., Edwards, R.L., Stoll, H., 2019. Ocean-atmosphere interconnections from the last interglacial to the early glacial: An integration of marine and cave records in the Iberian region. Quat. Sci. Rev. 226. https://doi.org/10.1016/j.quascirev.2019.106037

Torres, T., Valle, M., Ortiz, J.E., Soler, V., Araujo, R., Rivas, M.R., Delgado, A., Julià, R., Sánchez-Palencia, Y., 2020. 800 ka of Palaeoenvironmental changes in the Southwestern Mediterranean realm. J. Iber. Geol. 46, 117–144. https://doi.org/10.1007/s41513-020-00123-2

Toucanne, S., Mulder, T., Schönfeld, J., Hanquiez, V., Gonthier, E., 2007. Contourites of the Gulf of Cadiz: A high-resolution record of the paleocirculation of the Mediterranean outf low water during the last 50 , 000 years 246, 354–366. https://doi.org/10.1016/j.palaeo.2006.10.007

Toucanne, S., Jouet, G., Ducassou, E., Bassetti, M.A., Dennielou, B., Angue Minto'o, C.M., Lahmi, M., Touyet, N., Charlier, K., Lericolais, G., Mulder, T., 2012. A 130,000-year record of Levantine Intermediate Water flow variability in the Corsica Trough, western Mediterranean Sea. Quat. Sci. Rev. 33, 55–73. https://doi.org/10.1016/j.quascirev.2011.11.020

Toucanne, S., Soulet, G., Vázquez Riveiros, N., Boswell, S.M., Dennielou, B., Waelbroeck, C., Bayon, G., Mojtahid, M., Bosq, M., Sabine, M., Zaragosi, S., Bourillet, J.F., Mercier, H., 2021. The North Atlantic Glacial Eastern Boundary Current as a Key Driver for Ice-Sheet—AMOC Interactions and Climate Instability. Paleoceanogr. Paleoclimatology 36, 1–23. https://doi.org/10.1029/2020PA004068

Traverse, A., 2007. Paleopalynology. Springer Science & Business Media.

Tribovillard, N., Algeo, T.J., Baudin, F., Riboulleau, A., 2012. Analysis of marine environmental conditions based onmolybdenum-uranium covariation-Applications to Mesozoic paleoceanography. Chem. Geol. 324–325, 46–58. https://doi.org/10.1016/j.chemgeo.2011.09.009

Trigo, I.F., Bigg, G.R., Davies, T.D., 2002. Climatology of cyclogenesis mechanisms in the Mediterranean. Mon. Weather Rev. 130, 549–569. https://doi.org/10.1175/1520-0493(2002)130<0549:COCMIT>2.0.CO;2

Trigo, R. M., Palutikof, J. P., 2001. Precipitation scenarios over Iberia: a comparison between direct GCM output and different downscaling techniques, J. Climate , 14, 4442-4446, DOI:10.1175/1520-0442(2001)014<4422:PSOIAC>2.0.CO;2

Trigo, R.M., Osborn, T.J., Corte-Real, J.M., 2002. The North Atlantic Oscillation influence on Europe: Climate impacts and associated physical mechanisms. Clim. Res. 20, 9–17. https://doi.org/10.3354/cr020009

Trigo, R.M., Pozo-Vázquez, D., Osborn, T.J., Castro-Díez, Y., Gámiz-Fortis, S., Esteban-Parra, M.J., 2004. North Atlantic oscillation influence on precipitation, river flow

and water resources in the Iberian Peninsula. Int. J. Climatol. 24, 925–944. https://doi.org/10.1002/joc.1048

Trouet, V., Esper, J., Graham, N. E., Baker, A., Scourse, J. D., Frank, D. C., 2009. Persistent positive North Atlantic Oscillation mode dominated the Medieval Climate Anomaly, Science, 324, 78-80, DOI:10.1126/science.1166349

Tzedakis, P.C., Crucifix, M., Mitsui, T., Wolff, E.W., 2017. A simple rule to determine which insolation cycles lead to interglacials. Nat. Publ. Gr. 542, 427–432. https://doi.org/10.1038/nature21364

Tzedakis, P.C., Drysdale, R.N., Margari, V., Skinner, L.C., Menviel, L., Rhodes, R.H., Taschetto, A.S., Hodell, D.A., Crowhurst, S.J., Hellstrom, J.C., Fallick, A.E., Grimalt, J.O., Mcmanus, J.F., Martrat, B., Mokeddem, Z., Parrenin, F., Regattieri, E., Roe, K., Zanchetta, G., 2018. Enhanced climate instability in the North Atlantic and southern Europe during the Last Interglacial. Nat. Commun. 9, 4235. https://doi.org/10.1038/s41467-018-06683-3

Valbuena-Carabaña, M., de Heredia, U.L., Fuentes-Utrilla, P., González-Doncel, I., Gil, L., 2010. Historical and recent changes in the Spanish forests: A socio-economic process. Rev. Palaeobot. Palynol. 162, 492–506. https://doi.org/10.1016/j.revpalbo.2009.11.003

Valle, F.: Mapa de series de vegetación de Andalucía 1: 400 000, Editorial Rueda, Madrid, 2003.

Valle, F., Lorite, J., Salazar-Mendías, C., 2007. Series de Vegetación.

van der Weijden, C.H., 2002. Pitfalls of normalization of marine geochemical data using a common divisor. Mar. Geol. 184, 167–187. https://doi.org/10.1016/S0025-3227(01)00297-3

van Dijk, J., Ziegler, M., de Nooijer, L.J., Reichart, G.J., Xuan, C., Ducassou, E., Bernasconi, S.M., Lourens, L.J., 2018. A Saltier Glacial Mediterranean Outflow. Paleoceanogr. Paleoclimatology 33, 179–197. https://doi.org/10.1002/2017PA003228

Voelker, A.H.L., Lebreiro, S.M., Schönfeld, J., Cacho, I., Erlenkeuser, H., Abrantes, F., 2006. Mediterranean outflow strengthening during northern hemisphere coolings: A

salt source for the glacial Atlantic? Earth Planet. Sci. Lett. 245, 39–55. https://doi.org/10.1016/j.epsl.2006.03.014

Voelker, A.H.L., Abreu, L. de, 2011. A review of abrupt climate change events in the northeastern Atlantic Ocean (Iberian Margin): Latitudinal, longitudinal, and vertical gradients, in: Abrupt Climate Change: Mechanisms, Patterns, and Impacts. Geophysical Monograph Series, 193. pp. 15–37.

Vogts, A., Badewien, T., Rullkötter, J., Schefuß, E., 2016. Near-constant apparent hydrogen isotope fractionation between leaf wax n-alkanes and precipitation in tropical regions: Evidence from a marine sediment transect off SW Africa. Org. Geochem. https://doi.org/10.1016/j.orggeochem.2016.03.003

Walker, M., Head, M.J., Lowe, J., Berkelhammer, M., Björck, S., Cheng, H., Cwynar, L., Fisher, D., Gkinis, V., Long, A., Newnham, R.M., Rasmussen, S., Weiss, H., 2019. Subdividing the Holocene Series/Epoch: formalization of stages/ages and subseries/subepochs, and designation of GSSPs and auxiliary stratotypes. J. Quat. Sci. 34, 173–186. https://doi.org/10.1002/jqs.3097

Walczak, I. W., Baldini, J. U., Baldini, L. M., McDermott, F., Marsden, S., Standish, C. D., Richards, D. A., Andreo, B., Slater, J., 2015. Reconstructing high-resolution climate using CT scanning of unsectioned stalagmites: A case study identifying the mid-Holocene onset of the Mediterranean climate in southern Iberia, Quaternary Sci. Revi., 127, 117-128, DOI:10.1016/j.quascirev.2015.06.013

Wang, H., Lo Iacono, C., Wienberg, C., Titschack, J., Hebbeln, D., 2019. Cold-water coral mounds in the southern Alboran Sea (western Mediterranean Sea): Internal waves as an important driver for mound formation since the last deglaciation. Mar. Geol. 412, 1–18. https://doi.org/10.1016/j.margeo.2019.02.007

Wang, J., Xu, Y., Zhou, L., Shi, M., Axia, E., Jia, Y., Chen, Z., Li, J., Wang, G., 2018. Disentangling temperature effects on leaf wax n-alkane traits and carbon isotopic composition from phylogeny and precipitation. Org. Geochem. 126, 13–22. https://doi.org/10.1016/j.orggeochem.2018.10.008

Wang, N., Zong, Y., Brodie, C.R., Zheng, Z., 2014. An examination of the fidelity of n-alkanes as a palaeoclimate proxy from sediments of Palaeolake Tianyang, South China. Quat. Int. 333, 100–109. https://doi.org/10.1016/j.quaint.2014.01.044

Wang, Y. V., Larsen, T., Leduc, G., Andersen, N., Blanz, T., Schneider, R.R., 2013. What does leaf wax δD from a mixed C3/C4vegetation region tell us? Geochim. Cosmochim. Acta 111, 128–139. https://doi.org/10.1016/j.gca.2012.10.016

Wanner, H., Brönnimann, S., Casty, C., Gyalistras, D., Luterbacher, J., Schmutz, C., Stephenson, D. B., Xoplaki, E., 2001. North Atlantic Oscillation–concepts and studies, Surv. Geophys., 22, 321-381, DOI:10.1023/A:1014217317898

Wanner, H., Beer, J., Bütikofer, J., Crowley, T.J., Cubasch, U., Flückiger, J., Goosse, H., Grosjean, M., Joos, F., Kaplan, J.O., Küttel, M., Müller, S.A., Prentice, I.C., Solomina, O., Stocker, T.F., Tarasov, P., Wagner, M., Widmann, M., 2008. Mid- to Late Holocene climate change: an overview. Quat. Sci. Rev. 27, 1791–1828. https://doi.org/10.1016/j.quascirev.2008.06.013

Wehausen, R., Brumsack, H.J., 1999. Cyclic variations in the chemical composition of eastern Mediterranean Pliocene sediments: a key for understanding sapropel formation. Marine Geology 153, 161–176

Weijer, W., Cheng, W., Drijfhout, S.S., Fedorov, A. V., Hu, A., Jackson, L.C., Liu, W., McDonagh, E.L., Mecking, J. V., Zhang, J., 2019. Stability of the Atlantic Meridional Overturning Circulation: A Review and Synthesis. J. Geophys. Res. Ocean. 124, 5336–5375. https://doi.org/10.1029/2019JC015083

Wiersma, A. P., Jongma, J. I., 2010. A role for icebergs in the 8.2 ka climate event, Climate dynamics, 35, 535-549, DOI:10.1007/s00382-009-0645-1

Wiersma, A. P., Roche, D. M., Renssen, H., 2011. Fingerprinting the 8.2 ka event climate response in a coupled climate model, J. Quat. Sci., 26, 118-127, DOI:10.1002/jqs.1439

Xu, Z., Li, T., Chang, F., Wan, S., Choi, J., Lim, D., 2014. Clay-sized sediment provenance change in the northern Okinawa Trough since 22 kyr BP and its paleoenvironmental implication. Palaeogeogr. Palaeoclimatol. Palaeoecol. 399, 236–245. https://doi.org/10.1016/j.palaeo.2014.01.016

Yuan, F., 2017. A multi-element sediment record of hydrological and environmental changes from Lake Erie since 1800, J. Paleolimnol., 58, 23-42, DOI:10.1007/s10933-017-9953-3

Zanchetta, G., Drysdale, R. N., Hellstrom, J. C., Fallick, A. E., Isola, I., Gagan, M. K., Pareschi, M. T., 2007. Enhanced rainfall in the Western Mediterranean during deposition of sapropel S1: stalagmite evidence from Corchia cave (Central Italy), Quaternary Sci. Rev., 26, 279-286, DOI:10.1016/j.quascirev.2006.12.003

Zahn, R., Comas, M.C., Klaus, A., 1999. In: Proceedings of the Ocean Drilling Program, Scientific Results, vol. 161. (Ocean Drilling Program), College Station, TX.

Zaragosi, S., Bourillet, J.F., Eynaud, F., Toucanne, S., Denhard, B., Van Toer, A., Lanfumey, V., 2006. The impact of the last European deglaciation on the deep-sea turbidite systems of the Celtic-Armorican margin (Bay of Biscay). Geo-Marine Lett. 26, 317–329. https://doi.org/10.1007/s00367-006-0048-9

Zech, M., Zech, R., Glaser, B., 2007. A 240,000-year stable carbon and nitrogen isotope record from a loess-like palaeosol sequence in the Tumara Valley, Northeast Siberia. Chem. Geol. 242, 307–318. https://doi.org/10.1016/j.chemgeo.2007.04.002

Zielhofer, C., Fletcher, W.J., Mischke, S., De Batist, M., Campbell, J.F.E., Joannin, S., Tjallingii, R., El Hamouti, N., Junginger, A., Stele, A., Bussmann, J., Schneider, B., Lauer, T., Spitzer, K., Strupler, M., Brachert, T., Mikdad, A., 2017. Atlantic forcing of Western Mediterranean winter rain minima during the last 12,000 years. Quat. Sci. Rev. 157, 29–51. https://doi.org/10.1016/j.quascirev.2016.11.037

Zielhofer, C., Köhler, A., Mischke, S., Benkaddour, A., Mikdad, A., Fletcher, W.J., 2019. Western Mediterranean hydro-climatic consequences of Holocene ice-rafted debris (Bond) events. Clim. Past 15, 463–475. https://doi.org/10.5194/cp-15-463-2019

Zúñiga, Diana, Calafat, A., Sanchez-Vidal, A., Canals, M., Price, B., Heussner, S., Miserocchi, S., 2007a. Particulate organic carbon budget in the open Algero-Balearic Basin (Western Mediterranean): Assessment from a one-year sediment trap experiment. Deep. Res. Part I Oceanogr. Res. Pap. 54, 1530–1548. https://doi.org/10.1016/j.dsr.2007.06.001

Zúñiga, D., García-Orellana, J., Calafat, A., Price, N.B., Adatte, T., Sanchez-Vidal, A., Canals, M., Sanchez-Cabeza, J.A., Masqué, P., Fabres, J., 2007b. Late Holocene fine-grained sediments of the Balearic Abyssal Plain, Western Mediterranean Sea. Mar. Geol. 237, 25–36. https://doi.org/10.1016/j.margeo.2006.10.034

Zúñiga, D., Calafat, A., Heussner, S., Miserocchi, S., Sanchez-Vidal, A., Garcia-Orellana, J., Canals, M., Sánchez-Cabeza, J.A., Carbonne, J., Delsaut, N., Saragoni, G., 2008. Compositional and temporal evolution of particle fluxes in the open Algero-Balearic basin (Western Mediterranean). J. Mar. Syst. 70, 196–214. https://doi.org/10.1016/j.jmarsys.2007.05.007

X APPENDIX

X. Appendix

Other peer reviewed publications – JCR (SCI) – indexed journal papers:

Ramos-Román, M.J., Jiménez-Moreno, G., Anderson, R.S., García-Alix, A., Camuera, J., Mesa-Fernández, J.M., Manzano, S., 2019. Climate controlled historic olive tree occurrences and olive oil production in southern Spain. Global and Planetary Change, 182, 102996.

Jiménez-Moreno, G., Anderson, R.S., Ramos-Román, M.J., Camuera, J., Mesa-Fernández, J.M., García-Alix, A., Jiménez-Espejo, F.J., Carrión, J.S., López-Avilés, A., 2020. The Holocene Cedrus pollen record from Sierra Nevada (S Spain), a proxy for climate change in N Africa. Quaternary Science Reviews, 242, 106468.

Davis B.A.S., Chevalier, M., Sommer, P.S., et al., 2020. The Eurasian Modern Pollen Database (EMPD), version 2. Earth System Science Data, 12, 2423-2445.

López-Avilés, A., García-Alix, A., Jiménez-Moreno, G., Anderson, R.S., Toney, J.L., Mesa-Fernández, J.M., Jiménez-Espejo, F.J., 2021. Latest Holocene paleoenvironmental and paleoclimate reconstruction from an alpine bog in the Western Mediterranean region: The Borreguil de los Lavaderos de la Reina record (Sierra Nevada). Palaeogeography, Palaeoclimatology, Palaeoecology, 573, 110434.